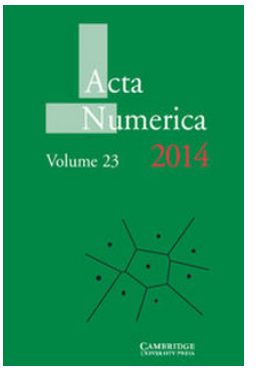

Mathematical analysis of variational isogeometric methods

L. Beirão da Veiga, A. Buffa, G. Sangalli and R. Vázquez

Acta Numerica / Volume 23 / May 2014, pp 157 - 287
DOI: 10.1017/S096249291400004X, Published online: 12 May 2014

Acta Numerica (2014), pp. 157–287
doi:10.1017/S096249291400004X

Mathematical analysis of variational isogeometric methods*

L. Beirão da Veiga[1,2]
A. Buffa[2]
G. Sangalli[3,2]
R. Vázquez[2]

[1] *Dipartimento di Matematica,*
Università di Milano,
via Saldini 50, 20133, Milano, Italy
E-mail: lourenco.beirao@unimi.it

[2] *Istituto di Matematica Applicata e Tecnologie Informatiche*
'E. Magenes' del CNR,
via Ferrata 1, 27100, Pavia, Italy
E-mail: {annalisa.buffa,vazquez}@imati.cnr.it

[3] *Dipartimento di Matematica,*
Università di Pavia,
via Ferrata 1, 27100, Pavia, Italy
E-mail: giancarlo.sangalli@unipv.it

This review paper collects several results that form part of the theoretical foundation of isogeometric methods. We analyse variational techniques for the numerical resolution of PDEs based on splines or NURBS and we provide optimal approximation and error estimates in several cases of interest. The theory presented also includes estimates for T-splines, which are an extension of splines allowing for local refinement. In particular, we focus our attention on elliptic and saddle point problems, and we define spline edge and face elements. Our theoretical results are demonstrated by a rich set of numerical examples. Finally, we discuss implementation and efficiency together with preconditioning issues for the final linear system.

* Colour online for monochrome figures available at journals.cambridge.org/anu.

CONTENTS

1 Introduction 158
2 Splines and NURBS: basics 162
3 Construction of isogeometric approximation spaces 179
4 Isogeometric spaces: scalar fields 186
5 Isogeometric spaces: vector fields 207
6 Application to elliptic and saddle point problems 223
7 Local refinement via T-splines 242
8 Efficient implementation and computational cost 261
References 278

1. Introduction

This paper aims to collect the main recent results on the numerical analysis and mathematical foundations of *isogeometric analysis*, introduced in the seminal paper by Hughes, Cottrell and Bazilevs (2005) as a new approach to the discretization of partial differential equations (PDEs); see also the book by Cottrell, Hughes and Bazilevs (2009). Isogeometric analysis is indeed a collection of methods (henceforth referred to as isogeometric methods) that use splines, or some of their extensions such as NURBS (non-uniform rational B-splines) and T-splines, as functions to build approximation spaces which are then used to solve partial differential equations numerically.

The main challenge Hughes, Cottrell and Bazilevs wanted to address was to improve the interoperability between CAD and PDE solvers, and for this reason they proposed the use of CAD mathematical primitives, that is, splines and NURBS, to represent PDE unknowns as well. Indeed, full interoperability is a challenging aim, for a number of reasons. For example, CAD modellers give a parametrization only of the boundary of geometrical objects as collections of manifolds in three-dimensional space, while the approximation spaces need to be defined on a three-dimensional volume that represents the computational domain; moreover, these manifolds are often obtained by trimming (Cohen, Riesenfeld and Elber 2001, Cohen *et al.* 2010). In this respect, isogeometric methods have taken the first fundamental steps towards a satisfactory solution and have undoubtedly created strong interest in these questions, promoting interaction between the scientific communities concerned. This is clearly documented by the number of publications on isogeometric methods, from the perspectives of geometric modelling, mechanical engineering and numerical analysis of PDEs.

From the standpoint of geometric modelling, the paper by Cohen *et al.* (2010) essentially initiated the study of isogeometric techniques. Even in

two space dimensions, not all possible CAD geometric representations may be used within isogeometric methods, and the automatic construction of parametrizations which fit CAD standards and, at the same time, are compatible with the isogeometric framework is a challenge. The so-called T-splines can be used for this purpose, and we refer the reader to the thesis by Scott (2011) and the references therein. Moreover, questions related to the construction of isogeometric-suitable volumetric meshes are addressed in Wang, Zhang, Scott and Hughes (2011) and Wang, Zhang, Liu and Hughes (2013). In this paper we will also introduce and analyse T-splines (in Section 7), but from a different perspective. Other approaches are possible. For example, Xu, Mourrain, Duvigneau and Galligo (2013) (see also Xu, Mourrain, Duvigneau and Galligo 2011) propose optimization algorithms to generate volumetric parametrization which are suitable for isogeometric techniques (at least injective, for example). Finally, we should also mention Martin, Cohen and Kirby (2009), who constructed NURBS parametrizations from tetrahedral meshes, or Aigner *et al.* (2009), who constructed swept volume parametrizations.

From the standpoint of numerical solution of PDEs, the use of splines and NURBS as building blocks for the construction of discrete spaces paves the way to many new numerical schemes for the numerical simulations of PDEs enjoying features that would be extremely hard to achieve within a standard finite element framework. The smoothness of splines is a new ingredient that yields several advantages: for example, it improves the accuracy per degree of freedom and allows for the direct approximation of PDEs of order higher than two.

Isogeometric methods have been used and tested on a variety of problems of engineering interest. There is indeed a large engineering literature on isogeometric methods showing the beneficial effects of higher regularity in several practical problems. Without any hope of completeness, we report here a few references that may be useful to the interested reader. Isogeometric methods have been proposed for flow simulations in the presence of turbulence (Bazilevs *et al.* 2007, Bazilevs, Michler, Calo and Hughes 2010*b*, Bazilevs and Hughes 2008), with conservative schemes (Buffa, de Falco and Sangalli 2011*a*, Evans and Hughes 2013*b*, Evans and Hughes 2013*c*), and for higher-order models such as Cahn–Hilliard (Gómez, Calo, Bazilevs and Hughes 2008, Gómez, Hughes, Nogueira and Calo 2010); for plate and shell analysis (Kiendl *et al.* 2010, Benson, Bazilevs, Hsu and Hughes 2011, Kiendl, Bletzinger, Linhard and Wuchner 2009, Beirão da Veiga *et al.* 2012*b*) where, in particular, the use of Kirchhoff models is made possible by the higher regularity of splines; for nonlinear solid mechanics (Elguedj, Bazilevs, Calo and Hughes 2008, Lipton *et al.* 2010, Echter and Bischoff 2010, Auricchio, Beirão da Veiga, Lovadina and Reali 2010*a*), shape optimization (Wall, Frenzel and Cyron 2008), fluid–structure interaction (Bazilevs, Calo, Hughes and

Zhang 2008, Bazilevs *et al.* 2011); and for electromagnetic problems (Buffa, Sangalli and Vázquez 2010*b*, Crouseilles, Ratnani and Sonnendrücker 2012, Vázquez, Buffa and Di Rienzo 2012, Vázquez, Buffa and Di Rienzo 2014). Moreover, regularity of splines has also been exploited in the design of contact algorithms in De Lorenzis, Temizer, Wriggers and Zavarise (2011) and Temizer, Wriggers and Hughes (2012), for example, and the effect of regularity on the spectral behaviour has been studied by Cottrell, Reali, Bazilevs and Hughes (2006), Hughes, Reali and Sangalli (2008) and more recently by Hughes, Evans and Reali (2014). Finally, again thanks to the regularity of splines, an isogeometric collocation method may be implemented, as proposed by Auricchio *et al.* (2010*b*) and Schillinger *et al.* (2013), for example, although its mathematical understanding is still incomplete.

From a more theoretical perspective, the mathematical analysis of isogeometric methods, on one hand, borrows from classical spline theory (see, *e.g.*, de Boor 2001 and Schumaker 2007), but on the other hand it has stimulated new developments and interesting new open questions. The theory of h-refinement of isogeometric spaces and methods, that is, the study of convergence that is achieved by refining the mesh, was developed in Bazilevs *et al.* (2006) and Beirão da Veiga, Cho and Sangalli (2012*c*), the latter covering anisotropic refinement. Another important issue of a theoretical nature concerns the use of splines/NURBS of high order, where convergence is achieved by raising the degree and possibly the inter-element regularity, known as k-refinement in the isogeometric literature. This is a challenging topic, and the relation between degree, regularity, and approximation properties is still not fully understood: we refer to the partial theoretical results in Beirão da Veiga, Buffa, Rivas and Sangalli (2011) and useful numerical studies in Evans, Bazilevs, Babuška and Hughes (2009). Exponential convergence for singular solutions in one dimension was investigated in Buffa, Sangalli and Schwab (2014*a*).

The stability of isogeometric methods has also been studied beyond the elliptic case, with special attention to saddle point problems and to compatible discretization in the sense of Arnold, Falk and Winther (2006). In this framework, smoothness offers innovative possibilities in method design, gives higher accuracy, and introduces new challenges in the analysis: we refer to the results obtained for the Stokes problem in Bressan (2011), Bressan and Sangalli (2013), Evans and Hughes (2013*a*), Auricchio *et al.* (2007), Buffa *et al.* (2011*a*), for Navier–Stokes in Evans and Hughes (2013*b*, 2013*c*), for the plate problem in Beirão da Veiga *et al.* (2012*b*), for the Maxwell problem in frequency and time domain in Buffa *et al.* (2010*b*) and Ratnani and Sonnendrücker (2012). As far as the approximation of vector fields is concerned, it is often important to preserve some fundamental structure of the continuous problem at a discrete level. In some of the previous references, de Rham-compatible edge and face elements, based on splines, have been

used; they were developed and fully analysed in Buffa *et al.* (2010*b*) and Buffa, Rivas, Sangalli and Vázquez (2011*b*), again showing that smoothness is beneficial since it allows for the design of spaces that are suitable for use in wider contexts.

An important topic is the generalization of spline constructions, which allow for local refinement by breaking the global tensor product structure of multivariate splines and NURBS. In the current literature there are three different definitions of splines on rectangular tilings with hanging nodes: T-splines, locally refinable (LR) splines and hierarchical splines. In this paper we have decided to focus on T-splines, reviewing and extending the results from Scott, Li, Sederberg and Hughes (2012), Beirão da Veiga, Buffa, Cho and Sangalli (2012*a*), Beirão da Veiga, Buffa, Sangalli and Vázquez (2013*a*) and Bressan, Buffa and Sangalli (2013). We refer the reader interested in hierarchical and LR splines to the following references: hierarchical splines were first introduced in Kraft (1997) and studied within the isogeometric paradigm in the papers by Vuong, Giannelli, Jüttler and Simeon (2011), Giannelli, Jüttler and Speleers (2012), Giannelli and Jüttler (2013), Schillinger *et al.* (2012) and others; LR splines were defined in Dokken, Lyche and Pettersen (2013) and further investigated in Johannessen, Kvamsdal and Dokken (2014) and Bressan (2013). Furthermore, splines can be defined over triangulations (see Lai and Schumaker 2007 and the references therein), but the construction cannot easily be extended to three space dimensions. Their use in isogeometric methods was investigated in Speleers, Manni, Pelosi and Sampoli (2012) (see also Speleers 2013 and Cohen, Lyche and Riesenfeld 2013) and warrants further study.

Finally, the modern theory of linear solvers, and in particular the set-up of preconditioners, needs to be reworked. This is an important aim from the viewpoint of real-world application of isogeometric methods, and also a mathematical challenge, particularly with regard to the high-degree high-regularity case. Some of the modern approaches for finite elements have been extended to the isogeometric context, for example the overlapping Schwarz approach (Beirão da Veiga, Cho, Pavarino and Scacchi 2012*d*, Beirão da Veiga, Cho, Pavarino and Scacchi 2013*c*), the BPX approach (Buffa, Harbrecht, Kunoth and Sangalli 2013), or domain-decomposition-based approaches such as BDDC or FETI (see Beirão da Veiga, Cho, Pavarino and Scacchi 2013*b* and Kleiss, Pechstein, Jüttler and Tomar 2012).

In this paper we give a unified review of the results and theorems which are part of the theoretical basis of isogeometric methods. In Section 2 we present a quick introduction to concepts and properties from classical spline theory that are needed for the rest of the paper. In Section 3 we introduce the main ideas behind isogeometric methods, together with the isoparametric–isogeometric concept. In this section we also make clear which class of computational domains we are able to treat within the isogeometric frame-

work. In Sections 4 and 5 we analyse the approximation properties of spline spaces for both scalar and vector fields. In Section 6 we present some numerical testing with the aim of demonstrating the theory developed in previous sections, and of showing that convergence and good approximation properties are achieved beyond the assumptions needed for the theoretical results. In Section 7 we approach the subject of local refinement via T-splines. Finally, in Section 8, we summarize some implementation issues and discuss the computational efficiency of the isogeometric method with relation to the smoothness of the underlying spline space, the construction of solvers for the linear systems and, in particular, the design of efficient preconditioners.

2. Splines and NURBS: basics

In this section we give a brief overview of B-splines and NURBS, which is mainly intended to fix the notation and to introduce the main definitions and results that will be used throughout the paper. Since this work is mainly focused on the numerical analysis of isogeometric methods, in this introduction we will present some basic definitions for B-splines, along with the construction and the approximation properties of some interpolants and quasi-interpolants. The reference books by Schumaker (2007) and de Boor (2001) cover the contents of this section together with many more results, while the basic ingredients for the practical use of splines in the context of isogeometric Galerkin methods are summarized in Cottrell *et al.* (2009).

In view of our focus, most of the properties that have made B-splines and NURBS the most successful technology for geometric modelling and computer aided design have been omitted from this introduction. For readers interested in obtaining a better understanding of this field we recommend the books by Cohen *et al.* (2001), Piegl and Tiller (1997) and Rogers (2001).

This section is divided into two parts. In Section 2.1 we present the definition of B-spline and NURBS basis functions in the one-dimensional case, the construction of free-form parametric curves with these bases, and the definition and approximation properties of some quasi-interpolants. All these definitions are extended to the multi-dimensional case by tensor products in Section 2.2.

2.1. Univariate B-splines: splines and NURBS curves

We start by presenting the definition and properties of B-splines and NURBS in the univariate case.

2.1.1. Definition and properties of univariate B-splines

Given two positive integers p and n, we say that $\Xi := \{\xi_1, \dots, \xi_{n+p+1}\}$ is a p-open knot vector if

$$\xi_1 = \cdots = \xi_{p+1} < \xi_{p+2} \leq \cdots \leq \xi_n < \xi_{n+1} = \cdots = \xi_{n+p+1},$$

where repeated knots are allowed. Without loss of generality, we assume in the following that $\xi_1 = 0$ and $\xi_{n+p+1} = 1$.

We also introduce the vector $Z = \{\zeta_1, \dots, \zeta_N\}$ of knots without repetitions, also called breakpoints, and denote by m_j the multiplicity of the breakpoint ζ_j, such that

$$\Xi = \{\underbrace{\zeta_1, \dots, \zeta_1}_{m_1 \text{ times}}, \underbrace{\zeta_2, \dots, \zeta_2}_{m_2 \text{ times}}, \dots, \underbrace{\zeta_N, \dots, \zeta_N}_{m_N \text{ times}}\}, \tag{2.1}$$

with $\sum_{i=1}^{N} m_i = n + p + 1$. We assume $m_j \leq p + 1$ for all internal knots. Note that the points in Z form a partition of the unit interval $I = (0, 1)$, that is, a mesh, and the local mesh size of the element $I_i = (\zeta_i, \zeta_{i+1})$ is called $h_i = \zeta_{i+1} - \zeta_i$, for $i = 1, \dots, N - 1$.

From the knot vector Ξ, B-spline functions of degree p are defined following the well-known Cox–de Boor recursive formula. We start with piecewise constants ($p = 0$):

$$\widehat{B}_{i,0}(\zeta) = \begin{cases} 1 & \text{if } \xi_i \leq \zeta < \xi_{i+1}, \\ 0 & \text{otherwise,} \end{cases} \tag{2.2}$$

and for $p \geq 1$ the *B-spline* functions are defined by the recursion

$$\widehat{B}_{i,p}(\zeta) = \frac{\zeta - \xi_i}{\xi_{i+p} - \xi_i} \widehat{B}_{i,p-1}(\zeta) + \frac{\xi_{i+p+1} - \zeta}{\xi_{i+p+1} - \xi_{i+1}} \widehat{B}_{i+1,p-1}(\zeta), \tag{2.3}$$

where it is formally assumed that $0/0 = 0$.

This gives a set of n B-splines that, among many other properties, are non-negative and form a partition of unity. They also form a basis of the space of *splines*, that is, piecewise polynomials of degree p with $k_j := p - m_j$ continuous derivatives at the points ζ_j, for $j = 1, \dots, N$. Therefore, $-1 \leq k_j \leq p - 1$, and the maximum multiplicity allowed, $m_j = p + 1$, gives $k_j = -1$, which stands for a discontinuity at ζ_j. The *regularity vector* $\mathbf{k} = \{k_1, \dots, k_N\}$ will collect the regularity of the basis functions at the internal knots, with $k_1 = k_N = -1$ for the boundary knots, because of the open knot vector structure. An example of B-splines is given in Figure 2.1.

We let

$$S_p(\Xi) = \operatorname{span}\{\widehat{B}_{i,p},\ i = 1, \dots, n\} \tag{2.4}$$

denote the *univariate spline space* spanned by the B-splines.

Note that the definition of each B-spline $\widehat{B}_{i,p}$ depends only on $p+2$ knots, which are collected in the *local knot vector*

$$\Xi_{i,p} := \{\xi_i, \dots,\ \xi_{i+p+1}\}.$$

When necessary, we will stress this fact by adopting the notation

$$\widehat{B}_{i,p}(\zeta) = \widehat{B}[\Xi_{i,p}](\zeta). \tag{2.5}$$

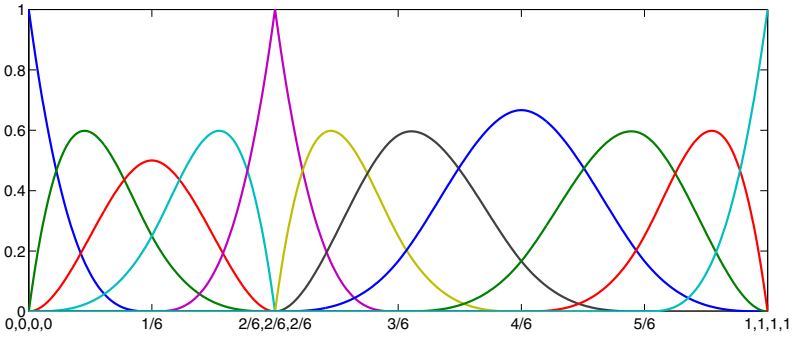

Figure 2.1. Cubic B-splines and the corresponding knot vector with repetitions.

The support of each basis function is exactly $\operatorname{supp}(\widehat{B}_{i,p}) = [\xi_i, \xi_{i+p+1}]$. Moreover, given an interval $I_j = (\zeta_j, \zeta_{j+1})$ of the partition, which can also be written as (ξ_i, ξ_{i+1}) for a certain (unique) i, we associate the *support extension* $\widetilde{I}_j$ defined by

$$\widetilde{I}_j := (\xi_{i-p}, \xi_{i+p+1}), \tag{2.6}$$

that is, the interior of the union of the supports of basis functions whose support intersects I_j.

Assuming the maximum multiplicity of the internal knots is less than or equal to the degree p, that is, the B-spline functions are at least continuous, the derivative of each B-spline $\widehat{B}_{i,p}$ is given by the expression

$$\frac{\mathrm{d}\widehat{B}_{i,p}}{\mathrm{d}\zeta}(\zeta) = \frac{p}{\xi_{i+p} - \xi_i}\widehat{B}_{i,p-1}(\zeta) - \frac{p}{\xi_{i+p+1} - \xi_{i+1}}\widehat{B}_{i+1,p-1}(\zeta), \tag{2.7}$$

where we have assumed that $\widehat{B}_{1,p-1}(\zeta) = \widehat{B}_{n+1,p-1}(\zeta) = 0$. In fact, the derivative belongs to the spline space $S_{p-1}(\Xi')$, where $\Xi' = \{\xi_2, \ldots, \xi_{n+p}\}$ is a $(p-1)$-open knot vector. Moreover, it is easy to see that $\mathrm{d}/\mathrm{d}\zeta : S_p(\Xi) \to S_{p-1}(\Xi')$ is a surjective application. For later use, we define the so-called *Curry–Schoenberg spline basis* (see, *e.g.*, de Boor 2001, Chapter IX) as follows:

$$\widehat{D}_{i,p-1}(\zeta) = \frac{p}{\xi_{i+p+1} - \xi_{i+1}}\widehat{B}_{i+1,p-1}(\zeta), \quad \text{for } i = 1, \ldots, n-1.$$

The indices for the new basis have been shifted in order to start the numbering from 1. Then formula (2.7) becomes

$$\frac{\mathrm{d}\widehat{B}_{i,p}}{\mathrm{d}\zeta}(\zeta) = \widehat{D}_{i-1,p-1}(\zeta) - \widehat{D}_{i,p-1}(\zeta), \tag{2.8}$$

where, again, we adopt the convention $\widehat{D}_{0,p-1} = \widehat{D}_{n,p-1} = 0$.

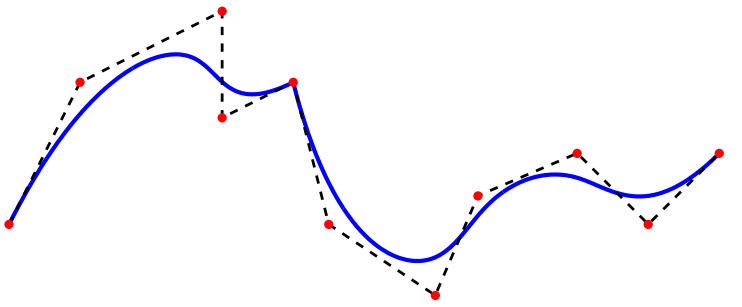

Figure 2.2. Spline curve (solid line), control polygon (dashed line) and control points (dots).

2.1.2. Splines and NURBS curves

A *spline curve* in $\mathbb{R}^d$, $d = 2, 3$ is a linear combination of B-splines and control points as follows:

$$\mathbf{C}(\zeta) = \sum_{i=1}^{n} \mathbf{c}_i \, \widehat{B}_{i,p}(\zeta) \quad \mathbf{c}_i \in \mathbb{R}^d, \tag{2.9}$$

where $\{\mathbf{c}_i\}_{i=1}^n$ are called control points. Given a spline curve $\mathbf{C}(\zeta)$, we call control polygon $\mathbf{C}_P(\zeta)$ the piecewise linear curve obtained by joining the control points $\{\mathbf{c}_i\}_{i=1}^n$ (see Figure 2.2). The control polygon has several properties and some of them are at the very core of the geometric modelling. We refer to Cohen *et al.* (2001) for details.

Despite the many advantages of splines, there exist several curves important for design that cannot be represented with piecewise polynomials, and in particular all conic curves except the parabola. It is known that conic sections can be parametrized by rational polynomials of the form

$$x(\zeta) = \frac{X(\zeta)}{W(\zeta)}, \quad y(\zeta) = \frac{Y(\zeta)}{W(\zeta)}.$$

For example, the circle of radius 1 can be parametrized with

$$X(\zeta) = 1 - \zeta^2, \quad Y(\zeta) = 2\zeta, \quad W(\zeta) = 1 + \zeta^2.$$

This motivated the introduction of *non-uniform rational B-splines*, better known as NURBS,[1] which are now the most widespread technology for geometric modelling, thanks to their versatility in representing both free-form and sculptured surfaces and conic sections. A discussion of the need for rational curves and surfaces can be found in Piegl and Tiller (1997, Section 1.4).

[1] Non-uniform refers to the distance between the knots.

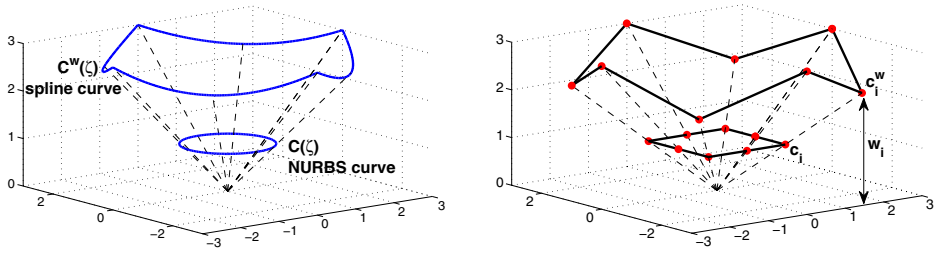

Figure 2.3. The circle as the projection of a non-rational spline curve.

In order to define NURBS, we set the *weight*,

$$W(\zeta) = \sum_{\ell=1}^{n} w_\ell \widehat{B}_{\ell,p}(\zeta),$$

where the positive coefficients $w_\ell > 0$ for $\ell = 1, \ldots, n$ are usually called *weights*. After setting the weight, we define the NURBS basis functions

$$\widehat{N}_{i,p}(\zeta) = \frac{w_i \widehat{B}_{i,p}(\zeta)}{\sum_{\ell=1}^{n} w_\ell \widehat{B}_{\ell,p}(\zeta)} = \frac{w_i \widehat{B}_{i,p}(\zeta)}{W(\zeta)}, \quad i = 1, \ldots, n, \tag{2.10}$$

which are clearly rational B-splines. Since the basis functions depend on the choice of weight W, we denote the corresponding NURBS space by

$$N_p(\Xi, W) = \operatorname{span}\{\widehat{N}_{i,p},\ i = 1, \ldots, n\}. \tag{2.11}$$

Similar to splines, a NURBS curve is defined by associating one control point with each basis function, in the form

$$\mathbf{C}(\zeta) = \sum_{i=1}^{n} \mathbf{c}_i\, \widehat{N}_{i,p}(\zeta) \quad \mathbf{c}_i \in \mathbb{R}^d. \tag{2.12}$$

In fact the NURBS curve is a projection into $\mathbb{R}^d$ of a non-rational B-spline curve in the space $\mathbb{R}^{d+1}$, which is defined by

$$\mathbf{C}^w(\zeta) = \sum_{i=1}^{n} \mathbf{c}_i^w\, \widehat{B}_{i,p}(\zeta),$$

where $\mathbf{c}_i^w = [\mathbf{c}_i, w_i] \in \mathbb{R}^{d+1}$ (see Figure 2.3). For more details about NURBS we refer to Piegl and Tiller (1997).

2.1.3. Knot insertion and degree elevation

In the context of geometric modelling, refinement refers to the possibility of adding new control points into a spline or NURBS curve without changing its parametrization $\mathbf{C}(\zeta)$. In order to do so, a refined space must be defined

which contains the space of the parametrization. Given the spline space $S_{p^0}(\Xi^0)$, we say that $S_p(\Xi)$ is a *refinement* of $S_{p^0}(\Xi^0)$ if

$$S_{p^0}(\Xi^0) \subset S_p(\Xi). \tag{2.13}$$

In the case of NURBS, since the parametrization must not change during refinement, the weight $W(\zeta)$ must also remain the same. Thus, given a NURBS space $N_{p^0}(\Xi^0, W)$, we say that $N_p(\Xi, W)$ is a refinement if

$$N_{p^0}(\Xi^0, W) \subset N_p(\Xi, W).$$

In fact, since W does not change, the previous condition reduces to (2.13) on the corresponding spline spaces.

For splines and NURBS curves, refinement is performed by knot insertion and degree elevation algorithms, which allow us to recompute the control points and the weights of the parametrization in the refined space. By combining these two algorithms, three kinds of refinement are possible in isogeometric methods, as explained in Hughes *et al.* (2005).

(1) *h-refinement*, which corresponds to mesh refinement and is obtained by knot insertion. Let $\bar{\Xi} := \Xi \cup \{\bar{\xi}\}$ be the knot vector after inserting the knot $\bar{\xi}$ into Ξ, and assume that $\xi_j \le \bar{\xi} \le \xi_{j+1}$. Denoting the knots in $\bar{\Xi}$ by $\bar{\xi}_\ell$ and the corresponding B-spline functions by $\bar{B}_{i,p}$, the original B-spline functions can be expressed in terms of the refined B-splines by

$$\widehat{B}_{i,p}(\zeta) = \alpha_i \bar{B}_{i,p}(\zeta) + (1 - \alpha_{i+1}) \bar{B}_{i+1,p}(\zeta) \tag{2.14}$$

with the coefficients

$$\alpha_i = \begin{cases} 1 & i = 1, \dots, j-p, \\ \dfrac{\bar{\xi} - \bar{\xi}_i}{\bar{\xi}_{i+p+1} - \bar{\xi}_i} & i = j-p+1, \dots, j, \\ 0 & i = j+1, \dots, n+1. \end{cases} \tag{2.15}$$

When $\bar{\xi}$ is equal to ξ_j or ξ_{j+1} or to both, the knot insertion corresponds to reduction of the inter-element regularity at $\bar{\xi}$.

(2) *p-refinement*, which corresponds to degree raising with fixed inter-element regularity. Successive application of p-refinement generates a sequence of nested spaces.

(3) *k-refinement*, which corresponds to applying degree elevation to the curve in the space $N_{p^0}(\Xi^0, W)$, and then knot insertion. By doing so, regularity is maintained at the knots of Ξ^0, but it is increased along with the degree in all the other knots. Therefore, successive application of k-refinement generates a sequence of spaces that are not nested. The name 'k-refinement' was coined by Hughes *et al.* (2005).

2.1.4. Greville sites and control polygon

For each B-spline basis function $\widehat{B}_{j,p}$ we associate a *Greville site*, also called the knot average:

$$\gamma_{j,p} = \frac{\xi_{j+1} + \cdots + \xi_{j+p}}{p}, \quad j = 1, \ldots, n. \tag{2.16}$$

Greville sites are the coefficients of the identity in the expansion with respect to a B-spline basis, that is,

$$\zeta = \sum_{j=1}^{n} \gamma_{j,p}\, \widehat{B}_{j,p}(\zeta). \tag{2.17}$$

Clearly, the Greville abscissa $\gamma_{j,p}$ depends only on the local knot vector $\Xi_{j,p}$. When necessary, we will adopt the notation $\gamma_{j,p} = \gamma[\Xi_{j,p}]$.

It is immediate to see that, when the multiplicity of the internal knots is $m_j \leq p$, for $j = 2, \ldots, n-1$, the Greville points $\gamma_{j,p}$ are all distinct and form a partition of the interval $[0, 1]$, which we call the *Greville mesh*. We let $\{\varphi_{j,p}\}_{j=1,\ldots,n}$ denote the standard hat functions associated to the Greville mesh, that is, the piecewise linear functions satisfying $\varphi_{j,p}(\gamma_{i,p}) = \delta_{i,j}$.

Given a spline (or a NURBS) curve in $\mathbb{R}^d$ as defined in (2.9) (or (2.12), respectively) with control points $\{\mathbf{c}_i\}_{i=1,\ldots,n}$, the corresponding control polygon $\mathbf{C}_P$ is defined by

$$\mathbf{C}_P = \sum_{i=1}^{n} \mathbf{c}_i \varphi_{i,p}(\zeta). \tag{2.18}$$

When splines (or NURBS) are used to describe functions, then the corresponding *control field* is a piecewise linear finite element function defined on the Greville mesh. Indeed, if $f \in S_p(\Xi)$, that is, $f = \sum_{j=1}^{n} f_j \widehat{B}_{j,p}$, then the *control points* associated with f, or with the graph of f, are $\mathbf{c}_j(f) = [\gamma_{j,p}, f_j]^T$, and the associated *control field* is $f_{\mathsf{cp}} = \sum_{j=1}^{n} f_j \varphi_{j,p}$.

Finally, it can be shown that when applying knot insertion and degree elevation, the control polygon converges to the curve (or the control field converges to the function). Indeed, assuming that the spline curve $\mathbf{C}$ is continuously differentiable, and applying knot insertion, there exists a constant C independent of the curve such that

$$\sup |\mathbf{C}(\zeta) - \mathbf{C}_P(\zeta)| \leq C h^2 \sup |\mathbf{C}''(\zeta)|,$$

where h is the mesh size of the refined knot vector by knot insertion. Moreover, when refining the spline space by degree elevation, Cohen and Schumaker (1985) proved that

$$\sup |\mathbf{C}(\zeta) - \mathbf{C}_P(\zeta)| \leq \frac{C}{p} \sup |\mathbf{C}'(\zeta)|.$$

2.1.5. Projections and quasi-interpolation operators

In this section we introduce interpolation and projection operators onto the space of splines $S_p(\Xi)$, whereas projections onto the NURBS spaces will be provided in Section 3. There are several ways to define projections for splines, and here we only describe the ones that will be needed below.

In the present contribution we will often make use of the following local quasi-uniformity condition on the knot vector, which is a classical assumption in the mathematical isogeometric literature.

Assumption 2.1. The partition defined by the knots $\zeta_1, \zeta_2, \ldots, \zeta_N$ is locally quasi-uniform, that is, there exists a constant $\theta \geq 1$ such that the mesh sizes $h_i = \zeta_{i+1} - \zeta_i$ satisfy the relation $\theta^{-1} \leq h_i/h_{i+1} \leq \theta$, for $i = 1, \ldots, N-2$.

Since splines are not, in general, interpolatory, a common way to define projections is by giving a dual basis, that is,

$$\Pi_{p,\Xi} : C^\infty([0,1]) \to S_p(\Xi), \quad \Pi_{p,\Xi}(f) = \sum_{j=1}^{n} \lambda_{j,p}(f)\widehat{B}_{j,p}, \tag{2.19}$$

where $\lambda_{j,p}$ are dual functionals satisfying

$$\lambda_{j,p}(\widehat{B}_{k,p}) = \delta_{jk}, \tag{2.20}$$

where δ_{jk} is the standard Kronecker symbol. Thanks to this property, it is trivial to prove that the quasi-interpolant $\Pi_{p,\Xi}$ preserves splines, that is,

$$\Pi_{p,\Xi}(f) = f, \quad \text{for all } f \in S_p(\Xi). \tag{2.21}$$

In spline theory, projections defined by dual bases are commonly called *quasi-interpolant operators.* There are several possible choices for the dual basis $\{\lambda_{j,p}\}$, $j = 1, \ldots, n$, and we refer the reader to Lee, Lyche and Mørken (2001) for a very general construction and theory of quasi-interpolant operators. Here we adopt the dual basis defined in Schumaker (2007, Section 4.6):

$$\lambda_{j,p}(f) = \int_{\xi_j}^{\xi_{j+p+1}} f(s) D^{p+1}\psi_j(s)\,\mathrm{d}s, \tag{2.22}$$

where $\psi_j(\zeta) = G_j(\zeta)\phi_j(\zeta)$, with

$$\phi_j(\zeta) = \frac{(\zeta - \xi_{j+1}) \cdots (\zeta - \xi_{j+p})}{p!},$$

and

$$G_j(\zeta) = g\left(\frac{2\zeta - \xi_j - \xi_{j+p+1}}{\xi_{j+p+1} - \xi_j}\right),$$

where g is the transition function of Schumaker (2007, Theorem 4.37). In

the same reference it is proved that the functionals $\lambda_{j,p}(\cdot)$ are dual to B-splines in the sense of (2.20) and stable (see Schumaker 2007, Theorem 4.41), that is,

$$|\lambda_{j,p}(f)| \leq C(\xi_{j+p+1} - \xi_j)^{-1/2} \|f\|_{L^2(\xi_j, \xi_{j+p+1})}, \tag{2.23}$$

where the constant C grows exponentially with respect to the polynomial degree p with the upper bound

$$C \leq (2p+3)9^p, \tag{2.24}$$

slightly improved in the literature following the results reported in Schumaker (2007). Note that these dual functionals are locally defined and only depend on the corresponding local knot vector, that is, adopting notation as in (2.5), we can write

$$\lambda_{i,p}(f) = \lambda[\Xi_{i,p}](f). \tag{2.25}$$

The reasons for this choice of dual basis are mainly historical, in that the first paper on the numerical analysis of isogeometric methods (Bazilevs *et al.* 2006) used this projection, but also because it satisfies the following important stability property.

Proposition 2.2. For any non-empty knot span $I_i = (\zeta_i, \zeta_{i+1})$, we have

$$\|\Pi_{p,\Xi}(f)\|_{L^2(I_i)} \leq C \|f\|_{L^2(\widetilde{I}_i)}, \tag{2.26}$$

where the constant C depends only on the degree p, and $\widetilde{I}_i$ is the support extension defined in (2.6). Moreover, if Assumption 2.1 holds, we also have

$$|\Pi_{p,\Xi}(f)|_{H^1(I_i)} \leq C |f|_{H^1(\widetilde{I}_i)}, \tag{2.27}$$

where the constant C depends only on p and θ, and where H^1 denotes the Sobolev space of order one, endowed with the standard norm and seminorm.

Proof. We first show (2.26). There exists a unique index j such that $I_i = (\zeta_i, \zeta_{i+1}) = (\xi_j, \xi_{j+1})$, and using the definition of B-splines at the beginning of Section 2.1.1, and in particular their support, it immediately follows that

$$\big\{\ell \in \{1, 2, \ldots, n\} : \mathrm{supp}(\widehat{B}_{\ell,p}) \cap I_i \neq \emptyset\big\} = \{j-p, j-p+1, \ldots, j\}. \tag{2.28}$$

Let h_i denote the length of I_i and let $\widetilde{h}_i$ indicate the length of $\widetilde{I}_i$. First by definition (2.19), and then recalling that the B-spline basis is positive and

a partition of unity, we obtain

$$\begin{aligned}\|\Pi_{p,\Xi}(f)\|_{L^2(I_i)} &= \Big\| \sum_{\ell=j-p}^{j} \lambda_{\ell,p}(f)\widehat{B}_{\ell,p} \Big\|_{L^2(I_i)} \\ &\le \max_{j-p\le\ell\le j} |\lambda_{\ell,p}(f)| \, \Big\| \sum_{\ell=j-p}^{j} \widehat{B}_{\ell,p} \Big\|_{L^2(I_i)} \\ &= h_i^{1/2} \max_{j-p\le\ell\le j} |\lambda_{\ell,p}(f)|.\end{aligned}$$

We now apply bound (2.23) and obtain

$$\begin{aligned}\|\Pi_{p,\Xi}(f)\|_{L^2(I_i)} &\le C h_i^{1/2} \max_{j-p\le\ell\le j} (\xi_{\ell+p+1}-\xi_\ell)^{-1/2} \|f\|_{L^2(\xi_\ell,\xi_{\ell+p+1})} \\ &\le C h_i^{1/2} \max_{j-p\le\ell\le j} (\xi_{\ell+p+1}-\xi_\ell)^{-1/2} \|f\|_{L^2(\widetilde{I}_i)},\end{aligned}$$

which yields (2.26), since clearly $h_i \le (\xi_{\ell+p+1}-\xi_\ell)$ for all ℓ in $\{j-p,\dots,j\}$.

We now show (2.27). For any real constant c, since the operator $\Pi_{p,\Xi}$ preserves constant functions and using a standard inverse estimate for polynomials on I_i, we obtain

$$\begin{aligned}|\Pi_{p,\Xi}(f)|_{H^1(I_i)} &= |\Pi_{p,\Xi}(f)-c|_{H^1(I_i)} = |\Pi_{p,\Xi}(f-c)|_{H^1(I_i)} \\ &\le C h_i^{-1} \|\Pi_{p,\Xi}(f-c)\|_{L^2(I_i)}.\end{aligned}$$

We now apply (2.26) and a standard approximation estimate for constant functions, yielding

$$|\Pi_{p,\Xi}(f)|_{H^1(I_i)} \le C h_i^{-1} \|f-c\|_{L^2(\widetilde{I}_i)} \le C h_i^{-1} \widetilde{h}_i |f|_{H^1(\widetilde{I}_i)}.$$

Using Assumption 2.1, it is immediate to check that $\widetilde{h}_i \le C h_i$ with $C = C(p,\theta)$, so that (2.27) follows. □

The operator $\Pi_{p,\Xi}$ can be modified in order to match boundary conditions. We can define, for all $f \in C^\infty([0,1])$,

$$\widetilde{\Pi}_{p,\Xi}(f) = \sum_{j=1}^{n} \widetilde{\lambda}_{j,p}(f)\widehat{B}_{j,p} \quad \text{with} \tag{2.29}$$

$$\widetilde{\lambda}_{1,p}(f) = f(0),\ \widetilde{\lambda}_{n,p}(f) = f(1),\ \widetilde{\lambda}_{j,p}(f) = \lambda_{j,p}(f), \quad j = 2,\dots,n-1.$$

Clearly, the L^2-stability stated for $\Pi_{p,\Xi}$ cannot be valid for $\widetilde{\Pi}_{p,\Xi}$, but a similar result holds.

Proposition 2.3. For any non-empty knot span $I_i = (\zeta_i, \zeta_{i+1})$, we have

$$\|\widetilde{\Pi}_{p,\Xi}(f)\|_{L^2(I_i)} \le C\big(\|f\|_{L^2(\widetilde{I}_i)} + \widetilde{h}_i |f|_{H^1(\widetilde{I}_i)}\big), \tag{2.30}$$

where the constant C depends on the degree p, and $\widetilde{I}_i$ is the support extension defined in (2.6), and $\widetilde{h}_i$ its length. Moreover, if Assumption 2.1 holds, we also have

$$|\widetilde{\Pi}_{p,\Xi}(f)|_{H^1(I_i)} \leq C\|f\|_{H^1(\widetilde{I}_i)}, \tag{2.31}$$

where the constant C depends only on p, θ and where the symbol H^1 was introduced in the previous proposition.

Proof. We concentrate only on the first estimate and merely sketch the proof, since it makes use of arguments similar to the previous one. Following Schumaker (2007) and by standard Sobolev inequalities, we have, analogous to (2.23),

$$|\widetilde{\lambda}_{\ell,p}(f)| \leq C(\xi_{\ell+p+1}-\xi_\ell)^{-1/2}\|f\|_{L^2(\xi_\ell,\xi_{\ell+p+1})}+(\xi_{\ell+p+1}-\xi_\ell)^{1/2}|f|_{H^1(\xi_\ell,\xi_{\ell+p+1})}.$$

Then, recalling that the B-splines that do not vanish in I_i are given by (2.28), we deduce, using $\|\widehat{B}_{\ell,p}\|_{L^2(\xi_{\ell+p+1}-\xi_\ell)} \leq C(\xi_{\ell+p+1}-\xi_\ell)^{1/2}$,

$$\begin{aligned}\|\widetilde{\Pi}_{p,\Xi}(f)\|_{L^2(I_i)} &\leq C\sum_{\ell=j-p}^{j} |\widetilde{\lambda}_{\ell,p}(f)|\ \|\widehat{B}_{\ell,p}\|_{L^2(\xi_{\ell+p+1}-\xi_\ell)} \\ &\leq C\|f\|_{L^2(\widetilde{I}_i)} + \widetilde{h}_i|f|_{H^1(\widetilde{I}_i)}.\end{aligned}$$

H^1-stability follows easily. □

We remark that the constant appearing in estimates (2.26)–(2.27) and (2.30)–(2.31) depends exponentially on the polynomial degree p, because of (2.23)–(2.24), and this prevents the use of such a quasi-interpolant for explicit estimates with respect to p. By no means does this fact demonstrate that the spline spaces have no 'good' properties with respect to p since (i) the proof, in its present form, does not provide the optimal constant, (ii) other, wiser, choices of dual functionals may lead to different estimates. The behaviour of the spline spaces as an approximation space for functions enjoying a fixed Sobolev regularity is studied numerically in Evans *et al.* (2009).

To our knowledge, the results of Beirão da Veiga *et al.* (2011) are among the few that are explicit in the degree and the regularity of the spline spaces. There, the attention is focused on splines of reduced regularity: it is required that $p \geq 2k+1$, where p is the polynomial degree and $k = \min\{k_2, \ldots, k_{N-1}\}$ is the smallest regularity across internal knots. Under this limitation, a Hermite-type interpolation operator can be defined and used. Although this operator might be recast in the framework of quasi-interpolants, we prefer to present it in the following form, to preserve clarity.

We assume for simplicity that all the internal knot multiplicities are the same, and thus the number of continuous derivatives is $k_i = k$ for all $i = 2, \dots, N-1$, and that $p \geq 2k+1$. We define the projection operator

$$\pi_{p,k} \colon H^{k+1}(0,1) \to S_p(\Xi)$$

as follows. Let $I_i = (\zeta_i, \zeta_{i+1})$, for $i = 1, \dots, N-1$, denote the ith element of the mesh defined in (2.1). Then, for all $f \in H^{k+1}(0,1)$

$$\begin{aligned} (\pi_{p,k} f)^{(j)}(\zeta_i) &= f^{(j)}(\zeta_i), && i = 1, \dots, N,\ j = 0, \dots, k, \\ (\pi_{p,k} f)^{(k+1)}|_{I_i} &= P^{I_i}_{p-k-1}(f^{(k+1)}) && i = 1, \dots, N-1, \end{aligned} \tag{2.32}$$

where $P^{I_i}_{p-k}$ denotes the L^2-projection onto the space of polynomials of degree $p-k$ living on I_i. Note that the above operator is well defined (Beirão da Veiga *et al.* 2011), although this is not immediately obvious. Clearly this operator does not enjoy the stability property (2.26), and its approximation properties are discussed in Section 4.1.3.

We end this section with the construction of another quasi-interpolant that will be useful later on, and concerns the construction of commuting projectors. In particular, given a projector $\Pi_{p,\Xi}$ constructed as above, we define

$$\Pi^c_{p-1,\Xi'} g\,(\zeta) := \frac{\mathrm{d}}{\mathrm{d}\zeta} \Pi_{p,\Xi} \int_0^\zeta g(s)\,\mathrm{d}s, \tag{2.33}$$

for all functions g such that $f(\zeta) = \int_0^\zeta g(s)\,\mathrm{d}s$ is in the domain of definition of $\Pi_{p,\Xi}$. The superscript c stands for commuting, and it is indeed trivial to see that

$$\Pi^c_{p-1,\Xi'} \frac{\mathrm{d}}{\mathrm{d}\zeta} f = \frac{\mathrm{d}}{\mathrm{d}\zeta} \Pi_{p,\Xi} f \tag{2.34}$$

for all f in the domain of definition of $\Pi_{p,\Xi}$. Moreover, and as a consequence of the spline preserving property (2.21), it is also immediate to prove that $\Pi^c_{p-1,\Xi'}$ preserves B-splines, that is,

$$\Pi^c_{p-1,\Xi'} g = g \quad \text{for all } g \in S_{p-1}(\Xi'). \tag{2.35}$$

Thus, we have the following commutative diagram:

$$\begin{array}{ccccccc} \mathbb{R} & \longrightarrow & H^1(0,1) & \xrightarrow{\frac{\mathrm{d}}{\mathrm{d}\zeta}} & L^2(0,1) & \longrightarrow & 0 \\ & & \Pi_{p,\Xi} \downarrow & & \Pi^c_{p-1,\Xi'} \downarrow & & \\ \mathbb{R} & \longrightarrow & S_p(\Xi) & \xrightarrow{\frac{\mathrm{d}}{\mathrm{d}\zeta}} & S_{p-1}(\Xi') & \longrightarrow & 0. \end{array} \tag{2.36}$$

We prove the following proposition.

Proposition 2.4. Let $g \in L^2(0,1)$, and let the projector $\Pi_{p,\Xi}$ be defined as in (2.19), that is,

$$\Pi_{p,\Xi} f(\zeta) = \sum_{i=1}^{n} \lambda_{i,p}(f) \widehat{B}_{i,p}(\zeta)$$

for any $f \in L^2(0,1)$. Then we have

$$\Pi^c_{p-1,\Xi'} g(\zeta) = \sum_{j=1}^{n-1} \lambda^c_{j,p-1}(g) \widehat{D}_{j,p-1}(\zeta),$$

with

$$\lambda^c_{j,p-1}(g) = \lambda_{j+1,p}\bigg(\int_{\xi_j}^{\zeta} g(s)\,\mathrm{d}s\bigg) - \lambda_{j,p}\bigg(\int_{\xi_j}^{\zeta} g(s)\,\mathrm{d}s\bigg). \tag{2.37}$$

Moreover, if Assumption 2.1 is satisfied, then for all $I_i = (\zeta_i, \zeta_{i+1})$ we have

$$\|\Pi^c_{p-1,\Xi'} g\|_{L^2(I_i)} \le C \|g\|_{L^2(\widetilde{I}_i)}, \tag{2.38}$$

where $\widetilde{I}_i$ is the support extension of I_i defined in (2.6).

Proof. Let $f(\zeta) := \int_0^\zeta g(s)\,\mathrm{d}s$. By definition of $\Pi^c_{p-1,\Xi'}$ and $\Pi_{p,\Xi}$, and then using the expression for the derivative (2.8), we have

$$\begin{aligned}\Pi^c_{p-1,\Xi'} g(\zeta) &= \frac{\mathrm{d}}{\mathrm{d}\zeta} \Pi_{p,\Xi} f(\zeta) = \frac{\mathrm{d}}{\mathrm{d}\zeta} \sum_{i=1}^{n} \lambda_{i,p}(f) \widehat{B}_{i,p}(\zeta) \\ &= \sum_{i=1}^{n} \lambda_{i,p}(f) (\widehat{D}_{i-1,p}(\zeta) - \widehat{D}_{i,p}(\zeta)),\end{aligned}$$

and recalling the convention $\widehat{D}_{0,p}(\zeta) = \widehat{D}_{n,p}(\zeta) = 0$, we obtain

$$\Pi^c_{p-1,\Xi'} g(\zeta) = \sum_{j=1}^{n-1} \big(\lambda_{j+1,p}(f) - \lambda_{j,p}(f)\big) \widehat{D}_{j,p-1}(\zeta).$$

Due to the linearity of the functionals $\lambda_{j,p}$, we have, for any given $\zeta^* \in \mathbb{R}$,

$$\lambda_{j,p}(f) = \lambda_{j,p}\bigg(\int_0^{\zeta^*} g(s)\,\mathrm{d}s\bigg) + \lambda_{j,p}\bigg(\int_{\zeta^*}^{\zeta} g(s)\,\mathrm{d}s\bigg),$$

and noting that the term $\int_0^{\xi_j} g(s)\,\mathrm{d}s$ is a constant, thanks to the partition of unity of the B-spline functions $\widehat{B}_{i,p}$ we have

$$\lambda_{j+1,p}\bigg(\int_0^{\xi_j} g(s)\,\mathrm{d}s\bigg) = \lambda_{j,p}\bigg(\int_0^{\xi_j} g(s)\,\mathrm{d}s\bigg).$$

Combining the last three equations, we obtain (2.37).

To prove (2.38), we again use the definition of $\Pi^c_{p-1,\Xi'}$, and then the stability of the projector $\Pi_{p,\Xi}$ from (2.27), to obtain

$$\|\Pi^c_{p-1,\Xi'} g\|_{L^2(I_i)} = |\Pi_{p,\Xi} f|_{H^1(I_i)} \leq C|f|_{H^1(\widetilde{I}_i)} = C\|g\|_{L^2(\widetilde{I}_i)},$$

and the result is proved. □

Remark 2.5. The same construction can be repeated, replacing $\Pi_{p,\Xi}$ with $\widetilde{\Pi}_{p,\Xi}$ in the definition of $\Pi^c_{p-1,\Xi'}$, and we set

$$\widetilde{\Pi}^c_{p-1,\Xi'} g\,(\zeta) := \frac{\mathrm{d}}{\mathrm{d}\zeta} \widetilde{\Pi}_{p,\Xi} \int_0^\zeta g(s)\,\mathrm{d}s. \tag{2.39}$$

The operator $\widetilde{\Pi}^c_{p-1,\Xi'}$ enjoys the same properties as $\Pi^c_{p-1,\Xi'}$, that is, Proposition 2.4 holds also for $\widetilde{\Pi}^c_{p-1,\Xi'}$.

Remark 2.6. Note that the definition of the dual functional $\lambda^c_{j,p-1}$ depends on the local knot vectors $\Xi_{j,p}$ and $\Xi_{j+1,p}$, and therefore it goes beyond the support of $\widehat{D}_{j,p-1}$. Moreover, in the estimate (2.38), the support extension $\widetilde{I}_i$ is defined for degree p, not $p-1$. This means that the projector $\Pi^c_{p-1,\Xi'}$ loses some locality with respect to $\Pi_{p-1,\Xi'}$, which would be the quasi-interpolant defined in Schumaker (2007, Section 4.6). This is the price paid to obtain the commutative diagram.

2.2. Multivariate splines and NURBS: tensorization

Multivariate B-splines are defined from univariate B-splines by simple tensor products. In this section we define our notation for function spaces, basis functions and indices. Since the tensorization argument is quite standard, we proceed without too many details, and we refer the reader to Schumaker (2007) and de Boor (2001), or to the book by Cottrell *et al.* (2009).

2.2.1. Multivariate splines and NURBS geometries

Let d be the space dimension (in practical cases, $d = 2, 3$). Assume $n_\ell \in \mathbb{N}$, the degree $p_\ell \in \mathbb{N}$ and the p_ℓ-open knot vector $\Xi_\ell = \{\xi_{\ell,1}, \ldots, \xi_{\ell,n_\ell+p_\ell+1}\}$ are given, for $\ell = 1, \ldots, d$. We set the polynomial degree vector $\mathbf{p} = (p_1, \ldots, p_d)$ and $\boldsymbol{\Xi} = \Xi_1 \times \cdots \times \Xi_d$. The corresponding knot values without repetitions are given for each direction ℓ by $Z_\ell = \{\zeta_{\ell,1}, \ldots, \zeta_{\ell,N_\ell}\}$.

The knots Z_ℓ form a Cartesian grid in the *parametric domain* $\widehat{\Omega} = (0,1)^d$, giving the *parametric Bézier mesh*, which is denoted by $\widehat{\mathcal{M}}$:

$$\widehat{\mathcal{M}} = \{Q_{\mathbf{j}} = I_{1,j_1} \times \cdots \times I_{d,j_d} : I_{\ell,j_\ell} = (\zeta_{\ell,j_\ell}, \zeta_{\ell,j_\ell+1}) \text{ for } 1 \leq j_\ell \leq N_\ell - 1\}. \tag{2.40}$$

For a generic Bézier element $Q_{\mathbf{j}} \in \widehat{\mathcal{M}}$, we also define its *support extension*

$$\widetilde{Q}_{\mathbf{j}} = \widetilde{I}_{1,j_1} \times \cdots \times \widetilde{I}_{d,j_d},$$

with $\widetilde{I}_{\ell,j_\ell}$ the univariate support extension given by (2.6).

B-spline spaces are defined by tensor product. We first introduce the set of multi-indices $\mathbf{I} = \{\mathbf{i} = (i_1, \ldots, i_d) : 1 \le i_\ell \le n_\ell\}$, and for each multi-index $\mathbf{i} = (i_1, \ldots, i_d)$, we define the local knot vector

$$\boldsymbol{\Xi}_{\mathbf{i},\mathbf{p}} = \Xi_{i_1,p_1} \times \cdots \times \Xi_{i_d,p_d}.$$

Then we introduce the set of multivariate B-splines

$$\big\{\widehat{B}_{\mathbf{i},\mathbf{p}}(\boldsymbol{\zeta}) = \widehat{B}[\Xi_{i_1,p_1}](\zeta_1) \cdots \widehat{B}[\Xi_{i_d,p_d}](\zeta_d), \text{ for all } \mathbf{i} \in \mathbf{I}\big\}. \tag{2.41}$$

Greville sites are constructed accordingly:

$$\boldsymbol{\gamma}_{\mathbf{i},\mathbf{p}} = (\gamma[\Xi_{i_1,p_1}], \ldots, \gamma[\Xi_{i_d,p_d}]).$$

The spline space in the parametric domain $\widehat{\Omega}$ is then

$$S_{\mathbf{p}}(\boldsymbol{\Xi}) = \operatorname{span}\{\widehat{B}_{\mathbf{i},\mathbf{p}}(\boldsymbol{\zeta}),\ \mathbf{i} \in \mathbf{I}\},$$

which is the space of piecewise polynomials of degree $\mathbf{p}$ with the regularity across Bézier elements given by the knot multiplicity. The Greville sites, as in the univariate case, are the coefficients of the identity in the B-spline basis:

$$\boldsymbol{\zeta} = \sum_{\mathbf{i}\in\mathbf{I}} \gamma_{\mathbf{i},\mathbf{p}} \widehat{B}_{\mathbf{i},\mathbf{p}}(\boldsymbol{\zeta}), \quad \boldsymbol{\zeta} \in \widehat{\Omega} = (0,1)^d. \tag{2.42}$$

Multivariate NURBS are defined as rational tensor product B-splines. Given a set of *weights* $\{w_{\mathbf{i}},\ \mathbf{i} \in \mathbf{I}\}$, and the weight function

$$W(\boldsymbol{\zeta}) = \sum_{\mathbf{j}\in\mathbf{I}} w_{\mathbf{j}} \widehat{B}_{\mathbf{j},\mathbf{p}}(\boldsymbol{\zeta}),$$

we define the NURBS basis functions

$$\widehat{N}_{\mathbf{i},\mathbf{p}}(\boldsymbol{\zeta}) = \frac{w_{\mathbf{i}} \widehat{B}_{\mathbf{i},\mathbf{p}}(\boldsymbol{\zeta})}{\sum_{\mathbf{j}\in\mathbf{I}} w_{\mathbf{j}} \widehat{B}_{\mathbf{j},\mathbf{p}}(\boldsymbol{\zeta})} = \frac{w_{\mathbf{i}} \widehat{B}_{\mathbf{i},\mathbf{p}}(\boldsymbol{\zeta})}{W(\boldsymbol{\zeta})}.$$

The NURBS space in the parametric domain $\widehat{\Omega}$ is then

$$N_{\mathbf{p}}(\boldsymbol{\Xi}, W) = \operatorname{span}\{\widehat{N}_{\mathbf{i},\mathbf{p}}(\boldsymbol{\zeta}),\ \mathbf{i} \in \mathbf{I}\}.$$

As in the case of NURBS curves, the choice of the weight depends on the geometry to parametrize, and should remain fixed after refinement.

Remark 2.7. Note that $S_{\mathbf{p}}(\boldsymbol{\Xi}) = \otimes_{\ell=1}^{d} S_{p_\ell}(\Xi_\ell)$. The same is not true for NURBS, since the weight W is not defined from the tensor product of univariate weights.

As for curves, we can now define spline (resp. NURBS) parametrizations of multivariate geometries in $\mathbb{R}^m$, $m = 2, 3$. A spline (resp. NURBS) parametrization is then any linear combination of B-spline (resp. NURBS) basis functions via control points $\mathbf{c_i} \in \mathbb{R}^m$,

$$\mathbf{F}(\boldsymbol{\zeta}) = \sum_{\mathbf{i} \in \mathbf{I}} \mathbf{c_i} \widehat{B}_{\mathbf{i},\mathbf{p}}(\boldsymbol{\zeta}), \quad \text{with } \boldsymbol{\zeta} \in \widehat{\Omega}, \tag{2.43}$$

and a NURBS parametrization is just a linear combination of NURBS instead of splines. Depending on the values of d and m, the map (2.43) can define a planar surface in $\mathbb{R}^2$ ($d = 2, m = 2$), a manifold in $\mathbb{R}^3$ ($d = 2, m = 3$), or a volume in $\mathbb{R}^3$ ($d = 3, m = 3$).

The refinement algorithms of knot insertion and degree elevation, to recompute the control points in finer spaces, can be generalized to multivariate splines and NURBS (Piegl and Tiller 1997). As in the univariate case, given a spline space $S_{\mathbf{p}^0}(\boldsymbol{\Xi}^0)$ we say that $S_{\mathbf{p}}(\boldsymbol{\Xi})$ is a refinement if $S_{\mathbf{p}^0}(\boldsymbol{\Xi}^0) \subset S_{\mathbf{p}}(\boldsymbol{\Xi})$. For NURBS spaces, the weight function W must remain fixed after refinement, and the refinement algorithms also recompute the set of weights. Thus, given a NURBS space $N_{\mathbf{p}^0}(\boldsymbol{\Xi}^0, W)$ we say that $N_{\mathbf{p}}(\boldsymbol{\Xi}, W)$ is a refinement if $N_{\mathbf{p}^0}(\boldsymbol{\Xi}^0, W) \subset N_{\mathbf{p}}(\boldsymbol{\Xi}, W)$. The three possibilities of refinement introduced in Section 2.1.3 also apply to multivariate splines and NURBS spaces.

Finally, the definition of the control polygon is generalized for multivariate splines and NURBS to a control mesh, which is given by the control points $\mathbf{c_i}$. To define it precisely, let $\boldsymbol{\gamma}_{\mathbf{i},\mathbf{p}}$ be the Greville points introduced above. As in the univariate case, the Greville points define a Cartesian grid in the parametric domain $\widehat{\Omega}$, which we call a *Greville mesh*, denoted by $\widehat{\mathcal{M}}_G$. Now let $\{\varphi_{\mathbf{i},\mathbf{p}}\}_{\mathbf{i} \in \mathbf{I}}$ be the piecewise bilinear or trilinear functions (depending on d) associated with the mesh $\widehat{\mathcal{M}}_G$. We define the *control mesh* as the image of $\widehat{\mathcal{M}}_G$ via the mapping

$$\mathbf{F}_{\mathsf{cp}} = \sum_{\mathbf{i} \in \mathbf{I}} \mathbf{c_i} \varphi_{\mathbf{i},\mathbf{p}}(\boldsymbol{\zeta}), \quad \boldsymbol{\zeta} \in [0,1]^d, \tag{2.44}$$

denoted by $\mathcal{M}_G$. Note, moreover, that since B-splines and NURBS functions are not interpolatory, the control mesh is not a mesh on the domain Ω (see Figure 2.4).

As in the univariate case, when splines (or NURBS) are used to describe functions in the domain $\widehat{\Omega}$, which take the form $f = \sum_{\mathbf{i} \in \mathbf{I}} f_{\mathbf{i}} \widehat{B}_{\mathbf{i},\mathbf{p}}(\boldsymbol{\zeta})$, then the control points associated with f, or with the graph of f, are $\mathbf{c}_{\mathbf{i},\mathbf{p}} = [\gamma_{\mathbf{i},\mathbf{p}}, f_{\mathbf{i}}]^T$, and the associated *control field* is

$$f_{\mathsf{cp}} = \sum_{\mathbf{i} \in \mathbf{I}} f_{\mathbf{i}} \varphi_{\mathbf{i},\mathbf{p}}(\boldsymbol{\zeta}).$$

The coefficients $f_{\mathbf{i}}$ are called the *control variables*.

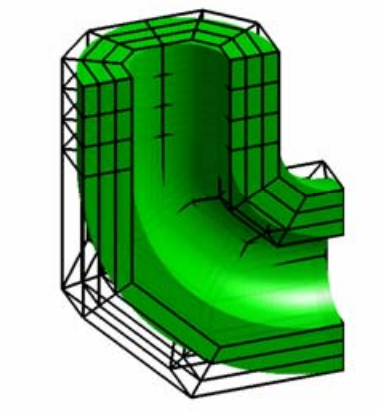

Figure 2.4. The control mesh for the shaded pipe.

Finally, as in the univariate case, it can be proved that when applying knot insertion and degree elevation, the control mesh converges to the surface or volume, and the control field converges to the function.

2.2.2. Multivariate quasi-interpolants

The univariate interpolation and quasi-interpolation operators introduced in Section 2.1.5 can also be extended to the multi-dimensional case by a tensor product construction. For $i = 1, \dots, d$, let the symbol $\Pi^i_{p_i}$ denote any one of the univariate operators onto the space $S_{p_i}(\Xi_i)$, either $\Pi_{p,\Xi}$, $\widetilde{\Pi}_{p,\Xi}$ or $\pi_{p,k}$. We define

$$\Pi_{\mathbf{p}}(f) = (\Pi^1_{p_1} \otimes \cdots \otimes \Pi^d_{p_d})(f), \tag{2.45}$$

where the tensorization must be interpreted in the sense explained in the next few lines. For the time being let f denote a sufficiently regular function on $[0,1]^d$. Then, for all $i = 1, \dots, d$ and $(x_1, \dots, x_{i-1}, x_{i+1}, \dots, x_d) \in [0,1]^{d-1}$, we define the one-dimensional functions

$$f^i_{(x_1,\dots,x_{i-1},x_{i+1},\dots,x_d)}(x) = f(x_1, \dots, x_{i-1}, x, x_{i+1}, \dots, x_d) \quad \text{for all } x \in [0,1].$$

By first introducing the auxiliary operators $\breve{\Pi}^i$,

$$(\breve{\Pi}^i f)(x_1, \dots, x_d) = \big(\Pi^i_{p_i} f^i_{(x_1,\dots,x_{i-1},x_{i+1},\dots,x_d)}\big)(x_i)$$

for all $(x_1, \dots, x_d) \in [0,1]^d$, we can finally define the tensorization in (2.45):

$$\Pi^1_{p_1} \otimes \cdots \otimes \Pi^d_{p_d} = \breve{\Pi}^1 \circ \cdots \circ \breve{\Pi}^d. \tag{2.46}$$

By abuse of notation, we will always use $\Pi^\ell_{p_\ell}$ even when $\breve{\Pi}^\ell$ should be used instead.

It is easy to check that, due to the tensor product structure of the spline space, the above operator is indeed a projection on $S_{\mathbf{p}}(\boldsymbol{\Xi})$. Note, moreover,

that the above operators $\Pi^i_{p_i}$ commute and the order of the operation in (2.46) has no effect on the final result. The definition above is given for any smooth f and then extended by continuity to the correct functional space. For instance, in the case of quasi-interpolants the L^2-regularity requirement stays unchanged and the operator $\Pi_{\mathbf{p}}$ is well defined for all $f \in L^2([0,1]^d)$. In contrast, for the Hermite interpolant of Section 2.1.5 it turns out that derivatives of order dk are required to be well defined at all the 'element vertices'. More details are given below in Section 4.2.3.

In the following, we will use the notation $\Pi_{\mathbf{p},\boldsymbol{\Xi}}$, $\widetilde{\Pi}_{\mathbf{p},\boldsymbol{\Xi}}$ and $\Pi_{\mathbf{p},\mathbf{k}}$ to refer to the multivariate projectors constructed from the univariate projectors (2.19), (2.29) and (2.32), respectively. We will use $\Pi_{\mathbf{p}}$ to denote any generic projector defined as in (2.45).

Finally, it is important to note that when the univariate quasi-interpolants are defined from a dual basis, as in (2.19) (or as in (2.29)), then the multivariate quasi-interpolant is also defined from a dual basis. Indeed, we have

$$\Pi_{\mathbf{p},\boldsymbol{\Xi}}(f) = \sum_{\mathbf{i}\in\mathbf{I}} \lambda_{\mathbf{i},\mathbf{p}}(f)\widehat{B}_{\mathbf{i},\mathbf{p}},$$

where each dual functional is defined from the univariate dual bases by the expression

$$\lambda_{\mathbf{i},\mathbf{p}} = \lambda_{i_1,p_1} \otimes \cdots \otimes \lambda_{i_d,p_d}. \tag{2.47}$$

Tensor products of dual functionals are defined along exactly the same lines as (2.46), and all details can be found in de Boor (2001, Chapter XVII).

We close this section with a useful note on the tensorized operator for boundary conditions $\widetilde{\Pi}_{p,\Xi}$:

$$\widetilde{\Pi}_{\mathbf{p},\boldsymbol{\Xi}} = \widetilde{\Pi}_{p_1,\Xi_1} \otimes \cdots \otimes \widetilde{\Pi}_{p_d,\Xi_d} : C^0([0,1]^d) \longrightarrow S_{\mathbf{p}}(\boldsymbol{\Xi}). \tag{2.48}$$

The operator $\widetilde{\Pi}_{\mathbf{p},\boldsymbol{\Xi}}$ enjoys a strong locality property when considering the boundary $\partial\widehat{\Omega}$ of $\widehat{\Omega} = (0,1)^d$. In particular, if Γ is a face of $\partial\widehat{\Omega}$, the following holds:

$$(\widetilde{\Pi}_{\mathbf{p},\boldsymbol{\Xi}} f)|_\Gamma \text{ depends only on } f|_\Gamma. \tag{2.49}$$

More precisely, $(\widetilde{\Pi}_{\mathbf{p},\boldsymbol{\Xi}} f)|_\Gamma$ corresponds to the (d–1)-dimensional tensor product operator obtained from $\widetilde{\Pi}_{\mathbf{p},\boldsymbol{\Xi}}$ by excluding $\widetilde{\Pi}_{p_j,\Xi_j}$, where ζ_j is the only coordinate that is constant on face Γ.

3. Construction of isogeometric approximation spaces

The aim of this section is to present the basic concepts of isogeometric methods introduced in Hughes *et al.* (2005), in order to perform their numerical analysis. We will assume that the computational domain is given by a NURBS geometry, and the finite-dimensional space for the discretization

will be defined directly on the NURBS geometry and on its mesh, without any need for re-meshing.

Hughes *et al.* (2005) proposed using the isoparametric concept, that is, the same space that generates the geometry is mapped to the physical domain using the NURBS parametrization. We will show how this concept can be relaxed without changing the essence of isogeometric analysis: roughly speaking it is necessary for the space describing the geometry and the space describing the solution to share the same mesh. For example, spline spaces can be defined on a NURBS geometry, or vector fields can be mapped by pull-back as Piola transforms, as we will see in Section 5. In this section we restrict to the isoparametric case; the other cases will be introduced in the following sections.

To study the approximation properties of spline or NURBS spaces mapped to the computational domain, it is also necessary to introduce suitable projectors defined in the physical domain, which is achieved by mapping the interpolants and quasi-interpolants defined in the previous section. At the end of the section we extend the definitions to the case of the so-called multi-patch domains, where the computational domain is represented by the union of several NURBS geometries.

3.1. Isogeometric spaces in a single-patch domain

We start by defining the spaces when the physical domain is given as the image of the unit square, or the unit cube, by a single NURBS parametrization.

3.1.1. Parametrization, mesh and discrete space

In isogeometric methods, the computational domain Ω is often assumed to be given via a NURBS transformation of the parametric domain $\widehat{\Omega}$. More precisely, for a given degree vector $\mathbf{p}^0$, the knot vectors $\boldsymbol{\Xi}^0$ and a weight function $W \in S_{\mathbf{p}^0}(\boldsymbol{\Xi}^0)$, we assume that there exists a map $\mathbf{F} \in (N_{\mathbf{p}^0}(\boldsymbol{\Xi}^0, W))^d$ such that $\Omega = \mathbf{F}(\widehat{\Omega})$, as in Figure 3.1.

We saw in Section 2.2.1 that the parametrization $\mathbf{F}$ is related to the control grid $\mathcal{M}_G$. Apart from defining the geometry, the control grid also plays a role in the definition of the space in multi-patch domains, as we will see below. However, the control grid is not a real mesh in Ω, because in general the control points do not lie in the geometry. In order to define a mesh in Ω, we consider the $\mathbf{F}$-*image*, that is, the image under $\mathbf{F}$, of the partition given by the knot vectors, as shown in Figure 3.1. This mesh, commonly referred to as the *Bézier mesh*, is the mesh used for the numerical computations, as we will see in Section 8.

More precisely, we have introduced the parametric Bézier mesh $\widehat{\mathcal{M}}$ in (2.40), as the mesh associated to the knot vectors $\boldsymbol{\Xi}$, and we now define the

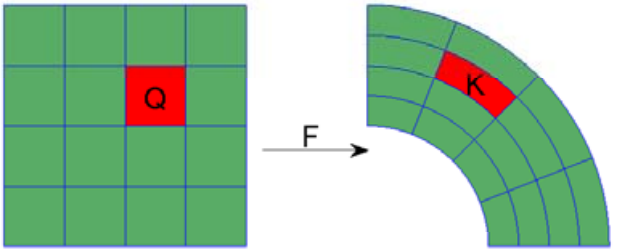

Figure 3.1. Mesh $\widehat{\mathcal{M}}$ in the parametric domain, and its image $\mathcal{M}$ in the physical domain.

physical Bézier mesh, or simply Bézier mesh, as the **F**-image of the (open) elements in $\widehat{\mathcal{M}}$:

$$\mathcal{M} := \{K \subset \Omega : K = \mathbf{F}(Q), Q \in \widehat{\mathcal{M}}\} \tag{3.1}$$

(see Figure 3.1). The meshes for the coarsest knot vector $\boldsymbol{\Xi}^0$ will be denoted by $\widehat{\mathcal{M}}_0$ and $\mathcal{M}_0$. For any element $K = \mathbf{F}(Q) \in \mathcal{M}$, we define its support extension as $\widetilde{K} = \mathbf{F}(\widetilde{Q})$, where $\widetilde{Q}$ is the support extension of Q, defined in Section 2.2.1. Moreover, we denote the element size of any element $Q \in \widehat{\mathcal{M}}$ by $h_Q = \operatorname{diam}(Q)$, and the global mesh size is $h = \max\{h_Q : Q \in \widehat{\mathcal{M}}\}$. Analogously, we define the element sizes $h_K = \operatorname{diam}(K)$ and $h_{\widetilde{K}} = \operatorname{diam}(\widetilde{K})$. Assumption 3.1 below will ensure that $h_Q \simeq h_K$.

In the following, we will make use of a regularity assumption on **F**.

Assumption 3.1 (regularity of F). The parametrization $\mathbf{F} : \widehat{\Omega} \to \Omega$ is a bi-Lipschitz homeomorphism. Moreover, $\mathbf{F}_{|\bar{Q}}$ is in $C^\infty(\bar{Q})$ for all $Q \in \widehat{\mathcal{M}}_0$, where $\bar{Q}$ denotes the closure of Q, and $\mathbf{F}^{-1}_{|\bar{K}}$ is in $C^\infty(\bar{K})$ for all $K \in \mathcal{M}_0$.

The assumption prevents the existence of singularities in the parametrization **F**. In the two-dimensional case, for instance, the most common singularities occur when a rectangular element in $\widehat{\mathcal{M}}$ is mapped by **F** to a curvilinear triangular element (see Figure 3.2), which is not allowed under Assumption 3.1. We remark that the study of isogeometric methods in the case of a parametrization with singularities began in Takacs and Jüttler (2011, 2012).

The discrete approximation spaces for isogeometric methods, as introduced in Hughes *et al.* (2005), are constructed as the **F**-image of refined splines or NURBS spaces. In more detail, let $\widehat{V}_h = N_{\mathbf{p}}(\boldsymbol{\Xi}, W)$ be a refinement of $N_{\mathbf{p}^0}(\boldsymbol{\Xi}^0, W)$, and define

$$V_h = \{f \circ \mathbf{F}^{-1} : f \in \widehat{V}_h\}, \tag{3.2}$$

where h parametrizes the family of spaces and stands for the mesh size,

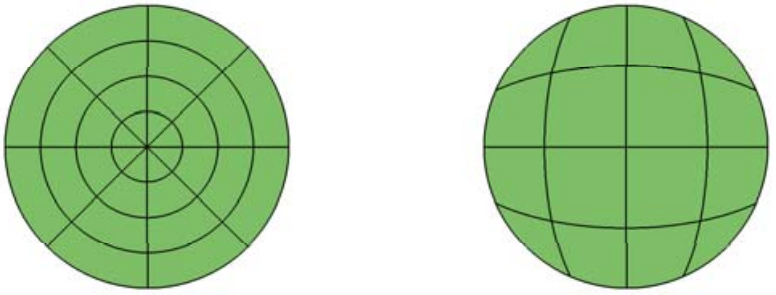

(a) (b)

Figure 3.2. Two possible singular parametrizations of the circle: (a) one singularity at the origin, and (b) four singularities on the boundary.

as usual. It is also important to provide a basis for the discrete space V_h. Under Assumption 3.1, it is clear that

$$V_h = \operatorname{span}\{N_{\mathbf{i},\mathbf{p}}(\mathbf{x}) := \widehat{N}_{\mathbf{i},\mathbf{p}} \circ \mathbf{F}^{-1}(\mathbf{x}),\ \mathbf{i} \in \mathbf{I}\}, \tag{3.3}$$

and the functions $N_{\mathbf{i},\mathbf{p}}$ form a basis of the space V_h.

We will also make use of spaces with boundary conditions. Let $\Gamma_D \subset \partial\Omega$ be a non-empty part of the boundary. We let

$$V_{h,\Gamma_D} = \{f \in V_h : f|_{\Gamma_D} = 0\}, \tag{3.4}$$

denote the space with homogeneous Dirichlet boundary conditions on Γ_D. For simplicity, we will always make the following assumption.

Assumption 3.2. The boundary region $\Gamma_D \subset \partial\Omega$ is the union of full faces of the boundary. More precisely, $\Gamma_D = \mathbf{F}(\widehat{\Gamma}_D)$, with $\widehat{\Gamma}_D$ a collection of full faces of the parametric domain $\widehat{\Omega}$.

3.1.2. Definition of the projector in the physical domain

Now we define a projector for the discrete space V_h in (3.2). We recall that the space V_h is constructed by applying the map $\mathbf{F}$ to the NURBS space $N_{\mathbf{p}}(\boldsymbol{\Xi}, W)$, which is constructed from $S_{\mathbf{p}}(\boldsymbol{\Xi})$ using the weight W. Therefore, the most natural definition of the projector is the one introduced in Bazilevs *et al.* (2006). Let $\Pi_{\mathbf{p}}$ be the spline projector (2.45), as defined by any of the univariate projectors in Section 2.1.5. We define the projector $\Pi_{V_h} : \mathcal{V}(\Omega) \to V_h$ as

$$\Pi_{V_h} f := \frac{\Pi_{\mathbf{p}}(W(f \circ \mathbf{F}))}{W} \circ \mathbf{F}^{-1}, \tag{3.5}$$

where $\mathcal{V}(\Omega)$ is some sufficiently regular functional space, which will depend on the choice of the univariate projectors, and will be specified when needed.

The approximation properties of Π_{V_h} will be studied in Section 4. Here we only prove the following result.

Proposition 3.3. It holds that $\Pi_{V_h} v_h = v_h$ for all $v_h \in V_h$. That is, Π_{V_h} is a projector.

Proof. Let $v_h \in V_h$, which can be written as $v_h = \widehat{v}_h \circ \mathbf{F}^{-1}$ for a unique $\widehat{v}_h \in \widehat{V}_h = N_{\mathbf{p}}(\boldsymbol{\Xi}, W)$. Moreover, $\widehat{v}_h = \widehat{u}_h / W$ for a unique $\widehat{u}_h \in S_{\mathbf{p}}(\boldsymbol{\Xi})$. Using definition (3.5) and these two previous expressions, and recalling that $\Pi_{\mathbf{p}}$ is a projector onto the space $S_{\mathbf{p}}(\boldsymbol{\Xi})$, the result is proved. □

Remark 3.4. Note that the space V_h is defined from the NURBS space $N_{\mathbf{p}}(\boldsymbol{\Xi}, W)$. Abandoning the isoparametric paradigm, we can analogously construct the approximation space as the image under the NURBS parametrization $\mathbf{F}$ of the spline space $\widehat{V}_h = S_{\mathbf{p}}(\boldsymbol{\Xi})$, which is a refinement of $S_{\mathbf{p}^0}(\boldsymbol{\Xi}^0)$. In this case the basis functions are $B_{\mathbf{i},\mathbf{p}} := \widehat{B}_{\mathbf{i},\mathbf{p}} \circ \mathbf{F}^{-1}$, and the projector Π_{V_h} is defined as in (3.5) taking $W = 1$. This non-isoparametric approach will be used in Section 5.

3.2. Isogeometric spaces in a multi-patch domain

In the previous section the domain Ω was defined as the $\mathbf{F}$-image of the unit square or the unit cube. In order to enhance flexibility and allow for more complex geometries, we generalize the definition of tensor product spline and NURBS parametrized domains to domains that are the union of several images of squares or cubes.

3.2.1. Multi-patch domain and discrete space

Let Ω be an open, bounded and connected set, which is defined as the union of M_p subdomains, in the form

$$\overline{\Omega} = \bigcup_{j=1}^{M_p} \overline{\Omega^{(j)}}, \tag{3.6}$$

where the subdomains $\Omega^{(j)} = \mathbf{F}^{(j)}(\widehat{\Omega})$ are referred to as *patches*, and are assumed to be disjoint. Each patch has its own parametrization $\mathbf{F}^{(j)}$, defined using the NURBS space $N_{\mathbf{p}^{(j)}}(\boldsymbol{\Xi}^{(j)}, W^{(j)})$, which differs from patch to patch. The whole Ω is then referred to as a *multi-patch* domain. In the following, the super-index (j) will identify the mathematical entities that are different on each patch $\Omega^{(j)}$, such as the basis functions and the control points.

Let us assume for simplicity that the degree vector $\mathbf{p}^{(j)} = \mathbf{p}$ is the same for all the patches, and all the components of $\mathbf{p}$ are equal to p. Noting that the knot vectors may be different from patch to patch, we define in $\Omega^{(j)}$ the discrete space

$$V_h^{(j)} = \operatorname{span}\{N_{\mathbf{i},\mathbf{p}}^{(j)}(\mathbf{x}) := \widehat{N}_{\mathbf{i},\mathbf{p}}^{(j)} \circ {\mathbf{F}^{(j)}}^{-1}(\mathbf{x}),\ \mathbf{i} \in \mathbf{I}^{(j)}\}, \quad j = 1, \ldots, M_p.$$

For the definition of the discrete space in the whole domain Ω, we take the functions which, restricted to each patch, belong to $V_h^{(j)}$, and possibly impose the continuity at the interfaces between patches, that is,

$$V_h^s = \{f \in C^s(\Omega) : f|_{\Omega^{(j)}} \in V_h^{(j)} \text{ for } j = 1, \dots, M_p\}, \quad s = -1, 0, 1 \dots. \tag{3.7}$$

When $s = -1$, no continuity is imposed: the construction of a basis for V_h^{-1} and the related properties are simple. When $s \geq 1$, the construction of a basis and the properties of V_h^s are not well understood and are related to the questions of *extraordinary points*. We refer the reader to Scott (2011, Chapter 6) and the references therein. For this paper, the interesting case is when $s = 0$, that is, continuity is imposed across patches. We set $V_h = V_h^0$ and we focus our attention on the properties of V_h.

In order to construct a basis for the discrete space V_h, we introduce a suitable conformity assumption, which follows the one given in Kleiss, Pechstein, Jüttler and Tomar (2012).

Assumption 3.5. Let $\Gamma_{ij} = \partial\Omega^{(i)} \cap \partial\Omega^{(j)}$ be the interface between the patches $\Omega^{(i)}$ and $\Omega^{(j)}$, with $i \neq j$. We say that the two patches are *fully matching* if the two following conditions hold.

(i) Γ_{ij} is either a vertex, or the image of a full edge, or the image of a full face for both parametric domains.

(ii) For each $N_{\mathbf{k},\mathbf{p}}^{(i)} \in V_h^{(i)}$ such that

$$\operatorname{supp}(N_{\mathbf{k},\mathbf{p}}^{(i)}) \cap \Gamma_{ij} \neq \emptyset,$$

there exists a function $N_{\mathbf{l},\mathbf{p}}^{(j)} \in V_h^{(j)}$ such that

$$N_{\mathbf{k},\mathbf{p}}^{(i)}|_{\Gamma_{ij}} = N_{\mathbf{l},\mathbf{p}}^{(j)}|_{\Gamma_{ij}}$$

(and *vice versa*).

Assumption 3.5 means that the physical Bézier meshes $\mathcal{M}^{(i)}$ and $\mathcal{M}^{(j)}$ coincide on the interface Γ_{ij}, and the coincident knot vectors are affinely related, including knot repetitions. Thus the partition

$$\mathcal{M} = \cup_{j=1}^{M_p} \mathcal{M}^{(j)} \tag{3.8}$$

is a *conforming*, globally unstructured, locally (to each patch) structured mesh of the computational domain Ω.

Moreover, the control points and weights associated to the matching basis functions $N_{\mathbf{k},\mathbf{p}}^{(i)}$ and $N_{\mathbf{l},\mathbf{p}}^{(j)}$ must also coincide, *i.e.*, $\mathbf{c}_{\mathbf{k}}^{(i)} = \mathbf{c}_{\mathbf{l}}^{(j)}$ and $w_{\mathbf{k}}^{(i)} = w_{\mathbf{l}}^{(j)}$, and as a consequence the control meshes $\mathcal{M}_G^{(i)}$ and $\mathcal{M}_G^{(j)}$ must also match conformally (see Figure 3.3). Having conformity of the control meshes $\mathcal{M}_G^{(j)}$, the continuity condition is implemented very easily by generating a global

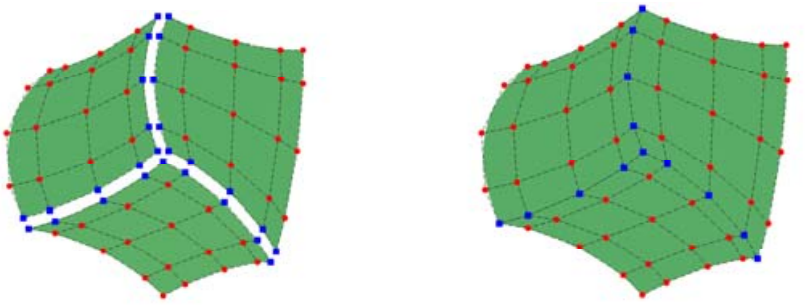

(a) (b)

Figure 3.3. Generation of a multi-patch domain with conforming meshes: control mesh of (a) the three separate patches, and (b) the multi-patch domain. The square control points are associated with basis functions that match on the interface.

numbering, in a process that resembles the generation of the connectivity array in finite element meshes. For each non-empty interface Γ_{ij}, we collect the pairs of coincident basis functions $N^{(i)}_{\mathbf{k},\mathbf{p}}$ and $N^{(j)}_{\mathbf{l},\mathbf{p}}$, and identify them as one single function, constraining their associated degrees of freedom to coincide. Note that for corners and edges (in the three-dimensional case), the new function may be generated from the contribution of functions coming from more than two patches.

More rigorously, we define for each patch $\Omega^{(j)}$, and precisely for the multi-index set $\mathbf{I}^{(j)}$, an application $G^{(j)} : \mathbf{I}^{(j)} \to \mathcal{I} = \{1, \dots, N_{V_h}\}$, in such a way that

$$G^{(i)}(\mathbf{k}) = G^{(j)}(\mathbf{l}) \Leftrightarrow \Gamma_{ij} \neq \emptyset \quad \text{and} \quad N^{(i)}_{\mathbf{k},\mathbf{p}}|_{\Gamma_{ij}} = N^{(j)}_{\mathbf{l},\mathbf{p}}|_{\Gamma_{ij}}.$$

The scalar N_{V_h} is the dimension of V_h, which is equal to the number of vertices of the control mesh $\mathcal{M}_G$. Moreover, we define for each global index $\ell \in \mathcal{I}$ the set of pairs $\mathcal{I}_\ell = \{(j, \mathbf{k}) : G^{(j)}(\mathbf{k}) = \ell\}$, which collects the local contributions to the global function. To conclude, for each $\ell \in \mathcal{I}$, we define the global basis function

$$N_\ell(\mathbf{x}) := \begin{cases} N^{(j)}_{\mathbf{k},\mathbf{p}}(\mathbf{x}) & \text{if } \mathbf{x} \in \overline{\Omega^{(j)}} \text{ and } (j, \mathbf{k}) \in \mathcal{I}_\ell, \\ 0 & \text{otherwise,} \end{cases} \tag{3.9}$$

which is continuous due to Assumption 3.5, and $V_h = \operatorname{span}\{N_\ell(\mathbf{x}) : \ell \in \mathcal{I}\}$.

Remark 3.6. In this paper we only address the multi-patch case with conforming meshes. The study of multi-patch domains with non-conforming meshes began in Cottrell, Hughes and Reali (2007) and Kleiss *et al.* (2012), which dealt with the case where one of the meshes on the interface is a refinement of the other, and imposed some constraints to ensure C^0-continuity between patches. The general case of non-conforming meshes has recently

been considered in Ruess, Schillinger, Özcan and Rank (2014), Apostolatos, Schmidt, Wüchner and Bletzinger (2014) and Nguyen *et al.* (2014), imposing the continuity between patches in a weak form.

Remark 3.7. It should be noted that classical hexahedral finite elements can be seen as a special case of multi-patch spline spaces. Indeed, we recover finite elements by having each patch composed of only one element. In this case, the basis selected comprises mapped Bernstein polynomials, while control points and the corresponding control mesh provide a localization of degrees of freedom similar to the one associated with Lagrangian bases.

3.2.2. Definition of the projector for multi-patch domains

Projectors onto the multi-patch spline or NURBS spaces could be constructed starting from any local (to patches) projectors defined in (3.5), with suitable averaging at control points shared by two or more patches.

Here, for simplicity, we present only a specific projector. Let

$$\Pi_{V_h^{(j)}} : C^0(\bar{\Omega}^{(j)}) \to V_h^{(j)},$$

defined as in (3.5) when considering $\widetilde{\Pi}_{p,\Xi}$ of (2.29). We construct the multi-patch interpolant

$$(\Pi_{V_h} f)|_{\Omega^{(j)}} = \Pi_{V_h^{(j)}}(f|_{\Omega^{(j)}}) \quad j = 1, \dots, M_p. \tag{3.10}$$

Thanks to the locality property of $\widetilde{\Pi}_{p,\Xi}$ (2.49) and to Assumption 3.5, it is immediate to see that the following proposition holds.

Proposition 3.8. The operator $\Pi_{V_h} : C^0(\bar{\Omega}) \to V_h$ is a projector.

Proof. By (2.49) and using that each $\Pi_{V_h^{(j)}}$ is defined by (3.5), we have that the quantity $(\Pi_{V_h^{(j)}}(f|_{\Omega^{(j)}}))|_{\Gamma_{ij}}$ depends only on $f|_{\Gamma_{ij}}$, for all non-empty $\Gamma_{ij} = \partial\Omega^{(j)} \cap \partial\Omega^{(i)}$. Thanks to Assumption 3.5, if $f \in C^0(\bar{\Omega})$ we have

$$(\Pi_{V_h^{(j)}}(f|_{\Omega^{(j)}}))|_{\Gamma_{ij}} = (\Pi_{V_h^{(i)}}(f|_{\Omega^{(i)}}))|_{\Gamma_{ij}}.$$

Therefore, also recalling Proposition 3.3, the result holds. □

4. Isogeometric spaces: scalar fields

From a theoretical standpoint, the approximation properties of the mapped NURBS space used to generate the discrete solution of the PDE of interest are fundamental. Although many results already exist for B-splines, which are the starting point for the construction of NURBS, the presence of the map $\mathbf{F}$ (representing the geometry) and the weight W (NURBS are *rational*) adds a further degree of complexity.

As usual in approximation estimates, we will make use of standard Sobolev spaces on a domain D, which can be either Ω or $\widehat{\Omega}$ or any of their relevant subsets as Q, $\widetilde{Q}$, K or $\widetilde{K}$. We let $H^s(D)$, $s \in \mathbb{N}$ denote the space of square-integrable functions $f \in L^2(\Omega)$ such that its derivatives up to order s are square-integrable. As is well known (see, *e.g.*, Adams 1975), the definition of Sobolev spaces extends to real regularity exponent s, but we will use this extension very rarely.

Conventional Sobolev spaces are not suitable for studying the approximation estimates of the space V_h defined in (3.2). Indeed, since the mapping $\mathbf{F}$ is not arbitrarily regular across mesh lines, even if a scalar function f in physical space satisfies $f \in H^s(\Omega)$, its pull-back $\widehat{f} = f \circ \mathbf{F}$ is not guaranteed to be in $H^s(\widehat{\Omega})$. As a consequence, the natural functional space in parameter space, in order to study the approximation properties of mapped NURBS, is not the standard Sobolev space H^s but rather a 'bent' version that allows for less regularity across mesh lines. This new class of spaces is defined rigorously below and used extensively in the rest of the section.

The approximation estimates with respect to the mesh size h (often called h-estimates) for isogeometric spaces are carried out in two papers, Bazilevs *et al.* (2006) and Beirão da Veiga *et al.* (2012*c*). The analysis in Bazilevs *et al.* (2006) is based on a generalized Bramble–Hilbert lemma and requires shape-regular and quasi-uniform meshes, while Beirão da Veiga *et al.* (2012*c*) introduce a new argument that strongly uses the tensor product structure and provide approximation estimates under much weaker assumptions. Here we present the analysis proposed in Beirão da Veiga *et al.* (2012*c*).

The analysis mentioned above yields h-approximation bounds, in the sense that the involved constants are uniform in h but not in p, k. Fully satisfactory h, p, k approximation estimates for B-splines and mapped NURBS spaces are still lacking in the literature. An initial result was obtained in Beirão da Veiga *et al.* (2011), but only for the case $p \geq 2k + 1$, and requiring high regularity of the target function. We also briefly describe the p-estimates of Beirão da Veiga *et al.* (2011).

The h-estimate and p-estimate above share a similar argument when it comes to extending the one-dimensional bound to the multivariate NURBS case. In contrast, the two one-dimensional interpolants and the ensuing approximation arguments are totally different.

The present section is organized as follows. After some preliminaries on bent Sobolev spaces, we consider the univariate case. We first address the h-analysis and then the p-analysis. Afterwards, in Section 4.2 we move on to the multivariate case, focusing on the two-dimensional setting for simplicity of exposition but also presenting general d-dimensional results. As in the univariate case, we consider h-estimates first and then, more briefly, p-estimates. In Section 4.3 we finally consider the case of mapped NURBS

spaces in physical space, which are the spaces actually used in isogeometric methods, following the usual order between the h and p cases. Moreover, notes on approximation estimates for multi-patch geometries can be found at the end of the section.

In the following, as usual, C will denote a constant, possibly different at each occurrence, but independent of the knot vector's characteristic size h. Note that, unless stated otherwise, C may depend on the polynomial degree p.

4.1. Univariate approximation estimates in the parametric domain

As already noted, we start with approximation estimates for univariate B-spline spaces.

4.1.1. Bent Sobolev spaces

Let $d = 1$, Ξ be a knot vector, and let p be the polynomial degree. Recalling from Section 2.1.1 that $I = (0, 1)$, and that $I_i = (\zeta_i, \zeta_{i+1})$ are the intervals of the partition given by the knot vector, we define for any $q \in \mathbb{N}$ the piecewise polynomial space

$$\mathcal{P}_q(\Xi) = \{v \in L^2(I) : v|_{I_i} \text{ is a } q\text{-degree polynomial, for } i = 1, \dots, N-1\}.$$

We recall that, given $s \in \mathbb{N}$ and any sub-interval $E \subset I$, we indicate by $H^s(E)$ the usual Sobolev space endowed with norm $\|\cdot\|_{H^s(E)}$ and seminorm $|\cdot|_{H^s(E)}$. We are now ready to introduce the bent Sobolev spaces, starting with the one-dimensional case. We define the bent Sobolev space (see Bazilevs *et al.* 2006) on I as

$$\mathcal{H}^s(I) = \left\{ \begin{array}{l} f \in L^2(I) : f|_{I_i} \in H^s(I_i) \text{ for } i = 1, \dots, N-1, \text{ and} \\ D_-^k f(\zeta_i) = D_+^k f(\zeta_i), \text{ for } k = 0, \dots, \min\{s-1, k_i\},\ i = 2, \dots, N-1, \end{array} \right\} \tag{4.1}$$

where $D_\pm^k$ denote the k-order left and right derivative (or left and right limit for $k = 0$), and k_i is the number of continuous derivatives at the breakpoint ζ_i, as defined in Section 2.1. Note that, although we leave this implicit in the notation, the space $\mathcal{H}^s(I)$ depends on the knot vector Ξ. We endow the above space with the broken norm and seminorms

$$\|f\|^2_{\mathcal{H}^s(I)} = \sum_{j=0}^{s} |f|^2_{\mathcal{H}^j(I)}, \quad |f|^2_{\mathcal{H}^j(I)} = \sum_{i=1}^{N-1} |f|^2_{H^j(I_i)} \quad \text{for all } j = 0, 1, \dots, s,$$

where $|\cdot|_{H^0(I_i)} = \|\cdot\|_{L^2(I_i)}$. Moreover, we indicate with $\mathcal{H}^s(E)$, for any sub-interval $E \subset I$, the restriction of $\mathcal{H}^s(I)$ to E, with the obvious norm and seminorms as above.

Given an integer s such that $0 \leq s \leq p$, we define the space

$$\widetilde{S}_{s,p}(\Xi) = \mathcal{P}_s(\Xi) \cap S_p(\Xi). \tag{4.2}$$

Clearly $S_p(\Xi) = \widetilde{S}_{p,p}(\Xi)$, and, for any $s < p$, $\widetilde{S}_{s,p}(\Xi)$ is still a spline space but clearly associated to a knot vector different from Ξ. For all $s \leq s' \leq p$ we also have the inclusion

$$\widetilde{S}_{s,p}(\Xi) \subseteq \widetilde{S}_{s',p}(\Xi). \tag{4.3}$$

Finally, we also note that

$$S_p(\Xi) = \mathcal{P}_p(\Xi) \cap \mathcal{H}^p(I).$$

4.1.2. Approximation estimates in h

In the present section we prove one-dimensional approximation estimates for B-splines, which are more general than the classical ones in Schumaker (2007). These more general estimates are needed in order to derive the approximation estimates for mapped NURBS spaces that follow. The following results are largely inspired by Beirão da Veiga *et al.* (2012*c*).

We need the following preliminary results in order to prove the approximation estimates for functions in bent Sobolev spaces (4.1), stated in Proposition 4.3.

Lemma 4.1. Let $s \in \mathbb{N}$, $s \leq p+1$. There exists a projector $\Gamma : \mathcal{H}^s(I) \to \widetilde{S}_{s-1,p}(\Xi)$ such that, for all $f \in \mathcal{H}^s(I)$,

$$f - \Gamma(f) \in H^s(I). \tag{4.4}$$

If $s \geq 2$, it is also possible to define Γ such that

$$\Gamma(f)(\zeta_1) = \Gamma(f)(\zeta_N) = 0. \tag{4.5}$$

Proof. Obviously one can assume $s = p+1$, and construct $\Gamma : \mathcal{H}^{p+1}(I) \to S_p(\Xi)$. The proof is identical for $s < p+1$.

In order to show (4.4) we have to construct $\Gamma(f) \in S_p(\Xi)$ such that

$$D_+^k(f - \Gamma(f))(\zeta_i) = D_-^k(f - \Gamma(f))(\zeta_i)$$

for all $i = 2, \ldots, N-1$ and $k = 0, 1, \ldots, p$. Due to the definition (4.1), this is equivalent to

$$D_+^k(\Gamma(f))(\zeta_i) - D_-^k(\Gamma(f))(\zeta_i) = D_+^k(f)(\zeta_i) - D_-^k(f)(\zeta_i) \tag{4.6}$$

for all $i = 2, \ldots, N-1$ and $k = k_i + 1, k_i + 2, \ldots, p$, since for smaller values of k both the left- and right-hand sides above are null.

For all $i = 2, \ldots, N-1$ and $q = k_i + 1, k_i + 2, \ldots, p$, let the functions $\varphi_i^q : I \to \mathbb{R}$ be defined as

$$\varphi_i^q(x) = \big(\max\{0, x - \zeta_i\}\big)^q \quad \text{for all } x \in I, \tag{4.7}$$

where in the above definition we assume the convention that $0^0 = 0$. The above functions φ_i^q are in $S_p(\Xi)$ and are smooth everywhere in I but ζ_i. Moreover, it is immediate to check that, for all admissible indices q, i and for all $k \in \mathbb{N}$, the left and right derivatives

$$D_-^k \varphi_i^q(\zeta_i) = 0, \quad D_+^k \varphi_i^q(\zeta_i) = q!\, \delta_{qk}, \tag{4.8}$$

with δ_{qk} the Kronecker symbol. We now define $\Gamma(f) \in S_p(\Xi)$ as

$$\Gamma(f)(x) = \sum_{i=2}^{N-1} \sum_{q=k_i+1}^{p} \frac{c_i^q}{q!}\, \varphi_i^q(x) \quad \text{for all } x \in I, \tag{4.9}$$

where, for $i = 2, \dots, N-1$ and $k_i + 1 \le q \le p$, we set

$$c_i^q = D_+^q f(\zeta_i) - D_-^q f(\zeta_i). \tag{4.10}$$

The function $\Gamma(f)$ satisfies (4.6).

If $p \ge 1$, we can then define

$$\Gamma_0(f)(x) = (\zeta_N - \zeta_1)\Gamma(f)(x) - (x - \zeta_1)\Gamma(f)(\zeta_N),$$

which fulfils the previous property (4.6) and vanishes at the boundary $x = \zeta_1$ and $x = \zeta_N$. □

We recall that the length of the element $I_i = (\zeta_i, \zeta_{i+1})$ is denoted by h_i, and the global mesh size is represented by $h = \max\{h_i, 1 \le i \le N-1\}$. In the following we will also denote by $\widetilde{h}_i$ the length of the support extensions $\widetilde{I}_i$, defined in (2.6), for $i = 1, \dots, N-1$.

Let $\Pi_{p,\Xi}$ be the quasi-interpolant on the space $S_p(\Xi)$ introduced in Section 2.1.5. We have the following approximation estimate.

Proposition 4.2. There exists a positive constant C, depending only on p, such that, for all $s \in \mathbb{N}$, $s \le p+1$, and all $f \in H^s(I)$,

$$\|f - \Pi_{p,\Xi}(f)\|_{L^2(I_i)} \le C(\widetilde{h}_i)^s |f|_{H^s(\widetilde{I}_i)} \quad \text{for all } i = 1, \dots, N-1. \tag{4.11}$$

Furthermore, let the knot vector Ξ satisfy Assumption 2.1. Then, there exists a constant C depending only on p and θ such that, for all $r, s \in \mathbb{N}$, $0 < r \le s \le p+1$, and all $f \in H^s(I)$,

$$|f - \Pi_{p,\Xi}(f)|_{H^r(I_i)} \le C(\widetilde{h}_i)^{s-r} |f|_{H^s(\widetilde{I}_i)} \quad \text{for all } i = 1, \dots, N-1. \tag{4.12}$$

Proof. Let any non-empty knot span $I_i = (\zeta_i, \zeta_{i+1})$ and let q be any polynomial of degree at most p living on $[0,1]$. Noting that, since $q \in S_p(\Xi)$, we have $\Pi_{p,\Xi}(q) = q$, and using Proposition 2.2, it follows that

$$\|f - \Pi_{p,\Xi}(f)\|_{L^2(I_i)} \le \|f - q\|_{L^2(I_i)} + \|\Pi_{p,\Xi}(q - f)\|_{L^2(I_i)} \le C\|f - q\|_{L^2(\widetilde{I}_i)}.$$

The term above is bounded by standard polynomial approximation estimates in one dimension, leading immediately to (4.11). We note that, since

the restriction of $S_p(\Xi)$ to any element I_i is a polynomial of fixed degree p, we can apply inverse estimates. Therefore, regarding (4.12), we have

$$\begin{aligned}|f-\Pi_{p,\Xi}(f)|_{H^r(I_i)} &\le |f-q|_{H^r(I_i)} + |\Pi_{p,\Xi}(q-f)|_{H^r(I_i)}\\ &\le |f-q|_{H^r(I_i)} + Ch_i^{-r}\|\Pi_{p,\Xi}(q-f)\|_{L^2(I_i)}\\ &\le |f-q|_{H^r(I_i)} + Ch_i^{-r}\|f-q\|_{L^2(\widetilde{I}_i)}.\end{aligned}$$

Due to Assumption 2.1, it is easy to check that $h_i \le \widetilde{h}_i \le C'h_i$ for some fixed positive constant C'. Therefore, again applying standard polynomial approximation estimates, we obtain

$$|f-\Pi_{p,\Xi}(f)|_{H^r(I_i)} \le C\big(h_i^{s-r} + (\widetilde{h}_i)^s h_i^{-r}\big)|f|_{H^s(\widetilde{I}_i)}. \le C(\widetilde{h}_i)^{s-r}|f|_{H^s(\widetilde{I}_i)}. \ \square$$

Lemma 4.1 and Proposition 4.2 yield the following improved approximation result.

Proposition 4.3. There exists a positive constant $C = C(p)$ such that, for all $s \in \mathbb{N}$, $s \le p+1$, and all $f \in \mathcal{H}^s(I)$,

$$\|f-\Pi_{p,\Xi}(f)\|_{L^2(I_i)} \le C(\widetilde{h}_i)^s|f|_{\mathcal{H}^s(\widetilde{I}_i)} \quad \text{for all } i=1,\dots,N-1. \tag{4.13}$$

Moreover, under Assumption 2.1, there exists a constant $C = C(p,\theta)$ such that, for all $r,s \in \mathbb{N}$, $0 < r \le s \le p+1$, and all $f \in \mathcal{H}^s(I)$,

$$|f-\Pi_{p,\Xi}(f)|_{H^r(I_i)} \le C(\widetilde{h}_i)^{s-r}|f|_{\mathcal{H}^s(\widetilde{I}_i)} \quad \text{for all } i=1,\dots,N-1. \tag{4.14}$$

Proof. Let i be in $\{1,\dots,N-1\}$. We apply Lemma 4.1 and, since $\Gamma(f) \in \widetilde{S}_{s-1,p}(\Xi) \subset S_p(\Xi)$, we have

$$f-\Pi_{p,\Xi}(f) = (f-\Gamma(f)) - \Pi_{p,\Xi}(f-\Gamma(f)). \tag{4.15}$$

Again noting that $\Gamma(f) \in \widetilde{S}_{s-1,p}(\Xi)$, it follows that $|\Gamma(f)|_{H^s(I_j)} = 0$ for all $1 \le j \le N-1$. Moreover, since $(f-\Gamma(f)) \in H^s(I)$ due to (4.4), we can use Proposition 4.2 and get

$$\begin{aligned}|f-\Pi_{p,\Xi}(f)|_{H^r(I_i)} &= |f-\Gamma(f)-\Pi_{p,\Xi}(f-\Gamma(f))|_{H^r(I_i)}\\ &\le C(\widetilde{h}_i)^{s-r}|f-\Gamma(f)|_{H^s(\widetilde{I}_i)}\\ &= C(\widetilde{h}_i)^{s-r}\sum_{I_j\subset\widetilde{I}_i}|f-\Gamma(f)|_{H^s(I_j)}\\ &= C(\widetilde{h}_i)^{s-r}\sum_{I_j\subset\widetilde{I}_i}|f|_{H^s(I_j)}\\ &= C(\widetilde{h}_i)^{s-r}|f|_{\mathcal{H}^s(\widetilde{I}_i)}.\end{aligned}$$

This gives (4.13)–(4.14), for $r=0$ and $r>0$ respectively. $\square$

Remark 4.4. Due to Assumption 2.1, we can replace $\widetilde{h}_i$ by h_i in (4.12) and in (4.14).

Remark 4.5. Setting $0 \leq r = s \leq p+1$, (4.13)–(4.14) also guarantees the stability of $\Pi_{p,\Xi}$ in Sobolev seminorms:

$$|\Pi_{p,\Xi}(f)|_{H^r(I_i)} \leq C|f|_{\mathcal{H}^r(\widetilde{I}_i)} \quad \text{for all } i = 1, \ldots, N-1, \text{ and } f \in \mathcal{H}^r(\widetilde{I}_i).$$

Remark 4.6. When $p \geq 1$, one can easily deal with spaces with boundary conditions. For instance, using the simple variant for Γ in (4.5), the proof in the case of homogeneous boundary conditions at one or both ends follows using the same argument shown above. The approximation result is therefore the same as in Proposition 4.3.

4.1.3. Approximation estimates in p

In the present section we derive approximation error estimates that are explicit in h, p, k for the (univariate) Hermite-type interpolant (2.32) introduced in Section 2.1.5. The Hermite-type interpolant is completely local to the element, and as a consequence the error estimates on each element I_i will not depend on the support extension $\widetilde{I}_i$, as occurs for the quasi-interpolant of the previous section. This local property comes at the cost of reduced continuity between the elements.

We assume for simplicity of exposition that all the internal knot multiplicities are equal, so that the regularity indices satisfy $k_i = k$ for all $i = 2, \ldots, N-1$. We recall the assumption $p \geq 2k+1$, which is needed in order for the present interpolant to be well defined.

We do not show the proof of the following result, which is derived by using truncated Legendre series and a scaling argument. The proof can be found in Beirão da Veiga *et al.* (2011).

Proposition 4.7. Given the subdivision $\{0 = \zeta_1, \ldots, \zeta_N = 1\}$ of the reference domain $(0,1)$, let $I_i = (\zeta_i, \zeta_{i+1})$ for $i = 1, \ldots, N-1$. Let also k, p be non-negative integers with $p \geq 2k+1$ and $f \in H^s(0,1)$ for some $0 \leq \sigma \leq \kappa = p - k$. The following holds for all $i = 1, \ldots, N-1$, and for $r = 0, \ldots, k+1$:

$$|f - \pi_{p,k} f|^2_{H^r(I_i)} \leq \left(\frac{h_i}{2}\right)^{2(\sigma+k+1-r)} \frac{(\kappa-\sigma)!\,(\kappa-(k-r+1))!}{(\kappa+\sigma)!\,(\kappa+(k-r+1))!} |f^{(k+1)}|^2_{H^\sigma(I_i)}, \tag{4.16}$$

where $h_i = \zeta_{i+1} - \zeta_i$ is the element size.

Then, we have the following theorem, stating the *hpk* approximation properties of the one-dimensional interpolant $\pi_{p,k}$, explicit in p, k and h.

Theorem 4.8. Under the assumptions of Proposition 4.7, with

$$h = \max\{h_i : i = 1, \ldots, N-1\},$$

we have

$$|f-\pi_{p,k}f|_{H^r(0,1)} \le Ch^{s-r}(p-k)^{-(s-r)}|f|_{H^s(0,1)}, \tag{4.17}$$

for $k+1 \le s \le p+1$, $r=0,\dots,k+1$, and C independent of s, r, h, p and k. In particular, when $p=2k+1$,

$$|f-\pi_{p,k}f|_{H^r(0,1)} \le Ch^{s-r}\left(\frac{p+1}{2}\right)^{-(s-r)}|f|_{H^s(0,1)}, \quad r=0,\dots,k+1. \tag{4.18}$$

Proof. Let $\kappa = p-k$. Summing (4.16) over the elements, we have

$$\begin{aligned} &|f-\pi_{p,k}f|^2_{H^r(0,1)} \\ &\quad \le \sum_{i=1}^{N-1}\left(\frac{h_i}{2}\right)^{2(\sigma+k+1-r)}\frac{(\kappa-\sigma)!}{(\kappa+\sigma)!}\frac{(\kappa-(k+1-r))!}{(\kappa+(k+1-r))!}|f^{(k+1)}|^2_{H^\sigma(I_i)}. \end{aligned} \tag{4.19}$$

Now, take $\sigma = s-k-1$:

$$\begin{aligned} &|f-\pi_{p,k}f|^2_{H^r(0,1)} \\ &\quad \le \sum_{i=1}^{N-1}\left(\frac{h_i}{2}\right)^{2(s-r)}\frac{(\kappa-(s-k-1))!}{(\kappa+(s-k-1))!}\frac{(\kappa-(k+1-r))!}{(\kappa+(k+1-r))!}|f^{(k+1)}|^2_{H^{s-k-1}(I_i)}. \end{aligned}$$

Taking into account the definition of h and the well-known Stirling formula, there exists a positive constant C such that

$$\begin{aligned} &|f-\pi_{p,k}f|^2_{H^r(0,1)} \\ &\quad \le C\left(\frac{h}{2}\right)^{2(s-r)}\left(\frac{\mathrm{e}}{2}\right)^{2(s-k-1)}\kappa^{-2(s-k-1)}\left(\frac{\mathrm{e}}{2}\right)^{2(k+1-r)}\kappa^{-2(k+1-r)}|f|^2_{H^s(0,1)} \\ &\quad \le Ch^{2(s-r)}\left(\frac{\mathrm{e}}{4}\right)^{2(s-r)}\kappa^{-2(s-r)}|f|^2_{H^s(0,1)}, \end{aligned}$$

so that (4.17) follows from the definition of κ and the fact that $\mathrm{e}/4 \le 1$.

Further, if $p=2k+1$, then $\kappa = k+1 = (p+1)/2$ and a direct substitution in (4.17) yields (4.18). □

Remark 4.9. Let us assume that the partition $Z = \{\zeta_1,\dots,\zeta_N\}$ is a quasi-uniform mesh on $(0,1)$. It is easy to see that the dimension of $S_p(\Xi)$ is

$$n = (N-1)(p+1) - (k+1)(N-2) = (N-1)(p-k) + k + 1,$$

then $(p-k)/h \sim n-k-1$ and the estimate (4.17) can therefore be rewritten in terms of n:

$$|f-\pi_{p,k}f|_{H^r(0,1)} \le C(n-k-1)^{-(s-r)}|f|_{H^s(0,1)}.$$

In particular, for $r=0$ we have

$$\|f-\pi_{p,k}f\|_{L^2(0,1)} \le C(n-k-1)^{-s}|f|_{H^s(0,1)}.$$

The previous estimate shows that splines of reduced regularity enjoy the same approximation properties as standard continuous finite elements. The exploratory study in Evans *et al.* (2009) seems to show that this result is indeed sub-optimal.

4.2. Multivariate approximation estimates in the parametric domain

We now address the multi-dimensional tensor product case for B-splines in the parametric domain, following the notation of the previous sections. The multivariate analysis takes the steps from the one-dimensional estimates of the previous two sections, extended to the multi-dimensional case by a tensor product argument. Since the argument in the case of the h- and p-analysis is similar, we focus on the h-error bounds and address the p-analysis in brief.

4.2.1. Tensor product bent Sobolev spaces

In more dimensions, the tensor product bent Sobolev spaces are defined as follows. Let $\mathbf{s} = (s_1, s_2, \dots, s_d)$ in $\mathbb{N}^d$. By a tensor product construction starting from (4.1), we define the tensor product bent Sobolev spaces in the parametric domain $\widehat{\Omega} := (0,1)^d$,

$$\mathcal{H}^{\mathbf{s}}(\widehat{\Omega}) := \mathcal{H}^{s_1}(0,1) \otimes \mathcal{H}^{s_2}(0,1) \otimes \cdots \otimes \mathcal{H}^{s_d}(0,1),$$

iteratively as follows. For all $j = 2, \dots, d$,

$$\begin{aligned} \mathcal{H}^{(s_1,\dots,s_j)}((0,1)^j) &:= \mathcal{H}^{(s_1,\dots,s_{j-1})}((0,1)^{j-1}) \otimes \mathcal{H}^{s_j}(0,1) \\ &\equiv \mathcal{H}^{(s_1,\dots,s_{j-1})}((0,1)^{j-1}; \mathcal{H}^{s_j}(0,1)). \end{aligned}$$

We endow the above spaces with the norm and seminorms

$$\begin{aligned} \|f\|^2_{\mathcal{H}^{\mathbf{s}}(\widehat{\Omega})} &= \sum_{r_1=0}^{s_1} \cdots \sum_{r_d=0}^{s_d} |f|^2_{\mathcal{H}^{(r_1,\dots,r_d)}(\widehat{\Omega})}, \\ |f|^2_{\mathcal{H}^{(r_1,\dots,r_d)}(\widehat{\Omega})} &= \sum_{Q \in \widehat{\mathcal{M}}} |f|^2_{\mathcal{H}^{(r_1,\dots,r_d)}(Q)}, \end{aligned} \tag{4.20}$$

where for the elements $Q \in \widehat{\mathcal{M}}$ we have used the local seminorm

$$|f|_{\mathcal{H}^{(r_1,\dots,r_d)}(Q)} = \left\| \frac{\partial^{r_1} \cdots \partial^{r_d} f}{\partial \zeta_1^{r_1} \cdots \partial \zeta_d^{r_d}} \right\|_{L^2(Q)}.$$

The above definition clearly extends immediately to the case of any hyper-rectangle $E \subset \widehat{\Omega}$ that is a union of elements in $\widehat{\mathcal{M}}$.

We finally note that these bent Sobolev spaces are related but not equal to those introduced in Bazilevs *et al.* (2006), but they will provide the desired estimates on the physical domain, as is explained in Section 4.3.

4.2.2. Approximation estimates in h

For simplicity of exposition, we restrict the detailed analysis to the two-dimensional case and present the general dimensional case without proof at the end of the section. As in the one-dimensional case, we introduce the following local quasi-uniformity assumption.

Assumption 4.10. Assumption 2.1 holds for each univariate partition $Z_j = \{\zeta_{j,1}, \dots, \zeta_{j,N_j}\}$.

Let $\Pi_{p_i,\Xi_i} : L^2(I) \to S_{p_i}(\Xi_i)$, for $i = 1, 2$, indicate the univariate quasi-interpolant associated to the knot vector Ξ_i and polynomial degree p_i introduced in Section 2.1.5. Moreover, let $\Pi_{\mathbf{p},\boldsymbol{\Xi}} = \Pi_{p_1,\Xi_1} \otimes \Pi_{p_2,\Xi_2}$ from $L^2(\Omega)$ to $S_{\mathbf{p}}(\boldsymbol{\Xi})$ denote the tensor product quasi-interpolant built using the Π_{p_i,Ξ_i} above according to the construction in (2.45) for $d = 2$.

Given any sufficiently regular function $f : \widehat{\Omega} \to \mathbb{R}$, we will indicate the partial derivative operators with the symbol

$$\widehat{D}^{\mathbf{r}} f = \frac{\partial^{r_1}\partial^{r_2} f}{\partial\zeta_1^{r_1}\partial\zeta_2^{r_2}} \quad \mathbf{r} = (r_1, r_2) \in \mathbb{N}^2. \tag{4.21}$$

Let $E \subset \widehat{\Omega}$ be any union of elements $Q \in \widehat{\mathcal{M}}$ of the spline mesh. Then, in the following we will adopt the notation

$$\|f\|^2_{L^2_h(E)} := \sum_{\substack{Q\in\widehat{\mathcal{M}}\\ Q\subset E}} \|f\|^2_{L^2(Q)},$$

which will be useful for distributions f which are not in $L^2(E)$.

Finally, the element size of a generic element $Q_{\mathbf{i}} = I_{1,i_1} \times \cdots \times I_{d,i_d} \in \widehat{\mathcal{M}}$ (see Section 2.2.1) will be denoted by $h_{Q_{\mathbf{i}}} = \operatorname{diam}(Q_{\mathbf{i}})$. Moreover, we will indicate the length of the edges of $Q_{\mathbf{i}}$ by $h_{1,i_1}, h_{2,i_2}, \dots, h_{d,i_d}$, and the length of the edges of its extended patch $\widetilde{Q}_{\mathbf{i}}$ by $\widetilde{h}_{1,i_1}, \widetilde{h}_{2,i_2}, \dots, \widetilde{h}_{d,i_d}$.

We are now able to show the following result.

Proposition 4.11. Let Assumption 4.10 hold. Let the integers $0 \le r_1 \le s_1 \le p_1 + 1$ and $0 \le r_2 \le s_2 \le p_2 + 1$. Then, there exists a constant C depending only on $\mathbf{p}, \theta$ such that for all elements $Q_{\mathbf{i}} \in \widehat{\mathcal{M}}$, we have

$$\begin{aligned}&\|\widehat{D}^{(r_1,r_2)}(f - \Pi_{\mathbf{p},\boldsymbol{\Xi}} f)\|_{L^2(Q_{\mathbf{i}})}\\ &\qquad \le C\big((\widetilde{h}_{1,i_1})^{s_1-r_1}\|\widehat{D}^{(s_1,r_2)} f\|_{L^2_h(\widetilde{Q}_{\mathbf{i}})} + (\widetilde{h}_{2,i_2})^{s_2-r_2}\|\widehat{D}^{(r_1,s_2)} f\|_{L^2_h(\widetilde{Q}_{\mathbf{i}})}\big)\end{aligned}$$

for all f in $\mathcal{H}^{(s_1,r_2)}(\widehat{\Omega}) \cap \mathcal{H}^{(r_1,s_2)}(\widehat{\Omega})$. When $(r_1, r_2) = (0, 0)$, Assumption 4.10 is not needed and C depends only on $\mathbf{p}$.

Proof. Let f be as above and let $Q_{\mathbf{i}} = I_{1,i_1} \times I_{2,i_2}$ be any element of the mesh. From the definition of $\Pi_{\mathbf{p},\boldsymbol{\Xi}}$ as in (2.45), and the triangle inequality,

it immediately follows that

$$\|\widehat{D}^{(r_1,r_2)}(f-\Pi_{\mathbf{p},\boldsymbol{\Xi}}f)\|_{L^2(Q_{\mathbf{i}})} \le T_1+T_2, \tag{4.22}$$

with the terms

$$T_1=\|\widehat{D}^{(r_1,r_2)}(f-\Pi_{p_1,\Xi_1}f)\|_{L^2(Q_{\mathbf{i}})},\quad T_2=\|\widehat{D}^{(r_1,r_2)}(\Pi_{p_1,\Xi_1}f-\Pi_{\mathbf{p},\boldsymbol{\Xi}}f)\|_{L^2(Q_{\mathbf{i}})}.$$

It is easy to check that the derivative with respect to ζ_2 and the operator Π_{p_1,Ξ_1} commute. Then we have

$$\widehat{D}^{(r_1,r_2)}\Pi_{p_1,\Xi_1}=\widehat{D}^{(r_1,0)}\Pi_{p_1,\Xi_1}\widehat{D}^{(0,r_2)}.$$

Setting $w=\widehat{D}^{(0,r_2)}f$ and using Proposition 4.3, we get

$$\begin{aligned}(T_1)^2&=\|\widehat{D}^{(r_1,0)}(w-\Pi_{p_1,\Xi_1}w)\|^2_{L^2(Q_{\mathbf{i}})}\\&=\int_{I_{2,i_2}}\int_{I_{1,i_1}}\big(\widehat{D}^{(r_1,0)}(w-\Pi_{p_1,\Xi_1}w)\big)^2\,\mathrm{d}\zeta_1\,\mathrm{d}\zeta_2\\&=\int_{I_{2,i_2}}|w-\Pi_{p_1,\Xi_1}w|^2_{H^{r_1}(I_{1,i_1})}\,\mathrm{d}\zeta_2\\&\le C(\widetilde{h}_{1,i_1})^{2(s_1-r_1)}\int_{I_{2,i_2}}|w|^2_{\mathcal{H}^{s_1}(\widetilde{I}_{1,i_1})}\,\mathrm{d}\zeta_2\\&\le C(\widetilde{h}_{1,i_1})^{2(s_1-r_1)}\|\widehat{D}^{(s_1,r_2)}f\|^2_{L^2_h(\widetilde{Q}_{\mathbf{i}})}.\end{aligned} \tag{4.23}$$

Now let $v=\widehat{D}^{(r_1,0)}f$. Again using the property

$$\widehat{D}^{(r_1,r_2)}\Pi_{p_1,\Xi_1}=\widehat{D}^{(r_1,0)}\Pi_{p_1,\Xi_1}\widehat{D}^{(0,r_2)},$$

the similar property

$$\widehat{D}^{(r_1,r_2)}\Pi_{p_2,\Xi_2}=\widehat{D}^{(0,r_2)}\Pi_{p_2,\Xi_2}\widehat{D}^{(r_1,0)}$$

and recalling Remark 4.5, we obtain

$$\begin{aligned}(T_2)^2&=\|\widehat{D}^{(r_1,0)}\Pi_{p_1,\Xi_1}\widehat{D}^{(0,r_2)}(f-\Pi_{p_2,\Xi_2}f)\|^2_{L^2(Q_{\mathbf{i}})}\\&=\int_{I_{2,i_2}}|\Pi_{p_1,\Xi_1}\widehat{D}^{(0,r_2)}(f-\Pi_{p_2,\Xi_2}f)|^2_{H^{r_1}(I_{1,i_1})}\,\mathrm{d}\zeta_2\\&\le C\int_{I_{2,i_2}}|\widehat{D}^{(0,r_2)}(f-\Pi_{p_2,\Xi_2}f)|^2_{\mathcal{H}^{r_1}(\widetilde{I}_{1,i_1})}\,\mathrm{d}\zeta_2\\&=C\|\widehat{D}^{(r_1,r_2)}(f-\Pi_{p_2,\Xi_2}f)\|^2_{L^2_h(\widetilde{I}_{1,i_1}\times I_{2,i_2})}\\&=C\|\widehat{D}^{(0,r_2)}(v-\Pi_{p_2,\Xi_2}v)\|^2_{L^2_h(\widetilde{I}_{1,i_1}\times I_{2,i_2})}.\end{aligned} \tag{4.24}$$

The last term in (4.24) is bounded as for (4.23), simply exchanging the role of ζ_1 and ζ_2. We obtain

$$(T_2)^2\le C(\widetilde{h}_{2,i_2})^{2(s_2-r_2)}\|\widehat{D}^{(r_1,s_2)}f\|^2_{L^2_h(\widetilde{Q}_{\mathbf{i}})}. \tag{4.25}$$

The result follows by combining (4.22) with (4.23) and (4.25). □

The case of three or higher dimensions follows obviously with the same arguments used above. We have the following result in general dimension d, where $\Pi_{\mathbf{p},\boldsymbol{\Xi}}$ is now the quasi-interpolant built following the tensor product construction (2.45) and using the one-dimensional operators Π_{p_i,Ξ_i}, $i = 1, 2, \ldots, d$.

Proposition 4.12. Let Assumption 4.10 hold. Let the integers $0 \leq r_\ell \leq s_\ell \leq p_\ell + 1$ for all $\ell = 1, \ldots, d$. Then, there exists a constant C depending only on $\mathbf{p}, \theta$ such that, for all elements $Q_{\mathbf{i}} \in \widehat{\mathcal{M}}$, we obtain

$$\|\widehat{D}^{(r_1,\ldots,r_d)}(f - \Pi_{\mathbf{p},\boldsymbol{\Xi}} f)\|_{L^2(Q_{\mathbf{i}})} \leq C\Bigg(\sum_{\ell=1,\ldots,d} (\widetilde{h}_{\ell,i_\ell})^{s_\ell - r_\ell} \|\widehat{D}^{(r_1,\ldots,r_{\ell-1},s_\ell,r_{\ell+1},\ldots,r_d)} f\|_{L^2_{\widetilde{h}}(\widetilde{Q}_{\mathbf{i}})}\Bigg)$$

for all f in $\mathcal{H}^{(s_1,r_2,\ldots,r_d)}(\widehat{\Omega}) \cap \mathcal{H}^{(r_1,s_2,r_3,\ldots,r_d)}(\widehat{\Omega}) \cap \ldots \cap \mathcal{H}^{(r_1,\ldots,r_{d-1},s_d)}(\widehat{\Omega})$. When $r_\ell = 0$ for all $\ell = 1, \ldots, d$, Assumption 4.10 is not needed and C depends only on $\mathbf{p}$.

Remark 4.13. Due to Remark 4.6, it is immediate to extend the results of this section to spaces with boundary conditions on the whole $\partial\widehat{\Omega}$ or on some faces of $\widehat{\Omega}$.

4.2.3. Approximation estimates in p

As in the univariate case, for the p estimates we limit ourselves to showing the main results without proofs, which can be found in Beirão da Veiga *et al.* (2011). We focus attention on the two-dimensional case, while a note on the three-dimensional case can be found at the end of the section. Now let $\Pi_{\mathbf{p},\mathbf{k}}$ represent the multivariate interpolation operator built following construction (2.45) for $d = 2$, starting from the one-dimensional operators π_{p_i,k_i} in (2.32), each associated to the degree p_i and knot vector Ξ_i, $i = 1, 2$.

We assume for simplicity that all the internal knots in the knot vectors Ξ_i have the same multiplicity m_i, $i = 1, 2$, so that the integer $k_i = p_i - m_i$ represents the regularity index for the ith coordinate. Moreover, we assume $p_1 = p_2 = p$; we refer to Beirão da Veiga *et al.* (2011) for more general forms of the estimates below. We finally recall the condition $p \geq 2k_i + 1$ for $i = 1, 2$, which is needed in order for the operator $\Pi_{\mathbf{p},\mathbf{k}}$ to be well defined.

As usual, let $Q_{\mathbf{i}} = I_{1,i_1} \times I_{2,i_2}$ denote a generic element in $\widehat{\mathcal{M}}$ with diameter $h_{Q_{\mathbf{i}}}$. We then have the following approximation result.

Proposition 4.14. Let $\Pi_{\mathbf{p},\mathbf{k}}$ be the projection operator described above, and let k_1, k_2 and s be such that $k_1 + k_2 + 2 \leq s \leq p + 1$. Then there exists a positive constant C, independent of s, p, k_1 and k_2, such that for

all $f \in H^s(\widehat{\Omega})$ and for all $r_1 = 0, \dots, k_1 + 1$, and $r_2 = 0, \dots, k_2 + 1$,

$$\left\| \widehat{D}^{(r_1,r_2)}(f - \Pi_{\mathbf{p},\mathbf{k}} f) \right\|_{L^2(Q_{\mathbf{i}})} \leq C(p - k^*)^{-(s-(r_1+r_2))} h_{Q_{\mathbf{i}}}^{(s-(r_1+r_2))} |f|_{H^s(Q_{\mathbf{i}})}, \tag{4.26}$$

for all elements $Q_{\mathbf{i}} \in \widehat{\mathcal{M}}$ and where $k^* = \max\{k_1, k_2\}$.

We also have the following corollary.

Corollary 4.15. Under the same hypotheses and notation as Proposition 4.14, for all integers $0 \leq r \leq k_* := \min\{k_1, k_2\} + 1$, we have

$$|f - \Pi_{\mathbf{p},\mathbf{k}} f|^2_{H^r(Q_{\mathbf{i}})} \leq C(p - k^*)^{-2(s-r)} h_{Q_{\mathbf{i}}}^{2(s-r)} |f|^2_{H^s(Q_{\mathbf{i}})}. \tag{4.27}$$

We close the section by noting that extending these k, p approximation results to the three-dimensional case is not straightforward unless we accept more severe requirements on the discrete parameters k, p and on the target function regularity. In particular, following the above steps would give in Proposition 4.14 the condition $k_1 + k_2 + k_3 + 3 \leq s \leq p + 1$, where k_i, $i = 1, 2, 3$, represents as usual the continuity constant for the ith variable. Considering, for instance, the case $k_1 = k_2 = k_3 = k$, this would enforce the relation $p \geq 3k + 2$, which is definitely more severe than that required to define the interpolation operator ($p \geq 2k + 1$).

4.3. NURBS approximation estimates in the physical domain

Here we finally present error estimates for the mapped NURBS spaces introduced in (3.2), by taking the steps from the B-spline approximation results in the parametric domain of the previous section. Again we focus mainly on the h-estimates in order to show the idea of the argument. Indeed, although there are different technical aspects, the general path to obtaining approximation estimates in the physical domain, starting from estimates in the parametric domain, is similar for the h and p cases. Both estimates are based on the projector $\Pi_{V_h} : \mathcal{V}(\Omega) \to V_h$, which we introduced in (3.5), but the regularity required in each case is different, and depends on the choice of the univariate projectors, as we show precisely in the following.

Throughout the present section we will require that the mapping $\mathbf{F}$ satisfies Assumption 3.1.

4.3.1. Approximation estimates in h

From the spline projector in the parametric domain $\Pi_{\mathbf{p},\boldsymbol{\Xi}}$, introduced in Section 4.2.2, we can define the projector Π_{V_h} in (3.5) giving precisely its domain of definition $\mathcal{V}(\Omega)$. Indeed, we define $\Pi_{V_h} : L^2(\Omega) \to V_h$,

$$\Pi_{V_h} f = \frac{\Pi_{\mathbf{p},\boldsymbol{\Xi}}(W(f \circ \mathbf{F}))}{W} \circ \mathbf{F}^{-1} \quad f \in L^2(\Omega).$$

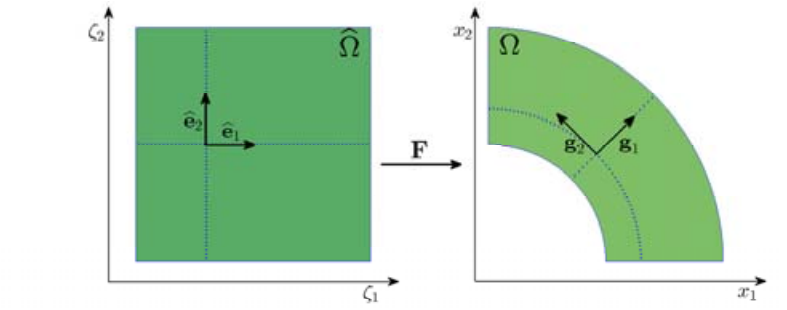

Figure 4.1. Definition of the **F**-coordinate system in the physical domain.

Before proving the approximation estimates for the projector, we need to introduce some notation and intermediate results. As usual, for simplicity of exposition we will show the details and proofs for the bivariate case and present the multi-dimensional case briefly at the end of the section, the proofs for $d > 2$ being a simple extension of the $d = 2$ argument.

In the physical domain $\Omega = \mathbf{F}(\widehat{\Omega})$, as well as the Cartesian coordinates x_1 and x_2, we also introduce the coordinate system naturally induced by the geometrical map $\mathbf{F}$, referred to as the **F**-coordinate system, which associates to a point $\mathbf{x} \in \Omega$ the Cartesian coordinates in $\widehat{\Omega}$ of its counter-image $\mathbf{F}^{-1}(\mathbf{x})$. At each $\mathbf{x} \in K \in \mathcal{M}_0$ (more generally, at each $\mathbf{x}$ where $\mathbf{F}$ is differentiable) the tangent *base vectors* $\mathbf{g}_1$ and $\mathbf{g}_2$ of the **F**-coordinate system can be defined by

$$\mathbf{g}_i = \mathbf{g}_i(\mathbf{x}) = \frac{\partial \mathbf{F}}{\partial \zeta_i}(\mathbf{F}^{-1}(\mathbf{x})), \quad i = 1, 2. \tag{4.28}$$

These are the images of the canonical base vectors $\widehat{\mathbf{e}}_i$ in $\widehat{\Omega}$, and represent the axis directions of the **F**-coordinate system (see Figure 4.1).

In analogy to the derivatives in the parametric domain (4.21), the derivatives of $f : \Omega \to \mathbb{R}$ in Cartesian coordinates are denoted by

$$D^{\mathbf{r}} f = \frac{\partial^{r_1} \partial^{r_2} f}{\partial x_1^{r_1} \partial x_2^{r_2}} \quad \mathbf{r} = (r_1, r_2) \in \mathbb{N}^2.$$

We also consider the derivatives of $f : \Omega \to \mathbb{R}$ with respect to the **F**-coordinates. These are just the directional derivatives. For first order we have

$$\frac{\partial f}{\partial \mathbf{g}_i}(\mathbf{x}) = \nabla f(\mathbf{x}) \cdot \mathbf{g}_i(\mathbf{x}) = \lim_{t \to 0} \frac{f(\mathbf{x} + t\mathbf{g}_i(\mathbf{x})) - f(\mathbf{x})}{t}, \tag{4.29}$$

which is well defined for any $\mathbf{x}$ in the (open) elements of the coarse triangulation $\mathcal{M}_0$, as already noted. Higher-order derivatives are defined similarly:

$$\frac{\partial^{r_i} f}{\partial \mathbf{g}_i^{r_i}} = \frac{\partial}{\partial \mathbf{g}_i}\left(\frac{\partial^{r_i - 1} f}{\partial \mathbf{g}_i^{r_i - 1}}\right) = \left(\frac{\partial}{\partial \mathbf{g}_i}\left(\cdots\left(\frac{\partial}{\partial \mathbf{g}_i}\left(\frac{\partial f}{\partial \mathbf{g}_i}\right)\right)\right)\right).$$

More generally, we adopt the notation

$$D_{\mathbf{F}}^{\mathbf{r}} f = \frac{\partial^{r_1}}{\partial \mathbf{g}_1^{r_1}} \frac{\partial^{r_2} f}{\partial \mathbf{g}_2^{r_2}} \quad \mathbf{r} = (r_1, r_2) \in \mathbb{N}^2. \tag{4.30}$$

Derivatives with respect to the $\mathbf{F}$-coordinates are directly related to derivatives in the parametric domain, as stated in the following proposition.

Proposition 4.16. Let $f : \Omega \to \mathbb{R}$. For all $K \in \mathcal{M}$, $\mathbf{r} \in \mathbb{N}^2$, we have

$$D_{\mathbf{F}}^{\mathbf{r}} f = \big(\widehat{D}^{\mathbf{r}}(f \circ \mathbf{F})\big) \circ \mathbf{F}^{-1}. \tag{4.31}$$

Proof. From the chain rule and (4.28),

$$\frac{\partial (f \circ \mathbf{F})}{\partial \zeta_i} = (\nabla f) \circ \mathbf{F} \cdot \frac{\partial \mathbf{F}}{\partial \zeta_i} = (\nabla f \cdot \mathbf{g}_i) \circ \mathbf{F}.$$

Recalling (4.29)–(4.30), the above identity yields

$$\begin{aligned} \widehat{D}^{(1,0)}(f \circ \mathbf{F}) &= \big(D_{\mathbf{F}}^{(1,0)} f\big) \circ \mathbf{F}, \\ \widehat{D}^{(0,1)}(f \circ \mathbf{F}) &= \big(D_{\mathbf{F}}^{(0,1)} f\big) \circ \mathbf{F}, \end{aligned}$$

which is (4.31) for $\mathbf{r} = (1, 0)$ and $\mathbf{r} = (0, 1)$.

The general case is shown by induction. Assuming (4.31) holds for order (r_1, r_2), it is easy to get it for order (r_1+1, r_2) and (r_1, r_2+1). For example,

$$\begin{aligned} D_{\mathbf{F}}^{(r_1+1,r_2)} f &= D_{\mathbf{F}}^{(r_1,r_2)} \big(D_{\mathbf{F}}^{(1,0)} f\big) \\ &= D_{\mathbf{F}}^{(r_1,r_2)} \big(\big(\widehat{D}^{(1,0)}(f \circ \mathbf{F})\big) \circ \mathbf{F}^{-1}\big) \\ &= \big(\widehat{D}^{(r_1,r_2)} \big(\widehat{D}^{(1,0)}(f \circ \mathbf{F})\big)\big) \circ \mathbf{F}^{-1} \\ &= \big(\widehat{D}^{(r_1+1,r_2)}(f \circ \mathbf{F})\big) \circ \mathbf{F}^{-1}. \end{aligned}$$

□

Let E be a union of elements $K \in \mathcal{M}$. We introduce the norms and seminorms

$$\begin{aligned} \|f\|^2_{\mathcal{H}_{\mathbf{F}}^{(s_1,s_2)}(E)} &= \sum_{r_1=0}^{s_1} \sum_{r_2=0}^{s_2} |f|^2_{\mathcal{H}_{\mathbf{F}}^{(r_1,r_2)}(E)}, \\ |f|^2_{\mathcal{H}_{\mathbf{F}}^{(s_1,s_2)}(E)} &= \sum_{\substack{K \in \mathcal{M} \\ K \subset E}} |f|^2_{H_{\mathbf{F}}^{(s_1,s_2)}(K)}, \end{aligned} \tag{4.32}$$

where

$$|f|_{H_{\mathbf{F}}^{(s_1,s_2)}(K)} = \big\| D_{\mathbf{F}}^{(s_1,s_2)} f \big\|_{L^2(K)}.$$

We also introduce the space

$$H_{\mathbf{F}}^{(s_1,s_2)}(\Omega) = \text{closure of } C^\infty(\Omega) \text{ with respect to the norm } \|\cdot\|_{\mathcal{H}_{\mathbf{F}}^{(s_1,s_2)}(\Omega)},$$

endowed with the norm

$$\|\cdot\|_{H_{\mathbf{F}}^{(s_1,s_2)}(\Omega)} = \|\cdot\|_{\mathcal{H}_{\mathbf{F}}^{(s_1,s_2)}(\Omega)}.$$

Note that the space $H_{\mathbf{F}}^{(s_1,s_2)}(\Omega)$ is a kind of tensor product Sobolev space with respect to the physical coordinates. For instance, we have

$$H^{s_1+s_2}(\Omega) \subseteq H_{\mathbf{F}}^{(s_1,s_2)}(\Omega) \subseteq H^{\min(s_1,s_2)}(\Omega),$$

where as usual $H^t(\Omega)$ represents, for $t \in \mathbb{N}$, the standard Sobolev space of order t on Ω.

We then have the following proposition, which is a consequence of Assumption 3.1 and the inter-element continuity of the parametrization $\mathbf{F}$. The simple proof can be found in Beirão da Veiga *et al.* (2012*c*).

Proposition 4.17. Let $f : \Omega \to \mathbb{R}$ and $\mathbf{s} \in \mathbb{N}^2$. If $f \in H_{\mathbf{F}}^{(s_1,s_2)}(\Omega)$, then its pull-back $\widehat{f} = f \circ \mathbf{F}$ is in the bent Sobolev space $\mathcal{H}^{(s_1,s_2)}(\widehat{\Omega})$. Moreover, there exists a positive constant $C = C(\mathbf{F})$ such that, for all $K = \mathbf{F}(Q) \in \mathcal{M}$, $\mathbf{s} \in \mathbb{N}^2$, we have

$$C^{-1}\|f\|_{H_{\mathbf{F}}^{(s_1,s_2)}(K)} \leq \|\widehat{f}\|_{H^{(s_1,s_2)}(Q)} \leq C\|f\|_{H_{\mathbf{F}}^{(s_1,s_2)}(K)}. \tag{4.33}$$

The following theorem from Beirão da Veiga *et al.* (2012*c*) states the main estimate for the approximation error of $\Pi_{V_h} f$ and, making use of derivatives in the $\mathbf{F}$-coordinate system, it is suitable for anisotropic meshes. We recall that, for a generic element $K_{\mathbf{i}} = \mathbf{F}(Q_{\mathbf{i}}) \in \mathcal{M}$, the notation $\widetilde{K}_{\mathbf{i}} = \mathbf{F}(\widetilde{Q}_{\mathbf{i}})$ indicates its support extension. Moreover, $\widetilde{h}_{1,i_1}$ and $\widetilde{h}_{2,i_2}$ indicate the edge lengths of $\widetilde{Q}_{\mathbf{i}}$, as in Proposition 4.11.

Theorem 4.18. Let Assumption 4.10 hold. Let the integers r_i, s_i be such that $0 \leq r_i \leq s_i \leq p_i+1$, $i = 1, 2$. Then, there exists a constant C depending only on $\mathbf{p}, \theta, \mathbf{F}, W$ such that, for all elements $K_{\mathbf{i}} = \mathbf{F}(Q_{\mathbf{i}}) \in \mathcal{M}$,

$$\begin{aligned} &|f - \Pi_{V_h} f|_{\mathcal{H}_{\mathbf{F}}^{(r_1,r_2)}(K_{\mathbf{i}})} \\ &\quad \leq C\big((\widetilde{h}_{1,i_1})^{s_1-r_1}\|f\|_{\mathcal{H}_{\mathbf{F}}^{(s_1,r_2)}(\widetilde{K}_{\mathbf{i}})} + (\widetilde{h}_{2,i_2})^{s_2-r_2}\|f\|_{\mathcal{H}_{\mathbf{F}}^{(r_1,s_2)}(\widetilde{K}_{\mathbf{i}})}\big), \end{aligned} \tag{4.34}$$

for all f in $H_{\mathbf{F}}^{(s_1,r_2)}(\Omega) \cap H_{\mathbf{F}}^{(r_1,s_2)}(\Omega)$. When $(r_1, r_2) = (0, 0)$, Assumption 4.10 is not needed.

Proof. The argument is similar to that in Bazilevs *et al.* (2006). We first use (4.31) and perform a change of variable:

$$\begin{aligned} &\big\|D_{\mathbf{F}}^{(r_1,r_2)}(f - \Pi_{V_h} f)\big\|_{L^2(K_{\mathbf{i}})} \\ &\qquad \leq C\big\|\widehat{D}^{(r_1,r_2)}\big(f \circ \mathbf{F} - (\Pi_{V_h} f) \circ \mathbf{F}\big)\big\|_{L^2(Q_{\mathbf{i}})} \\ &\qquad = C\left\|\widehat{D}^{(r_1,r_2)}\left(\frac{W\,(f \circ \mathbf{F}) - \Pi_{\mathbf{p},\boldsymbol{\Xi}}(W(f \circ \mathbf{F}))}{W}\right)\right\|_{L^2(Q_{\mathbf{i}})}, \end{aligned} \tag{4.35}$$

where $K_{\mathbf{i}} = \mathbf{F}(Q_{\mathbf{i}})$, and the constant C takes into account the factor $\det(\nabla \mathbf{F})$

in the change of variable. We now note that, due to the regularity of f and using Proposition 4.17, it follows that

$$W\,(f\circ\mathbf{F})\in\mathcal{H}^{(s_1,r_2)}(\widehat{\Omega})\cap\mathcal{H}^{(r_1,s_2)}(\widehat{\Omega}).$$

Then we use the Leibniz formula

$$\left\|\widehat{D}^{(r_1,r_2)}\left(\frac{\phi}{W}\right)\right\|^2_{L^2(Q_{\mathbf{i}})}\leq C\sum_{q_i=0,\dots,r_i}\|\widehat{D}^{(q_1,q_2)}\phi\|^2_{L^2(Q_{\mathbf{i}})},$$

where C depends on the derivatives (inside the elements) of W^{-1}, and then we use Proposition 4.11, yielding

$$\begin{aligned}
&\left\|\widehat{D}^{(r_1,r_2)}\left(\frac{W\,(f\circ\mathbf{F})-\Pi_{\mathbf{p},\boldsymbol{\Xi}}(W\,(f\circ\mathbf{F}))}{W}\right)\right\|^2_{L^2(Q_{\mathbf{i}})} \qquad (4.36)\\
&\quad\leq C\sum_{q_i=0,\dots,r_i}\|\widehat{D}^{(q_1,q_2)}\big(W\,(f\circ\mathbf{F})-\Pi_{\mathbf{p},\boldsymbol{\Xi}}(W\,(f\circ\mathbf{F}))\big)\|^2_{L^2(Q_{\mathbf{i}})}\\
&\quad\leq C(\widetilde{h}_{1,i_1})^{2(s_1-r_1)}\sum_{q_2=0,\dots,r_2}\|\widehat{D}^{(s_1,q_2)}\big(W\,(f\circ\mathbf{F})\big)\|^2_{L^2_h(\widetilde{Q}_{\mathbf{i}})}\\
&\qquad+C(\widetilde{h}_{2,i_2})^{2(s_2-r_2)}\sum_{q_1=0,\dots,r_1}\|\widehat{D}^{(q_1,s_2)}\big(W\,(f\circ\mathbf{F})\big)\|^2_{L^2_h(\widetilde{Q}_{\mathbf{i}})}.
\end{aligned}$$

The last step is to use the Leibniz formula again (now with C depending on the derivatives of W), identity (4.31) and the change of variable again. We obtain

$$\begin{aligned}
&\sum_{q_2=0,\dots,r_2}\|\widehat{D}^{(s_1,q_2)}\big(W\,(f\circ\mathbf{F})\big)\|^2_{L^2_h(\widetilde{Q}_{\mathbf{i}})} \qquad (4.37)\\
&\qquad\leq C\sum_{q_1=0,\dots,s_1}\sum_{q_2=0,\dots,r_2}\|\widehat{D}^{(q_1,q_2)}\big(f\circ\mathbf{F}\big)\|^2_{L^2_h(\widetilde{Q}_{\mathbf{i}})}\\
&\qquad\leq C\sum_{q_1=0,\dots,s_1}\sum_{q_2=0,\dots,r_2}\|D^{(q_1,q_2)}_{\mathbf{F}}f\|^2_{L^2_h(\widetilde{K}_{\mathbf{i}})},
\end{aligned}$$

and

$$\begin{aligned}
&\sum_{q_1=0,\dots,r_1}\|\widehat{D}^{(q_1,s_2)}\big(W\,(f\circ\mathbf{F})\big)\|^2_{L^2_h(\widetilde{Q}_{\mathbf{i}})} \qquad (4.38)\\
&\qquad\leq C\sum_{q_1=0,\dots,r_1}\sum_{q_2=0,\dots,s_2}\|\widehat{D}^{(q_1,q_2)}\big(f\circ\mathbf{F}\big)\|^2_{L^2_h(\widetilde{Q}_{\mathbf{i}})}\\
&\qquad\leq C\sum_{q_1=0,\dots,r_1}\sum_{q_2=0,\dots,s_2}\|D^{(q_1,q_2)}_{\mathbf{F}}f\|^2_{L^2_h(\widetilde{K}_{\mathbf{i}})}.
\end{aligned}$$

Collecting (4.35)–(4.38) together finally yields (4.34). □

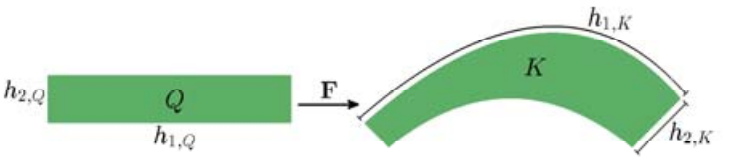

Figure 4.2. Q is mapped by the geometrical map $\mathbf{F}$ to K.

Under Assumption 4.10, it clearly holds that $\widetilde{h}_{\ell,i_\ell} \simeq h_{\ell,i_\ell}$, $\ell = 1, 2$. Therefore, the parametric mesh sizes $\widetilde{h}_{\ell,i_\ell}$ appearing in (4.34) can also be substituted by h_{ℓ,i_ℓ}, $\ell = 1, 2$. Note that, since the mapping $\mathbf{F}$ is fixed at the coarse level of discretization (and thus it is elementwise uniformly regular), and thanks to Assumption 3.1, the lengths h_{ℓ,i_ℓ} are equivalent to the lengths of the corresponding edges of the physical element $K_{\mathbf{i}} = \mathbf{F}(Q_{\mathbf{i}})$, as shown in Figure 4.2.

Remark 4.19. As occurs with standard finite elements, the regularity assumption in Theorem 4.18 can be made weaker. In particular, on mesh lines associated with C^k-regularity of V_h, $k \in \mathbb{N}$, it is sufficient for the target function f and its derivatives up to order k to have merging traces. This observation is based on the fact that in such cases we still have $W(f \circ \mathbf{F}) \in \mathcal{H}^{(s_1,r_2)}(\widehat{\Omega}) \cap \mathcal{H}^{(r_1,s_2)}(\widehat{\Omega})$.

We have the following corollary of Theorem 4.18, which bounds the local approximation error in standard H^r Sobolev norms. We show this result directly in the general case of dimension d.

Corollary 4.20. Let Assumption 4.10 hold. Let the integers r, s_ℓ be such that $0 \le r \le s_\ell \le p_\ell + 1$, $\ell = 1, \dots, d$. Then, there exists a constant C depending only on $\mathbf{p}, \theta, \mathbf{F}, W$ such that, for all elements $K_{\mathbf{i}} = \mathbf{F}(Q_{\mathbf{i}}) \in \mathcal{M}$,

$$\|f - \Pi_{V_h} f\|_{H^r(K_{\mathbf{i}})} \le C \left(\sum_{\ell=1}^{d} (\widetilde{h}_{\ell,i_\ell})^{s_\ell - r} \sum_{j=0,\dots,s_\ell - r} \|D_{\mathbf{F}}^{j\mathbf{e}_\ell} f\|_{H^r(\widetilde{K}_{\mathbf{i}})} \right), \tag{4.39}$$

where $\mathbf{e}_\ell$ are the vectors of the canonical basis of $\mathbb{R}^d$, and the result holds for all $f \in H^r(\Omega)$ such that $D_{\mathbf{F}}^{(s_\ell - r)\mathbf{e}_\ell} f$ are in $H^r(\Omega)$ for $\ell = 1, 2, \dots, d$.

Proof. It is enough to remark that

$$\|f - \Pi_{V_h} f\|_{H^r(K_{\mathbf{i}})} \le C \sum_{\mathbf{r}:\ 0 \le r_1 + \cdots + r_d \le r} \|f - \Pi_{V_h} f\|_{\mathcal{H}^{\mathbf{r}}_{\mathbf{F}}(K_{\mathbf{i}})},$$

and the proof follows by applying Theorem 4.18. □

Finally, it is easy to see that, for r and s as in the corollary below, we have

$$\sum_{j=0,\dots,s-r} \|D_{\mathbf{F}}^{j\mathbf{e}_\ell} f\|_{H^r(\widetilde{K}_{\mathbf{i}})} \leq \|f\|_{H^s(\widetilde{K}_{\mathbf{i}})},$$

and thus the following is true.

Corollary 4.21. Let Assumption 4.10 hold. Let the integers r, s be such that $0 \leq r \leq s \leq \min(p_1, \dots, p_d) + 1$. Then there exists a constant C depending only on $\mathbf{p}, \theta, \mathbf{F}, W$ such that

$$\begin{aligned} \|f - \Pi_{V_h} f\|_{H^r(K_{\mathbf{i}})} &\leq C(h_{\widetilde{K}_{\mathbf{i}}})^{s-r} \|f\|_{H^s(\widetilde{K}_{\mathbf{i}})} \quad \text{for all } K_{\mathbf{i}} \in \mathcal{M}, \\ \|f - \Pi_{V_h} f\|_{H^r(\Omega)} &\leq C h^{s-r} \|f\|_{H^s(\Omega)}, \end{aligned} \tag{4.40}$$

for all f in $H^s(\Omega)$.

Note that the above result is very similar to that in Bazilevs *et al.* (2006, Theorem 3.1), but without the uniformity assumption on the mesh.

Remark 4.22. As already commented in the previous sections, the cases with boundary conditions are handled similarly and are thus not detailed here. We can therefore set homogeneous boundary conditions on $\Gamma_D \subset \partial\Omega$ which is the $\mathbf{F}$-image of a collection of faces of $\widehat{\Omega}$, as in Assumption 3.2, and define a projector $\Pi_{V_{h,\Gamma_D}}$ into the space with boundary conditions (3.4), with the same approximation properties as Π_{V_h}.

4.3.2. Approximation estimates in p

In this section we briefly show the approximation error of the h, k, p-interpolant in the physical domain, and in the case $d = 2$. The simpler one-dimensional case is in fact trivially obtained from the previous results, while treating the $d = 3$ case is not straightforward, for the reason mentioned at the end of Section 4.2.3. We do not show the details of the proofs, which can be found in Beirão da Veiga *et al.* (2011) and which follow similar arguments as for the h-estimates.

Just as for the h-estimates, we now define precisely the projector Π_{V_h} and its domain of definition $\mathcal{V}(\Omega)$ in (3.5). We recall the spline interpolant in parameter space $\Pi_{\mathbf{p},\mathbf{k}}$ described in Section 4.2.3. This interpolant is extended to a NURBS interpolant in physical space $\Pi_{V_h} : H^s(\Omega) \to V_h$, $s \geq k_1 + k_2 + 2$,

$$\Pi_{V_h} f = \frac{\Pi_{\mathbf{p},\mathbf{k}}(W\,(f \circ \mathbf{F}))}{W} \circ \mathbf{F}^{-1} \quad f \in H^s(\Omega).$$

Then, the local estimates for splines in Corollary 4.15 yield the following analogous bounds in physical space. As usual we assume $p_1 = p_2 = p$ and $p \geq 2k_i + 1$, $i = 1, 2$, with the same meaning for the integers k_1, k_2 as in Section 4.2.3.

Theorem 4.23. Let $K_{\mathbf{i}} \in \mathcal{M}$ and $f \in H^s(K_{\mathbf{i}})$ with $k_1+k_2+2 \leq s \leq p+1$ and the non-negative integer $r \leq k_* = \min\{k_1, k_2\} + 1$. Then we have

$$|f - \Pi_{V_h}(f)|_{H^r(K_{\mathbf{i}})} \leq C(p-k^*)^{-(s-r)} h_K^{s-r} \|f\|_{H^s(K_{\mathbf{i}})}, \tag{4.41}$$

where h_K indicates the diameter of $K_{\mathbf{i}}$, and $k^* = \max\{k_1, k_2\}$.

We finally have the following global error estimate (a more general version can be found in Beirão da Veiga *et al.* (2011)).

Theorem 4.24. Let $f \in H^s(\Omega)$ with $k_1 + k_2 + 2 \leq s \leq p+1$ and the non-negative integer $r \leq k_*$. Then we have

$$|f - \Pi_{V_h}(f)|_{H^r(\Omega)} \leq C(p-k^*)^{-(s-r)} h^{s-r} \|f\|_{H^s(\Omega)}, \tag{4.42}$$

where h indicates the maximum diameter of the elements $K_{\mathbf{i}} \in \mathcal{M}$.

4.4. Approximation on multi-patch geometries

Approximation estimates for mapped NURBS on general multi-patch geometries are missing from the isogeometric literature. In the present section we introduce an initial result for the multi-patch interpolant introduced in (3.10), restricting the analysis to the case of isotropic bounds and the L^2-error norm, for simplicity. The main motivation of this section is to show that the previous analysis can be used as a foundation to develop approximation estimates on multi-patch geometries. Deriving sharper and more general error bounds would need a deeper investigation.

As already noted, we consider the multi-patch interpolant introduced in (3.10). This operator is defined by making use of the patchwise projectors $\Pi_{V_h^{(j)}} : C^0(\bar{\Omega}^{(j)}) \to V_h^{(j)}$, which are defined as in (3.5) when considering $\widetilde{\Pi}_{\mathbf{p},\boldsymbol{\Xi}}$ of (2.48). The projection $\widetilde{\Pi}_{\mathbf{p},\boldsymbol{\Xi}}$ is in turn built as a tensor product operator using the one-dimensional projectors $\widetilde{\Pi}_{p_j,\Xi_j}$, $j = 1, 2, \ldots, d$.

A stability estimate for the one-dimensional operators $\widetilde{\Pi}_{p_j,\Xi_j}$ was derived in Proposition 2.3. Using this stability result and following the same steps as in Propositions 4.2 and 4.3, the approximation result below follows easily. We express it directly for a general operator $\widetilde{\Pi}_{p,\Xi}$ on the interval $[0,1]$.

Proposition 4.25. There exists a positive constant C, depending only on p, such that for any non-empty knot span $I_i = (\zeta_i, \zeta_{i+1})$, for all $s \in \mathbb{N}$, $1 \leq s \leq p+1$, and all $f \in \mathcal{H}^s(I)$,

$$\|f - \widetilde{\Pi}_{p,\Xi}(f)\|_{L^2(I_i)} \leq C\,(\widetilde{h}_i)^s\, |f|_{\mathcal{H}^s(\widetilde{I}_i)}, \tag{4.43}$$

where $\widetilde{I}_i$ is the support extension defined in (2.6), and $\widetilde{h}_i$ is its length.

We have the following approximation result in two dimensions (a result for general dimension will be shown later) for the tensor product operator $\widetilde{\Pi}_{\mathbf{p},\boldsymbol{\Xi}}$

in parameter space. The proof can be derived using the same arguments as in Proposition 4.11 combined with (4.43) and Proposition 2.3, as shown below. For simplicity of exposition, we now present the global and isotropic version of the estimate.

Proposition 4.26. Let the polynomial degree $p = p_1 = p_2$ and the integer $2 \le s \le p+1$. Then, there exists a constant C depending only on p such that

$$\|f - \widetilde{\Pi}_{\mathbf{p},\boldsymbol{\Xi}} f\|_{L^2((0,1)^2)} \le C\, h^s \big(\|f\|_{\mathcal{H}^{(s,0)}((0,1)^2)} + \|f\|_{\mathcal{H}^{(0,s)}((0,1)^2)} + \|f\|_{\mathcal{H}^{(s-1,1)}((0,1)^2)} + \|f\|_{\mathcal{H}^{(1,s-1)}((0,1)^2)} \big)$$

for all f sufficiently regular for the right-hand side to make sense.

Proof. Let $Q_{\mathbf{i}} = I_{1,i_1} \times I_{2,i_2}$ be any element of the mesh. From definition (2.48) and the triangle inequality it immediately follows that

$$\|(f - \widetilde{\Pi}_{\mathbf{p},\boldsymbol{\Xi}} f)\|_{L^2(Q_{\mathbf{i}})} \le T_1 + T_2, \tag{4.44}$$

with the terms

$$T_1 = \|f - \widetilde{\Pi}_{p_1,\Xi_1} f\|_{L^2(Q_{\mathbf{i}})}, \quad T_2 = \|\widetilde{\Pi}_{p_1,\Xi_1} f - \widetilde{\Pi}_{\mathbf{p},\boldsymbol{\Xi}} f\|_{L^2(Q_{\mathbf{i}})}.$$

The first term is bounded easily using Proposition 4.25 applied to the operator $\widetilde{\Pi}_{p_1,\Xi_1}$:

$$\begin{aligned}(T_1)^2 &= \int_{I_{2,i_2}} \int_{I_{1,i_1}} (f - \widetilde{\Pi}_{p_1,\Xi_1} f)^2 \,\mathrm{d}\zeta_1 \,\mathrm{d}\zeta_2 = \int_{I_{2,i_2}} |f - \widetilde{\Pi}_{p_1,\Xi_1} f|^2_{L^2(I_{1,i_1})} \,\mathrm{d}\zeta_2 \\ &\le C(\widetilde{h}_{1,i_1})^{2s} \int_{I_{2,i_2}} |f|^2_{\mathcal{H}^s(\widetilde{I}_{1,i_1})} \,\mathrm{d}\zeta_2 \le C(\widetilde{h}_{1,i_1})^{2s} |f|^2_{\mathcal{H}^{(s,0)}(\widetilde{Q}_{\mathbf{i}})}. \end{aligned} \tag{4.45}$$

Now let $w = (f - \widetilde{\Pi}_{p_2,\Xi_2} f)$. Proposition 2.3 and the commuting property $\widehat{D}^{(1,0)} \widetilde{\Pi}_{p_2,\Xi_2} f = \widetilde{\Pi}_{p_2,\Xi_2} \widehat{D}^{(1,0)} f$ yield

$$\begin{aligned}(T_2)^2 &= \|\widetilde{\Pi}_{p_1,\Xi_1}(f - \widetilde{\Pi}_{p_2,\Xi_2} f)\|^2_{L^2(Q_{\mathbf{i}})} = \int_{I_{2,i_2}} \|\widetilde{\Pi}_{p_1,\Xi_1} w\|^2_{L^2(I_{1,i_1})} \,\mathrm{d}\zeta_2 \\ &\le C \int_{I_{2,i_2}} \|w\|^2_{L^2(\widetilde{I}_{1,i_1})} + (\widetilde{h}_{1,i_1})^2 |\widehat{D}^{(1,0)} w|^2_{L^2(\widetilde{I}_{1,i_1})} \,\mathrm{d}\zeta_2 \\ &= C \int_{\widetilde{I}_{1,i_1}} \|f - \widetilde{\Pi}_{p_2,\Xi_2} f\|^2_{L^2(I_{2,i_2})} \,\mathrm{d}\zeta_1 \\ &\quad + (\widetilde{h}_{1,i_1})^2 \int_{\widetilde{I}_{1,i_1}} |(\widehat{D}^{(1,0)} f) - \widetilde{\Pi}_{p_2,\Xi_2}(\widehat{D}^{(1,0)} f)|^2_{L^2(I_{2,i_2})} \,\mathrm{d}\zeta_1. \end{aligned}$$

The two terms above are bounded using Proposition 4.25 applied to the operator $\widetilde{\Pi}_{p_2,\Xi_2}$, as already shown in (4.45). Note that for the second term

the target function is $\widehat{D}^{(1,0)}f$ instead of f. We get

$$(T_2)^2 \leq C\big((\widetilde{h}_{2,i_2})^{2s}|f|^2_{\mathcal{H}^{(0,s)}(\widetilde{Q}_{\mathbf{i}})} + (\widetilde{h}_{1,i_1})^2(\widetilde{h}_{2,i_2})^{2(s-1)}|f|^2_{\mathcal{H}^{(1,s-1)}(\widetilde{Q}_{\mathbf{i}})}\big).$$

Finally, the global result in the proposition follows easily by summing for all elements $Q_{\mathbf{i}}$ and taking h as the maximum edge length. □

Note that in the above proposition we do not pursue an optimal result in terms of required regularity of the target function. This result could be obtained by making use of (bent) fractional Sobolev spaces in the proof.

We finally introduce the approximation results for the multi-patch quasi-interpolant in physical space (3.10). A key property of the quasi-interpolant (3.10) is that, by definition, the function $(\Pi_{V_h}f)|_{\Omega^{(j)}}$ depends only on $f|_{\Omega^{(j)}}$. This property allows us to derive the error estimates *patch by patch* separately. By combining the estimates in Proposition 4.26 with the mapping arguments of Section 4.3 on each single patch, the following result follows easily. We state it directly in general dimension d.

Proposition 4.27. Let the polynomial degree $p = p_1 = \cdots = p_d$ and the integer $d \leq s \leq p+1$. Then, there exists a constant C depending only on p such that

$$\|f - \Pi_{V_h}f\|_{L^2(\Omega)} \leq C\,h^s\left(\|f\|_{H^s(\Omega)}\right)$$

for all $f \in H^s(\Omega)$, where h denotes the maximum mesh size over all patches.

5. Isogeometric spaces: vector fields

This section is devoted to the definition and properties of spline approximation of vector fields. We mainly follow the two papers by Buffa *et al.* (2011*b*) and Buffa, Sangalli and Vázquez (2014*b*), and we focus our attention on the construction of the so-called spline complex, that is, spline approximation spaces for the de Rham diagram. In the finite element context, the construction of discrete de Rham complexes has been object of intense study and its various aspects have been object of three review papers: for computational electromagnetics (Hiptmair 2002), for discrete exterior calculus (Arnold *et al.* 2006) and for eigenvalue problems (Boffi 2010).

Throughout this section we will work in three space dimensions, with the exception of Section 5.5; however, the constructions and results apply to any space dimensions with obvious changes. The reason for this choice is to avoid the use of the language of differential forms and, hopefully, to improve clarity.

In Section 5.1 we briefly recall the de Rham diagram in a simple setting, and in Section 5.2 we construct the spline de Rham complex, called here *the spline complex* on the parametric domain $\widehat{\Omega} = (0,1)^3$, and we propose the approximation properties which are obtained following the lines of Section 4.

Finally, following Section 3, we construct the spline complex on the physical domain and analyse their approximation properties: Section 5.3 is devoted to the single-patch domain and Section 5.4 to multi-patch domains.

5.1. The de Rham complex

In this section we briefly introduce the concept of the de Rham complex and introduce our notation for the related spaces. We adopt the language of functional analysis and proxy fields rather than that of differential forms, and we mainly concentrate on the definition of pull-backs that will be needed in the next sections. Let $\widehat{\Omega} = (0,1)^3$ and Ω be a single-patch physical domain, that is, there exists a map $\mathbf{F} : \widehat{\Omega} \to \mathbb{R}^3$ satisfying Assumption 3.1 such that $\Omega = \mathbf{F}(\widehat{\Omega})$. Due to Assumption 3.1, the domain Ω is simply connected with connected boundary. We define the spaces

$$\widehat{X}^0 := H^1(\widehat{\Omega}), \quad \widehat{X}^1 := \mathbf{H}(\mathbf{curl};\widehat{\Omega}), \quad \widehat{X}^2 := \mathbf{H}(\mathrm{div};\widehat{\Omega}), \quad \widehat{X}^3 := L^2(\widehat{\Omega}),$$
$$X^0 := H^1(\Omega), \quad X^1 := \mathbf{H}(\mathbf{curl};\Omega), \quad X^2 := \mathbf{H}(\mathrm{div};\Omega), \quad X^3 := L^2(\Omega).$$

where for $D = \widehat{\Omega},\ \Omega$, $L^2(D)$ is the space of real-valued, square-integrable functions, and

$$\mathbf{H}(\mathbf{curl};D) := \{\mathbf{u} \in L^2(D)^3 : \mathbf{curl}\,\mathbf{u} \in L^2(D)^3\},$$
$$\mathbf{H}(\mathrm{div};D) := \{\mathbf{u} \in L^2(D)^3 : \mathrm{div}\,\mathbf{u} \in L^2(D)\}.$$

Note that $\widehat{X}^j$ and X^j are spaces of scalar fields for $j = 0, 3$ whereas they are spaces of vector fields for the indices $j = 1, 2$. The index j will be used throughout this section to identify these spaces.

Thanks to Assumption 3.1, both $\mathbf{F}$ and its inverse are smooth. We can then define the pull-backs that relate these spaces as (see Hiptmair 2002, Section 2.2):

$$\begin{aligned}
\iota^0(f) &:= f \circ \mathbf{F}, && f \in X^0,\\
\iota^1(\mathbf{f}) &:= (D\mathbf{F})^T(\mathbf{f} \circ \mathbf{F}), && \mathbf{f} \in X^1,\\
\iota^2(\mathbf{f}) &:= \det(D\mathbf{F})(D\mathbf{F})^{-1}(\mathbf{f} \circ \mathbf{F}), && \mathbf{f} \in X^2,\\
\iota^3(f) &:= \det(D\mathbf{F})(f \circ \mathbf{F}), && f \in X^3,
\end{aligned} \tag{5.1}$$

where $D\mathbf{F}$ is the Jacobian matrix of the mapping $\mathbf{F}$. Then, due to the curl and divergence conserving properties of ι^1 and ι^2, respectively (see, *e.g.*, Monk 2003, Section 3.9), the following commutative de Rham diagram is satisfied (see Hiptmair 2002, Section 2.2):

$$\begin{array}{ccccccccccc}
\mathbb{R} & \longrightarrow & \widehat{X}^0 & \xrightarrow{\widehat{\mathbf{grad}}} & \widehat{X}^1 & \xrightarrow{\widehat{\mathbf{curl}}} & \widehat{X}^2 & \xrightarrow{\widehat{\mathrm{div}}} & \widehat{X}^3 & \longrightarrow & 0\\
 & & \iota^0\uparrow & & \iota^1\uparrow & & \iota^2\uparrow & & \iota^3\uparrow & & \\
\mathbb{R} & \longrightarrow & X^0 & \xrightarrow{\mathbf{grad}} & X^1 & \xrightarrow{\mathbf{curl}} & X^2 & \xrightarrow{\mathrm{div}} & X^3 & \longrightarrow & 0.
\end{array} \tag{5.2}$$

5.2. The spline complex on the parametric domain

In this section we may use a 'verbose' notation. For example, the space $S_{\mathbf{p}}(\boldsymbol{\Xi})$ will also be denoted by $S_{p_1,p_2,p_3}(\Xi_1,\Xi_2,\Xi_3)$. The reason for this choice will be clear in the next lines.

First of all, using the expression for the derivative (2.7) in three dimensions, it is clear that, for example,

$$\frac{\partial}{\partial\zeta_1} : S_{p_1,p_2,p_3}(\Xi_1,\Xi_2,\Xi_3) \to S_{p_1-1,p_2,p_3}(\Xi_1',\Xi_2,\Xi_3),$$

where we recall that Ξ_1' is defined as the knot vector $\{\xi_{1,2},\dots,\xi_{1,n_1+p_1}\}$.

Following the same rationale, we define the spaces on the parametric domain $\widehat{\Omega}$:

$$\begin{aligned}
\widehat{X}_h^0 &:= S_{p_1,p_2,p_3}(\Xi_1,\Xi_2,\Xi_3),\\
\widehat{X}_h^1 &:= S_{p_1-1,p_2,p_3}(\Xi_1',\Xi_2,\Xi_3)\times S_{p_1,p_2-1,p_3}(\Xi_1,\Xi_2',\Xi_3)\\
&\qquad\qquad \times S_{p_1,p_2,p_3-1}(\Xi_1,\Xi_2,\Xi_3'),\\
\widehat{X}_h^2 &:= S_{p_1,p_2-1,p_3-1}(\Xi_1,\Xi_2',\Xi_3')\times S_{p_1-1,p_2,p_3-1}(\Xi_1',\Xi_2,\Xi_3')\\
&\qquad\qquad \times S_{p_1-1,p_2-1,p_3}(\Xi_1',\Xi_2',\Xi_3),\\
\widehat{X}_h^3 &:= S_{p_1-1,p_2-1,p_3-1}(\Xi_1',\Xi_2',\Xi_3').
\end{aligned} \tag{5.3}$$

In order for $\widehat{X}_h^1$, $\widehat{X}_h^2$ and $\widehat{X}_h^3$ to be meaningful, we require $0 \le m_{\ell,i} \le p_\ell$, for $i = 2,\dots,N_\ell - 1$ and $\ell = 1,2,3$. This means that the functions in $\widehat{X}_h^0$ are at least continuous. Then, thanks to (2.7) it is easily seen that

$$\widehat{\mathbf{grad}}(\widehat{X}_h^0) \subset \widehat{X}_h^1,$$

and analogously, from the definition of the curl and the divergence operators, we get

$$\widehat{\mathbf{curl}}(\widehat{X}_h^1) \subset \widehat{X}_h^2 \quad \text{and} \quad \widehat{\mathrm{div}}(\widehat{X}_h^2) \subset \widehat{X}_h^3.$$

Moreover, it is proved in Buffa *et al.* (2011*b*) that the kernel of each operator is exactly the image of the preceding one. In other words, these spaces form an exact sequence:

$$\mathbb{R} \longrightarrow \widehat{X}_h^0 \xrightarrow{\widehat{\mathbf{grad}}} \widehat{X}_h^1 \xrightarrow{\widehat{\mathbf{curl}}} \widehat{X}_h^2 \xrightarrow{\widehat{\mathrm{div}}} \widehat{X}_h^3 \longrightarrow 0, \tag{5.4}$$

that is, the first line of (5.2).

Remark 5.1. The spaces defined above do not have boundary conditions, but everything presented in this section can be extended with minor changes to spaces where homogeneous boundary conditions are applied to a set of faces Γ_D of $\partial\Omega$, as in Assumption 3.2.

5.2.1. Choice of bases and topological structure

First of all, we define an appropriate basis for the spline spaces which will show that the topological structure of the spline complex is closely related to that of the Greville mesh $\widehat{\mathcal{M}}_G$. We remark that, although the mesh $\widehat{\mathcal{M}}$ is the same for all the spaces of the complex, the Greville mesh $\widehat{\mathcal{M}}_G$ is different for each space (and for each component). In the following $\widehat{\mathcal{M}}_G$ will always refer to the Greville mesh corresponding to the space $\widehat{X}_h^0$.

We start with a simple one-dimensional argument. Let us first recall formula (2.8):

$$\frac{\mathrm{d}\widehat{B}_{i,p}}{\mathrm{d}\zeta}(\zeta) = \widehat{D}_{i-1,p-1}(\zeta) - \widehat{D}_{i,p-1}(\zeta).$$

This means that on the segment $[0,1]$, if we choose

$$\{\widehat{B}_{i,p}, i = 1, \dots, n\} \quad \text{and} \quad \{\widehat{D}_{i,p-1}, i = 1, \dots, n-1\}$$

as the basis for $S_p(\Xi)$ and $S_{p-1}(\Xi')$, respectively, then the matrix representing the derivative is the lower triangular, bidiagonal matrix which represents the *vertex-to-edge* relation on the one-dimensional Greville mesh constructed from Ξ and p, that is, with vertices given by (2.16). This means that we are implicitly setting an association between the edges of the Greville mesh and functions $\widehat{D}_{i,p-1}$. In a standard spline setting, it would be more natural to define a new Greville mesh, constructed from Ξ' and the degree $p-1$, but this would not help us understand the topological structure of the spline complex.

As in Ratnani and Sonnendrücker (2012) and Buffa *et al.* (2014*b*), inspired by this observation, we can choose the following set of basis for the spaces in the spline complex:

$$\widehat{X}_h^0 = \operatorname{span}\big\{ \widehat{B}_{i_1,p_1}(\zeta_1)\widehat{B}_{i_2,p_2}(\zeta_2)\widehat{B}_{i_3,p_3}(\zeta_3) \quad \text{with } 1 \le i_\ell \le n_\ell,\ \ell = 1,2,3 \big\}, \tag{5.5}$$

$$\widehat{X}_h^1 = \operatorname{span}\,(\mathrm{I} \cup \mathrm{II} \cup \mathrm{III}), \text{ with} \tag{5.6}$$

$$\mathrm{I} = \big\{ \widehat{D}_{i_1,p_1-1}(\zeta_1)\widehat{B}_{i_2,p_2}(\zeta_2)\widehat{B}_{i_3,p_3}(\zeta_3)\widehat{\mathbf{e}}_1 \quad \text{with } 1 \le i_1 \le n_1 - 1,\ 1 \le i_\ell \le n_\ell,\ \ell = 2,3 \big\},$$

$$\mathrm{II} = \big\{ \widehat{B}_{i_1,p_1}(\zeta_1)\widehat{D}_{i_2,p_2-1}(\zeta_2)\widehat{B}_{i_3,p_3}(\zeta_3)\widehat{\mathbf{e}}_2 \quad \text{with } 1 \le i_2 \le n_2 - 1,\ 1 \le i_\ell \le n_\ell,\ \ell = 1,3 \big\},$$

$$\mathrm{III} = \big\{ \widehat{B}_{i_1,p_1}(\zeta_1)\widehat{B}_{i_2,p_2}(\zeta_2)\widehat{D}_{i_3,p_3-1}(\zeta_3)\widehat{\mathbf{e}}_3 \quad \text{with } 1 \le i_3 \le n_3 - 1,\ 1 \le i_\ell \le n_\ell,\ \ell = 1,2 \big\},$$

$$\widehat{X}_h^2 = \text{span}\,(\mathrm{I} \cup \mathrm{II} \cup \mathrm{III}),\ \text{with} \tag{5.7}$$

$$\mathrm{I} = \big\{ \widehat{B}_{i_1,p_1}(\zeta_1)\widehat{D}_{i_2,p_2-1}(\zeta_2)\widehat{D}_{i_3,p_3-1}(\zeta_3)\widehat{\mathbf{e}}_1 \quad \text{with } 1 \le i_1 \le n_1,\ 1 \le i_\ell \le n_\ell - 1,\ \ell = 2,3 \big\},$$

$$\mathrm{II} = \big\{ \widehat{D}_{i_1,p_1-1}(\zeta_1)\widehat{B}_{i_2,p_2}(\zeta_2)\widehat{D}_{i_3,p_3-1}(\zeta_3)\widehat{\mathbf{e}}_2 \quad \text{with } 1 \le i_2 \le n_2,\ 1 \le i_\ell \le n_\ell - 1,\ \ell = 1,3 \big\},$$

$$\mathrm{III} = \big\{ \widehat{D}_{i_1,p_1-1}(\zeta_1)\widehat{D}_{i_2,p_2-1}(\zeta_2)\widehat{B}_{i_3,p_3}(\zeta_3)\widehat{\mathbf{e}}_3 \quad \text{with } 1 \le i_3 \le n_3,\ 1 \le i_\ell \le n_\ell - 1,\ \ell = 1,2 \big\},$$

$$\widehat{X}_h^3 = \text{span}\big\{ \widehat{D}_{i_1,p_1-1}(\zeta_1)\widehat{D}_{i_2,p_2-1}(\zeta_2)\widehat{D}_{i_3,p_3-1}(\zeta_3) \quad \text{with } 1 \le i_\ell \le n_\ell - 1,\ \ell = 1,2,3 \big\}, \tag{5.8}$$

where $\{\widehat{\mathbf{e}}_\ell\}_{\ell=1,2,3}$ denotes the canonical basis of $\mathbb{R}^3$. We remark that all basis functions defined in (5.5)–(5.8) are non-negative.

Moreover, by using the formula (2.8) and a tensor product argument, we can analyse the structure of the basis functions. For instance, we consider the set I in (5.6). By construction, we have one of these functions for each edge of $\widehat{\mathcal{M}}_G$ in the ζ_1-direction, and these functions share the edge directions. Applying the same reasoning to the other set of basis functions in (5.5)–(5.8), together with the structure of the matrices representing differential operators, we have the following.

Proposition 5.2. With the choices (5.5)–(5.8), the matrices representing differential operators $\widehat{\mathbf{grad}}$, $\widehat{\mathbf{curl}}$, and $\widehat{\mathrm{div}}$ are the incidence matrices of the tensor product mesh $\widehat{\mathcal{M}}_G$. Thus, the spline complex $(\widehat{X}_h^0, \widehat{X}_h^1, \widehat{X}_h^2, \widehat{X}_h^3)$ is isomorphic to the co-chain complex associated with mesh $\widehat{\mathcal{M}}_G$.

The previous proposition states that the spline complex has exactly the same structure as the well-known Whitney forms when defined on the tensor product mesh $\widehat{\mathcal{M}}_G$; see, for example, Section 3 in Hiptmair (2002).

5.2.2. Commuting projections and approximation estimates

It is now necessary to define appropriate projectors into the discrete spaces. This is done by using the definition of interpolants and quasi-interpolants that we have given in Section 2.1.5. To alleviate notation, from this point we will not detail the knot vector in the interpolant, that is, we will denote

$$\Pi_p \equiv \Pi_{p,\Xi} \quad \text{and} \quad \Pi^c_{p-1} \equiv \Pi^c_{p-1,\Xi'}.$$

The choice of the interpolants follows from the definition of the spaces

$$\widehat{X}_h^0, \ldots, \widehat{X}_h^3,$$

and precisely we set

$$\widehat{\Pi}^0 := \Pi_{p_1} \otimes \Pi_{p_2} \otimes \Pi_{p_3}, \tag{5.9}$$

$$\widehat{\Pi}^1 := (\Pi^c_{p_1-1} \otimes \Pi_{p_2} \otimes \Pi_{p_3}) \times (\Pi_{p_1} \otimes \Pi^c_{p_2-1} \otimes \Pi_{p_3}) \times (\Pi_{p_1} \otimes \Pi_{p_2} \otimes \Pi^c_{p_3-1}), \tag{5.10}$$

$$\widehat{\Pi}^2 := (\Pi_{p_1} \otimes \Pi^c_{p_2-1} \otimes \Pi^c_{p_3-1}) \times (\Pi^c_{p_1-1} \otimes \Pi_{p_2} \otimes \Pi^c_{p_3-1}) \times (\Pi^c_{p_1-1} \otimes \Pi^c_{p_2-1} \otimes \Pi_{p_3}), \tag{5.11}$$

$$\widehat{\Pi}^3 := \Pi^c_{p_1-1} \otimes \Pi^c_{p_2-1} \otimes \Pi^c_{p_3-1}. \tag{5.12}$$

The next lemma shows that the interpolants are projectors onto the corresponding spline spaces.

Lemma 5.3. The interpolants (5.9)–(5.12) satisfy the spline preserving property, that is,

$$\widehat{\Pi}^j \widehat{f}_h = \widehat{f}_h, \quad \text{for all } \widehat{f}_h \in \widehat{X}^j_h,\ j = 0, 3,$$
$$\widehat{\Pi}^j \widehat{\mathbf{f}}_h = \widehat{\mathbf{f}}_h, \quad \text{for all } \widehat{\mathbf{f}}_h \in \widehat{X}^j_h,\ j = 1, 2.$$

Proof. The result is an immediate consequence of the spline preserving property of the interpolants Π_{p_ℓ} and $\Pi^c_{p_\ell-1}$, $\ell = 1, 2, 3$, given in (2.21) and in (2.35), respectively. □

Lemma 5.4. Under Assumption 4.10, the following inequalities hold for any $Q \in \widehat{\mathcal{M}}$:

$$\|\widehat{\Pi}^j \widehat{f}\|_{L^2(Q)} \le C \|\widehat{f}\|_{L^2(\widetilde{Q})} \quad \text{for all } \widehat{f} \in L^2(\widehat{\Omega}),\ j = 0, 3,$$
$$\|\widehat{\Pi}^j \widehat{\mathbf{f}}\|_{L^2(Q)^3} \le C \|\widehat{\mathbf{f}}\|_{L^2(\widetilde{Q})^3} \quad \text{for all } \widehat{\mathbf{f}} \in L^2(\widehat{\Omega})^3,\ j = 1, 2.$$

Proof. The result follows immediately from (2.26) and (2.38), which state that the relevant one-dimensional operators Π_{p_ℓ} and $\Pi^c_{p_\ell-1}$, $\ell = 1, 2, 3$ are L^2-stable. □

The commutativity of the interpolants with the differential operators is stated in the following lemma.

Lemma 5.5. We have

$$\widehat{\mathbf{grad}}(\widehat{\Pi}^0 \widehat{f}) = \widehat{\Pi}^1(\widehat{\mathbf{grad}}\, \widehat{f}) \quad \text{for all } \widehat{f} \in \widehat{X}^0, \tag{5.13}$$

$$\widehat{\mathbf{curl}}(\widehat{\Pi}^1 \widehat{\mathbf{f}}) = \widehat{\Pi}^2(\widehat{\mathbf{curl}}\, \widehat{\mathbf{f}}) \quad \text{for all } \widehat{\mathbf{f}} \in \widehat{X}^1, \tag{5.14}$$

$$\widehat{\mathrm{div}}(\widehat{\Pi}^2 \widehat{\mathbf{f}}) = \widehat{\Pi}^3(\widehat{\mathrm{div}}\, \widehat{\mathbf{f}}) \quad \text{for all } \widehat{\mathbf{f}} \in \widehat{X}^2. \tag{5.15}$$

Proof. The proof is based on the commutativity property (2.34) and the tensor product structure of the spaces and interpolants. First consider (5.13): let $\widehat{f}$ be a smooth scalar field with compact support in $\widehat{\Omega}$. With the

same abuse of notation as in Section 2.2.2, the first component of $\widehat{\mathbf{grad}}(\widehat{\Pi}^0\widehat{f})$ is given by

$$\begin{aligned}\partial_{\widehat{x}}(\widehat{\Pi}^0\widehat{f}) &= \partial_{\widehat{x}}((\Pi_{p_1}\otimes\Pi_{p_2}\otimes\Pi_{p_3})\,\widehat{f}) = \partial_{\widehat{x}}(\Pi_{p_1}(\Pi_{p_2}(\Pi_{p_3}\,\widehat{f})))\\ &= \Pi^c_{p_1-1}\partial_{\widehat{x}}(\Pi_{p_2}(\Pi_{p_3}\,\widehat{f})) = (\Pi^c_{p_1-1}\otimes\Pi_{p_2}\otimes\Pi_{p_3})\,\partial_{\widehat{x}}\widehat{f},\end{aligned}$$

which is the first component of $\widehat{\Pi}^1(\widehat{\mathbf{grad}}\,\widehat{f})$. A similar reasoning, using the commutativity of the univariate interpolants, yields

$$\begin{aligned}\partial_{\widehat{y}}(\widehat{\Pi}^0\widehat{f}) &= (\Pi_{p_1}\otimes\Pi^c_{p_2-1}\otimes\Pi_{p_3})\,\partial_{\widehat{y}}\widehat{f},\\ \partial_{\widehat{z}}(\widehat{\Pi}^0\widehat{f}) &= (\Pi_{p_1}\otimes\Pi_{p_2}\otimes\Pi^c_{p_3-1})\,\partial_{\widehat{z}}\widehat{f},\end{aligned}$$

which proves that $\widehat{\mathbf{grad}}(\widehat{\Pi}^0\widehat{f}) = \widehat{\Pi}^1(\widehat{\mathbf{grad}}\,\widehat{f})$. By a density argument (5.13) follows, thanks to Lemma 5.4. The proof of (5.14)–(5.15) is similar, from the definition of the interpolants and the expression of the curl and divergence operators. □

5.2.3. Approximation estimates

This section is devoted to the study of the approximation estimates of the complex $(\widehat{X}^0_h,\dots,\widehat{X}^3_h)$. The content of this section is based on Buffa *et al.* (2011*b*) and the approximation results are extended to the case of possibly anisotropic meshes, in the spirit of Section 4.

We start from the definition of the bent Sobolev spaces that we need. Since the inter-element regularity changes from space to space (and from component to component), we need to make the notation more explicit, starting from the one-dimensional definition: we denote by $\mathcal{H}^s_{\mathbf{k}}(I)$ the space defined in (4.1), where $\mathbf{k}=(k_2,\dots,k_{N-1})$ and k_i is the number of continuous derivatives at the point $\zeta_i\in Z$.

In three dimensions, given $\mathbf{r}=(r_1,r_2,r_3)\in\mathbb{N}^3$ and the three vectors $\mathbf{k}_1,\mathbf{k}_2,\mathbf{k}_3$ constructed from $\boldsymbol{\Xi}$, we set

$$\begin{aligned}\mathcal{H}^{0,\mathbf{r}} &= \mathcal{H}^{\mathbf{r}}_{\mathbf{k}_1,\mathbf{k}_2,\mathbf{k}_3},\\ \mathcal{H}^{1,\mathbf{r}} &= \mathcal{H}^{\mathbf{r}}_{\mathbf{k}_1-1,\mathbf{k}_2,\mathbf{k}_3}\times\mathcal{H}^{\mathbf{r}}_{\mathbf{k}_1,\mathbf{k}_2-1,\mathbf{k}_3}\times\mathcal{H}^{\mathbf{r}}_{\mathbf{k}_1,\mathbf{k}_2,\mathbf{k}_3-1},\\ \mathcal{H}^{2,\mathbf{r}} &= \mathcal{H}^{\mathbf{r}}_{\mathbf{k}_1,\mathbf{k}_2-1,\mathbf{k}_3-1}\times\mathcal{H}^{\mathbf{r}}_{\mathbf{k}_1-1,\mathbf{k}_2,\mathbf{k}_3-1}\times\mathcal{H}^{\mathbf{r}}_{\mathbf{k}-1,\mathbf{k}_2-1,\mathbf{k}_3},\\ \mathcal{H}^{3,\mathbf{r}} &= \mathcal{H}^{\mathbf{r}}_{\mathbf{k}-1,\mathbf{k}_2-1,\mathbf{k}_3-1}.\end{aligned}\tag{5.16}$$

This choice is made in order to ensure that $\widehat{X}^j_h\subset\mathcal{H}^{j,\mathbf{r}}$, for all $\mathbf{r}\in\mathbb{N}^3$, $j=1,2,3$, that is, the inter-element regularity of $\mathcal{H}^{j,\mathbf{r}}$ is *no higher* than that of $\widehat{X}^j_h$. The corresponding norms and seminorms are defined as in (4.20), component by component for the spaces $\mathcal{H}^{1,\mathbf{r}}$ and $\mathcal{H}^{2,\mathbf{r}}$, and we will make use of the set of notation introduced in Section 4 for directional derivatives. The following holds.

Proposition 5.6. Let Assumption 4.10 hold, let $Q_{\mathbf{i}}$ be an element of $\widehat{\mathcal{M}}$, and let $\widetilde{Q}_{\mathbf{i}}$ be its extension. Then, for $j = 0, 3$ we obtain

$$\begin{aligned}\|\widehat{D}^{(r_1,r_2,r_3)}(\widehat{f} - \widehat{\Pi}^j \widehat{f})\|_{L^2(Q_{\mathbf{i}})} \le C\big(&(\widetilde{h}_{1,i_1})^{s_1-r_1}\|\widehat{D}^{(s_1,r_2,r_3)}\widehat{f}\|_{L^2_h(\widetilde{Q}_{\mathbf{i}})} \\ &+ (\widetilde{h}_{2,i_2})^{s_2-r_2}\|\widehat{D}^{(r_1,s_2,r_3)}\widehat{f}\|_{L^2_h(\widetilde{Q}_{\mathbf{i}})} \\ &+ (\widetilde{h}_{3,i_3})^{s_3-r_3}\|\widehat{D}^{(r_1,r_2,s_3)}\widehat{f}\|_{L^2_h(\widetilde{Q}_{\mathbf{i}})}\big),\end{aligned} \tag{5.17}$$

for all $\widehat{f} \in \mathcal{H}^{j,(s_1,r_2,r_3)} \cap \mathcal{H}^{j,(r_1,s_2,r_3)} \cap \mathcal{H}^{j,(r_1,r_2,s_3)}$, and when $j = 0$, $0 \le r_\ell \le s_\ell \le p_\ell + 1$; whereas when $j = 3$, $0 \le r_\ell \le s_\ell \le p_\ell$, for $\ell = 1, 2, 3$.

Further, for $j = 1, 2$ we have

$$\begin{aligned}\|\widehat{D}^{(r_1,r_2,r_3)}(\widehat{\mathbf{f}} - \widehat{\Pi}^j\widehat{\mathbf{f}})\|_{L^2(Q_{\mathbf{i}})^3} \le C\big(&(\widetilde{h}_{1,i_1})^{s_1-r_1}\|\widehat{D}^{(s_1,r_2,r_3)}\widehat{\mathbf{f}}\|_{L^2_h(\widetilde{Q}_{\mathbf{i}})^3} \\ &+ (\widetilde{h}_{2,i_2})^{s_2-r_2}\|\widehat{D}^{(r_1,s_2,r_3)}\widehat{\mathbf{f}}\|_{L^2_h(\widetilde{Q}_{\mathbf{i}})^3} \\ &+ (\widetilde{h}_{3,i_3})^{s_3-r_3}\|\widehat{D}^{(r_1,r_2,s_3)}\widehat{\mathbf{f}}\|_{L^2_h(\widetilde{Q}_{\mathbf{i}})^3}\big),\end{aligned} \tag{5.18}$$

for all $\widehat{\mathbf{f}} \in \mathcal{H}^{j,(s_1,r_2,r_3)} \cap \mathcal{H}^{j,(r_1,s_2,r_3)} \cap \mathcal{H}^{j,(r_1,r_2,s_3)}$and $0 \le s_\ell \le p_\ell$, $\ell = 1, 2, 3$.

Proof. The proof follows that of Proposition 4.12 (see also Proposition 4.11), since the spaces $\mathcal{H}^{j,\mathbf{r}}$, $\mathbf{r} = (r_1, r_2, r_3)$, $j = 1, 2, 3$ are constructed on purpose. For vector fields, that is, for $j = 1$ and $j = 2$, the proof can be done component by component. □

5.3. The spline complex in the single-patch physical domain

As in Section 3, we suppose Ω is obtained from $\widehat{\Omega}$ via a NURBS (or spline) single-patch mapping $\mathbf{F} \in (N_{\mathbf{p}^0}(\boldsymbol{\Xi}^0, W))^3$, satisfying Assumption 3.1. To construct the spaces (5.3) in the parametric domain, first we choose the space

$$\widehat{X}^0_h = S_{p_1,p_2,p_3}(\Xi_1, \Xi_2, \Xi_3) = S_{\mathbf{p}}(\boldsymbol{\Xi}),$$

in such a way that $S_{\mathbf{p}^0}(\boldsymbol{\Xi}^0) \subset S_{\mathbf{p}}(\boldsymbol{\Xi})$. That is, the space $\widehat{X}^0_h$ is a refinement of the spline space used to define the NURBS geometry (neglecting the weight). Once the first space of the spline complex is chosen, the others are defined from (5.3).

We recall from Section 3 that $\mathcal{M}$ and $\mathcal{M}_G$ denote the image of $\widehat{\mathcal{M}}$ and $\widehat{\mathcal{M}}_G$ under the mappings $\mathbf{F}$ and $\mathbf{F}_{\mathsf{cp}}$, respectively. As in the parametric space, in the following the control mesh $\mathcal{M}_G$ is the one associated with the first space, and will be linked with the topological structure of the complex.

The discrete spaces $X^0_h, \dots, X^3_h$ on the physical domain Ω can be defined from the spaces (5.3) on the parametric domain $\widehat{\Omega}$ by *push-forward*, that is, the inverse of the transformations defined in (5.1), that commute with the

differential operators (as given by the diagrams (5.2))

$$\begin{array}{ccccccccccc}
\mathbb{R} & \longrightarrow & \widehat{X}_h^0 & \xrightarrow{\widehat{\mathbf{grad}}} & \widehat{X}_h^1 & \xrightarrow{\widehat{\mathbf{curl}}} & \widehat{X}_h^2 & \xrightarrow{\widehat{\mathrm{div}}} & \widehat{X}_h^3 & \longrightarrow & 0 \\
 & & \iota^0 \uparrow & & \iota^1 \uparrow & & \iota^2 \uparrow & & \iota^3 \uparrow & & \\
\mathbb{R} & \longrightarrow & X_h^0 & \xrightarrow{\mathbf{grad}} & X_h^1 & \xrightarrow{\mathbf{curl}} & X_h^2 & \xrightarrow{\mathrm{div}} & X_h^3 & \longrightarrow & 0,
\end{array} \tag{5.19}$$

that is, the discrete spaces in the physical domain are defined by

$$\begin{aligned}
X_h^j &:= \{f_h : \iota^j(f_h) \in \widehat{X}_h^j\}, \qquad \text{for } j = 0, 3, \\
X_h^j &:= \{\mathbf{f}_h : \iota^j(\mathbf{f}_h) \in \widehat{X}_h^j\}, \qquad \text{for } j = 1, 2.
\end{aligned} \tag{5.20}$$

We remark that the space X_h^1, which is a discretization of $\mathbf{H}(\mathbf{curl}; \Omega)$, is defined via the curl conserving transformation ι^1, and that the space X_h^2, which is a discretization of $\mathbf{H}(\mathrm{div}; \Omega)$, is defined via the divergence conforming transformation ι^2. These are equivalent to the curl and divergence preserving transformations that are used to define edge and face elements, respectively (see Monk 2003, Section 3.9).

Thanks to the properties of the operators (5.1), the spaces $X_h^0, \ldots, X_h^3$ inherit the same fundamental properties of $\widehat{X}_h^0, \ldots, \widehat{X}_h^3$ discussed in the previous section, as follows.

- They form an exact de Rham complex:

$$\mathbb{R} \longrightarrow X_h^0 \xrightarrow{\mathbf{grad}} X_h^1 \xrightarrow{\mathbf{curl}} X_h^2 \xrightarrow{\mathrm{div}} X_h^3 \longrightarrow 0. \tag{5.21}$$

- The basis functions for $X_h^0, \ldots, X_h^3$ are defined by push-forward of the basis functions of $\widehat{X}_h^0, \ldots, \widehat{X}_h^3$ defined in (5.5)–(5.8), similarly to (5.20).
- By (5.19), the matrices associated with the differential operators **grad**, **curl** and div on Ω are the same as the matrices of $\widehat{\mathbf{grad}}$, $\widehat{\mathbf{curl}}$ and $\widehat{\mathrm{div}}$ on $\widehat{\Omega}$, that is, they are the incidence matrices of the mesh $\mathcal{M}_G$.
- In view of Proposition 5.2 and the properties of the pull-back operators (5.1), we know that the spline complex $(X_h^0, \ldots, X_h^3)$ is isomorphic to the co-chain complex of the control mesh $\mathcal{M}_G$. As a consequence, degrees of freedom can be associated to geometric entities of the control mesh $\mathcal{M}_G$, to vertices for X_h^0, edges for X_h^1 and so on. Figure 5.1 shows degrees-of-freedom locations for X_h^0 and for X_h^1.

Remark 5.7. Buffa *et al.* (2014*b*) introduced the concept of control fields, which are Whitney forms defined on the control mesh $\mathcal{M}_G$. In view of the properties listed above, of Proposition 5.2, and the properties of the pull-back operators, the Whitney vector fields can be interpreted as control fields, that is, exactly in the spirit of control points, fields which 'carry' the degrees of freedom for the spline complex. It should be noted that, just as

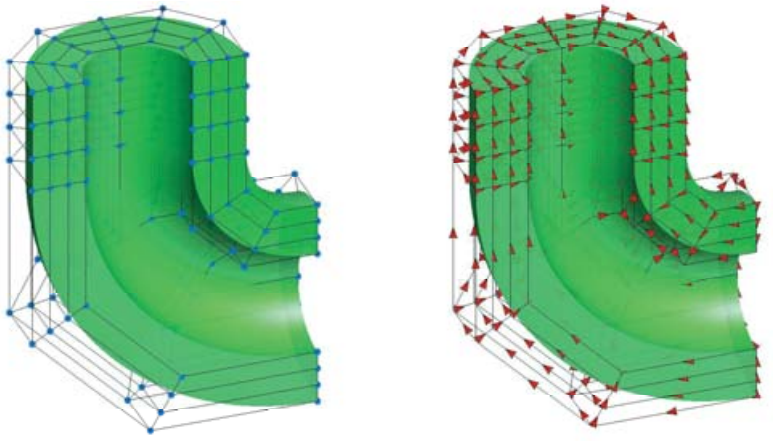

(a) (b)

Figure 5.1. (a) The degrees-of-freedom location (dots) for the space X_h^0. (b) The degrees-of-freedom location (arrows) for the space X_h^1.

for degrees of freedom, the spline complex enjoys approximation properties of order h^p, where $p = \min\{p_1, p_2, p_3\}$, whereas the underlying Whitney forms provide only low-order approximation rates.

5.3.1. Approximation estimates on the single-patch physical domain
As the first step to studying the approximation estimates in the physical domain, we start by introducing the projectors for each space X_h^j of the complex. These projectors are defined from the ones in the parametric domain (5.9)–(5.12), and the corresponding pull-backs ι^j, in such a way that they are uniquely characterized by the equations

$$\begin{aligned} \iota^j(\Pi^j f) &= \widehat{\Pi}^j(\iota^j(f)) \qquad j = 0, 3, \\ \iota^j(\Pi^j \mathbf{f}) &= \widehat{\Pi}^j(\iota^j(\mathbf{f})) \qquad j = 1, 2. \end{aligned} \tag{5.22}$$

The following proposition is an immediate consequence of these definitions, together with the commutativity properties of Lemma 5.5.

Proposition 5.8. The following diagram commutes:

$$\begin{array}{ccccccccc} \mathbb{R} & \longrightarrow & X^0 & \xrightarrow{\mathbf{grad}} & X^1 & \xrightarrow{\mathbf{curl}} & X^2 & \xrightarrow{\mathrm{div}} & X^3 \longrightarrow 0 \\ & & \Pi^0 \downarrow & & \Pi^1 \downarrow & & \Pi^2 \downarrow & & \Pi^3 \downarrow \\ \mathbb{R} & \longrightarrow & X_h^0 & \xrightarrow{\mathbf{grad}} & X_h^1 & \xrightarrow{\mathbf{curl}} & X_h^2 & \xrightarrow{\mathrm{div}} & X_h^3 \longrightarrow 0. \end{array} \tag{5.23}$$

Therefore, to study the approximation error of these projectors, we follow the same steps as in Section 4.3, and we will make use of the spaces, norms

and derivatives defined there without recalling their definition. We first prove the following proposition, which is the analogue of Proposition 4.17; see also Lemma 3.6 in Buffa *et al.* (2011*b*).

Proposition 5.9. Let $\mathbf{s} = (s_1, s_2, s_3)$, $f \in H^{\mathbf{s}}_{\mathbf{F}}(\Omega)$, and $\mathbf{f} \in H^{\mathbf{s}}_{\mathbf{F}}(\Omega)^3$. Then

$$\begin{aligned} \iota^j(f) &\in \mathcal{H}^{j,\mathbf{s}} \quad j = 0, 3, \\ \iota^j(\mathbf{f}) &\in \mathcal{H}^{j,\mathbf{s}} \quad j = 1, 2. \end{aligned} \tag{5.24}$$

Moreover, there exists a constant C such that for all elements $K = \mathbf{F}(Q) \in \mathcal{M}$, with $Q \in \widehat{\mathcal{M}}$, we have

$$\begin{aligned} C^{-1}\|f\|_{H^{\mathbf{s}}_{\mathbf{F}}(K)} \leq \|\iota^j(f)\|_{H^{\mathbf{s}}(Q)} \leq C\|f\|_{H^{\mathbf{s}}_{\mathbf{F}}(K)} \qquad j = 0, 3, \\ C^{-1}\|\mathbf{f}\|_{H^{\mathbf{s}}_{\mathbf{F}}(K)^3} \leq \|\iota^j(\mathbf{f})\|_{H^{\mathbf{s}}(Q)^3} \leq C\|\mathbf{f}\|_{H^{\mathbf{s}}_{\mathbf{F}}(K)^3} \quad j = 1, 2. \end{aligned}$$

Proof. First of all we show (5.24), and we focus on the case $j = 1$ since all other cases are similar. For a given $\mathbf{f} \in H^{\mathbf{s}}_{\mathbf{F}}(\Omega)^3$, let

$$\widehat{\mathbf{f}} = \iota^1(\mathbf{f}) = (D\mathbf{F})^T(\mathbf{f} \circ \mathbf{F}).$$

Since $\mathbf{F}$ is regular inside each element, we just need to check that the inter-element continuity is the one we expect. It is easy to see that, for example,

$$\frac{\partial \mathbf{F}}{\partial \zeta_1} \in \mathcal{H}^{\mathbf{s}'}_{\mathbf{k}_1 - 1, \mathbf{k}_2, \mathbf{k}_3}, \quad \text{for all } \mathbf{s}' \in \mathbb{N}^3,$$

and a similar result for the other partial derivatives implies that $\iota^1(\mathbf{f}) \in \mathcal{H}^{1,\mathbf{s}}$.

Applying the chain rule, and Proposition 4.16, we have

$$D^{\mathbf{s}}_{\mathbf{F}}\mathbf{f} = \big(\widehat{D}^{\mathbf{s}}\big(D\mathbf{F}^{-T}\,\widehat{\mathbf{f}}\big)\big) \circ \mathbf{F}^{-1},$$

where $D^{\mathbf{s}}_{\mathbf{F}}\mathbf{f}$ stands for the directional derivatives defined in Section 4.3 applied to each component of the vector $\mathbf{f}$. Then, from that expression and Proposition 4.17, and using Assumption 3.1 for the regularity of $\mathbf{F}$, we have

$$\begin{aligned} \|D^{\mathbf{s}}_{\mathbf{F}}\mathbf{f}\|_{L^2(K)^3} &\leq C(\mathbf{F}) \sum_{r_1, r_2, r_3 = 0}^{s_1, s_2, s_3} \|\big(\widehat{D}^{(r_1, r_2, r_3)}\widehat{\mathbf{f}}\big) \circ \mathbf{F}^{-1}\|_{L^2(K)^3} \\ &\leq C(\mathbf{F}) \sum_{r_1, r_2, r_3 = 0}^{s_1, s_2, s_3} \|\widehat{D}^{(r_1, r_2, r_3)}\widehat{\mathbf{f}}\|_{L^2(Q)^3}. \end{aligned}$$

On the other hand

$$\widehat{D}^{\mathbf{s}}(\widehat{\mathbf{f}}) = \widehat{D}^{\mathbf{s}}((D\mathbf{F})^T(\mathbf{f} \circ \mathbf{F})),$$

and we can again use the chain rule to obtain

$$\begin{aligned}\|\widehat{D}^{\mathbf{s}}(\widehat{\mathbf{f}})\|_{L^2(Q)^3} &\leq C(\mathbf{F}) \sum_{r_1,r_2,r_3=0}^{s_1,s_2,s_3} \|\widehat{D}^{(r_1,r_2,r_3)}(\mathbf{f}\circ\mathbf{F})\|_{L^2(Q)^3} \\ &\leq C(\mathbf{F}) \sum_{r_1,r_2,r_3=0}^{s_1,s_2,s_3} \|D_{\mathbf{F}}^{(r_1,r_2,r_3)}\mathbf{f}\|_{L^2(K)^3}.\end{aligned}$$

All other inequalities can be proved in the same way. □

We are now ready to write the approximation estimate for the projectors Π^j, $j = 1, 2, 3$.

Theorem 5.10. Let Assumption 4.10 hold, and let $\mathbf{s} = (s_1, s_2, s_3)$. Then there exists a constant C depending only on $\mathbf{p}, \theta, \mathbf{F}$ such that, for all elements $K = \mathbf{F}(Q) \in \mathcal{M}$, with $\widetilde{K} = \mathbf{F}(\widetilde{Q})$, for $j = 0$ and $j = 3$ we have

$$\begin{aligned}|f - \Pi^j f|_{\mathcal{H}_{\mathbf{F}}^{(r_1,r_2,r_3)}(K)} \leq C\big(&(\widetilde{h}_{1,i_1})^{s_1-r_1}\|f\|_{\mathcal{H}_{\mathbf{F}}^{(s_1,r_2,r_3)}(\widetilde{K})} \\ &+ (\widetilde{h}_{2,i_2})^{s_2-r_2}\|f\|_{\mathcal{H}_{\mathbf{F}}^{(r_1,s_2,r_3)}(\widetilde{K})} \\ &+ (\widetilde{h}_{3,i_3})^{s_3-r_3}\|f\|_{\mathcal{H}_{\mathbf{F}}^{(r_1,r_2,s_3)}(\widetilde{K})}\big),\end{aligned} \tag{5.25}$$

for all f in $H_{\mathbf{F}}^{(s_1,r_2,r_3)}(\Omega) \cap H_{\mathbf{F}}^{(r_1,s_2,r_3)}(\Omega) \cap H_{\mathbf{F}}^{(r_1,r_2,s_3)}(\Omega)$, and $\mathbf{r}, \mathbf{s}$ such that, when $j = 0$, $0 \leq r_\ell \leq s_\ell \leq p_\ell + 1$, $\ell = 1, 2, 3$; whereas when when $j = 3$, $0 \leq r_\ell \leq s_\ell \leq p_\ell$, $\ell = 1, 2, 3$.

For $j = 1$ and $j = 2$ we have

$$\begin{aligned}|\mathbf{f} - \Pi^j\mathbf{f}|_{\mathcal{H}_{\mathbf{F}}^{(r_1,r_2,r_3)}(K)^3} \leq C\big(&(\widetilde{h}_{1,i_1})^{s_1-r_1}\|\mathbf{f}\|_{\mathcal{H}_{\mathbf{F}}^{(s_1,r_2,r_3)}(\widetilde{K})^3} \\ &+ (\widetilde{h}_{2,i_2})^{s_2-r_2}\|\mathbf{f}\|_{\mathcal{H}_{\mathbf{F}}^{(r_1,s_2,r_3)}(\widetilde{K})^3} \\ &+ (\widetilde{h}_{3,i_3})^{s_3-r_3}\|\mathbf{f}\|_{\mathcal{H}_{\mathbf{F}}^{(r_1,r_2,s_3)}(\widetilde{K})^3}\big),\end{aligned} \tag{5.26}$$

for all $\mathbf{f}$ in $H_{\mathbf{F}}^{(s_1,r_2,r_3)}(\Omega)^3 \cap H_{\mathbf{F}}^{(r_1,s_2,r_3)}(\Omega)^3 \cap H_{\mathbf{F}}^{(r_1,r_2,s_3)}(\Omega)^3$, and $\mathbf{r}, \mathbf{s}$ such that $0 \leq r_\ell \leq s_\ell \leq p_\ell$, $\ell = 1, 2, 3$.

Proof. The proof of the estimate of $j = 0$ is very similar to that of Theorem 4.18. The other estimates are proved in a similar way. We describe the proof of (5.26) for $j = 1$, but the reasoning is the same for all other estimates. Using Proposition 5.9 and the definition of the projectors (5.22), for $\widehat{\mathbf{f}} = \iota^1(\mathbf{f})$, we have

$$\begin{aligned}|\mathbf{f} - \Pi^1\mathbf{f}|_{\mathcal{H}_{\mathbf{F}}^{(r_1,r_2,r_3)}(K)^3} &= \|D_{\mathbf{F}}^{(r_1,r_2,r_3)}(\mathbf{f} - \Pi^1\mathbf{f})\|_{L^2(K)^3} \\ &\leq C\|\widehat{\mathbf{f}} - \widehat{\Pi}^1\widehat{\mathbf{f}}\|_{\mathcal{H}_{\mathbf{F}}^{(r_1,r_2,r_3)}(Q)^3}.\end{aligned}$$

Then, applying Propositions 5.6 and 5.9 again, and from the definition of the norms in (4.32), we have, for every $0 \le q_\ell \le r_\ell$, $\ell = 1, 2, 3$,

$$\begin{aligned}
&\|\widehat{D}^{(q_1,q_2,q_3)}(\widehat{\mathbf{f}} - \widehat{\Pi}^1\widehat{\mathbf{f}})\|_{L^2(Q)^3} \\
&\quad \le C\Big((\widetilde{h}_{1,i_1})^{s_1-q_1} \|\widehat{D}^{(s_1,q_2,q_3)}\widehat{\mathbf{f}}\|_{L^2_h(\widetilde{Q})^3} \\
&\qquad + (\widetilde{h}_{2,i_2})^{s_2-q_2} \|\widehat{D}^{(q_1,s_2,q_3)}\widehat{\mathbf{f}}\|_{L^2_h(\widetilde{Q})^3} + (\widetilde{h}_{3,i_3})^{s_3-q_3} \|\widehat{D}^{(q_1,q_2,s_3)}\widehat{\mathbf{f}}\|_{L^2_h(\widetilde{Q})^3} \Big) \\
&\quad \le C\Big((\widetilde{h}_{1,i_1})^{s_1-q_1} \|\mathbf{f}\|_{\mathcal{H}^{(s_1,q_2,q_3)}_{\mathbf{F}}(\widetilde{K})^3} \\
&\qquad + (\widetilde{h}_{2,i_2})^{s_2-q_2} \|\mathbf{f}\|_{\mathcal{H}^{(q_1,s_2,q_3)}_{\mathbf{F}}(\widetilde{K})^3} + (\widetilde{h}_{3,i_3})^{s_3-q_3} \|\mathbf{f}\|_{\mathcal{H}^{(q_1,q_2,s_3)}_{\mathbf{F}}(\widetilde{K})^3} \Big).
\end{aligned}$$

Finally, since the previous inequality is valid for $0 \le q_\ell \le r_\ell$, recalling again the definition of the norms (4.32), and since $\widetilde{h}_{\ell,i_\ell} \le 1$, we get

$$\begin{aligned}
&\|(\widehat{\mathbf{f}} - \widehat{\Pi}^1\widehat{\mathbf{f}})\|_{\mathcal{H}^{(r_1,r_2,r_3)}_{\mathbf{F}}(Q)^3} \\
&\quad \le C\Big((\widetilde{h}_{1,i_1})^{s_1-r_1} \|\mathbf{f}\|_{\mathcal{H}^{(s_1,r_2,r_3)}_{\mathbf{F}}(\widetilde{K})^3} \\
&\qquad + (\widetilde{h}_{2,i_2})^{s_2-r_2} \|\mathbf{f}\|_{\mathcal{H}^{(r_1,s_2,r_3)}_{\mathbf{F}}(\widetilde{K})^3} + (\widetilde{h}_{3,i_3})^{s_3-r_3} \|\mathbf{f}\|_{\mathcal{H}^{(r_1,r_2,s_3)}_{\mathbf{F}}(\widetilde{K})^3} \Big),
\end{aligned}$$

and the result is proved. □

Remark 5.11. Note that we have decided to write the estimates (5.26) only for $s_\ell \le p_\ell$, $\ell = 1, 2, 3$ regardless of the component and the direction of derivatives. This can surely be improved in the spirit of Buffa, Costabel and Dauge (2005), but the development of complete anisotropic estimates for vector fields would be technical and falls beyond the scope of this review.

We end this section with a bound for the approximation error in standard H^r Sobolev norms. The proof is analogous to that of Corollary 4.21, and we do not detail it here.

Corollary 5.12. Let Assumption 4.10 hold, and let $p = \min(p_1, p_2, p_3)$. Then there exists a constant C, depending only on $\mathbf{p}, \theta, \mathbf{F}$, such that

$$\begin{aligned}
&\|f - \Pi^0 f\|_{H^r(\Omega)} \le C h^{s-r} \|f\|_{H^s(\Omega)} && 0 \le r \le s \le p+1, \\
&\|\mathbf{f} - \Pi^1 \mathbf{f}\|_{H^r(\Omega)^3} \le C h^{s-r} \|\mathbf{f}\|_{H^s(\Omega)^3} && 0 \le r \le s \le p, \\
&\|\mathbf{f} - \Pi^2 \mathbf{f}\|_{H^r(\Omega)^3} \le C h^{s-r} \|\mathbf{f}\|_{H^s(\Omega)^3} && 0 \le r \le s \le p, \\
&\|f - \Pi^3 f\|_{H^r(\Omega)} \le C h^{s-r} \|f\|_{H^s(\Omega)} && 0 \le r \le s \le p,
\end{aligned}$$

for all $f \in H^s(\Omega)$ and $\mathbf{f} \in H^s(\Omega)^3$.

The approximation estimates in the previous corollary are presented in high-order Sobolev norms, as in Section 4. In particular this gives the error in the L^2-norm, which, together with the commutative diagram implied by

Lemma 5.5, will imply the approximation estimates in the graph norms for the spaces $\widehat{X}^j$.

5.4. The spline complex on the multi-patch physical domain

In this section we extend the definition of the spline complex to multi-patch domains. Here we will make use of the notation introduced in Section 3.2. For simplicity, and to avoid dealing with harmonic functions, we assume that the multi-patch domain Ω is simply connected with connected boundary.

If we let $(X^{0,(j)}, \dots, X^{3,(j)})$ denote the spline complex in the domain $\Omega^{(j)}$, the spline complex in Ω is defined by

$$\begin{aligned} X_h^0(\Omega) &= \{f \in H^1(\Omega) : f_{|\Omega^{(j)}} \in X_h^{0,(j)}\}, \\ X_h^1(\Omega) &= \{\mathbf{f} \in \mathbf{H}(\mathbf{curl};\Omega) : \mathbf{f}_{|\Omega^{(j)}} \in X_h^{1,(j)}\}, \\ X_h^2(\Omega) &= \{\mathbf{f} \in \mathbf{H}(\mathrm{div};\Omega) : \mathbf{f}_{|\Omega^{(j)}} \in X_h^{2,(j)}\}, \\ X_h^3(\Omega) &= \{f \in L^2(\Omega) : f_{|\Omega^{(j)}} \in X_h^{3,(j)}\}. \end{aligned} \tag{5.27}$$

A few remarks are due. Thanks to Assumption 3.5, the control mesh $\mathcal{M}_G$ defined in (3.8) is a conforming mesh associated to Ω. Following Section 3.2, $\mathcal{M}_G$ is generated by identifying control points, or vertices, of the meshes $\mathcal{M}_G^{(i)}$, $i = 1, \dots, M_p$ which coincide. The same identification applies to edges and faces, where the orientation matters too.

With these premises, the functions in $X_h^0(\Omega)$ are obtained by identifying control variables (*i.e.*, coefficients) associated with control points that have been identified. Similarly, vector fields in $X_h^1(\Omega)$ (or $X_h^2(\Omega)$) are obtained by identifying the control variables associated to edges (or faces, respectively) that have been identified in the construction of $\mathcal{M}_G$, with a possible change of orientation. In Figure 5.2, we describe this identification for the space $X_h^1(\Omega)$. Finally, functions in $X_h^3(\Omega)$ are discontinuous across the patch interfaces.

This construction is exactly the one that would be performed in the finite element context, but we recall that this standard procedure, when applied to the control mesh $\mathcal{M}_G$, provides the correct interface condition for the underlying spline complex.

It is very easy to see that the following holds.

Proposition 5.13. Under Assumption 3.5, the spaces $(X_h^0(\Omega), \dots, X_h^3(\Omega))$ form a complex:

$$\mathbb{R} \longrightarrow X_h^0(\Omega) \xrightarrow{\mathbf{grad}} X_h^1(\Omega) \xrightarrow{\mathbf{curl}} X_h^2(\Omega) \xrightarrow{\mathrm{div}} X_h^3(\Omega) \longrightarrow 0. \tag{5.28}$$

The construction and study of commuting quasi-interpolants for multi-patch domains is beyond the scope of this work. Indeed, based on the

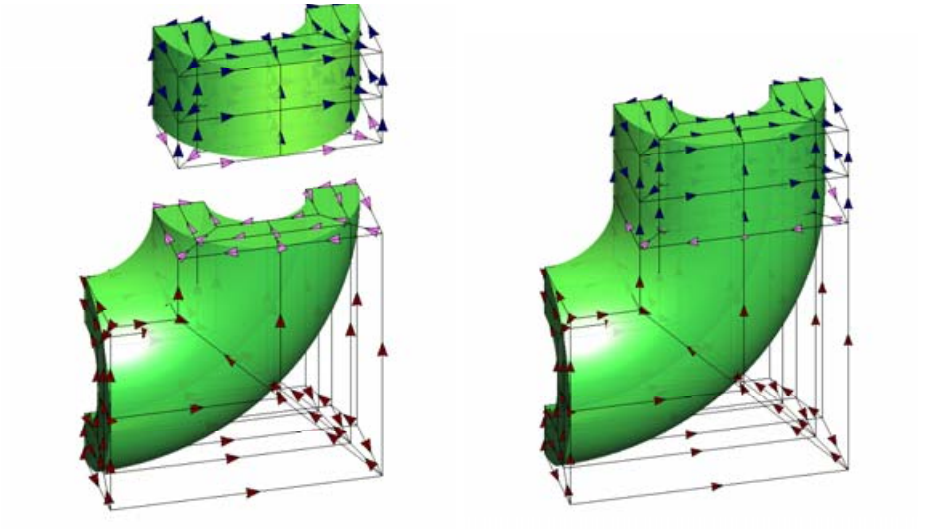

(a) (b)

Figure 5.2. Implementing continuity for $X_h^1(\Omega)$ on a two-patch domain: control variables of (a) the two patches, and (b) the merged patch. The orientation of the degrees of freedom associated to the interface edges (light arrows) is chosen as that of the lower patch. The orientation for degrees of freedom not on the interface (dark arrows) remains unchanged after merging.

definition and theory given in Section 4.4, commuting interpolants may be constructed, but they would not be L^2-stable as required by the exterior calculus theory developed in Arnold, Falk and Winther (2010). This is the reason why we do not develop them here, and we leave the construction of L^2-stable commuting projectors to future works.

5.5. The spline complex in two-dimensional domains

For convenience of the reader, we also present the construction of the spline complexes in the two-dimensional case. We do not study the approximation properties, since all the results are analogous to those in previous sections.

In the two-dimensional setting we have two different curl operators, that is, $\operatorname{rot}\mathbf{u} = (\partial_{x_1}u_2 - \partial_{x_2}u_1)$ is the scalar rotor, and $\mathbf{rot}\, u = (\partial_{x_2}u, -\partial_{x_1}u)^T$ is the vector rotor. We need to define the vector space

$$\mathbf{H}(\operatorname{rot};\Omega) = \{\mathbf{u} \in L^2(\Omega)^2 : \operatorname{rot}\mathbf{u} \in L^2(\Omega)\},$$

and setting

$$X^0 := H^1(\Omega),\ X^1 := \mathbf{H}(\operatorname{rot};\Omega),\ X^{1*} := \mathbf{H}(\operatorname{div};\Omega),\ X^2 := L^2(\Omega),$$

we have two different diagrams, namely

$$\begin{aligned} \mathbb{R} \longrightarrow X^0 \xrightarrow{\mathbf{grad}} X^1 \xrightarrow{\mathrm{rot}} X^2 \longrightarrow 0, \\ \mathbb{R} \longrightarrow X^0 \xrightarrow{\mathbf{rot}} X^{1*} \xrightarrow{\mathrm{div}} X^2 \longrightarrow 0. \end{aligned} \tag{5.29}$$

The pull-backs that relate the spaces in the physical and the parametric domain are given by

$$\begin{aligned} \iota^0(f) &:= f \circ \mathbf{F} && f \in X^0, \\ \iota^1(\mathbf{f}) &:= (D\mathbf{F})^T(\mathbf{f} \circ \mathbf{F}) && \mathbf{f} \in X^1, \\ \iota^{1*}(\mathbf{f}) &:= \det(D\mathbf{F})(D\mathbf{F})^{-1}(\mathbf{f} \circ \mathbf{F}) && \mathbf{f} \in X^{1*}, \\ \iota^2(f) &:= \det(D\mathbf{F})(f \circ \mathbf{F}) && f \in X^2. \end{aligned} \tag{5.30}$$

Following the same reasoning as for the definition of the spaces (5.3) in the three-dimensional case, we define the spline spaces in the parametric domain $\widehat{\Omega} = (0,1)^2$ by

$$\begin{aligned} \widehat{X}_h^0 &:= S_{p_1,p_2}(\Xi_1, \Xi_2), \\ \widehat{X}_h^1 &:= S_{p_1-1,p_2}(\Xi_1', \Xi_2) \times S_{p_1,p_2-1}(\Xi_1, \Xi_2'), \\ \widehat{X}_h^{1*} &:= S_{p_1,p_2-1}(\Xi_1, \Xi_2') \times S_{p_1-1,p_2}(\Xi_1', \Xi_2), \\ \widehat{X}_h^2 &:= S_{p_1-1,p_2-1}(\Xi_1', \Xi_2'). \end{aligned}$$

Note that choosing the basis functions analogously to (5.5)–(5.8), both X_h^1 and X_h^{1*} have one basis function associated to each edge of the Greville mesh $\widehat{\mathcal{M}}_G$. These functions are tangent to the edges for the space X_h^1, and normal to the edges for X_h^{1*}.

Finally, the spline complex in the physical domain is constructed as in (5.20), by simply applying the corresponding pull-backs, that is,

$$\begin{aligned} X_h^j &= \{f_h : \iota^j(f_h) \in \widehat{X}_h^j\}, && \text{for } j = 0, 2, \\ X_h^j &= \{\mathbf{f}_h : \iota^j(\mathbf{f}_h) \in \widehat{X}_h^j\}, && \text{for } j = 1, 1^*, \end{aligned} \tag{5.31}$$

and with this construction, we have the two complexes

$$\begin{aligned} \mathbb{R} \longrightarrow X_h^0 \xrightarrow{\mathbf{grad}} X_h^1 \xrightarrow{\mathrm{rot}} X_h^2 \longrightarrow 0, \\ \mathbb{R} \longrightarrow X_h^0 \xrightarrow{\mathbf{rot}} X_h^{1*} \xrightarrow{\mathrm{div}} X_h^2 \longrightarrow 0. \end{aligned} \tag{5.32}$$

The definition of the quasi-interpolants and the approximation properties for the two-dimensional spaces are very similar to those in Sections 5.2 and 5.3 for the three-dimensional case, with obvious changes. The construction of conforming spaces for two-dimensional multi-patch domains is also similar.

6. Application to elliptic and saddle point problems

After introducing the relevant discrete spaces and their approximation estimates in the previous two sections, we now apply isogeometric methods for the solution of partial differential equations by Galerkin's method, and perform some numerical testing. We will discuss the well-posedness of the discrete problem, and the convergence of the computed numerical solution to the exact one. The theory is the general one of Galerkin's methods, that is, similar to that of the finite element method, so we will not give all the details in the proofs.

This section is divided into three parts. In Section 6.1 we present the approximation of a scalar elliptic problem, and the analysis is based on the results of Section 4. In Section 6.2 we deal with the linear elasticity problem, in particular in the nearly incompressible regime, and we analyse the use of different isogeometric spaces both in displacement and displacement-pressure (*i.e.*, mixed) formulations. Finally, in Section 6.3, we consider some electromagnetic problems in the harmonic regime, using the spaces in Section 5. Along with the numerical analysis, we present for each problem some numerical tests that confirm the theoretical results, and in particular show that high-continuity splines can be efficiently used to approximate singular functions.

For simplicity the theory in this section will focus on a single-patch domain, but these can be generalized to multi-patch domains, which will indeed be used in some of the numerical tests. Throughout this section we will assume that the degree is the same in all directions, that is, $p_\ell = p$ for $\ell = 1, \dots, d$.

6.1. Scalar elliptic problems

As the first example we apply the isogeometric method to the discretization of the scalar elliptic problem (advection–reaction–diffusion equation):

$$\begin{aligned} -\operatorname{div}(A(\mathbf{x})\,\mathbf{grad}\,u) + \mathbf{b}(\mathbf{x}) \cdot \mathbf{grad}\,u + c(\mathbf{x})u = f \quad & \text{in } \Omega, \\ u = 0 \quad & \text{on } \Gamma_D, \\ \frac{\partial u}{\partial \mathbf{n}} = g_N \quad & \text{on } \Gamma_N, \end{aligned}$$

with $f \in L^2(\Omega)$ and $g_N \in L^2(\Gamma_N)$. For the coefficients, we assume that $\mathbf{b} \in \mathbf{W}^{1,\infty}(\Omega)$, $c \in L^\infty(\Omega)$ and $A(\mathbf{x}) = (a_{ij}(\mathbf{x}))_{1 \le i,j \le d}$ is a symmetric tensor with $a_{ij} \in L^\infty(\Omega)$, which satisfies the ellipticity condition

$$\sum_{i,j=1}^{d} a_{ij}(\mathbf{x})\phi_i\phi_j \ge \alpha|\boldsymbol{\phi}|^2 \quad \text{for all } \boldsymbol{\phi} \in \mathbb{R}^d.$$

We introduce the following bilinear form defined on $H^1(\Omega)$:

$$a(v,w) = \int_\Omega A(\mathbf{x})\,\mathbf{grad}\,v \cdot \mathbf{grad}\,w\,\mathrm{d}\mathbf{x} + \int_\Omega \mathbf{b}(\mathbf{x})\cdot\mathbf{grad}\,v\,w\,\mathrm{d}\mathbf{x} + \int_\Omega c(\mathbf{x})v\,w\,\mathrm{d}\mathbf{x},$$

which is continuous and coercive, provided $c(\mathbf{x}) - \frac{1}{2}\,\mathrm{div}\,\mathbf{b}(\mathbf{x}) \geq 0$ a.e. in Ω. Introducing the space

$$V_{0,\Gamma_D} = \{v \in H^1(\Omega) : v|_{\Gamma_D} = 0\},$$

the variational formulation of the problem reads as follows: find $u \in V_{0,\Gamma_D}$ such that

$$a(u,v) = \int_\Omega f\,v\,\mathrm{d}\mathbf{x} + \int_{\Gamma_N} g_N\,v\,\mathrm{d}\Gamma, \quad \text{for all } v \in V_{0,\Gamma_D}. \tag{6.1}$$

The existence and uniqueness of the solution follows from the continuity and coercivity of $a(\cdot,\cdot)$, using the Lax–Milgram lemma. The coercivity of $a(\cdot,\cdot)$ also implies the stability of the problem: there exists a constant $C > 0$ such that

$$\|u\|_{H^1(\Omega)} \leq C\big(\|f\|_{L^2(\Omega)} + \|g_N\|_{L^2(\Gamma_N)}\big). \tag{6.2}$$

We assume that the domain Ω is given by a NURBS parametrization $\mathbf{F}$, and that $\Gamma_D \subset \partial\Omega$ is the $\mathbf{F}$-image of a collection of faces of $\widehat{\Omega}$, as in Assumption 3.2. Then, we define the finite-dimensional space V_{h,Γ_D} as in (3.4), and the discrete version of problem (6.1) is as follows: find $u_h \in V_{h,\Gamma_D}$ such that

$$a(u_h,v_h) = \int_\Omega f\,v_h\,\mathrm{d}\mathbf{x} + \int_{\Gamma_N} g_N\,v_h\,\mathrm{d}\Gamma, \quad \text{for all } v_h \in V_{h,\Gamma_D}. \tag{6.3}$$

As in the continuous case, the existence and uniqueness of the solution follows from the Lax–Milgram lemma, and the stability result (6.2) is also valid for u_h. Finally, we have the following error estimate.

Theorem 6.1. Let u the solution to (6.1) belong to $H^{s+1}(\Omega)$, with $s > 0$. Then there exists a constant C independent of the mesh size h such that the solution to (6.3) satisfies

$$\|u - u_h\|_{H^1(\Omega)} \leq C h^q \|u\|_{H^{q+1}(\Omega)},$$

with $q = \min\{p, s\}$.

Proof. The proof requires the use of the quasi-interpolant $\Pi_{V_{h,\Gamma_D}}$ from Remark 4.22, which has the same approximation properties as Π_{V_h}. Since $V_{h,\Gamma_D} \subset V_{0,\Gamma_D}$, we can first apply Céa's lemma, and then the estimate for the quasi-interpolant in Corollary 4.21 with $r = 1$, to obtain

$$\begin{aligned}\|u - u_h\|_{H^1(\Omega)} &\leq C \inf_{v_h \in V_{h,\Gamma_D}} \|u - v_h\|_{H^1(\Omega)} \leq C\|u - \Pi_{V_{h,\Gamma_D}} u\|_{H^1(\Omega)} \\ &\leq C h^q \|u\|_{H^{q+1}(\Omega)}.\end{aligned}$$

□

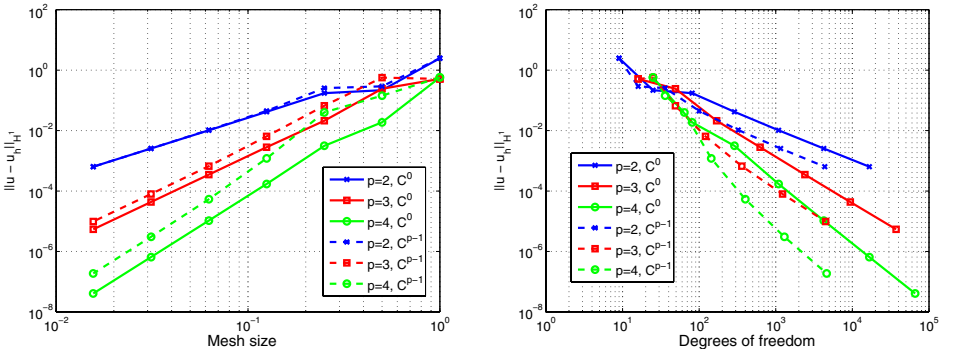

(a) (b)

Figure 6.1. Absolute error in the H^1-norm in the quarter-ring: error in terms of (a) the mesh size, and (b) the degrees of freedom.

Remark 6.2. Homogeneous Dirichlet conditions are imposed, setting to zero the degrees of freedom associated to boundary control points. To impose non-homogeneous Dirichlet conditions, a lifting $\widetilde{u}_h \in H^1(\Omega)$ satisfying $\widetilde{u}_h|_{\Gamma_D} = g_D$ must be constructed. Since B-splines and NURBS are not interpolatory at the knots, the lifting can be computed using a surface fitting technique, such as the least-squares approximation; see, for instance, Cottrell *et al.* (2009, Chapter 3) and Govindjee, Strain, Mitchell and Taylor (2012).

Numerical tests

Test 1. The first numerical test consists of a simple geometry: a quarter-ring with inner and outer radius equal to 1 and 2, respectively, and described via a quadratic NURBS parametrization, such as the one in Figure 3.1. We solve the Poisson problem, that is, $\mathbf{b} = \mathbf{0}$ and $c = 0$, with non-homogeneous Dirichlet boundary conditions on the boundary. The right-hand side f is imposed to obtain the exact solution $u = \mathrm{e}^{x_1} \sin(x_2)$, which is infinitely smooth.

We solve the problem in a set of successively refined meshes, for degree p varying from 2 to 4, and in NURBS spaces of maximum (C^{p-1}) and minimum (C^0) continuity. In Figure 6.1 we present the error in the H^1-norm with respect to the mesh size h, and with respect to the number of degrees of freedom N_{dof}. The results in terms of the mesh size confirm the estimate of Theorem 6.1, and show that in the same mesh lower continuity gives better accuracy, since the C^{p-1}-space is contained in the C^0-space. In terms of the degrees of freedom, the result always converges like $O(N_{\mathrm{dof}}^{-p/2})$, and in this case the C^{p-1}-spaces give better results. The relation between the number of degrees of freedom and the computational cost will be discussed in Section 8.

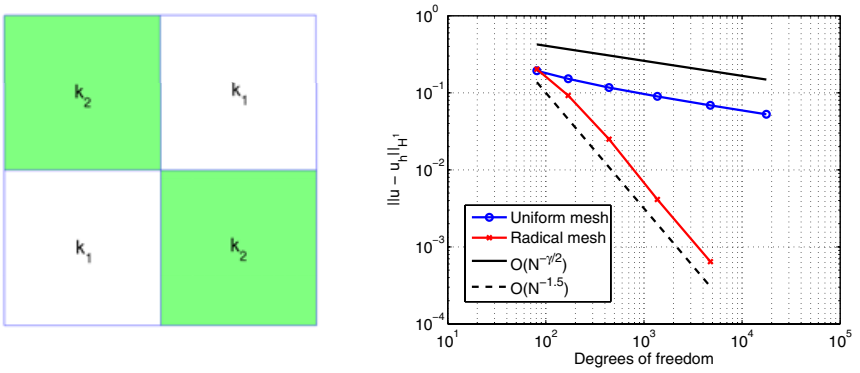

(a) (b)

Figure 6.2. Chessboard domain: distribution of the coefficients and error in the H^1-norm. (a) Coefficients in the chessboard pattern. (b) Absolute error in the H^1-norm.

Test 2. For the second numerical test we choose the same problem with discontinuous coefficients given in Morin, Nochetto and Siebert (2002) and Petzoldt (2001), and derived from the results in Kellogg (1974/75). The domain is the square $\Omega = (-1,1)^2$, with the coefficient $A = k_i I$ in the ith quadrant, with I the identity tensor, and again $\mathbf{b} = \mathbf{0}$ and $c = 0$. An exact weak solution for $f = 0$, and for non-homogeneous Dirichlet boundary conditions, is given in polar coordinates by $u = r^\gamma \mu(\theta)$, with

$$\mu(\theta) = \begin{cases} \cos((\pi/2-\sigma)\gamma)\,\cos((\theta-\pi/2+\rho)\gamma) & \text{if } 0 \le \theta \le \pi/2, \\ \cos(\rho\gamma)\,\cos((\theta-\pi+\sigma)\gamma) & \text{if } \pi/2 \le \theta \le \pi, \\ \cos(\sigma\gamma)\,\cos((\theta-\pi-\rho)\gamma) & \text{if } \pi \le \theta \le 3\pi/2, \\ \cos((\pi/2-\rho)\gamma)\,\cos((\theta-3\pi/2-\sigma)\gamma) & \text{if } 3\pi/2 \le \theta \le 2\pi. \end{cases}$$

The scalars γ, ρ and σ, and the coefficients k_i must be chosen in such a way that the function μ satisfies the condition along the interfaces,

$$k_{i-1}\mu'(\theta_i^-) = k_i \mu'(\theta_i^+), \quad i = 1, \dots, 4,$$

with $\theta_i = (i-1)\pi/2$, and assuming for convenience $k_0 = k_4$. In the most common examples, the materials are configured in a chessboard pattern, as in Figure 6.2(a). In this case, one can choose $\gamma \in (0,1]$ and then set $\rho = \pi/4$, $\sigma = (1+\frac{1}{\gamma})\frac{\pi}{2} - \rho$, and the interface conditions are satisfied with $k_1 = k_3 = -\tan(\gamma\sigma)$ and $k_2 = k_4 = \tan(\gamma\rho)$. This produces a singular solution $u \notin H^{1+\gamma}(\Omega)$ and $u \in H^{1+\gamma-\varepsilon}(\Omega)$ for any $\varepsilon > 0$.

We have solved the problem in the chessboard domain for the ratio $k_1/k_2 = 10$, which corresponds to $\gamma \approx 0.39$. The square is divided into four

patches, and the problem is discretized with cubic splines and C^2-continuity within each patch, setting C^0-continuity along the interfaces. The results in Figure 6.2(b) show that, in a uniform mesh, the absolute error in the H^1-norm converges like $O(N_{\text{dof}}^{-\gamma/2})$, with N_{dof} the number of degrees of freedom. Using a tensor product radical graded mesh as in Beirão da Veiga *et al.* (2012*c*) (see also Babuška and Strouboulis 2001, Section 3.4), with the univariate knots on each patch defined as

$$\zeta_j = \left(\frac{j-1}{N-1}\right)^{\alpha}$$

and $\alpha = 7$, we can recover the optimal convergence $O(N_{\text{dof}}^{-p/2})$. However, for stronger singularities and high degree p, the optimal convergence may not be recovered unless higher precision is employed in the numerical computation, as already noticed for the finite element case in Babuška and Strouboulis (2001, Section 3.4) and references therein.

Remark 6.3. In all the previous tests we have considered a pure diffusion case, with $\mathbf{b} = \mathbf{0}$ and $c = 0$. Design and numerical benchmarking of isogeometric methods for advection-dominated or reaction-dominated problems can be found in Hughes *et al.* (2005), Buffa, Cho and Kumar (2012), Dörfel, Jüttler and Simeon (2010) and Speleers *et al.* (2012).

6.2. Linear elasticity

We consider the linear elasticity model problem, which consists of finding the displacement vector $\mathbf{u} \in H^1(\Omega)^d$ such that

$$\begin{aligned} -\operatorname{div}(\sigma(\mathbf{u})) &= \mathbf{f} && \text{in } \Omega, \\ \sigma(\mathbf{u})\mathbf{n} &= \mathbf{g}_N && \text{on } \Gamma_N, \\ \mathbf{u} &= \mathbf{0} && \text{on } \Gamma_D, \end{aligned}$$

with $\mathbf{f} \in L^2(\Omega)^d$, $\mathbf{g}_N \in L^2(\Gamma_N)^d$ and $\sigma(\mathbf{u})$ the Cauchy stress tensor, which is given by

$$\sigma(\mathbf{u}) = 2\mu\epsilon(\mathbf{u}) + \lambda \operatorname{div}(\mathbf{u}) I,$$

where I is the identity matrix, $\lambda > 0$ and $\mu > 0$ are the Lamé parameters of the material, and $\epsilon(\mathbf{u})$ is the strain tensor, which is the symmetric part of the displacement gradient. In the engineering literature, it is more usual to give the material properties in terms of Young's modulus E, and Poisson's ratio ν. These are related to Lamé parameters by the equations

$$\lambda = \frac{\nu E}{(1+\nu)(1-2\nu)}, \quad \mu = \frac{E}{2(1+\nu)},$$

which for $d = 2$ represents a problem in the plane strain regime.

Let us now introduce the following bilinear form defined on $H^1(\Omega)^d$,

$$a(\mathbf{u},\mathbf{v}) = \int_\Omega 2\mu\,\epsilon(\mathbf{u}) : \epsilon(\mathbf{v})\,\mathrm{d}\mathbf{x} + \int_\Omega \lambda\,\mathrm{div}\,\mathbf{u}\,\mathrm{div}\,\mathbf{v}\,\mathrm{d}\mathbf{x},$$

and the space $V_{0,\Gamma_D} := \{u \in H^1(\Omega) : u = 0 \text{ on } \Gamma_D\}$. Then the problem in weak form reads as follows: find $\mathbf{u} \in (V_{0,\Gamma_D})^d$ such that

$$a(\mathbf{u},\mathbf{v}) = \int_\Omega \mathbf{f}\cdot\mathbf{v}\,\mathrm{d}\mathbf{x} + \int_{\Gamma_N} \mathbf{g}_N\cdot\mathbf{v}\,\mathrm{d}\Gamma \quad \text{for all } \mathbf{v} \in (V_{0,\Gamma_D})^d. \tag{6.4}$$

The existence and uniqueness of the solution to this problem, provided that $\Gamma_D \neq \emptyset$, is a classical result. It follows from the continuity and coercivity of $a(\cdot,\cdot)$, which is a consequence of Korn's inequality: see Section 1.2 in Ciarlet (2002).

For the discretization we again assume that the domain Ω is given by a NURBS parametrization $\mathbf{F}$, and as before, the boundary Γ_D is the $\mathbf{F}$-image of a collection of faces of $\widehat{\Omega}$. We are going to solve the problem with several choices for the discrete space, and thus we write the variational formulation of the problem for any finite-dimensional space $X_{h,\Gamma_D} \subset (V_{0,\Gamma_D})^d$. With this notation, the discrete problem takes the following general form: find $\mathbf{u}_h \in X_{h,\Gamma_D}$ such that

$$a(\mathbf{u}_h,\mathbf{v}_h) = \int_\Omega \mathbf{f}\cdot\mathbf{v}_h\,\mathrm{d}\mathbf{x} + \int_{\Gamma_N} \mathbf{g}_N\cdot\mathbf{v}_h\,\mathrm{d}\Gamma \quad \text{for all } \mathbf{v}_h \in X_{h,\Gamma_D}. \tag{6.5}$$

Since this is a conforming discretization, that is, $X_{h,\Gamma_D} \subset (V_{0,\Gamma_D})^d$, the well-posedness of the problem is proved exactly as for the continuous case.

The most common choice to solve (6.5) is to make use of the isoparametric paradigm, and to consider the space of vector fields $X_{h,\Gamma_D} = (V_{h,\Gamma_D})^d$, with the scalar space V_{h,Γ_D} given by (3.4). With this choice the following theorem, which is the analogue of Theorem 6.1 for the elliptic scalar problem, gives the convergence of the method to the exact solution. We do not present the proof here, as it is very similar to the one in the scalar case.

Theorem 6.4. Let $\mathbf{u}$, the solution to (6.4), belong to $H^{s+1}(\Omega)^d$, with $s > 0$. Then there exists a constant C independent of the mesh size h, but dependent on the parameters μ and λ, such that the solution to (6.5) satisfies

$$\|\mathbf{u} - \mathbf{u}_h\|_{H^1(\Omega)^d} \leq C h^q \|\mathbf{u}\|_{H^{q+1}(\Omega)^d},$$

with $q = \min\{p, s\}$.

An interesting feature of the solution of elasticity problems with the isogeometric method proposed above is the representation of the deformed geometry. In fact, each control point of the control net is associated to d degrees of freedom, which are the components of the displacement. Writing

these d degrees of freedom as a vector, it is trivial to see that the deformed geometry is obtained as a NURBS parametrization, by applying the computed displacement to their corresponding control points. Indeed, recalling the definition of the basis functions (3.3), the position of the material points after deformation is given by

$$\mathbf{x} + \mathbf{u}_h(\mathbf{x}) = \mathbf{F}(\boldsymbol{\zeta}) + \sum_{\mathbf{i}\in\mathbf{I}} \boldsymbol{\alpha}_\mathbf{i} N_{\mathbf{i},\mathbf{p}}(\mathbf{x}) = \sum_{\mathbf{i}\in\mathbf{I}} \mathbf{c}_\mathbf{i} \widehat{N}_{\mathbf{i},\mathbf{p}}(\boldsymbol{\zeta}) + \sum_{\mathbf{i}\in\mathbf{I}} \boldsymbol{\alpha}_\mathbf{i} \widehat{N}_{\mathbf{i},\mathbf{p}}(\boldsymbol{\zeta}), \quad (6.6)$$

which is a NURBS parametrization with control points $\mathbf{c}_\mathbf{i} + \boldsymbol{\alpha}_\mathbf{i}$. This property is particularly interesting for the approximation of nonlinear problems, where the nonlinearity is solved with an iterative procedure, and the deformed geometry must be recomputed at every iteration. This representation of the deformed geometry as a NURBS holds due to the isoparametric concept. If one were to discretize the problem in a NURBS geometry with the spline space as in Remark 3.4, which is non-isoparametric, the same would not hold.

6.2.1. Nearly incompressible elasticity

In the case of nearly incompressible elasticity, that is, when $\nu \approx 0.5$ (and consequently $\lambda \gg 1$), the discretization above suffers from 'volumetric locking' due to lack of stability, similar to classical finite elements. A possible approach is to rewrite the problem in an equivalent mixed form. In this section we start presenting some possibilities for the discretization of the mixed problem with isogeometric methods. Moreover, we take advantage of the higher continuity of splines with respect to finite elements to present a solution of the problem based on the $\mathbf{H}(\mathrm{div})$-conforming space defined in Section 5. We remark that the same space has been applied to the solution of incompressible Stokes and Navier–Stokes equations in Buffa *et al.* (2011*a*) and Evans and Hughes (2013*a*, 2013*b*, 2013*c*), to obtain numerical solutions which are pointwise divergence-free.

First we introduce the equivalent mixed formulation of the problem. Introducing the pressure $\pi = \lambda \operatorname{div} \mathbf{u}$, problem (6.4) is equivalent to the following one: find $\mathbf{u} \in (V_{0,\Gamma_D})^d$ and $\pi \in L^2(\Omega)$ such that

$$\int_\Omega 2\mu\, \epsilon(\mathbf{u}) : \epsilon(\mathbf{v})\, \mathrm{d}\mathbf{x} + \int_\Omega \pi \operatorname{div} \mathbf{v}\, \mathrm{d}\mathbf{x} = \int_\Omega \mathbf{f} \cdot \mathbf{v}\, \mathrm{d}\mathbf{x} + \int_{\Gamma_N} \mathbf{g}_N \cdot \mathbf{v}\, \mathrm{d}\Gamma$$

for all $\mathbf{v} \in (V_{0,\Gamma_D})^d$, and

$$-\int_\Omega \frac{1}{\lambda} \pi\, q\, \mathrm{d}\mathbf{x} + \int_\Omega q \operatorname{div} \mathbf{u}\, \mathrm{d}\mathbf{x} = 0$$

for all $q \in L^2(\Omega)$.

To solve this problem, it is necessary to choose a pair of finite-dimensional spaces, one for the displacement and one for the pressure. As before,

we write the discrete version of the problem for a general pair of spaces (X_{h,Γ_D}, P_h) such that $X_{h,\Gamma_D} \subset (V_{0,\Gamma_D})^d$ and $P_h \subset L^2(\Omega)$. With this notation, the problem is to find $\mathbf{u}_h \in X_{h,\Gamma_D}$ and $\pi_h \in P_h$ such that

$$\int_\Omega 2\mu\,\epsilon(\mathbf{u}_h) : \epsilon(\mathbf{v}_h)\,\mathrm{d}\mathbf{x} + \int_\Omega \pi_h \operatorname{div}\mathbf{v}_h\,\mathrm{d}\mathbf{x} = \int_\Omega \mathbf{f}\cdot\mathbf{v}_h\,\mathrm{d}\mathbf{x} + \int_{\Gamma_N} \mathbf{g}_N\cdot\mathbf{v}_h\,\mathrm{d}\Gamma \tag{6.7a}$$

for all $\mathbf{v}_h \in X_{h,\Gamma_D}$, and

$$-\int_\Omega \frac{1}{\lambda}\pi_h\, q_h\,\mathrm{d}\mathbf{x} + \int_\Omega q_h \operatorname{div}\mathbf{u}_h\,\mathrm{d}\mathbf{x} = 0 \tag{6.7b}$$

for all for all $q_h \in P_h$.

To ensure stability of the problem, the pair of discrete spaces (X_{h,Γ_D}, P_h) must satisfy the following inf-sup condition (see, *e.g.*, Section 5.5 in Boffi, Brezzi and Fortin 2013). There exists a constant $\alpha > 0$, independent of the mesh size h, such that

$$\sup_{\mathbf{v}_h \in X_{h,\Gamma_D}} \frac{\int_\Omega q_h \operatorname{div}\mathbf{v}_h\,\mathrm{d}\mathbf{x}}{\|\mathbf{v}_h\|_{H^1(\Omega)^d}} \geq \alpha \|q_h\|_{L^2(\Omega)}, \quad \text{for all } q_h \in P_h. \tag{6.8}$$

Bressan and Sangalli (2013) have introduced sufficient conditions for pairs of NURBS spaces to ensure that the the inf-sup condition is satisfied. In particular, given a parametrization in the coarse space $\mathbf{F} \in (N_{\mathbf{p}^0}(\boldsymbol{\Xi}^0, W))^d$, it is proved that the following two families of spaces produce stable approximations.

- *Isogeometric Taylor–Hood* (Bazilevs *et al.* 2006, Bressan 2011, Bressan and Sangalli 2013). Let $N_{\mathbf{p}}(\boldsymbol{\Xi}, W)$ be a refinement of the coarse space $N_{\mathbf{p}^0}(\boldsymbol{\Xi}^0, W)$, and let $N_{\mathbf{p}+1}(\boldsymbol{\Xi}_{p+1}, W)$ be obtained by raising the degree to $p+1$ and maintaining the same regularity at the element interfaces as in $N_{\mathbf{p}}(\boldsymbol{\Xi}, W)$. Then we choose the pair of spaces

  $$X_h = \{\mathbf{v} = \widehat{\mathbf{v}} \circ \mathbf{F}^{-1} : \widehat{\mathbf{v}} \in (N_{\mathbf{p}+1}(\boldsymbol{\Xi}_{p+1}, W))^d\},\ X_{h,\Gamma_D} = X_h \cap (V_{0,\Gamma_D})^d,$$
  $$P_h = \{q = \widehat{q} \circ \mathbf{F}^{-1} : \widehat{q} \in N_{\mathbf{p}}(\boldsymbol{\Xi}, W)\}.$$

- *Isogeometric subgrid* (Bressan and Sangalli 2013, Rüberg and Cirak 2012). Let $N_{\mathbf{p}}(\boldsymbol{\Xi}, W)$ be constructed from the coarse space $N_{\mathbf{p}^0}(\boldsymbol{\Xi}^0, W)$ by k-refinement, and let $N_{\mathbf{p}+1}(\boldsymbol{\Xi}_{h/2}, W)$ be constructed by k-refinement, subdividing each element of the knot vector $\boldsymbol{\Xi}$ into 2^d elements. Then we consider the pair

  $$X_h = \{\mathbf{v} = \widehat{\mathbf{v}} \circ \mathbf{F}^{-1} : \widehat{\mathbf{v}} \in (N_{\mathbf{p}+1}(\boldsymbol{\Xi}_{h/2}, W))^d\},\ X_{h,\Gamma_D} = X_h \cap (V_{0,\Gamma_D})^d,$$
  $$P_h = \{q = \widehat{q} \circ \mathbf{F}^{-1} : \widehat{q} \in N_{\mathbf{p}}(\boldsymbol{\Xi}, W)\}.$$

  We note that the subgrid method attains maximum regularity for both displacement and pressure.

Now we present an alternative pair based on the spaces of Section 5. In the following we assume that the parametrization $\mathbf{F} \in (N_{\mathbf{p}}(\boldsymbol{\Xi}, W))^d$, and the functions of the space $\widehat{X}_h^0 = S_{\mathbf{p}}(\boldsymbol{\Xi})$, have at least C^1-continuity, that is, the multiplicity of the knots is $m_{\ell,i} \leq p_\ell - 1$. Under this assumption, the functions of the $\mathbf{H}(\mathrm{div})$-conforming spaces X_h^2 defined in (5.20) for $d = 3$, or X_h^{1*} defined in (5.31) for $d = 2$, are ensured to be continuous. That is, due to the higher continuity of splines and NURBS we have that $X_h^2 \subset H^1(\Omega)^3$ and $X_h^{1*} \subset H^1(\Omega)^2$. Concerning the boundary Γ_D, in addition to Assumption 3.2 we also assume that it is the $\mathbf{F}$-image of *disjoint* faces of $\widehat{\Omega}$. We then define the pair of spaces

$$X_h = \begin{cases} X_h^{1*} & \text{for } d = 2, \\ X_h^2 & \text{for } d = 3, \end{cases} \qquad X_{h,\Gamma_D} = X_h \cap (V_{0,\Gamma_D})^d,$$
$$P_h = \begin{cases} X_h^2 & \text{for } d = 2, \\ X_h^3 & \text{for } d = 3. \end{cases} \tag{6.9}$$

With the choices above for X_h and P_h and the assumption on the boundary Γ_D, the mixed variational formulation (6.7) is well posed from the algebraic point of view. This is a consequence of the following result.

Proposition 6.5. Let X_{h,Γ_D} and P_h as in (6.9). Then, for every $q_h \in P_h$ there exists $\mathbf{v}_h \in X_{h,\Gamma_D}$ such that $\operatorname{div} \mathbf{v}_h = q_h$.

Proof. It is enough to prove the result in the parametric domain $\widehat{\Omega}$, and then the same holds in the physical domain Ω using the diagram (5.19) and the regularity of $\mathbf{F}$ from Assumption 3.1. We write the proof for $d = 2$, but the same holds for $d = 3$.

Since Γ_D is the $\mathbf{F}$-image of disjoint faces of the unit square, it is the image of at most two faces, and we can assume without loss of generality that in the parametric domain we have either $\widehat{\Gamma}_D = \{0\} \times (0, 1)$, or $\widehat{\Gamma}_D = \{0, 1\} \times (0, 1)$. In the first case, given $\widehat{q}_h \in \widehat{P}_h := \widehat{X}_h^2$, we define the two components of $\widehat{\mathbf{v}}_h$ as

$$\widehat{v}_1(\zeta_1, \zeta_2) = \int_0^{\zeta_1} \widehat{q}_h(s, \zeta_2)\, \mathrm{d}s, \quad \widehat{v}_2(\zeta_1, \zeta_2) = 0,$$

and it is trivial to see that $\widehat{\mathbf{v}}_h \in \widehat{X}_h^{1*}$, $\widehat{\operatorname{div}}\, \widehat{\mathbf{v}}_h = \widehat{q}_h$ and $\widehat{\mathbf{v}}_h = \mathbf{0}$ on $\widehat{\Gamma}_D$. The construction in the second case is more intricate. We first note that, since $\widehat{q}_h \in \widehat{X}_h^2 = S_{p_1-1,p_2-1}(\Xi_1', \Xi_2')$, by the surjectivity of the univariate derivative there exists $\varphi \in S_{p_2}(\Xi_2)$ such that

$$\varphi'(\zeta_2) = \int_0^1 \widehat{q}_h(s, \zeta_2)\, \mathrm{d}s.$$

Let $b \in S_{p_1-1}(\Xi_1')$ such that $b(0) = b(1) = 0$ and $\int_0^1 b(s)\, \mathrm{d}s = 1$. Now we

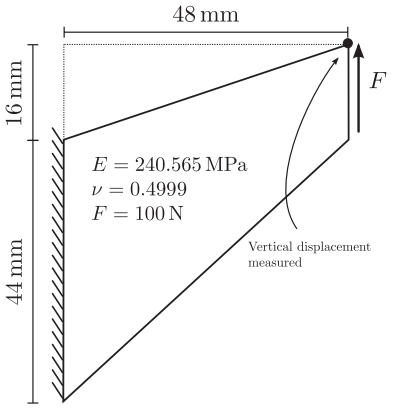

Figure 6.3. Cook's membrane: geometry, loads and material properties.

define the two components of $\widehat{\mathbf{v}}_h$ as

$$\widehat{v}_1(\zeta_1,\zeta_2) = \int_0^{\zeta_1} (\widehat{q}_h(s,\zeta_2) - b(s)\varphi'(\zeta_2))\,\mathrm{d}s, \quad \widehat{v}_2(\zeta_1,\zeta_2) = b(\zeta_1)\varphi(\zeta_2).$$

It is then easy to check that $\widehat{\mathbf{v}}_h \in \widehat{X}_h^{1*}$, $\widehat{\operatorname{div}}\,\widehat{\mathbf{v}}_h = \widehat{q}_h$ and $\widehat{\mathbf{v}}_h = \mathbf{0}$ on $\widehat{\Gamma}_D$. □

Remark 6.6. The previous result is valid thanks to the special choice of Γ_D as the image of disjoint faces of $\widehat{\Omega}$. The same is not true if Γ_D contains two adjacent faces, as was noted in Buffa *et al.* (2011*a*). In this case, one can prove a similar result for a space where only the normal components of the solution vanish at the boundary: see Proposition 5.3 in Evans and Hughes (2013*a*). The same paper proposes imposition of the boundary conditions for the tangential components in a weak form.

It is important to note that when we approximate the problem with the $\mathbf{H}(\mathrm{div})$-conforming space, the displacement and the mixed formulation are equivalent.

Proposition 6.7. Let X_{h,Γ_D} and P_h as in (6.9). Then $\mathbf{u}_h \in X_{h,\Gamma_D}$ is a solution to (6.5) if and only if $\mathbf{u}_h \in X_{h,\Gamma_D}$ and $\pi_h = \lambda \operatorname{div} \mathbf{u}_h \in P_h$ are solutions to (6.7).

Proof. The result is an immediate consequence of the surjectivity of the divergence onto P_h, proved in Proposition 6.5. □

Numerical tests

As the numerical test we consider Cook's membrane, a standard benchmark problem in the engineering literature, which has already been tested with isogeometric methods in Elguedj *et al.* (2008). The geometry and the setting of the problem are explained in Figure 6.3. The domain is a tapered panel

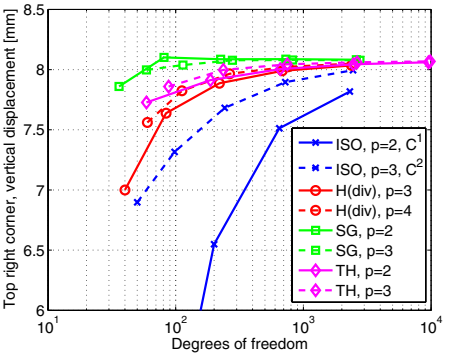

Figure 6.4. Cook's membrane: vertical displacement at the top right corner.

clamped on one side and subjected to a uniform shear load on the opposite side, which is imposed by the boundary condition $\mathbf{g}_N$. Note that $\nu \approx 0.5$, which is the condition of near-incompressibility.

To study the performance of the method, and in particular the locking effect, the standard approach is to measure the vertical displacement of the top right corner of the panel. In Figure 6.4 we compare the results obtained when solving the displacement formulation (6.5) by the standard isoparametric discretization, and with the $\mathbf{H}(\mathrm{div})$-conforming elements, and the mixed formulation (6.7) for isogeometric Taylor–Hood and subgrid elements. The comparison is done in terms of the total number of degrees of freedom, comprising the pressure space for the mixed methods. Since $\mathbf{H}(\mathrm{div})$-conforming elements are anisotropic with respect to the degree, we select degrees in order to compare approximations of the same order of accuracy (indeed, for mixed degrees p and $p-1$ we expect maximal convergence rate of order $p-1$ in the H^1-norm, according to Corollary 5.12).

The Taylor–Hood and subgrid-element mixed formulations are the most accurate. In particular, the subgrid approach, based on the smoothest splines, attains the best results: this is indeed consistent with the general observation that the k-refined method delivers the highest accuracy per degree of freedom. We also note the peculiar behaviour of the $\mathbf{H}(\mathrm{div})$-conforming element which, implemented in a displacement formulation, gives a far more accurate and locking-free displacement compared to the plain isoparametric–isogeometric element, with a stress (directly computed from the displacement) that is not polluted by unphysical oscillations (see Figure 6.5). It is possible to derive a displacement-only formulation from pressure-displacement mixed formulations as well, as is proposed for the $\bar{B}$ and $\bar{F}$ method. Although this typically produces a full stiffness matrix, it can be implemented efficiently as proposed in Elguedj *et al.* (2008), to which we refer for all the details.

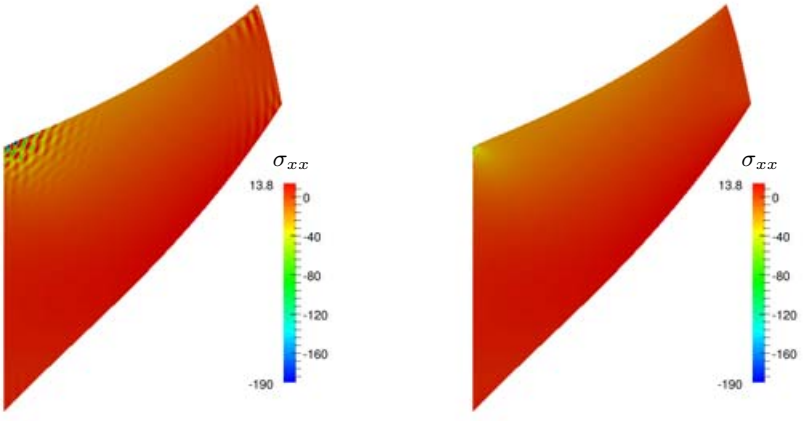

(a) (b)

Figure 6.5. Comparison of the σ_{xx} component of the stress tensor in the deformed configuration: (a) isoparametric discretization, and (b) $\mathbf{H}(\mathrm{div})$-conforming discretization.

6.3. Time-harmonic Maxwell equations

In this section we use the spline spaces for vector fields in Section 5 for the discretization of Maxwell equations. For the sake of simplicity, the theoretical discussion is restricted to the single-patch isogeometric method, but the numerical tests are performed in a more general setting.

6.3.1. Eigenvalue problem: cavity resonator

Given a bounded and simply connected domain $\Omega \subset \mathbb{R}^3$ with connected boundary $\partial\Omega$, we look for a scalar wavenumber κ and a non-zero electric field $\mathbf{E}$ such that

$$\begin{aligned} \mathbf{curl}(\mu_r^{-1}\,\mathbf{curl}\,\mathbf{E}) - \kappa^2\epsilon_r\mathbf{E} = \mathbf{0} \quad &\text{in } \Omega, \\ \mathbf{E}\times\mathbf{n} = \mathbf{0} \quad &\text{on } \partial\Omega, \end{aligned}$$

where μ_r and ϵ_r are the relative magnetic permeability and the relative electric permittivity, respectively. We assume that they are real-valued, strictly positive, and piecewise constant functions.

The variational formulation of the problem reads as follows: find $\mathbf{E} \in \mathbf{H}_0(\mathbf{curl};\Omega)$ and $\kappa \in \mathbb{R}$ such that

$$\int_\Omega \mu_r^{-1}\,\mathbf{curl}\,\mathbf{E}\cdot\mathbf{curl}\,\mathbf{v}\,\mathrm{d}\mathbf{x} = \kappa^2\int_\Omega \epsilon_r\mathbf{E}\cdot\mathbf{v}\,\mathrm{d}\mathbf{x}, \quad \text{for all } \mathbf{v}\in\mathbf{H}_0(\mathbf{curl};\Omega). \tag{6.10}$$

The solutions of the eigenvalue problem are closely related to the Helmholtz

decomposition:

$$\mathbf{H}_0(\mathbf{curl};\Omega) = \mathbf{Z}_0(\epsilon_r,\Omega) \oplus \mathbf{grad}(H^1_0(\Omega)), \tag{6.11}$$

with

$$\mathbf{Z}_0(\epsilon_r,\Omega) := \left\{ \mathbf{u} \in \mathbf{H}_0(\mathbf{curl};\Omega) : \int_\Omega \epsilon_r \mathbf{u} \cdot \mathbf{grad}\, \phi \,\mathrm{d}\mathbf{x} = 0 \text{ for all } \phi \in H^1_0(\Omega) \right\}.$$

We have the following result (Monk 2003, Theorem 4.18).

Theorem 6.8. The solutions of the eigenvalue problem (6.10) have the following properties.

- The eigenvalue $\kappa = 0$ is associated to an infinite family of eigenfunctions $\mathbf{E} = \mathbf{grad}\,\phi$ for any $\phi \in H^1_0(\Omega)$.
- There is an infinite set of eigenvalues $0 < \kappa_1 \le \kappa_2 \le \cdots$, with $\lim_{j\to\infty} \kappa_j = \infty$, and corresponding eigenfunctions $\mathbf{0} \neq \mathbf{E}_j \in \mathbf{Z}_0(\epsilon_r,\Omega)$.

Following Boffi, Fernandes, Gastaldi and Perugia (1999), the approximation of problem (6.10) with nodal finite elements is known to generate spurious eigenmodes, due to inexact approximations of the infinite family of zero eigenvalues. In contrast, Nédélec edge elements of the first class (Nédélec 1980), which are $\mathbf{H}(\mathbf{curl};\Omega)$-conforming, give good approximations of the same problem. The proof relies on the existence of a de Rham diagram with commuting projectors. With similar arguments, Buffa *et al.* (2011*b*) prove that a discretization of the eigenvalue problem based on the spline spaces in Section 5 is also spurious-free. We summarize the main results.

Assuming that the domain Ω is defined by a single-patch NURBS parametrization, we consider the discrete space $X^1_{0,h} = X^1_h \cap \mathbf{H}_0(\mathbf{curl};\Omega)$, with X^1_h defined as in (5.20). Then, the variational formulation of the discrete problem is as follows: find $\mathbf{E}_h \in X^1_{0,h}$ and $\kappa_h \in \mathbb{R}$ such that

$$\int_\Omega \mu_r^{-1}\, \mathbf{curl}\, \mathbf{E}_h \cdot \mathbf{curl}\, \mathbf{v}_h \,\mathrm{d}\mathbf{x} = \kappa_h^2 \int_\Omega \epsilon_r \mathbf{E}_h \cdot \mathbf{v}_h \,\mathrm{d}\mathbf{x}, \quad \text{for all } \mathbf{v}_h \in X^1_{0,h}. \tag{6.12}$$

Thanks to commutative diagram (5.23) (in fact its analogue with boundary conditions), we have for the space $X^1_{0,h}$ a discrete version of the Helmholtz decomposition (6.11):

$$X^1_{0,h} = \mathbf{Z}_{0,h}(\epsilon_r,\Omega) \oplus \mathbf{grad}(X^0_{0,h}),$$

with

$$\mathbf{Z}_{0,h}(\epsilon_r,\Omega) := \left\{ \mathbf{u}_h \in X^1_{0,h} : \int_\Omega \epsilon_r \mathbf{u}_h \cdot \mathbf{grad}\, \phi_h \,\mathrm{d}\mathbf{x} = 0 \text{ for all } \phi_h \in X^0_{0,h} \right\},$$

and $X^0_{0,h} = X^0_h \cap H^1_0(\Omega)$, the discrete scalar space with boundary conditions.

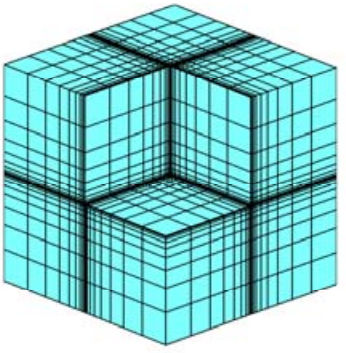

Figure 6.6. Mesh for Fichera's corner.

Moreover, and analogously to the continuous case, the eigenvalue $\kappa_h = 0$ is associated to the finite-dimensional space $\mathbf{grad}(X^0_{0,h})$. The rest of the eigenvalues are strictly positive, and their associated eigenfunctions belong to $\mathbf{Z}_{0,h}(\epsilon_r, \Omega)$.

The spectral correctness and the convergence of the solutions of the discrete eigenvalue problem (6.12) to those of (6.10) follow from the theory of finite element exterior calculus (Arnold *et al.* 2010). In particular, thanks to the classical compactness result from Picard (1984), the commutative diagram (5.23) and the stability of the projectors in the L^2-norm from Corollary 5.12, we can apply Theorem 3.19 in Arnold *et al.* (2010) to show the convergence of the associated vector Hodge–Laplacian eigenvalue problem:

$$\int_\Omega \phi_h \psi_h \,\mathrm{d}\mathbf{x} - \int_\Omega \epsilon_r \mathbf{E}_h \cdot \mathbf{grad}\, \psi_h \,\mathrm{d}\mathbf{x} = 0$$

for all $\psi_h \in X^0_{0,h}$, and

$$\int_\Omega \mu_r^{-1}\, \mathbf{curl}\, \mathbf{E}_h \cdot \mathbf{curl}\, \mathbf{v}_h \,\mathrm{d}\mathbf{x} + \int_\Omega \epsilon_r \mathbf{v}_h \cdot \mathbf{grad}\, \phi_h \,\mathrm{d}\mathbf{x} = \kappa_h^2 \int_\Omega \epsilon_r \mathbf{E}_h \cdot \mathbf{v}_h \,\mathrm{d}\mathbf{x}$$

for all $\mathbf{v}_h \in X^1_{0,h}$. The convergence for our problem follows from this one by using the commutative diagram and the Helmholtz decompositions, as is explained in Arnold *et al.* (2010, Section 3.6.1). See also Section 6 in the same paper to see how to deal with variable coefficients and boundary conditions.

Numerical test

We solve the eigenvalue problem in *Fichera's corner*, that is, the domain defined by $\Omega = (-1,1)^3 \setminus [0,1]^3$ and $\mu_r = \epsilon_r = 1$. Using linear splines, we define the domain as a multi-patch geometry given by seven patches. On each patch we impose a tensor product mesh with 12 elements in each direction, refined towards the corner and the re-entrant edges with a radical

Table 6.1. Eigenvalues in Fichera's corner, comparing finite element computations by Duruflé with isogeometric algorithms (IGA).

Eig.	Duruflé, $p=5$	IGA, $p=3$	IGA, $p=4$	IGA, $p=5$
1	3.21987401386	3.21987496658	3.21988066916	3.21988316848
2	5.88041891178	5.88041920051	5.88041871891	5.88041854438
3	5.88041891780	5.88041920051	5.88041871897	5.88041854605
4	10.6854921311	10.6854887693	10.6854782775	10.6854756735
5	10.6937829409	10.6937804726	10.6937680695	10.6937640480
6	10.6937829737	10.6937804726	10.6937680701	10.6937640484
7	12.3165204656	12.3165080267	12.3164992881	12.3164998491
8	12.3165204669	12.3165080267	12.3164992882	12.3164998498
d.o.f.	177720	62412	76365	92256

refinement, as in Beirão da Veiga *et al.* (2012*c*), in order to resolve the corner and edge singularities (see Figure 6.6). We note that, since the mesh is a tensor product, the refinement propagates away from the singularities too. We solve the problem with splines of degree 3, 4 and 5.

To our knowledge, reliable benchmark results are not yet available. In Table 6.1 we compare our results for isogeometric methods with the most accurate ones provided by M. Duruflé (Dauge 2014), which correspond to a finite element discretization of degree 5. We can observe that the results we obtain with degree 3 are very similar to those obtained with FEM, with around one third of the degrees of freedom. The results obtained with degrees 4 and 5 are even more accurate. In order to provide new benchmark results, the eigenvalues computed in finer meshes will be made available in Dauge (2014).

6.3.2. Source problem in a cavity

We now consider the source problem in a cavity. We look for a time-harmonic complex-valued electric field $\mathbf{E}$ corresponding to a given solenoidal current density $\mathbf{J} \in L^2(\Omega)^3$, subject to perfect conductor boundary conditions on $\Gamma_D \subset \partial\Omega$, and an impedance boundary condition on $\Sigma \subset \partial\Omega$. The equations of the problem are

$$\begin{aligned} \mathbf{curl}(\mu_r^{-1}\,\mathbf{curl}\,\mathbf{E}) - \kappa^2\epsilon_r\mathbf{E} &= \mathrm{i}\kappa\mu_0^{1/2}\mathbf{J} && \text{in } \Omega,\\ \mu_r^{-1}(\mathbf{curl}\,\mathbf{E})\times\mathbf{n} - \mathrm{i}\kappa\lambda\mathbf{E}_T &= \mathbf{g} && \text{on } \Sigma,\\ \mathbf{E}\times\mathbf{n} &= \mathbf{0} && \text{on } \Gamma_D, \end{aligned}$$

where κ, μ_r and ϵ_r are as in Section 6.3.1, μ_0 is the magnetic permeability of free space, $\mathbf{E}_T = (\mathbf{n}\times\mathbf{E})\times\mathbf{n}$, and the impedance λ is a positive function.

Following Monk (2003, Chapter 4), we define the space

$$X = \big\{\mathbf{u} \in \mathbf{H}(\mathbf{curl};\Omega) : \mathbf{u}\times\mathbf{n} = \mathbf{0} \text{ on } \Gamma_D,\ \mathbf{u}_T = (\mathbf{n}\times\mathbf{u})\times\mathbf{n} \in L^2(\Sigma)^3 \text{ on } \Sigma\big\},$$

equipped with the norm

$$\|\mathbf{u}\|_X^2 = \|\mathbf{u}\|^2_{\mathbf{H}(\mathbf{curl};\Omega)} + \|\mathbf{u}_T\|^2_{L^2(\Sigma)^3}.$$

Using this space, the variational formulation reads as follows: find $\mathbf{E} \in X$ such that

$$\int_\Omega \mu_r^{-1}\,\mathbf{curl}\,\mathbf{E}\cdot\mathbf{curl}\,\bar{\mathbf{v}}\,\mathrm{d}\mathbf{x} - \int_\Omega \kappa^2\epsilon_r\mathbf{E}\cdot\bar{\mathbf{v}}\,\mathrm{d}\mathbf{x} - \int_\Sigma \mathrm{i}\kappa\lambda\mathbf{E}_T\cdot\bar{\mathbf{v}}_T\,\mathrm{d}\Gamma = \int_\Omega \mathrm{i}\kappa\mu_0^{1/2}\mathbf{J}\cdot\bar{\mathbf{v}}\,\mathrm{d}\mathbf{x} + \int_\Sigma \mathbf{g}\cdot\bar{\mathbf{v}}\,\mathrm{d}\Gamma, \tag{6.13}$$

for all $\mathbf{v} \in X$.

The well-posedness of the problem follows using the Helmholtz decomposition and Fredholm alternative: see, for instance, Theorem 4.17 and Corollary 4.19 of Monk (2003), and Theorem 5.2 of Hiptmair (2002).

Theorem 6.9. Assume either that $\kappa \neq 0$ is such that κ^2 is not an eigenvalue of (6.10), or that $\Sigma \neq \emptyset$. Then there exists one unique solution $\mathbf{E}$ to (6.13) such that

$$\|\mathbf{E}\|_X \leq C(\|\mathbf{J}\|_{L^2(\Omega)^3} + \|\mathbf{g}\|_{L^2(\Sigma)^3}),$$

where C is independent of the data $\mathbf{J}$ and $\mathbf{g}$.

In order to discretize the problem with mixed boundary conditions, we first assume that both Σ and Γ_D are the $\mathbf{F}$-image of whole faces of $\widehat{\Omega}$, as in Assumption 3.2. Then we introduce the discrete space

$$X^1_{h,\Gamma_D} = \{\mathbf{u} \in X^1_h : \mathbf{u}\times\mathbf{n} = \mathbf{0} \ \text{ on } \Gamma_D\},$$

where X^1_h is the space defined in (5.20), and the variational formulation of the discrete problem reads as follows: find $\mathbf{E}_h \in X^1_{h,\Gamma_D}$ such that

$$\int_\Omega \mu_r^{-1}\,\mathbf{curl}\,\mathbf{E}_h\cdot\mathbf{curl}\,\bar{\mathbf{v}}_h\,\mathrm{d}\mathbf{x} - \int_\Omega \kappa^2\epsilon_r\mathbf{E}_h\cdot\bar{\mathbf{v}}_h\,\mathrm{d}\mathbf{x} - \int_\Sigma \mathrm{i}\kappa\lambda(\mathbf{E}_h)_T\cdot(\bar{\mathbf{v}}_h)_T\,\mathrm{d}\Gamma = \int_\Omega \mathrm{i}\kappa\mu_0^{1/2}\mathbf{J}\cdot\bar{\mathbf{v}}_h\,\mathrm{d}\mathbf{x} + \int_\Sigma \mathbf{g}\cdot\bar{\mathbf{v}}_h\,\mathrm{d}\Gamma, \tag{6.14}$$

for all $\mathbf{v}_h \in X^1_{h,\Gamma_D}$.

Using the commutative diagram and the approximation results of Section 5, the well-posedness of the discrete problem and error estimates are given in the following theorem. The proof can be found in Buffa *et al.* (2011*b*) and follows the same arguments used for the convergence of finite elements in Hiptmair (2002, Section 5).

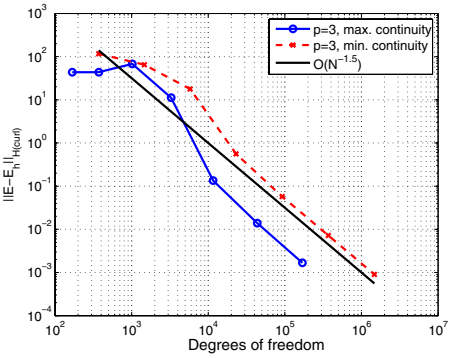

Figure 6.7. Comparison of the error in the $\mathbf{H}(\mathbf{curl})$-norm for the approximation of the plane wave.

Theorem 6.10. Assume either that $\kappa \neq 0$ is such that κ^2 is not an eigenvalue of (6.10), or that $\Sigma \neq \emptyset$. Then there exists $\bar{h} > 0$ such that, for all $h \leq \bar{h}$, problem (6.14) is well-posed and produces quasi-optimal approximation to (6.14), that is,

$$\|\mathbf{E} - \mathbf{E}_h\|_X \leq C \inf_{\boldsymbol{w}_h \in X^1_{h,\Gamma_D}} \|\mathbf{E} - \boldsymbol{w}_h\|_X. \tag{6.15}$$

Moreover, if $\mathbf{E}$ and $\mathbf{curl}\,\mathbf{E}$ are in $(H^s(\Omega))^3$ for some $s \leq p$, then

$$\|\mathbf{E} - \mathbf{E}_h\|_X \leq C h^s (\|\mathbf{E}\|_{H^s(\Omega)^3} + \|\,\mathbf{curl}\,\mathbf{E}\|_{H^s(\Omega)^3}). \tag{6.16}$$

Numerical tests

Test 1. The first numerical test consists of the propagation of a plane wave in free space, that is, $\mu_r = \epsilon_r = 1$. Written in polar coordinates, the domain is given by $\Omega = \{\mathbf{x} = (\rho, \theta) : \rho < 10\}$. We assume that $\mathbf{J} = \mathbf{0}$, and on $\Gamma_D = \partial\Omega$ we impose a Dirichlet boundary condition of the form $\mathbf{E} \times \mathbf{n} = \mathbf{E}^i \times \mathbf{n}$, where $\mathbf{E}^i$ is a plane wave given by $\mathbf{E}^i = \mathbf{p} \exp(\mathrm{i}\kappa \mathbf{x} \cdot \mathbf{d})$, with $\kappa = \sqrt{10}$ and the polarization $\mathbf{p} = (0, 1, 0)$ and direction of propagation $\mathbf{d} = (1, 0, 0)$.

We test a NURBS multi-patch parametrization of Ω, represented in Figure 6.8(a). The problem is discretized using the space X^1_{h,Γ_D} in a sequence of successively refined meshes. In Figure 6.7 we plot the error in the $\mathbf{H}(\mathbf{curl})$-norm for the discretization with degree $p = 3$, and compare the cases of maximum continuity (C^2-tangential continuity) and minimum continuity (C^0-tangential continuity) within each patch. As in Section 6.1, the results show a better convergence in terms of the degrees of freedom with higher continuity. Moreover, high-continuity splines are faster at reaching the asymptotic regime. This is indeed consistent with the known good behaviour of smooth splines in the approximation of the full spectrum of discrete differential operators (see, *e.g.*, Hughes *et al.* 2008).

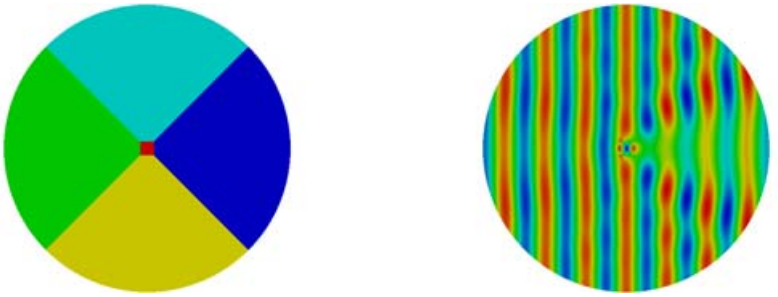

(a) (b)

Figure 6.8. Geometry and computed solution of the scattering problem: (a) geometry of the scattering problem using five patches, and (b) real part of the y-component of $\mathbf{E}_h$.

Test 2. For the second numerical test we consider the same domain Ω, and assume that the square region $(-1,1)^2$ is occupied by a dielectric material with $\epsilon_r = 10$ and $\mu_r = 1$. As before, we assume that $\mathbf{J} = \mathbf{0}$, and now we impose an absorbing boundary condition on $\Sigma = \partial\Omega$, which can be written as the impedance condition with $\lambda = 1$ and $\mathbf{g} = (\mathbf{curl}\,\mathbf{E}^i) \times \mathbf{n} - \mathrm{i}\kappa\mathbf{E}^i_T$, with the incidence field $\mathbf{E}^i$ the same plane wave as in the previous test.

The problem is discretized using the space X^1_h defined with degree $p = 3$ and maximum continuity within each patch, in a mesh formed by 1600 elements on each patch. In Figure 6.8(b) we show the real part of the second component of the computed electric field. We note that only tangential continuity is imposed across the patches, and in particular between the dielectric region and the free space. This allows a more accurate computation at interface regions, since the exact solution is only tangentially continuous due to the jump of the coefficient ϵ_r.

6.3.3. Mixed formulations: discretization with NURBS spaces

In some cases it may be convenient to introduce a mixed formulation of the problem, for instance to impose the divergence constraint in the case of a non-solenoidal source in (6.13), or to remove the null eigenvalues in (6.10). In particular, the non-zero eigenvalues of (6.10) are also solutions to the following mixed formulation:

$$\int_\Omega \mu_r^{-1}\,\mathbf{curl}\,\mathbf{E}\cdot\mathbf{curl}\,\mathbf{v}\,\mathrm{d}\mathbf{x} + \int_\Omega \epsilon_r\mathbf{v}\cdot\mathbf{grad}\,\phi\,\mathrm{d}\mathbf{x} = \kappa^2\int_\Omega \epsilon_r\mathbf{E}\cdot\mathbf{v}\,\mathrm{d}\mathbf{x}$$

for all $\mathbf{v} \in \mathbf{H}_0(\mathbf{curl};\Omega)$, and

$$\int_\Omega \epsilon_r\mathbf{E}\cdot\mathbf{grad}\,\psi\,\mathrm{d}\mathbf{x} = 0$$

for all $\psi \in H_0^1(\Omega)$. Boffi (2007) have proved that, due to the exact sequence (5.21) for the discrete spaces,[2] a discretization of the previous mixed formulation with $\mathbf{E}_h \in X_h^1 \cap \mathbf{H}_0(\mathbf{curl};\Omega)$ and $\phi_h \in X_h^0 \cap H_0^1(\Omega)$ is equivalent to solving the discrete problem (6.12) for $\kappa_h \neq 0$. An analogous result holds for the other mixed formulation introduced in Boffi *et al.* (1999). We will now present numerical results based on NURBS spaces, to show that having an exact sequence of discrete spaces is not a necessary condition for obtaining a good approximation of the mixed formulation.

As in Section 3, let us assume that the parametrization $\mathbf{F}$ is defined using the NURBS space $N_{\mathbf{p}^0}(\boldsymbol{\Xi}^0, W)$, let $\widehat{Y}_h^0 = N_{\mathbf{p}}(\boldsymbol{\Xi}, W)$ be a refinement of this space, and let $Y_h^0 = V_h$, defined as in (3.2). Varying the degree and the regularity in the same way as for defining the spline spaces (5.3), and applying the same transformations in (5.20) from $\widehat{\Omega}$ to the physical domain Ω, we can define similar NURBS spaces Y_h^1, Y_h^2 and Y_h^3.

It is obvious that the NURBS spaces Y_h^i do not form an exact sequence, since the derivative of a rational polynomial of degree p is a rational polynomial of degree $2p$. However, all extant numerical tests show that the NURBS spaces give stable and spurious-free discretizations of the mixed formulations (see the example below). These results suggest that, although there is no commutative diagram for the NURBS spaces, they probably satisfy the conditions for the convergence of eigenvalue problems in mixed form stated in Boffi, Brezzi and Gastaldi (1997) (see also Boffi 2010, Part 3). Unfortunately, at the moment we lack the mathematical explanation.

Remark 6.11. Given a parametrization

$$\mathbf{F} \in (N_{\mathbf{p}^0}(\boldsymbol{\Xi}^0, W))^d,$$

we can define the spline space $\widehat{X}_h^0 = S_{\mathbf{p}^0}(\boldsymbol{\Xi}^0)$ (or a refinement of it), and the other spaces $\widehat{X}_h^i$ follow from (5.3), in practice giving the knot vectors and neglecting the weight W. Instead, our construction of NURBS spaces $\widehat{Y}_h^i$ assumes that they are all defined with the same weight W, so all the spaces (or their components, for the vector-valued ones) must be a refinement of $N_{\mathbf{p}^0}(\boldsymbol{\Xi}^0, W)$, and the suitable degrees and regularities must be achieved by applying knot insertion and degree elevation.

Numerical test

For our numerical test we consider a thick curved L-shaped domain, which is an extrusion of the two-dimensional domain in Dauge (2014) (see Figure 6.9(a)). We solve the problem in a mesh of 432 elements and with degree $p = 3$, which correspond to 1729 degrees of freedom for the $\mathbf{H}(\mathbf{curl};\Omega)$-conforming space Y_h^1. Comparing all the computed eigenvalues with those

[2] In fact, the condition in Boffi (2007) is that $\mathbf{grad}(X_{0,h}^0) \subset X_{0,h}^1$.

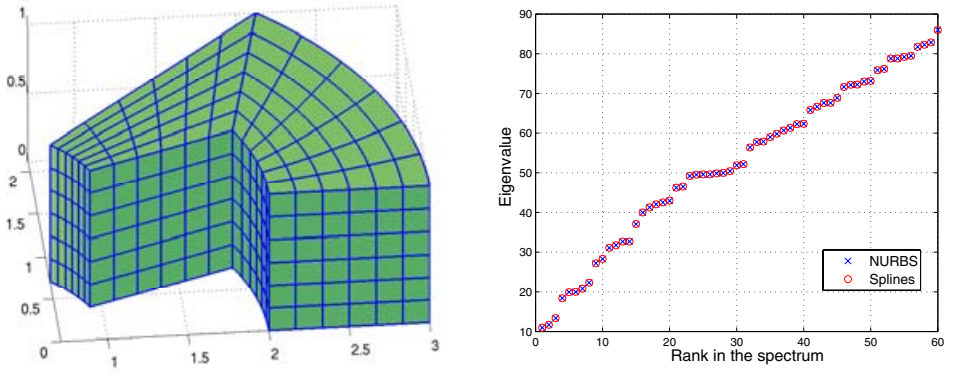

(a) (b)

Figure 6.9. Geometry and computed eigenvalues in a NURBS domain discretized with NURBS spaces: (a) curved thick L-shaped domain, and (b) computed eigenvalues using splines and NURBS.

obtained with a discretization based on the spline spaces X_h^i, the maximum relative error is less than 0.5%. We show in Figure 6.9(b) a plot of the first eigenvalues computed with both methods, to show that there is almost no discrepancy between them.

7. Local refinement via T-splines

Tensor product multivariate spline and NURBS spaces are easy to construct, and their mathematical properties directly extend from the univariate case, as in the case of the discrete de Rham complexes defined in Section 5. However, tensor products restrict local refinement, which is a severe limitation in problems that exhibit solutions with layers or singularities, as in some of the examples in Section 6. In this section we discuss an extension of spline spaces beyond the tensor product structure, which therefore allow local mesh refinement.

Three approaches have emerged in the isogeometric community, namely T-splines, locally refinable (LR) splines, and hierarchical splines. T-splines were proposed in Sederberg, Zheng, Bakenov and Nasri (2003) for applications to CAGD and have been adopted for isogeometric methods since Bazilevs *et al.* (2010*a*). Today they are probably the most popular approach among engineers: for example, they have been used for shell problems (Hosseini, Remmers, Verhoosel and Borst 2013), fluid–structure interaction problems (Bazilevs, Hsu and Scott 2012) and contact mechanics simulation (Dimitri *et al.* 2014). The algorithm for local refinement has

evolved since its introduction in Sederberg *et al.* (2004), and although the first approach was not efficient in isogeometric methods (see, *e.g.*, Dörfel *et al.* 2010), more recent developments (*e.g.*, Scott *et al.* 2012) have overcome the initial limitations. The mathematical literature on T-splines is very recent and mainly restricted to the two-dimensional case. It is based on the notion of analysis-suitable (AS) T-splines: these are a subset of T-splines, introduced in Li *et al.* (2012) and extended to arbitrary degree in Beirão da Veiga *et al.* (2013*a*), for which fundamental properties hold. LR-splines (Dokken *et al.* 2013) and hierarchical splines (Vuong *et al.* 2011) were proposed more recently in the isogeometric literature, and represent a valid alternative to T-splines. However, for reasons of space and because of our expertise, we restrict the presentation to T-splines.

This section is divided into five parts. In Section 7.1 we introduce the notion of a dual-compatible (DC) set of B-splines. This is a set of multivariate B-splines without a global tensor product structure, but endowed with a weaker structure that still guarantees some key properties. The main one is that their linear combination spans a space (called the DC space) which can be associated with a dual space by the construction of a dual basis analogous to that of Section 2. The existence of a 'good' dual space implies other mathematical properties that are needed in isogeometric methods: for example, (local) linear independence and partition of unity of the DC set of B-spline functions, and optimal approximation properties of the DC space. The framework we propose here is an extension of the one introduced in Beirão da Veiga *et al.* (2013*a*), and covers arbitrary space dimension.

In Section 7.2 we present the concept of T-mesh and T-spline spaces. For the sake of simplicity, the definition and all the examples are given in two dimensions, but for arbitrary degree. However, the extension to arbitrary dimension is briefly addressed in a dedicated paragraph.

Section 7.3 deals with the previously mentioned AS T-splines (from Scott *et al.* 2012 and Beirão da Veiga *et al.* 2013*a*), in two dimensions. Here we state the fundamental equivalence that a T-spline set is DC if and only if its T-mesh fulfils the topological conditions expressed by the AS definition. In this way, all the theoretical results of the first section are extended to AS T-splines.

In Section 7.4 we extend to AS T-splines the construction of discrete de Rham complexes, generalizing some of the results of Section 5, and finally show numerical tests in Section 7.5.

7.1. Dual-compatible B-splines

Consider a set of multivariate B-splines,

$$\big\{\widehat{B}_{\mathbf{A},\mathbf{p}},\ \mathbf{A} \in \mathcal{A}\big\}, \tag{7.1}$$

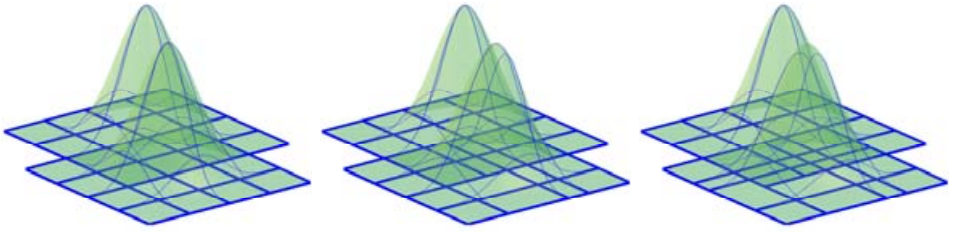

(a) (b) (c)

Figure 7.1. Examples of (a) overlapping, (b) partially overlapping, and (c) not partially overlapping B-splines. The thick solid lines represent the knot lines.

where $\mathcal{A}$ is a set of indices. This is a generalization of the tensor product set of multivariate splines (2.41) where the functions in (7.1) have the structure

$$\widehat{B}_{\mathbf{A},\mathbf{p}}(\boldsymbol{\zeta}) = \widehat{B}[\Xi_{\mathbf{A},1,p_1}](\zeta_1)\cdots\widehat{B}[\Xi_{\mathbf{A},d,p_d}](\zeta_d) \tag{7.2}$$

and generally have uncorrelated local knot vectors, that is, two different local knot vectors $\Xi_{\mathbf{A}',\ell,p_\ell}$ and $\Xi_{\mathbf{A}'',\ell,p_\ell}$ in the ℓ-direction are not, in general, sub-vectors of a global knot vector. This is equivalent to the definition of *point-based splines* in Sederberg *et al.* (2003). We assume that there is a one-to-one correspondence between $\mathbf{A} \in \mathcal{A}$ and $\widehat{B}_{\mathbf{A},\mathbf{p}}$.

We say that the two p-degree local knot vectors $\Xi' = \{\xi'_1, \dots \xi'_{p+2}\}$ and $\Xi'' = \{\xi''_1, \dots \xi''_{p+2}\}$ *overlap* if they are sub-vectors of the same knot vector (that depends on Ξ' and Ξ''). That is, there is a knot vector $\Xi = \{\xi_1, \dots \xi_k\}$ and k' and k'' such that:

$$\begin{aligned} &\text{for all } i = 1, \dots, p+2, \qquad \xi'_i = \xi_{i+k'} \\ &\text{for all } i = 1, \dots, p+2, \qquad \xi''_i = \xi_{i+k''}. \end{aligned} \tag{7.3}$$

Then we define for multivariate B-splines the notions of *overlap* and *partial overlap*, as follows.

Definition 7.1. Two B-splines $\widehat{B}_{\mathbf{A}',\mathbf{p}}$ $\widehat{B}_{\mathbf{A}'',\mathbf{p}}$ in (7.1) overlap if the local knot vectors in each direction overlap. Two B-splines $\widehat{B}_{\mathbf{A}',\mathbf{p}}$ $\widehat{B}_{\mathbf{A}'',\mathbf{p}}$ in (7.1) partially overlap if, when $\mathbf{A}' \neq \mathbf{A}''$, there exists a direction ℓ such that the local knot vectors $\Xi_{\mathbf{A}',\ell,p_\ell}$ and $\Xi_{\mathbf{A}'',\ell,p_\ell}$ are different and overlap.

From the previous definition, overlap implies partial overlap. Examples of B-splines overlapping, only partially overlapping, and not partially overlapping are depicted in Figure 7.1.

Definition 7.2. The set (7.1) is a dual-compatible (DC) set of B-splines if each pair of B-splines in it partially overlaps. Its span,

$$S_{\mathbf{p}}(\mathcal{A}) = \operatorname{span}\big\{\widehat{B}_{\mathbf{A},\mathbf{p}},\ \mathbf{A} \in \mathcal{A}\big\}, \tag{7.4}$$

is called a dual-compatible (DC) spline space.

Note that the partially overlapping condition in Definition 7.2 needs to be checked only for those B-spline pairs that have non-disjoint support. Indeed, by Definition 7.1, any two B-splines with disjoint supports are clearly partially overlapping.

A tensor product space (see Section 2.2) is clearly a DC spline space, since every pair of its multivariate B-splines always overlaps by construction. It is interesting to note that partial overlap is sufficient for the construction of a dual basis, similar to the ones in Section 2.2.2.

Proposition 7.3. Assume that (7.1) is a DC set, and consider an associated set of functionals

$$\big\{\lambda_{\mathbf{A},\mathbf{p}},\ \mathbf{A} \in \mathcal{A}\big\}, \tag{7.5}$$

where each $\lambda_{\mathbf{A},\mathbf{p}}$ is

$$\lambda_{\mathbf{A},\mathbf{p}} = \lambda[\Xi_{\mathbf{A},1,p_1}] \otimes \cdots \otimes \lambda[\Xi_{\mathbf{A},d,p_d}], \tag{7.6}$$

and $\lambda[\Xi_{\mathbf{A},\ell,p_\ell}]$ denotes a univariate functional that depends only on the local knot vector $\Xi_{\mathbf{A},\ell,p_\ell}$ and is dual to each univariate B-spline with overlapping knot vector. We assume that the local knot vectors in (7.6) are the same as (7.1)–(7.2). Then (7.5) is a dual basis for (7.1).

Proof. Consider any $\widehat{B}_{\mathbf{A}',\mathbf{p}}$ and $\lambda_{\mathbf{A}'',\mathbf{p}}$, with $\mathbf{A}', \mathbf{A}'' \in \mathcal{A}$. We then need to show

$$\lambda_{\mathbf{A}'',\mathbf{p}}(\widehat{B}_{\mathbf{A}',\mathbf{p}}) = \begin{cases} 1 & \text{if } \mathbf{A}'' = \mathbf{A}', \\ 0 & \text{otherwise.} \end{cases} \tag{7.7}$$

Clearly, if $\mathbf{A}' = \mathbf{A}''$ then we have $\lambda_{\mathbf{A}'',\mathbf{p}}(\widehat{B}_{\mathbf{A}',\mathbf{p}}) = 1$ from the definition of dual basis. If $\mathbf{A}' \neq \mathbf{A}''$, thanks to the partial overlap assumption there is a direction $\bar{\ell}$ such that the local knot vectors $\Xi_{\mathbf{A}',\ell,p_\ell}$ and $\Xi_{\mathbf{A}'',\ell,p_\ell}$ differ and overlap, and then

$$\lambda[\Xi_{\mathbf{A}'',\ell,p_\ell}](\widehat{B}[\Xi_{\mathbf{A}',\ell,p_\ell}]) = 0,$$

and from (7.6),

$$\lambda_{\mathbf{A}'',\mathbf{p}}(\widehat{B}_{\mathbf{A}',\mathbf{p}}) = \prod_{\ell=1}^{d} \lambda[\Xi_{\mathbf{A}'',\ell,p_\ell}](\widehat{B}[\Xi_{\mathbf{A}',\ell,p_\ell}]) = 0. \qquad \square$$

Observe that the assumptions on the functionals (7.5) stated in Proposition 7.3 are the natural ones when dual functionals are constructed for the tensor product B-splines. To simplify the following discussion, we assume that the dual functionals are defined from the local knot vectors as in (2.22)–(2.25) and (2.47).

The existence of dual functionals implies important properties for a DC set (7.1) and the related space $S_{\mathbf{p}}(\mathcal{A})$ in (7.4). We list these properties in the following propositions and remarks.

The first result is the linear independence of set (7.1), therefore forming a *basis*; they are also a partition of the unit.

Proposition 7.4. The B-splines in a DC set (7.1) are linearly independent. Moreover, if the constant function belongs to $S_{\mathbf{p}}(\mathcal{A})$, they form a partition of the unit.

Proof. Assume

$$\sum_{\mathbf{A}\in\mathcal{A}} C_{\mathbf{A}}\widehat{B}_{\mathbf{A},\mathbf{p}} = 0$$

for some coefficients $C_{\mathbf{A}}$. Then, for any $\mathbf{A}' \in \mathcal{A}$, applying $\lambda_{\mathbf{A}',\mathbf{p}}$ to the sum, using linearity and (7.7), we get

$$C_{\mathbf{A}'} = \lambda_{\mathbf{A}',\mathbf{p}}\Big(\sum_{\mathbf{A}\in\mathcal{A}} C_{\mathbf{A}}\widehat{B}_{\mathbf{A}',\mathbf{p}}\Big) = 0.$$

Similarly, let

$$\sum_{\mathbf{A}\in\mathcal{A}} C_{\mathbf{A}}\widehat{B}_{\mathbf{A},\mathbf{p}} = 1$$

for some coefficients $C_{\mathbf{A}}$. For any $\mathbf{A}' \in \mathcal{A}$, applying $\lambda_{\mathbf{A}',\mathbf{p}}$ as above, we get

$$C_{\mathbf{A}'} = \lambda_{\mathbf{A}',\mathbf{p}}\Big(\sum_{\mathbf{A}\in\mathcal{A}} C_{\mathbf{A}}\widehat{B}_{\mathbf{A},\mathbf{p}}\Big) = 1. \qquad \square$$

To each B-spline set (7.1) we can associate a parametric domain

$$\widehat{\Omega} = \bigcup_{\mathbf{A}\in\mathcal{A}} \operatorname{supp}(\widehat{B}_{\mathbf{A},\mathbf{p}}).$$

Moreover, we give the following extension of the notion of Bézier mesh (2.40).

Definition 7.5. A parametric Bézier mesh in the parametric domain, denoted by $\widehat{\mathcal{M}}$, is the collection of the the maximal open sets $Q \subset \widehat{\Omega}$ such that, for all $\mathbf{A} \in \mathcal{A}$, $\widehat{B}_{\mathbf{A},\mathbf{p}}$ is a polynomial in Q; these Q are called (Bézier) elements.

Proposition 7.6. In a DC set (7.1) there are at most $(p_1+1)\cdot\cdots\cdot(p_d+1)$ B-splines that are non-null in each element $Q \in \widehat{\mathcal{M}}$.

Proof. Given any point $\boldsymbol{\zeta} = (\zeta_1, \ldots, \zeta_d) \in \widehat{\Omega}$, let $\mathcal{A}(\boldsymbol{\zeta})$ denote the subset of $\mathbf{A} \in \mathcal{A}$ such that $\widehat{B}_{\mathbf{A},\mathbf{p}}(\boldsymbol{\zeta}) > 0$. It can be easily checked that $\mathcal{A}(\boldsymbol{\zeta})$ only depends on Q, for all $\boldsymbol{\zeta} \in Q$. Recalling (7.2) and introducing the notation $\Xi_{\mathbf{A},\ell,p_\ell} = \{\xi_{\ell,1}, \ldots, \xi_{\ell,p_\ell+2}\}$, to each $\mathbf{A} \in \mathcal{A}(\boldsymbol{\zeta})$ we can associate a multi-index $(i_{\mathbf{A},1}, \ldots, i_{\mathbf{A},d})$ such that, for all $\ell = 1, \ldots, d$,

$$1 \le i_{\mathbf{A},\ell} \le p_\ell + 1 \quad \text{and} \quad \xi_{\ell,i_{\mathbf{A},\ell}} \le \zeta_\ell < \xi_{\ell,i_{\mathbf{A},\ell}+1}. \tag{7.8}$$

From the DC assumption, if two $\widehat{B}_{\mathbf{A}',\mathbf{p}}$ and $\widehat{B}_{\mathbf{A}'',\mathbf{p}}$, with $\mathbf{A}' \neq \mathbf{A}''$, partially overlap, that is, there are different and overlapping $\Xi_{\mathbf{A}',\ell,p_\ell}$ and $\Xi_{\mathbf{A}'',\ell,p_\ell}$, then the indices in (7.8) fulfil the condition

$$\mathbf{A}' \neq \mathbf{A}'' \Rightarrow \exists \ell \quad \text{such that } i_{\mathbf{A}',\ell} \neq i_{\mathbf{A}'',\ell} \quad \text{for all } \mathbf{A}', \mathbf{A}'' \in \mathcal{A}(\boldsymbol{\zeta}). \tag{7.9}$$

The conclusion follows from (7.9), since from (7.8) there are at most $(p_1 + 1) \cdots (p_d + 1)$ distinct multi-indices $(i_{\mathbf{A},1}, \ldots, i_{\mathbf{A},d})$. □

It is interesting to note that an immediate consequence of Proposition 7.6 is that if the space of global polynomials of multi-degree $\mathbf{p}$ is contained in $S_{\mathbf{p}}(\mathcal{A})$, then the non-null B-splines restricted to the element are linearly independent. Assume now that each $\lambda_{\mathbf{A},\mathbf{p}}$ is defined on $L^2(\widehat{\Omega})$. An important consequence of Proposition 7.3 is that we can build a projection operator $\Pi_{\mathbf{p}} : L^2(\widehat{\Omega}) \to S_{\mathbf{p}}(\mathcal{A})$ by

$$\Pi_{\mathbf{p}}(f)(\boldsymbol{\zeta}) = \sum_{\mathbf{A} \in \mathcal{A}} \lambda_{\mathbf{A},\mathbf{p}}(f) \widehat{B}_{\mathbf{A},\mathbf{p}}(\boldsymbol{\zeta}) \quad \text{for all } f \in L^2(\widehat{\Omega}), \text{ and } \boldsymbol{\zeta} \in \widehat{\Omega}. \tag{7.10}$$

This allows us to prove the approximation properties of $S_{\mathbf{p}}(\mathcal{A})$. The following result will make use of the notion of support extension $\widetilde{Q}$ associated to an element $Q \subset \widehat{\Omega}$ (or a generic open subset $Q \subset \widehat{\Omega}$) and to the B-spline set (7.1), which is a generalization of the definition from Section 2.2:

$$\widetilde{Q} = \bigcup_{\substack{\mathbf{A} \in \mathcal{A} \\ \operatorname{supp}(\widehat{B}_{\mathbf{A},\mathbf{p}}) \cap Q \neq \emptyset}} \operatorname{supp}(\widehat{B}_{\mathbf{A},\mathbf{p}}).$$

Furthermore, we will denote by $\bar{Q}$ the smallest d-dimensional rectangle in $\widehat{\Omega}$ containing $\widetilde{Q}$. Then for the dual functionals defined as in (2.22)–(2.25) and (2.47), the following result holds.

Proposition 7.7. Let (7.1) be a DC set of B-splines. Then the projection operator $\Pi_{\mathbf{p}}$ in (7.10) is (locally) h-uniformly L^2-continuous, that is, there exists a constant C, depending only on $\mathbf{p}$, such that

$$\|\Pi_{\mathbf{p}}(f)\|_{L^2(Q)} \leq C \|f\|_{L^2(\widetilde{Q})} \quad \text{for all } Q \subset \widehat{\Omega}, \text{ and } f \in L^2(\widehat{\Omega}).$$

Proof. Let Q be an element in the parametric domain. From Proposition 7.6 and since each $B_{\mathbf{A},\mathbf{p}} \leq 1$, we have that, for any $\boldsymbol{\zeta} \in Q$,

$$\sum_{\mathbf{A} \in \mathcal{A}} \left| \widehat{B}_{\mathbf{A},\mathbf{p}}(\boldsymbol{\zeta}) \right| \leq C.$$

Therefore, given any point $\boldsymbol{\zeta} \in Q$, let $\mathcal{A}(\boldsymbol{\zeta})$ denote the subset of $\mathbf{A} \in \mathcal{A}$ such that $\widehat{B}_{\mathbf{A},\mathbf{p}}(\boldsymbol{\zeta}) > 0$, let $Q_{\mathbf{A}}$ denote the common support of $\widehat{B}_{\mathbf{A},\mathbf{p}}$ and $\lambda_{\mathbf{A},\mathbf{p}}$,

and let $|Q_{\mathbf{A}}|$ be its d-dimensional measure. Using (2.23) it follows that

$$\begin{aligned}\left|\Pi_{\mathbf{p}}(f)(\boldsymbol{\zeta})\right|^2 &= \left|\sum_{\mathbf{A}\in\mathcal{A}(\boldsymbol{\zeta})} \lambda_{\mathbf{A},\mathbf{p}}(f)\widehat{B}_{\mathbf{A},\mathbf{p}}(\boldsymbol{\zeta})\right|^2 \le C \max_{\mathbf{A}\in\mathcal{A}(\boldsymbol{\zeta})} \left|\lambda_{\mathbf{A},\mathbf{p}}(f)\right|^2 \qquad (7.11)\\ &\le C \max_{\mathbf{A}\in\mathcal{A}(\boldsymbol{\zeta})} |Q_{\mathbf{A}}|^{-1}\|f\|^2_{L^2(Q_{\mathbf{A}})}\\ &\le C|Q|^{-1}\|f\|^2_{L^2(\widetilde{Q})},\end{aligned}$$

where we have used in the last step that $Q \subset Q_{\mathbf{A}}$ for all $\mathbf{A} \in \mathcal{A}(\boldsymbol{\zeta})$ (and therefore $|Q| \le |Q_{\mathbf{A}}|$) and that $Q_{\mathbf{A}} \subset \widetilde{Q}$. Since the bound above holds for any $\boldsymbol{\zeta} \in Q$, integrating over Q and applying (7.11) yields

$$\|\Pi_{\mathbf{p}}(f)\|^2_{L^2(Q)} \le C\|f\|^2_{L^2(\widetilde{Q})}. \qquad \square$$

The continuity of $\Pi_{\mathbf{p}}$ implies the following approximation result in the L^2-norm.

Proposition 7.8. Assume that the space of global polynomials of degree $p = \min_{1\le\ell\le d}\{p_\ell\}$ is included in the space $S_{\mathbf{p}}(\mathcal{A})$ and that $\widehat{\Omega} = [0,1]^d$. Then there exists a constant C depending only on $\mathbf{p}$ such that, for $0 \le s \le p+1$,

$$\|f - \Pi_{\mathbf{p}}(f)\|_{L^2(Q)} \le C(h_{\bar{Q}})^s |f|_{H^s(\bar{Q})} \quad \text{for all } Q \subset \widehat{\Omega}, \text{ and } f \in H^s(\widehat{\Omega}),$$

where $h_{\bar{Q}}$ represents the diameter of $\bar{Q}$.

Proof. Let π be any p-degree polynomial. Since $\pi \in S_{\mathbf{p}}(\mathcal{A})$ and $\Pi_{\mathbf{p}}$ is a projection operator, using Proposition 7.7 it follows that

$$\begin{aligned}\|f - \Pi_{\mathbf{p}}(f)\|_{L^2(Q)} &= \|f - \pi + \Pi_{\mathbf{p}}(\pi - f)\|_{L^2(Q)}\\ &\le \|f - \pi\|_{L^2(Q)} + \|\Pi_{\mathbf{p}}(\pi - f)\|_{L^2(Q)}\\ &\le (1+C)\|f - \pi\|_{L^2(\widetilde{Q})} \le (1+C)\|f - \pi\|_{L^2(\bar{Q})}.\end{aligned}$$

The result finally follows by a standard polynomial approximation result. $\square$

We conclude this section with a final observation: the notion and construction of Greville sites are easily extended to DC sets of B-splines, and an analogous property to (2.42) holds.

Proposition 7.9. Assume that the linear polynomials belong to the space $S_{\mathbf{p}}(\mathcal{A})$. Then we have that

$$\zeta_\ell = \sum_{\mathbf{A}\in\mathcal{A}} \gamma[\Xi_{\mathbf{A},\ell,p_\ell}]\widehat{B}_{\mathbf{A},\mathbf{p}}(\boldsymbol{\zeta}), \quad \text{for all } \boldsymbol{\zeta} \in \widehat{\Omega}, \quad 1 \le \ell \le d, \qquad (7.12)$$

where $\gamma[\Xi_{\mathbf{A},\ell,p_\ell}]$ denotes the average of the p_ℓ internal knots of $\Xi_{\mathbf{A},\ell,p_\ell}$.

Proof. The identity (7.12) easily follows from the expansion of $\Pi_{\mathbf{p}}(\zeta_\ell)$ and the definition of dual functionals, which is the same as in the tensor product case, yielding $\lambda_{\mathbf{A},\mathbf{p}}(\zeta_\ell) = \gamma[\Xi_{\mathbf{A},\ell,p_\ell}]$. □

7.2. T-splines: definition and examples

T-splines are a particular case of the multivariate splines in the previous section, for which the multi-index and the local knot vectors are not arbitrary, but defined from a T-mesh. We explain the two-dimensional case in some detail, and in the final paragraph we briefly address the extension to the three-dimensional setting. The T-mesh, referred to as the *index* T-mesh, is a mesh in the index domain. This means that the T-mesh is defined on the knot indices. Knots and indices are not in a one-to-one correspondence: with T-splines, as for B-splines, we can have knot repetitions to allow spline variable regularity. For the sake of generality the T-mesh connectivity needs to be given on the indices. The present section follows the construction and notation introduced in Beirão da Veiga *et al.* (2013*a*).

An index T-mesh $\mathcal{T}$ is then a rectangular partition of the *index domain*

$$[\underline{n_1}, \overline{n_1}] \times [\underline{n_2}, \overline{n_2}],$$

with $\underline{n_1},\ \overline{n_1},\ \underline{n_2},\ \overline{n_2} \in \mathbb{Z}$, such that all element corners, that is, the *vertices* of $\mathcal{T}$, have integer coordinates. Precisely, $\mathcal{T}$ is the collection of all elements of the partition above, where the elements are taken as open sets. We also let $\mathcal{V}$ denote the collection of all the vertices of $\mathcal{T}$, considered as singletons (subset of $\mathbb{Z}^2$). An *edge* of $\mathcal{T}$ is a segment between vertices of $\mathcal{T}$ that does not intersect any element in $\mathcal{T}$. We further assume that edges do not contain vertices, and in particular that they are open at their endpoints. We denote by $h\mathcal{E}$ (resp. $v\mathcal{E}$) the collection of all horizontal (resp. vertical) edges, and by $\mathcal{E} = h\mathcal{E} \cup v\mathcal{E}$ the collection of all edges. The boundary of an element $E \in \mathcal{T}$ is denoted by ∂E, and the union of the two vertices $V^1, V^2 \in \mathcal{V}$ that are endpoints of an edge $e \in \mathcal{E}$ is denoted by ∂e. The *valence* of a vertex $V \in \mathcal{V}$ is the number of edges $e \in \mathcal{E}$ such that $V \subset \partial e$. Since elements are rectangular, only valence three or four is allowed for all the internal vertices $V \subset]\underline{n_1}, \overline{n_1}[\times]\underline{n_2}, \overline{n_2}[$, that is, in this setting so-called T-junctions are allowed but L-junctions or I-junctions (see Li *et al.* 2012) are not. The horizontal (resp. vertical) *skeleton* of the mesh is denoted by $h\mathcal{S}$ (resp. $v\mathcal{S}$), and is the union of all horizontal (resp. vertical) edges and all vertices. Finally, the union $\mathcal{S} = h\mathcal{S} \cup v\mathcal{S}$ is called the *skeleton*.

Given indices $\mathbf{p} = (p_1, p_2)$, we split the index domain $[\underline{n_1}, \overline{n_1}] \times [\underline{n_2}, \overline{n_2}]$ into an *active region* $\mathrm{AR}_{\mathbf{p}}$ and a *frame region* $\mathrm{FR}_{\mathbf{p}}$, such that

$$\begin{aligned}\mathrm{AR}_{\mathbf{p}} = [&\underline{n}_1 + \lfloor (p_1+1)/2 \rfloor, \overline{n}_1 - \lfloor (p_1+1)/2 \rfloor] \\ &\times [\underline{n}_2 + \lfloor (p_2+1)/2 \rfloor, \overline{n}_2 - \lfloor (p_2+1)/2 \rfloor],\end{aligned}$$

and

$$\begin{aligned}\mathrm{FR}_{\mathbf{p}} =&\big([\underline{n}_1, \underline{n}_1 + \lfloor (p_1+1)/2 \rfloor] \ \cup \ [\overline{n}_1 - \lfloor (p_1+1)/2 \rfloor, \overline{n}_1]\big) \times [\underline{n}_2, \overline{n}_2] \\ &\cup [\underline{n}_1, \overline{n}_1] \times \big([\underline{n}_2, \underline{n}_2, + \lfloor (p_2+1)/2 \rfloor] \ \cup \ [\overline{n}_2 - \lfloor (p_2+1)/2 \rfloor, \overline{n}_2]\big).\end{aligned}$$

Note that both $\mathrm{AR}_{\mathbf{p}}$ and $\mathrm{FR}_{\mathbf{p}}$ are closed regions.

Definition 7.10. An index T-mesh $\mathcal{T}$ belongs to $\mathrm{AD}_{\mathbf{p}}$, that is, it is *admissible* for degrees p_1 and p_2, if $\mathcal{S} \cap \mathrm{FR}_{\mathbf{p}}$ contains the vertical segments

$$\begin{aligned}\{\ell\} \times [\underline{n}_2, \overline{n}_2] \quad &\text{for } \ell = \underline{n}_1, \dots, \underline{n}_1 + p_1 \\ &\text{and } \ell = \overline{n}_1 - p_1, \dots, \overline{n}_1,\end{aligned}$$

and the horizontal segments

$$\begin{aligned}[\underline{n}_1, \overline{n}_1] \times \{\ell\} \quad &\text{for } \ell = \underline{n}_2, \dots, \underline{n}_2 + p_2 \\ &\text{and } \ell = \overline{n}_2 - p_2, \dots, \overline{n}_2,\end{aligned}$$

and all vertices $V \subset]\underline{n_1}, \overline{n_1}[\times]\underline{n_2}, \overline{n_2}[\cap \mathrm{FR}_{\mathbf{p}}$ have valence four.

Note that Definition 7.10 on admissible T-meshes is stronger than the one given in Beirão da Veiga *et al.* (2013*a*). This is needed to reproduce global polynomials, as we will see in Proposition 7.18 below. Furthermore, Definition 7.10 prevents the mesh from having T-junctions in the frame region (see Figure 7.2).

Remark 7.11. Observe that the indexing adopted here differs from that of Section 2. B-splines could be defined from a tensor product T-mesh, by taking $\underline{n_\ell} = 1$ and $\overline{n_\ell} = n_\ell + p_\ell + 1$. Moreover, the number of complete segments in Definition 7.10 is equal to $p_\ell + 1$ on each side, which is the same number as repetitions in the open knot vector. Note that this is different to the width of the frame.

In the following definition we give a further condition that prevents the existence of two facing T-junctions.

Definition 7.12. An index T-mesh $\mathcal{T} \in \mathrm{AD}_{\mathbf{p}}$ is said to belong to $\mathrm{AD}^+_{\mathbf{p}}$ if, for any pair of vertices $V^1 = \{(i_1, j_1)\}$, $V^2 = \{(i_2, j_2)\}$ in $\mathcal{V}$, such that $V^1, V^2 \subset \partial E$ for some $E \in \mathcal{T}$, and $i_1 = i_2$ (resp. $j_1 = j_2$), the open segment $\{i_1\}\times]j_1, j_2[$ (resp. $]i_1, i_2[\times\{j_1\}$) is contained in $\mathcal{S}$.

We are now ready to introduce the *anchors*. The active index T-mesh carries the anchors, which will then be associated to the spline basis functions, while the extra indices of $\mathrm{FR}_{\mathbf{p}}$ will be needed for the definition of the function when the anchor is close to the boundary. For T-splines of arbitrary degree, following Beirão da Veiga *et al.* (2013*a*), we define anchors as the vertices, edges or elements themselves.

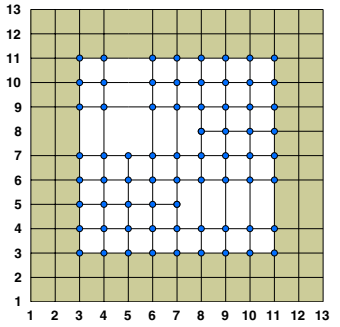

(a) $\mathbf{p} = (3,3)$

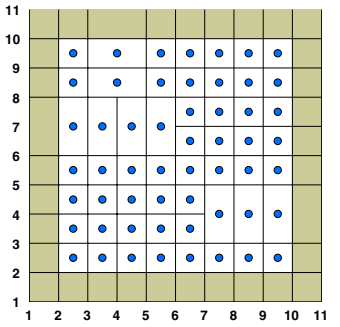

(b) $\mathbf{p} = (2,2)$

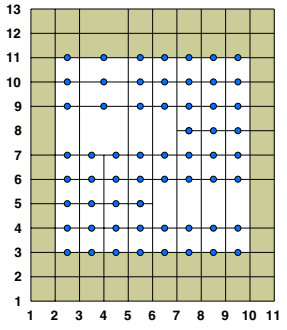

(c) $\mathbf{p} = (2,3)$

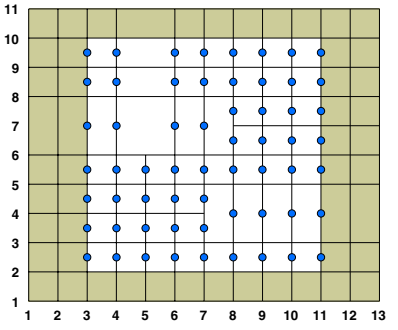

(d) $\mathbf{p} = (3,2)$

Figure 7.2. Admissible T-meshes and anchors for different values of $\mathbf{p} = (p_1, p_2)$. The frame region is shaded. Vertex anchors are represented by dots, and edge or element anchors are indicated by dots at the middle point of the edge or element.

Definition 7.13. Given a T-mesh $\mathcal{T} \in \mathrm{AD}_{\mathbf{p}}$, we define the set of anchors $\mathcal{A}_{\mathbf{p}}(\mathcal{T})$ as follows:

- if $p_1,\ p_2$ are odd, $\mathcal{A}_{\mathbf{p}}(\mathcal{T}) = \{\mathbf{A} \in \mathcal{V} : \mathbf{A} \subset \mathrm{AR}_{\mathbf{p}}\}$,
- if p_1 is even and p_2 is odd, $\mathcal{A}_{\mathbf{p}}(\mathcal{T}) = \{\mathbf{A} \in h\mathcal{E} : \mathbf{A} \subset \mathrm{AR}_{\mathbf{p}}\}$,
- if p_1 is odd and p_2 is even $\mathcal{A}_{\mathbf{p}}(\mathcal{T}) = \{\mathbf{A} \in v\mathcal{E} : \mathbf{A} \subset \mathrm{AR}_{\mathbf{p}}\}$,
- if $p_1,\ p_2$ are even $\mathcal{A}_{\mathbf{p}}(\mathcal{T}) = \{\mathbf{A} \in \mathcal{T} : \mathbf{A} \subset \mathrm{AR}_{\mathbf{p}}\}$.

The set of anchors for different values of $\mathbf{p}$ is represented in Figure 7.2.

Anchors $\mathbf{A} \in \mathcal{A}_{\mathbf{p}}$ are of type $a \times b$, where a and b are either elements of $\mathbb{Z}$ or open intervals with integer endpoints. We then define

$$\begin{aligned} h\mathcal{I}(a) &:= \{i \in \mathbb{Z} : \{i\} \times a \subset v\mathcal{S}\}, \\ v\mathcal{I}(a) &:= \{j \in \mathbb{Z} : a \times \{j\} \subset h\mathcal{S}\}, \end{aligned} \tag{7.13}$$

and we assume that these two sets are ordered.

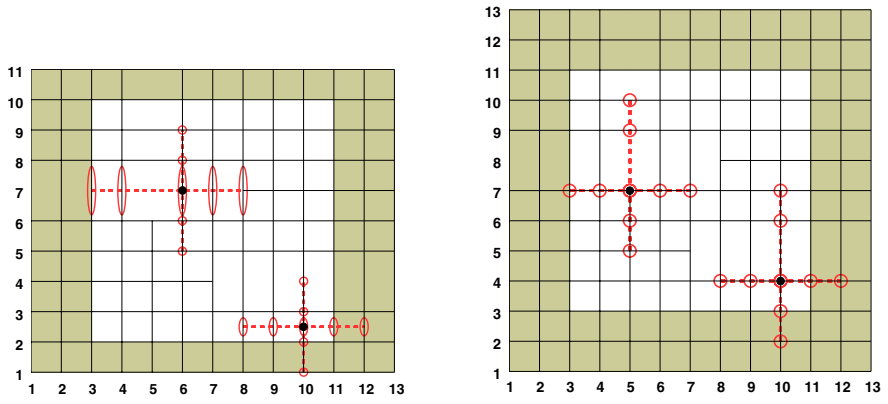

(a) $\mathbf{p} = (3, 2)$ (b) $\mathbf{p} = (3, 3)$

Figure 7.3. Construction of the horizontal and vertical index vector (empty ellipses joined with dashed lines), for some values of $\mathbf{p} = (p_1, p_2)$, and for the anchors marked as solid dots.

Definition 7.14. Given an anchor $\mathbf{A} = a \times b \in \mathcal{A}_{\mathbf{p}}(\mathcal{T})$, we define its horizontal (vertical) index vector $hv_{\mathbf{p}}(\mathbf{A})$ (resp. $vv_{\mathbf{p}}(\mathbf{A})$) as a subset of $h\mathcal{I}(b)$ (resp. $v\mathcal{I}(a)$) given by:

- if p is odd, $hv_{\mathbf{p}}(\mathbf{A}) = (i_1, \dots, i_{p_1+2}) \in \mathbb{Z}^{p_1+2}$ is made of the unique $p_1 + 2$ consecutive indices in $h\mathcal{I}(b)$ with $\{i_{(p_1+1)/2}\} = a$,
- if p_1 is even, $hv_{\mathbf{p}}(\mathbf{A}) = (i_1, \dots, i_{p_1+2}) \in \mathbb{Z}^{p_1+2}$ is made of the unique $p_1 + 2$ consecutive indices in $h\mathcal{I}(b)$ such that $]i_{p_1/2}, i_{p_1/2+1}[= a$.

The vertical index vector, denoted by

$$vv_{\mathbf{p}}(\mathbf{A}) = (j_1, \dots, j_{p_2+2}) \in \mathbb{Z}^{p_2+2},$$

is constructed in an analogous way, exchanging the roles of a and b.

Some examples of index vectors, for different values of $\mathbf{p} = (p_1, p_2)$, are given in Figure 7.3. For example, in Figure 7.3(b) ($p_1 = p_2 = 3$), the index vectors for the anchor $\mathbf{A} = \{5\} \times \{7\}$ are $hv_{\mathbf{p}}(\mathbf{A}) = (3, 4, 5, 6, 7)$ and $vv_{\mathbf{p}}(\mathbf{A}) = (5, 6, 7, 9, 10)$.

We are now in a position to define T-spline *blending functions* associated to a T-mesh $\mathcal{T}$. First we introduce $\Xi_1 = \{\xi_{1,\underline{n}_1}, \dots, \xi_{1,\overline{n}_1}\}$, a p_1-open knot vector on the interval $[0, 1]$ and $\Xi_2 = \{\xi_{2,\underline{n}_2}, \dots, \xi_{2,\overline{n}_2}\}$, a p_2-open knot vector on $[0, 1]$. Observe that the indexing adopted differs from that of Section 2. We associate to each anchor $\mathbf{A} = a \times b \in \mathcal{A}_{\mathbf{p}}(\mathcal{T})$ a bivariate B-spline function

of degree $\mathbf{p} = (p_1, p_2)$ defined in the form

$$\widehat{B}_{\mathbf{A},\mathbf{p}}(\zeta_1, \zeta_2) \tag{7.14}$$
$$= \widehat{B}[\{\xi_{1,i_1}, \xi_{1,i_2}, \dots, \xi_{1,i_{p_1+2}}\}](\zeta_1)\widehat{B}[\{\xi_{2,j_1}, \xi_{2,j_2}, \dots, \xi_{2,j_{p_2+2}}\}](\zeta_2),$$

where $hv_{\mathbf{p}}(\mathbf{A}) = (i_1, \dots, i_{p_1+2})$ and $vv_{\mathbf{p}}(\mathbf{A}) = (j_1, \dots, j_{p_2+2})$ denote the horizontal and vertical index vectors associated to the anchor $\mathbf{A}$; see Definition 7.14. The T-spline space is then defined as the space spanned by all these blending functions, namely

$$S^T_{\mathbf{p}}(\mathcal{A}_{\mathbf{p}}(\mathcal{T})) = \operatorname{span}\big\{\widehat{B}_{\mathbf{A},\mathbf{p}},\ \mathbf{A} \in \mathcal{A}_{\mathbf{p}}(\mathcal{T})\big\}. \tag{7.15}$$

Obviously, when the T-mesh is a tensor product grid the T-spline space defined above coincides with the B-spline space $S_{\mathbf{p}}(\boldsymbol{\Xi})$.

Once we have defined the T-spline space, the parametrization of a T-spline surface is constructed analogously to that of B-splines (2.43), by associating a control point to each blending function $\widehat{B}_{\mathbf{A},\mathbf{p}}$. Rational T-splines can also be constructed by defining the weight W as a linear combination of the T-spline blending functions.

After the definition of the T-spline parametrization, a discrete space for isogeometric analysis can be constructed as in (3.2), by choosing $\widehat{V}_h = S^T_{\mathbf{p}}(\mathcal{A}_{\mathbf{p}}(\mathcal{T}))$. However, in general it is not guaranteed that the constructed space is suitable to perform the analysis, and in particular a counter-example of linearly dependent T-splines was given in Buffa, Cho and Sangalli (2010*a*). In the next section we present a family of T-splines which show good properties for the analysis, and which are related to the dual-compatible splines defined in Section 7.1.

7.3. Analysis-suitable T-splines: fundamental properties

We will use the term *T-junctions* for the vertices of valence three in $\mathrm{AR}_{\mathbf{p}}$. Following Li *et al.* (2012), we adopt the notation $\perp$, $\top$, $\vdash$, $\dashv$ to indicate the four possible orientations of the T-junctions, and introduce the notion of a T-junction *extension*. T-junctions of type $\vdash$ and $\dashv$ (resp. $\perp$ and $\top$) and their extensions are called horizontal (resp. vertical). For the sake of simplicity, let us consider a T-junction $T = \{(\bar{\imath}, \bar{\jmath})\}$ of type $\dashv$. Clearly, $\bar{\imath}$ is one of the entries of $h\mathcal{I}(\{\bar{\jmath}\})$. We extract from $h\mathcal{I}(\{\bar{\jmath}\})$ the $p_1 + 1$ consecutive indices $i_1, i_2, \dots, i_{p_1+1}$ such that

$$\bar{\imath} = i_\kappa, \quad \text{with } \kappa = \lceil (p_1 + 1)/2 \rceil.$$

We let

$$\operatorname{ext}^e_{\mathbf{p}}(T) = [i_1, \bar{\imath}] \times \{\bar{\jmath}\}, \quad \operatorname{ext}^f_{\mathbf{p}}(T) =]\bar{\imath}, i_{p_1+1}] \times \{\bar{\jmath}\},$$
$$\operatorname{ext}_{\mathbf{p}}(T) = \operatorname{ext}^f_{\mathbf{p}}(T) \cup \operatorname{ext}^e_{\mathbf{p}}(T),$$

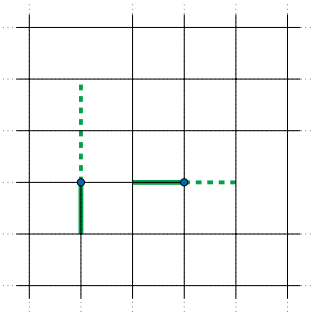

Figure 7.4. Extensions for degree $p_1 = 2$ (horizontal) and $p_2 = 3$ (vertical). The dashed lines represent the face extensions.

where $\mathrm{ext}^e_{\mathbf{p}}(T)$ is the *edge extension*, $\mathrm{ext}^f_{\mathbf{p}}(T)$ is the *face extension* and $\mathrm{ext}_{\mathbf{p}}(T)$ is just the *extension* of the T-junction T. The horizontal T-junction extension spans p_1 index intervals, referred to as *bays* in the literature. The edge extension spans $\lceil (p_1 - 1)/2 \rceil$ bays, and the face extension spans $\lfloor (p_1 + 1)/2 \rfloor$ bays. For the other type of T-junctions, the extensions are defined in a similar way, with the number of bays for vertical extensions depending on the value of p_2. An example with the length of the extensions is given in Figure 7.4.

Definition 7.15. A T-mesh $\mathcal{T} \in \mathrm{AD}_{\mathbf{p}}$ is *analysis-suitable* (AS) if horizontal T-junction extensions do not intersect vertical T-junction extensions. The class of analysis-suitable T-meshes is denoted by $\mathrm{AS}_{\mathbf{p}}$.

The fundamental result, stated for bicubic T-splines in Beirão da Veiga *et al.* (2012*a*) and generalized to arbitrary degree in Beirão da Veiga *et al.* (2013*a*), is that a T-mesh is AS if and only if the associated T-spline set is DC, up to minor technical assumptions. We report it below without proof.

Theorem 7.16. Let $\mathcal{T} \in \mathrm{AD}_{\mathbf{p}}$. If $\mathcal{T} \in \mathrm{AS}_{\mathbf{p}}$ then the set of T-spline blending functions (7.14) is DC. Furthermore, let $\mathcal{T} \in \mathrm{AD}^+_{\mathbf{p}}$. If the set of T-spline blending functions (7.14) is DC then $\mathcal{T} \in \mathrm{AS}_{\mathbf{p}}$.

It is worth noting that the definition of DC set of T-splines simplifies in two dimensions. The following characterization was taken as a definition in Beirão da Veiga *et al.* (2013*a*).

Proposition 7.17. In two dimensions, (7.14) is a DC set of splines if and only if each pair of T-splines in it have an overlapping local knot vector in at least one direction.

Furthermore, as remarked above, Definition 7.10 of the admissible T-mesh class is stronger than the definition from Beirão da Veiga *et al.* (2013*a*) and Li and Scott (2014). In particular the definition of $\mathrm{AD}^+_{\mathbf{p}}$ is equivalent to the

one in Bressan *et al.* (2013) and it implies the fundamental property below (which is an important corollary of the results in Bressan *et al.* 2013).

Proposition 7.18. Under the assumption $\mathcal{T} \in \mathrm{AD}_{\mathbf{p}}^{+} \cap \mathrm{AS}_{\mathbf{p}}$, the T-spline space (7.15) contains the polynomials of degree p_1 in the first variable and p_2 in the second variable.

Thanks to Propositions 7.3–7.9 and Propositions 7.16–7.18, we have the following theorem.

Theorem 7.19. If $\mathcal{T} \in \mathrm{AD}_{\mathbf{p}}^{+} \cap \mathrm{AS}_{\mathbf{p}}$, then T-spline blending functions in (7.14) are linearly independent, form a partition of unity, and the projection operator $\Pi_{\mathbf{p}} : L^2(\widehat{\Omega}) \to S_{\mathbf{p}}^{T}(\mathcal{A}_{\mathbf{p}}(\mathcal{T}))$ defined as in (7.10) gives optimal order of approximation, that is, there exists a constant C depending only on $\mathbf{p}$ such that, for $0 \leq s \leq \min\{p_1, p_2\} + 1$,

$$\|f - \Pi_{\mathbf{p}}(f)\|_{L^2(Q)} \leq C(h_{\bar{Q}})^s |f|_{H^s(\bar{Q})} \quad \text{for all } Q \subset \widehat{\Omega}, \text{ and } f \in H^s(\widehat{\Omega}),$$

where $h_{\bar{Q}}$ represents the diameter of $\bar{Q}$.

Beirão da Veiga *et al.* (2013*a*), Bressan *et al.* (2013) and Li and Scott (2014) provide another fundamental property of analysis-suitable T-splines. Define as $\mathrm{ext}_{\mathbf{p}}(\mathcal{T})$ the extended T-mesh in the index domain obtained by adding to $\mathcal{T}$ all the T-junction extensions, that is, the T-mesh having the union of $\mathcal{S}$ and all the T-junction extensions as skeleton. Let $\widehat{\mathcal{M}}$ denote the extended mesh in the parametric space, associated to $\mathcal{T}$, that is, the collection of *non-empty* elements of the form

$$Q =]\xi_{1,i_1}, \xi_{1,i_2}[\times]\xi_{2,j_1}, \xi_{2,j_2}[\neq \emptyset, \text{ with }]i_1, i_2[\times]j_1, j_2[\in \mathrm{ext}_{\mathbf{p}}(\mathcal{T}).$$

Beirão da Veiga *et al.* (2013*a*) show that $\widehat{\mathcal{M}}$ is the parametric Bézier mesh for an AS T-spline space (7.15), that is, the mesh of elements where T-splines are polynomials. Then, Bressan *et al.* (2013) further characterized the AS T-spline space as the space of piecewise polynomials on $\widehat{\mathcal{M}}$ that fulfil specific constraints at the mesh edges. The general result is technical, so in the following proposition we present a simple though interesting case (see Bressan *et al.* 2013, Proposition 6.1)

Proposition 7.20. Given $\mathcal{T} \in \mathrm{AD}_{\mathbf{p}}^{+} \cap \mathrm{AS}_{\mathbf{p}}$, if furthermore no T-junction extensions of any kind intersect each other or intersect mesh lines with multiplicity greater than one, then the T-spline space (7.15) is the space of all piecewise bivariate polynomials of degree (p_1, p_2) on $\widehat{\mathcal{M}}$ with the same continuity as the T-spline functions at the mesh lines.

We note that the approximation estimate from Theorem 7.19 is only valid in the parametric domain $\widehat{\Omega}$. Developing a similar result on the physical

domain Ω requires the definition of bent Sobolev spaces according to the characterization of T-spline spaces from Bressan *et al.* (2013), and is beyond the scope of this survey.

Finally, we comment on three-dimensional T-splines. These are defined and used mainly for the application of isogeometric methods in the engineering literature: see, for example, Bazilevs *et al.* (2010*a*), Zhang, Wang and Hughes (2012) and Wang *et al.* (2013). However, the definition of the class $\mathrm{AS}_{\mathbf{p}}$ in three dimensions is still absent. This is not a difficult extension *per se*, but we expect the study of mathematical properties of three-variate AS T-splines to be hard. On the other hand, the definition and study of DC set of B-splines in Section 7.1 is already dimension-independent, and this is therefore a framework for three-dimensional well-posed T-spline-based isogeometric methods that merits further investigation.

7.4. T-spline de Rham complex

The aim of this subsection is to introduce a two-dimensional de Rham complex based on AS T-splines, thus generalizing the tensor product construction of Section 5.5. For more details on this topic we refer to the recent publication by Buffa *et al.* (2014*b*). Throughout this section we assume, for the sake of simplicity, that $p_1 = p_2 = p$.

As for B-splines, T-spline vector fields are constructed by a suitable selection of the polynomial degree in the two directions. The main difference now is that we need to modify the index mesh at the boundary (similar to the change from Ξ_ℓ to Ξ'_ℓ for B-splines), but possibly also at T-junctions, depending on whether the degree is even or odd.

Let $p \in \mathbb{N}$, let Ξ_1, Ξ_2 be two p-open knot vectors, and let $\mathcal{T}^0 \in \mathrm{AS}_{(p,p)}$ be an index T-mesh on the index domain $[\underline{n}_1, \overline{n}_1] \times [\underline{n}_2, \overline{n}_2]$. On $\mathcal{T}^0$, we define the space of scalar fields as in (7.15):

$$\widehat{X}^0_h := S^T_{(p,p)}(\mathcal{A}_{(p,p)}(\mathcal{T}^0)). \tag{7.16}$$

The T-spline vector fields are defined from two T-meshes $\mathcal{T}^1_1$ (for one component) and $\mathcal{T}^1_2$ (for the other component). If p is even, $\mathcal{T}^1_1$ is equal to (with abuse of notation) $\mathcal{T}^0 \cap [\underline{n}_1 + 1, \overline{n}_1 - 1] \times [\underline{n}_2, \overline{n}_2]$, which means that

$$\mathcal{T}^1_1 = \big\{ E \in \mathcal{T}^0 : E \cap [\underline{n}_1 + 1, \overline{n}_1 - 1] \times [\underline{n}_2, \overline{n}_2] \neq \emptyset \big\}.$$

If p is odd, $\mathcal{T}^1_1$ is obtained from $\mathcal{T}^0 \cap [\underline{n}_1 + 1, \overline{n}_1 - 1] \times [\underline{n}_2, \overline{n}_2]$ by adding the first-bay face extension of all horizontal T-junctions. We define $\mathcal{T}^1_2$ analogously, reasoning in the vertical direction that if p is even, $\mathcal{T}^1_2$ is taken as $\mathcal{T}^0 \cap [\underline{n}_1, \overline{n}_1] \times [\underline{n}_2 + 1, \overline{n}_2 - 1]$, while if p is odd, $\mathcal{T}^1_2$ is defined by adding to $\mathcal{T}^0 \cap [\underline{n}_1, \overline{n}_1] \times [\underline{n}_2 + 1, \overline{n}_2 - 1]$ the first-bay face extension of all the vertical T-junctions. Then the vector fields and the rotated vector fields are defined

by

$$\widehat{X}_h^1 := S^T_{(p-1,p)}(\mathcal{A}_{(p-1,p)}(\mathcal{T}_1^1))) \times S^T_{(p,p-1)}(\mathcal{A}_{(p,p-1)}(\mathcal{T}_2^1)), \tag{7.17}$$

$$\widehat{X}_h^{1*} := S^T_{(p,p-1)}(\mathcal{A}_{(p,p-1)}(\mathcal{T}_2^1)) \times S^T_{(p-1,p)}(\mathcal{A}_{(p-1,p)}(\mathcal{T}_1^1)). \tag{7.18}$$

Finally, the last space $\widehat{X}_h^2$ is defined on the T-mesh $\mathcal{T}^2$: if p is even it is defined as $\mathcal{T}^0 \cap [\underline{n}_1+1, \overline{n}_1-1] \times [\underline{n}_2+1, \overline{n}_2-1]$, while for p odd $\mathcal{T}^2$ is obtained from $\mathcal{T}^0 \cap [\underline{n}_1+1, \overline{n}_1-1] \times [\underline{n}_2+1, \overline{n}_2-1]$ by adding all the first-bay face extensions (horizontal and vertical). Then

$$\widehat{X}_h^2 := S^T_{(p-1,p-1)}(\mathcal{A}_{(p-1,p-1)}(\mathcal{T}^2)). \tag{7.19}$$

That is, for even degree we only have to modify the boundary, whereas for odd degree we also need to add some extensions to the T-junctions. An example of the sequence of meshes is shown in Figure 7.5 for $p = 3$. The bases for $\widehat{X}_h^0, \ldots, \widehat{X}_h^2$, are formed by T-spline functions that can be scaled, as was done in (5.5)–(5.8).

We easily have the following result.

Proposition 7.21. Assuming $\mathcal{T}^0 \in \mathrm{AS}_{(p,p)}$, it holds that

$$\mathcal{T}_1^1 \in \mathrm{AS}_{(p-1,p)}, \quad \mathcal{T}_2^1 \in \mathrm{AS}_{(p,p-1)}, \quad \text{and} \quad \mathcal{T}^2 \in \mathrm{AS}_{(p-1,p-1)}.$$

Moreover, all the T-spline spaces defined in (7.16)–(7.19) share the same parametric Bézier mesh $\widehat{\mathcal{M}}$.

The definitions above become clear when considering the action of differential operators, as detailed in the following fundamental result, which generalizes to T-splines the two-dimensional spline complex in Section 5.5. The proof is given in Buffa *et al.* (2014*b*).

Theorem 7.22. Under the assumptions of Proposition 7.20, the following two-dimensional complexes are well defined and exact:

$$\mathbb{R} \longrightarrow \widehat{X}_h^0 \xrightarrow{\widehat{\mathbf{grad}}} \widehat{X}_h^1 \xrightarrow{\widehat{\mathrm{rot}}} \widehat{X}_h^2 \longrightarrow 0, \tag{7.20}$$

$$\mathbb{R} \longrightarrow \widehat{X}_h^0 \xrightarrow{\widehat{\mathbf{rot}}} \widehat{X}_h^{1*} \xrightarrow{\widehat{\mathrm{div}}} \widehat{X}_h^2 \longrightarrow 0. \tag{7.21}$$

Finally, we remark that when we have a NURBS parametrized geometry Ω, a similar complex is also valid in the physical domain obtained by applying the correct push-forwards, as in (5.31). The procedure is completely analogous to the one described in Section 5.5, and in fact it is not difficult to consider a (rational) T-spline geometry mapping defined using the space $S^T_{(p,p)}(\mathcal{A}_{(p,p)}(\mathcal{T}^0))$.

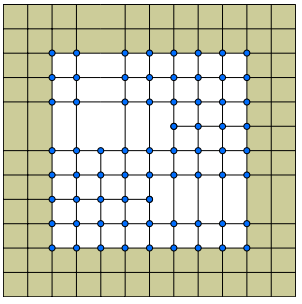

(a) mesh $\mathcal{T}^0$

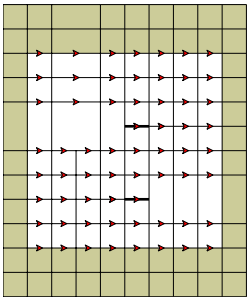

(b) mesh $\mathcal{T}_1^1$

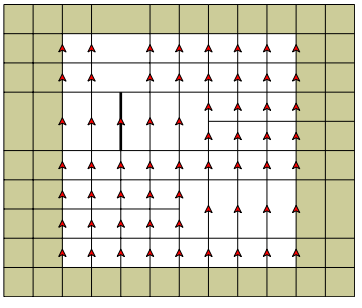

(c) mesh $\mathcal{T}_2^1$

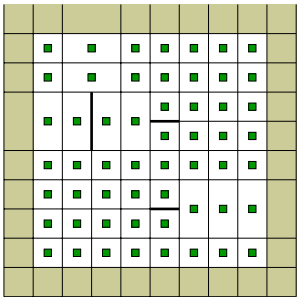

(d) mesh $\mathcal{T}^2$

Figure 7.5. Sequence of meshes for the T-spline complex, with their respective anchors, for $p = 3$: (a) mesh $\mathcal{T}^0$, anchors at the vertices, (b) mesh $\mathcal{T}_1^1$, anchors at the horizontal edges, (c) mesh $\mathcal{T}_2^1$, anchors at the vertical edges, and (d) mesh $\mathcal{T}^2$, anchors at the elements. The anchors are represented by dots for the scalar space $\widehat{X}_h^0$, arrows (indicating the vector component) for the vector space $\widehat{X}_h^1$, and squares for the scalar space $\widehat{X}_h^2$.

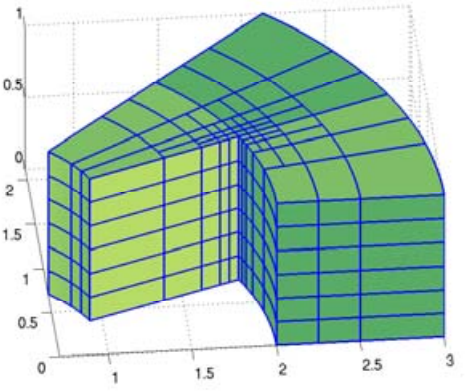

Figure 7.6. A mesh for the thick L-shaped domain: the lines represent the image of the T-mesh skeleton.

7.5. Application to a singular eigenvalue problem

In this section we present numerical tests showing the behaviour of a T-spline approximation for electromagnetic problems. For other tests we refer to Buffa *et al.* (2014*b*). We introduce a three-dimensional complex (on the parametric domain) by a tensor product of the two-dimensional T-spline complexes (7.20)–(7.21) and the one-dimensional B-spline complex (2.36). Then we define the spaces on the parametric domain $\widehat{\Omega} = (0,1)^3$:

$$\begin{aligned}
\widehat{Y}_h^0 &:= \widehat{X}_h^0 \otimes S_p(\Xi), \\
\widehat{Y}_h^1 &:= [\widehat{X}_h^1 \otimes S_p(\Xi)] \times [\widehat{X}_h^0 \otimes S_{p-1}(\Xi')], \\
\widehat{Y}_h^2 &:= [\widehat{X}_h^{1*} \otimes S_{p-1}(\Xi')] \times [\widehat{X}_h^2 \otimes S_p(\Xi)], \\
\widehat{Y}_h^3 &:= \widehat{X}_h^2 \otimes S_{p-1}(\Xi').
\end{aligned} \tag{7.22}$$

These form a de Rham complex:

$$\mathbb{R} \longrightarrow \widehat{Y}_h^0 \xrightarrow{\widehat{\mathbf{grad}}} \widehat{Y}_h^1 \xrightarrow{\widehat{\mathbf{curl}}} \widehat{Y}_h^2 \xrightarrow{\widehat{\mathrm{div}}} \widehat{Y}_h^3 \longrightarrow 0. \tag{7.23}$$

We assume a B-spline parametrized geometry Ω, such that the push-forwards (5.19) gives the correct de Rham complex on Ω:

$$\mathbb{R} \longrightarrow Y_h^0 \xrightarrow{\mathbf{grad}} Y_h^1 \xrightarrow{\mathbf{curl}} Y_h^2 \xrightarrow{\mathrm{div}} Y_h^3 \longrightarrow 0, \tag{7.24}$$

as for (5.21). This procedure is analogous to that described in Section 5.3 and it is not difficult to consider, more generally, a multi-patch (as in Section 5.4) or T-spline geometric mapping. This construction is not detailed here, but it is adopted in the numerical test proposed below.

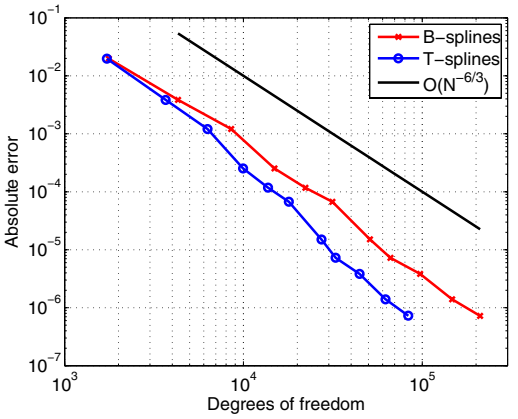

Figure 7.7. Error in the first computed eigenvalue versus the number of degrees of freedom.

For the numerical benchmark we consider the Maxwell eigenvalue problem (6.10) and solve it in the thick curved L-shaped domain, as in Section 6.3.3. The geometric representation differs from the one in that subsection, since the thick L-shaped domain is now parametrized as the union of three cubic patches (compare Figures 6.9(a) and 7.6). The scalar fields in Y_h^0 are bicubic ($p = 3$) and only continuous at the interfaces between patches, and the fields in Y_h^1 are only tangentially continuous at these interfaces (as for standard edge finite elements), but at least C^1 within patches.

The mesh is anisotropically and locally refined along the re-entrant edge, by use of T-splines with a dyadic partitioning. We perform the refinement first in the L-shaped two-dimensional section, and then propagate to the three-dimensional domain with a uniform mesh in the orthogonal direction. To construct the two-dimensional mesh, we first compute a one-dimensional dyadic partitioning, from which a quadrilateral mesh with T-junctions is created, and then some T-junction extensions are added to satisfy the conditions for an analysis-suitable T-mesh. For instance, one of these meshes is shown in Figure 7.6: the lines represent the image of the T-mesh skeleton.

For our numerical test we have solved the problem in a family of T-meshes, constructed from different one-dimensional partitions. We have computed the first Maxwell eigenvalue, which is related to the first eigenvalue of the Laplace eigenproblem in the two-dimensional section (see Costabel and Dauge 2006), and the corresponding eigenvector is singular at the re-entrant edge. In Figure 7.7 the eigenvalue error is plotted against the number of degrees of freedom for a sequence of T-meshes as described above and a family of tensor product meshes associated to the same global knot vectors. The T-mesh is clearly more effective and delivers an optimal order of approximation.

8. Efficient implementation and computational cost

In this section we discuss some relevant computational aspects of isogeometric methods. Since they are Galerkin methods, the computation of the discrete solution in isogeometric methods consists of two main steps, which are the same as in FEM: the assembly of the matrix and the vector of the finite-dimensional problem, and the solution of the corresponding linear system.

In the seminal paper by Hughes *et al.* (2005), and in all the early applications of isogeometric methods, the implementation is very similar to that of FEM. Each non-empty knot span is identified as an element of the mesh, and the local elementary matrices are computed by performing numerical quadrature within the element, and assembled into the global matrix as in FEM. Although there are several differences between the two methods, such as the use of rational polynomials and the fact that the basis functions are not interpolatory, the most important difference is the higher continuity of the basis functions. Indeed, the triple that defines an element in FEM (the geometric domain K, the space of functions P_K, and the degrees of freedom Σ_K) (Monk 2003) cannot be defined with splines or NURBS to be local to the element, since the degrees of freedom (the dual basis (2.47)) must be defined using the knots outside the element. To be precise, the functions on the element K are defined from the knots in the support extension $\widetilde{K}$.

In practice, high continuity has two immediate consequences from the computational perspective. The first is that when existing FEM codes are adapted to implement isogeometric methods, 'global' information from $\widetilde{K}$ must be used to compute the basis functions at the element level. The most common practice, at least for tensor product spaces, uses the algorithms in Piegl and Tiller (1997): we locate the position of the element in the global knot vectors, and then use those to compute the value of the basis functions. Another common approach is the so-called Bézier extraction, proposed in Borden, Scott, Evans and Hughes (2011), which allows us to express the high-continuity functions as linear combinations of C^0 Bernstein polynomials that are local to the element. We detail the procedure in Section 8.1.

The second important consequence is that high continuity increases the support of the basis functions and their interaction, affecting the sparsity pattern of the system matrix. In fact, higher continuity also implies a higher number of non-zero entries in the matrix, and increases the computational effort for the numerical solution of the linear system, as noted in Collier, Dalcin, Pardo and Calo (2013*a*). Moreover, Gaussian quadrature rules on each element are far from being optimal for B-splines, and at the moment the assembly of the matrix is the most time-consuming part of isogeometric codes. The development of optimal assembly procedures is an important task required to render isogeometric methods a competitive technology. In

Section 8.2 we explain in more detail how the continuity affects the computational cost.

Finally, another important aspect needs to be mentioned. It has recently become clear that, just as for standard high-degree Lagrangian finite elements, the matrices occurring in isogeometric methods suffer from large condition numbers when fine meshes and/or high degree p are used. However, the discrete spectrum of the isogeometric matrices differs from that of finite elements (see, *e.g.*, Hughes *et al.* 2008 and Garoni *et al.* 2014). This observation has driven various efforts in the isogeometric literature to build and analyse preconditioners that, in addition to allowing the handling of very fine meshes, can mitigate or even cancel such behaviour. We will review this area of study in Section 8.3.

We note that the scope of the present section is to address some of the computational issues associated to isogeometric methods, rather than to give a detailed description of their implementation. Details of the implementation can be found in Cottrell *et al.* (2009), which contains several algorithms written in pseudocode. There also exist several open-source codes in which isogeometric methods have been implemented. GeoPDEs (de Falco, Reali and Vázquez 2011) is an Octave/MATLAB code that can serve as an introduction to the basics of isogeometric methods, and it is the one we have used for the numerical experiments in this paper. Another MATLAB code, focused on solid mechanics, is MIGFEM (Nguyen, Bordas and Rabczuk 2012). For those readers aiming at high-performance computing and large applications, we recommend the general purpose C++ library igatools (Pauletti, Martinelli, Cavallini and Antolín 2013), or the PETSc-based library PetIGA (Collier, Dalcin and Calo 2013*b*).

8.1. Bézier extraction operators

As mentioned above, the high continuity of B-splines prevents us from computing the basis functions with the information contained in one single element, making it difficult to re-use existing FEM codes for the implementation of isogeometric methods. The solution proposed in Borden *et al.* (2011) is to express the B-spline basis functions on each Bézier element as linear combinations of Bernstein polynomials, which are local to the element, using the so-called Bézier extraction operators. These operators can be easily incorporated into existing FEM codes, without introducing changes in the matrix assembly. This procedure, which was introduced for NURBS in Borden *et al.* (2011), was extended to T-splines in Scott *et al.* (2011), and also works for the other local refinement strategies mentioned in Section 7, namely LR-splines and hierarchical splines. We explain here the construction of the extraction operators and, for simplicity, we assume that the parametrization is given by B-splines. The computations can be

easily extended to the NURBS case, taking into account the weights. We refer to Borden *et al.* (2011) for more details.

8.1.1. Univariate case

Bernstein polynomials provide a basis of the space of polynomials of degree p in the unit interval $[0,1]$. The $p+1$ Bernstein basis polynomials are given by the expression

$$b_{i+1,p}(t) = \binom{p}{i}(1-t)^{p-i}t^i, \quad \text{for } i = 0,\dots,p. \tag{8.1}$$

In fact, Bernstein polynomials are a particular case of B-splines for a p-open knot vector without internal knots, that is, $0 = \xi_1 = \cdots = \xi_{p+1} < \xi_{p+2} = \cdots = \xi_{2p+2} = 1$. Curves defined as linear combinations of Bernstein polynomials are called Bézier curves.

To compute the Bézier elements and the extraction operators, a B-spline curve given by the parametrization (2.9) is represented as a sequence of concatenated Bézier curves. The process is called Bézier decomposition, and it is achieved by performing knot insertion of the internal knots until their multiplicity is equal to p, that is, until the continuity at the knots is C^0. An example of Bézier decomposition is shown in Figure 8.1.

Let $\Xi = \{\xi_1,\dots,\xi_{n+p+1}\}$ be the knot vector of the original B-spline curve, and let $\{\bar{\xi}_1,\dots,\bar{\xi}_m\}$ be the set of knots, possibly repeated, required to be inserted for the Bézier decomposition. Let $\widehat{\mathbf{B}}(\zeta) = \{\widehat{B}_{i,p}(\zeta)\}_{i=1}^{n}$ denote the original B-splines, organized in a column vector, and let $\bar{\mathbf{B}}(\zeta) = \{\bar{B}_{i,p}(\zeta)\}_{i=1}^{n+m}$ denote the column vector of B-splines with C^0-continuity, obtained after inserting m new knots. By successively applying (2.14), the two sets of basis functions are related by the expressions

$$\widehat{\mathbf{B}}(\zeta) = \mathbf{E}\bar{\mathbf{B}}(\zeta), \tag{8.2}$$

where $\mathbf{E} \in \mathbb{R}^{n\times(n+m)}$ is a matrix defined by

$$\mathbf{E} = \mathbf{E}^1\mathbf{E}^2\cdots\mathbf{E}^m,$$

and the matrices $\mathbf{E}^j \in \mathbb{R}^{(n+j-1)\times(n+j)}$, for $j = 1,\dots,m$, are obtained by successive insertion of the knots $\bar{\xi}_j$, and have the form

$$\mathbf{E}^j = \begin{bmatrix} \alpha_1^j & 1-\alpha_2^j & 0 & \cdots & & & 0 \\ 0 & \alpha_2^j & 1-\alpha_3^j & 0 & \cdots & & 0 \\ \vdots & & & & & & \vdots \\ 0 & \cdots & & & 0 & \alpha_{n+j-1}^j & 1-\alpha_{n+j}^j \end{bmatrix}.$$

The coefficients α_i^j are given by (2.15), and correspond to inserting the knot $\bar{\xi}_j$ in the knot vector which already contains the previous $j-1$ new knots.

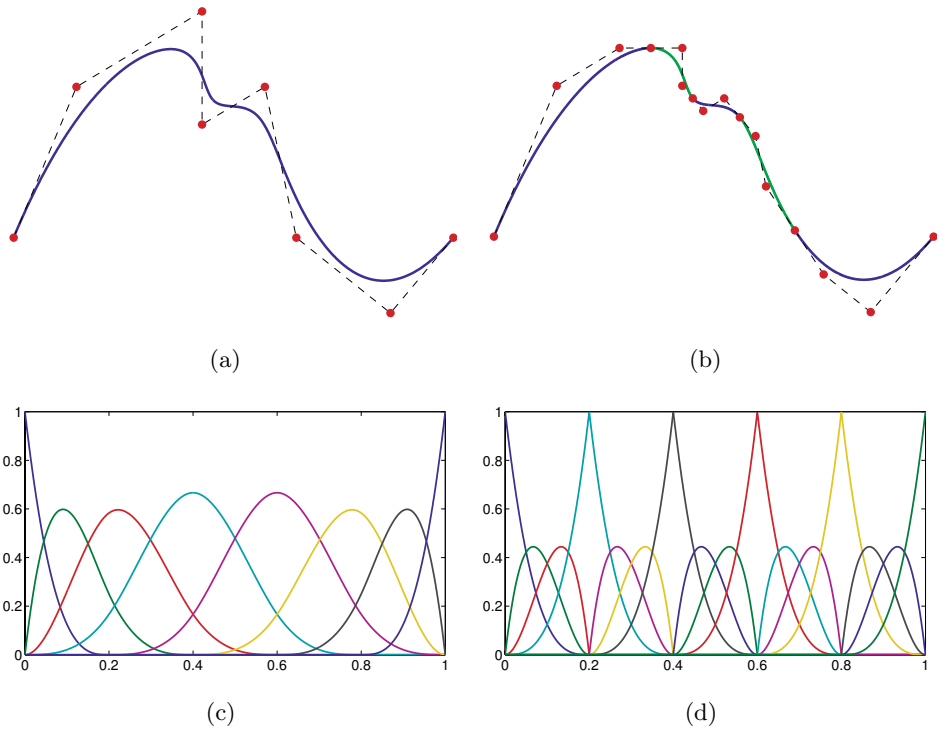

Figure 8.1. Bézier decomposition of a B-spline curve, and the corresponding basis functions: (a) initial B-spline curve, (b) the same curve after Bézier decomposition, (c) B-spline basis functions $\widehat{B}_{i,p}$, and (d) the B-spline basis functions with C^0-continuity, $\bar{B}_{i,p}$.

The matrix $\mathbf{E}$ is called the Bézier extraction operator. It relates not only the two sets of basis functions but also their associated control points. Indeed, if we let $\mathbf{c} = \{\mathbf{c}_i\}_{i=1}^{n}$ denote the set of control points of the original curve, and let $\bar{\mathbf{c}} = \{\bar{\mathbf{c}}_i\}_{i=1}^{n+m}$ denote the set of control points obtained after Bézier decomposition, applying (8.2) we have

$$\mathbf{F}(\zeta) = \mathbf{c}^T \widehat{\mathbf{B}}(\zeta) = \mathbf{c}^T \mathbf{E} \bar{\mathbf{B}}(\zeta) = \bar{\mathbf{c}}^T \bar{\mathbf{B}}(\zeta),$$

which yields

$$\bar{\mathbf{c}} = \mathbf{E}^T \mathbf{c}.$$

In practice, the extraction operator $\mathbf{E}$ is never computed globally. Instead, local extraction operators are computed on each Bézier element, taking into account the non-vanishing basis functions. Let us consider the kth Bézier element $I_k = (\zeta_k, \zeta_{k+1})$, which is also written as $(\xi_\ell, \xi_{\ell+1})$ for a certain (unique) ℓ. The non-vanishing B-spline basis functions are given by $\widehat{\mathbf{B}}^{I_k}(\zeta) = \{\widehat{B}_{i,p}(\zeta)\}_{i=\ell-p}^{\ell}$ and $\bar{\mathbf{B}}^{I_k}(\zeta) = \{\bar{B}_{i,p}(\zeta)\}_{i=kp-p+1}^{kp+1}$, and with the

same indices we have the sets of control points acting on the Bézier element, $\mathbf{c}^{I_k}$ and $\bar{\mathbf{c}}^{I_k}$. The basis functions and control points are related by the expression

$$\begin{aligned} \widehat{\mathbf{B}}^{I_k}(\zeta) &= \mathbf{E}^{I_k}\bar{\mathbf{B}}^{I_k}(\zeta), \\ \bar{\mathbf{c}}^{I_k} &= (\mathbf{E}^{I_k})^T\mathbf{c}^{I_k}, \end{aligned} \tag{8.3}$$

where the local extraction operator $\mathbf{E}^{I_k}$ is the square submatrix of $\mathbf{E}$:

$$\mathbf{E}^{I_k} = (E_{ij}), \quad i = \ell - p, \dots, \ell, \quad j = kp - p + 1, \dots, kp + 1.$$

The algorithm to compute the local extraction operators is a modification of the Bézier decomposition algorithm, and can be found in Borden *et al.* (2011).

In fact, on each Bézier element we can write the refined basis functions $\bar{\mathbf{B}}^{I_k}(\zeta)$ as Bernstein polynomials, by applying the change of variable

$$t = \frac{\zeta - \zeta_k}{\zeta_{k+1} - \zeta_k}.$$

Indeed, denoting $\mathbf{b}(t) = \{b_{i,p}(t)\}_{i=1}^{p+1}$, we have

$$\bar{\mathbf{B}}^{I_k}(\zeta) = \mathbf{b}(t),$$

and from (8.3) we immediately deduce

$$\widehat{\mathbf{B}}^{I_k}(\zeta) = \mathbf{E}^{I_k}\mathbf{b}(t), \quad \frac{\partial \widehat{\mathbf{B}}^{I_k}}{\partial \zeta} = \mathbf{E}^{I_k}\frac{\partial \mathbf{b}}{\partial t}\frac{\partial t}{\partial \zeta}.$$

8.1.2. Multivariate case

In the tensor product setting, the extraction operators are also defined by tensor product. As in Section 2.2, let d be the space dimension, and assume we are given the knot vectors $\Xi_\ell = \{\xi_{\ell,1}, \dots, \xi_{\ell,n_\ell+p_\ell+1}\}$, and the Bézier decomposition in each direction is obtained after inserting the knots $\{\bar{\xi}_{\ell,1}, \dots, \bar{\xi}_{\ell,m_\ell}\}$. Let us denote by $\mathbf{E}_\ell^{I_{k_\ell}}$ the element extraction operator for the k_ℓth Bézier element, $I_{k_\ell} = (\zeta_{\ell,k_\ell}, \zeta_{\ell,k_\ell+1})$, in the Ξ_ℓ knot vector. The element extraction operator for the Bézier element $Q \in \widehat{\mathcal{M}}$, $Q = I_{k_1} \times \cdots \times I_{k_d}$ is given by the (Kronecker) tensor product of the univariate matrices

$$\mathbf{E}^Q = \mathbf{E}_d^{I_{k_d}} \otimes \cdots \otimes \mathbf{E}_1^{I_{k_1}}. \tag{8.4}$$

The equalities (8.3) then become $\widehat{\mathbf{B}}^Q(\boldsymbol{\zeta}) = \mathbf{E}^Q\mathbf{b}(\mathbf{t})$, and $\bar{\mathbf{c}}^Q = (\mathbf{E}^Q)^T\mathbf{c}^Q$, from which we can also evaluate the parametrization $\mathbf{F}$ and its derivatives. In practice, rather than computing the extraction operator $\mathbf{E}^Q$, it is more efficient to compute the univariate B-splines from the univariate extraction operators, and multivariate basis functions are then computed by tensor product.

Remark 8.1. Bézier extraction operators can also be applied to the vector spaces in Section 5. In this case, a different extraction operator can be defined for each component of the vector field.

Remark 8.2. As was noted in Scott *et al.* (2011), the extraction operator can also be applied to T-splines, and is currently the most popular strategy for evaluating T-spline basis functions.

8.2. A discussion about continuity and computational cost

As we have seen in Section 6, high-continuity spaces give better accuracy results in terms of the degrees of freedom. However, the computational cost per degree of freedom typically increases, especially if algorithms for the C^0 finite element method are adopted. We report here some of the partial and most interesting results that are available in the literature following this approach (*e.g.*, Collier *et al.* 2012*b*, Collier *et al.* 2013*a*, Schillinger *et al.* 2013), but the discussion on this topic is still open. Indeed, we strongly believe that it is too early to assess the efficiency of the high-regularity high-degree k-refined isogeometric methods, and more effort needs to be directed towards the study of efficient implementation of isogeometric methods in order to exploit its full potential.

For simplicity we compare the computational cost of a discretization using NURBS spaces of maximum and minimum continuity, that is, C^{p-1} and C^0, respectively. We will focus on the Laplace problem, discretized with the space V_h in (3.2), as a model case. To simplify the analysis, we will assume in the following that periodic conditions (either C^0 or C^{p-1}) are imposed at the boundaries. In this case, for $N_{\rm el}$ elements the number of degrees of freedom is $N_{\rm dof} = p^d N_{\rm el}$ when C^0-functions are used, and $N_{\rm dof} = N_{\rm el}$ for C^{p-1}-functions. For other boundary conditions, these results hold asymptotically for $N_{\rm el} \gg p$.

8.2.1. Computation of the linear system matrix

The discussion in this section covers tensor product NURBS. The calculation of the local stiffness matrix is typically performed by numerical quadrature. The asymptotic number of floating point operations needed to compute the contribution to the local stiffness matrix at one quadrature point is $O(p^{2d})$. These values are valid for any continuity (from C^0 to C^{p-1}) of the basis functions and easily follow from the fact that there are, in all cases, $(p+1)^d$ non-vanishing functions at each point in the interior of a Bézier element, and neglecting the cost of computing the univariate B-spline.

Neglecting the cost of assembling the local matrices into the global one, the total number of FLOPS is then $O(p^{2d})$ multiplied by the total number of quadrature points, with a straightforward quadrature implementation.

Adopting a Gaussian quadrature rule of $(p+1)^d$ points per element, the total number of quadrature points is $N_{\rm el}(p+1)^d$. Therefore, the total number of operations to construct the stiffness matrix in terms of $N_{\rm el}$ is in proportion to $N_{\rm el}p^{3d}$ FLOPS for C^0- and C^{p-1}-functions. If we also take into account that the number of degrees of freedom is equal to $N_{\rm dof} = p^d N_{\rm el}$ when C^0-functions are used, and $N_{\rm dof} = N_{\rm el}$ for C^{p-1}-functions, then it is interesting to note that the cost of constructing the stiffness matrix results in $CN_{\rm dof}p^{3d}$ for C^0 and $CN_{\rm dof}p^{3(d+1)}$ for C^{p-1}-continuous NURBS. More details are given in Schillinger *et al.* (2013), where the focus is the comparison between the isogeometric Galerkin and isogeometric collocation methods.

It must be noted that if a *sum factorization* quadrature algorithm (see Melenk, Gerdes and Schwab 2001) is adopted, the total cost can be reduced to $CN_{\rm el}p^{2d+1}$, though to our knowledge this is not used in existing isogeometric codes.

We remark that, in existing isogeometric codes, matrix construction is the most expensive part of the computation. To alleviate its cost, different quadrature rules have been proposed by Hughes, Reali and Sangalli (2010) and Auricchio *et al.* (2012) for high-continuity splines, which reduce the number of quadrature points for C^{p-1}-continuous NURBS, from $(p+1)^d N_{\rm dof}$ to $(p/2+1)^d N_{\rm dof}$. Other approaches have been proposed recently (*e.g.*, Mantzaflaris and Jüttler 2014) and are based on an explicit computation of integrals (by *ad hoc* formulae) of B-splines, but at present they are restricted to uniform knot vectors.

Finally, it is worth noting that Karatarakis, Karakitsios and Papadrakakis (2014) proposed computing each entry of the global stiffness matrix directly instead of performing an element-by-element assembly. This approach is referred to as a *control point pairwise* formulation, and it is more efficient than element-by-element computation and assembly. Furthermore, it is efficiently parallelizable on GPUs.

8.2.2. Sparsity of the linear system matrix

We report the estimates for the number of non-zero entries in the stiffness matrix coming from C^0 and C^{p-1} discretizations already computed in Collier *et al.* (2013*a*). The number of non-zero entries in each row is the number of interactions of the corresponding basis function with functions that have overlapping support, which will depend on the continuity.

We begin by considering the one-dimensional case. For C^0-functions, the number of interactions depends on the relative position of the basis function (see, *e.g.*, Figure 8.1(d)). A function interpolating at the knot interacts with $2p+1$ other functions, whereas an interior function only interacts with $p+1$ functions. Since we are using periodic conditions, for $N_{\rm el}$ elements we have $N_{\rm el}$ functions associated to the knots, and $(p-1)N_{\rm el}$ interior functions. Thus, in the one-dimensional case the number of non-zero entries for

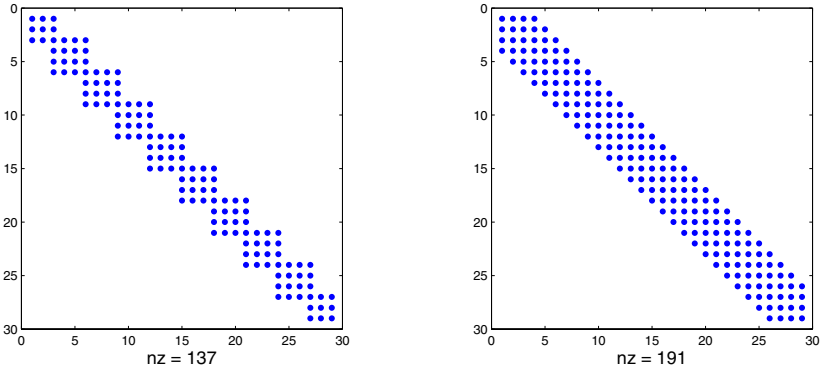

(a) (b)

Figure 8.2. Sparsity of the stiffness matrix for univariate splines: cubic splines with (a) C^0-continuity and (b) C^2-continuity.

C^0-functions is

$$\mathrm{nnz}^{C^0} = (2p+1)N_{\mathrm{el}} + (p+1)(p-1)N_{\mathrm{el}} = (p^2+2p)N_{\mathrm{el}} = (p+2)N_{\mathrm{dof}}.$$

In the case of C^{p-1}-continuity, the number of interactions is $2p+1$ for every function. Since we are using C^{p-1}-periodicity at the ends of the interval, the number of unknowns is equal to the number of elements N_{el}, and we obtain

$$\mathrm{nnz}^{C^{p-1}} = (2p+1)N_{\mathrm{el}} = (2p+1)N_{\mathrm{dof}}.$$

That is, although the bandwidth is equal to $2p+1$ independent of the continuity, high-continuity functions completely cover the band. A visual comparison of the sparsity of the stiffness matrix in the one-dimensional case is shown in Figure 8.2. Note that in the figure we do not use periodic boundary conditions.

In the tensor product setting, for C^0-continuous functions there are $d+1$ types of basis function on each element: vertex, edge and interior in two dimensions, and vertex, edge, face and interior in three dimensions. The number of functions of each type and the number of interactions are summarized in Table 3.1 in Collier *et al.* (2013*a*). Using that information, it is easy to see that the number of non-zero entries in the matrix is equal to

$$\mathrm{nnz}^{C^0} = (p+2)^d p^d N_{\mathrm{el}} = (p+2)^d N_{\mathrm{dof}}. \tag{8.5}$$

For C^{p-1}-continuous functions, the number of interactions is always $(2p+1)^d$, and since the number of degrees of freedom is $N_{\mathrm{dof}} = N_{\mathrm{el}}$, we have

$$\mathrm{nnz}^{C^{p-1}} = (2p+1)^d N_{\mathrm{el}} = (2p+1)^d N_{\mathrm{dof}}. \tag{8.6}$$

We note that in the multivariate case the band is not completely full.

Table 8.1. FLOPS estimates for a multi-frontal direct solver (Collier, Pardo, Paszynski and Calo 2012*a*).

	$k = 0$	$k = p - 1$
One dimension	$O(p^2 N_{\text{dof}})$	$O(p^2 N_{\text{dof}})$
Two dimensions	$O(p^4 N_{\text{dof}} + N_{\text{dof}}^{1.5})$	$O(p^3 N_{\text{dof}}^{1.5})$
Three dimensions	$O(p^6 N_{\text{dof}} + N_{\text{dof}}^{2})$	$O(p^3 N_{\text{dof}}^{2})$

Table 8.2. Memory estimates for a multi-frontal direct solver (Collier, Pardo, Paszynski and Calo 2012*a*).

	$k = 0$	$k = p - 1$
One dimension	$O(p\, N_{\text{dof}})$	$O(p\, N_{\text{dof}})$
Two dimensions	$O(p^2 N_{\text{dof}} + N_{\text{dof}} \log(N_{\text{dof}}/p^2))$	$O(p^2 N_{\text{dof}} \log(N_{\text{dof}}/p^2))$
Three dimensions	$O(p^3 N_{\text{dof}} + N_{\text{dof}}^{4/3})$	$O(p^2 N_{\text{dof}}^{4/3})$

8.2.3. Solution of the linear system: performance of direct solvers
The sparsity of the matrix has important consequences for the performance of the solvers. As we have just seen, the system matrix coming from a C^0 NURBS discretization shows a multi-block structure, as for standard finite elements. In this case, static condensation (Wilson 1974) can be applied in order to remove the internal degrees of freedom in every element, and in practice the solver can be applied to a smaller linear system, formed by the degrees of freedom shared by several elements. As noted in Collier *et al.* (2012*b*), in the case of a C^{p-1} NURBS discretization static condensation is not efficient, because due to the extended support of the basis functions only very few degrees of freedom can be removed.

The performance of direct solvers for isogeometric discretizations has been studied both analytically and numerically by Collier *et al.* (2012*b*) (see also Collier, Pardo, Paszynski and Calo 2012*a*). Collier *et al.* (2012*b*) consider multi-frontal algorithms, which are the up-to-date technology for the solution of linear systems coming from finite elements. Their results, summarized in Tables 8.1 and 8.2, show that high continuity has an important cost in terms of both computational time and memory consumption, when solving with the same number of degrees of freedom.

8.2.4. Solution of the linear system: performance of iterative solvers
Analysis of the performance of iterative solvers is more intricate, since one should consider the computational cost of one iteration, the total number

of iterations for convergence, and the cost of setting up the preconditioner. Although there are some papers that present preconditioning techniques for isogeometric methods (see Section 8.3), the only work we are aware of that studies the computational cost of iterative solvers for isogeometric methods is Collier *et al.* (2013*a*), from which we report some of the results.

The cost of one iteration mainly depends on the cost of the matrix–vector product, which is in proportion to the number of non-zero entries both in the matrix of the system and in the preconditioner. From the estimates in (8.5) and (8.6), even for very high p the cost of matrix–vector multiplication is no more than 2^d times for C^{p-1}-spaces than for C^0-spaces, and for relatively small p the difference is even lower. For instance, for $p = 3$ the computational cost is only three times higher in the three-dimensional case. We must remark, however, that static condensation can also be applied as a first step in iterative solvers, reducing the cost of each iteration for C^0-spaces. We refer to Collier *et al.* (2013*a*) for more details.

Concerning the preconditioner, Collier *et al.* (2013*a*) estimate the cost of constructing several preconditioners, and present several numerical tests with the preconditioned conjugate gradient method, to compare their performance in terms of computational time and number of iterations. In particular, they consider the diagonal Jacobi preconditioner, SSOR, incomplete LU factorization with no fill-in (ILU), and two different additive Schwarz preconditioners, including the one in Beirão da Veiga *et al.* (2012*d*).

From their estimates, they conclude that the cost of constructing the Jacobi, SSOR and ILU preconditioners is very similar for C^0- and C^{p-1}-spaces. The construction of the additive Schwarz preconditioner in the C^{p-1} case is similar if a minimal overlap is used, while it is much more expensive (it increases as p^9) if a generous p-overlap is applied. Their numerical results confirm that, at least on the basis of the computational time, it may therefore not be a good choice to use a generous overlap in the high-continuity case. On the other hand the much better condition number for high p for the latter choice allows for higher precision in the computations, which is one of the reasons to use a high polynomial degree.

Concerning the number of iterations and computational time, a remarkable result is the good behaviour of the ILU preconditioner for C^{p-1}-spaces. Indeed, the results from Table 4.2 in Collier *et al.* (2013*a*) show that, although the number of iterations increases when reducing the mesh size h, it remains constant when raising the degree p.

8.3. Preconditioning

In this section we present a short description of the main ideas of various preconditioners that can be found in the isogeometric literature. These include overlapping Schwarz, BPX, multigrid, BDDC and FETI.

8.3.1. Overlapping Schwarz

Beirão da Veiga *et al.* (2012*d*) consider a scalar elliptic model problem in order to construct and study overlapping Schwarz preconditioners for NURBS-based isogeometric methods.

The basic construction starts from a tensor product subdivision of the parameter domain $\widehat{\Omega} = (0,1)^d$ into disjoint rectangular subdomains. For simplicity of exposition, we first focus on the one-dimensional case $\widehat{\Omega} = [0,1]$.

The interval $[0,1]$ is first partitioned into N_{sub} disjoint sub-intervals $\widehat{I}_r = [\zeta_{i_r}, \zeta_{i_{r+1}}]$ (see (2.1) for the definitition of ζ_i) with $r = 1, \dots, N_{\text{sub}}$. A fundamental step is then to subdivide the parameter spline space $S_p(\Xi)$ into subspaces S_r, each one associated to a subdomain $\widehat{I}_r$. Recalling that we have n B-spline basis functions, we subdivide the set of indices $\{1, 2, \dots, n\}$ into N_{sub} (overlapping) sets

$$\{1, 2, \dots, \widehat{i}_1\},\ \{\widehat{i}_1, \widehat{i}_1 + 1, \dots, \widehat{i}_2\}, \dots, \{\widehat{i}_{N_{\text{sub}}-1}, \widehat{i}_{N_{\text{sub}}-1} + 1, \dots, n\}$$

with the property that, for all $i = 2, \dots, N_{\text{sub}}$, the interface point ζ_{i_r} is in the support of the basis function $\widehat{B}_{\widehat{i}_{r-1},p}$. We then set, for $r = 1, \dots, N_{\text{sub}}$,

$$S_r := \text{span}\big\{\widehat{B}_{i,p}\big\}_{i=\widehat{i}_{r-1}}^{\widehat{i}_r},$$

with the convention $\widehat{i}_0$=1 and $\widehat{i}_{N_{\text{sub}}} = n$.

More overlap can be enforced on the subspaces $\{S_r\}_{r=1}^{N_{\text{sub}}}$ simply by increasing the overlap in index space of the above sets; what is presented above is the so-called *minimal* overlap. The above construction can be easily extended to general dimension d by a simple tensor product construction. The subdivisions above can be introduced for each coordinate direction $\ell = 1, \dots, d$ and the subdomains defined by the Cartesian product of the associated intervals. Finally, note that the above construction in parameter space trivially extends to the mapped NURBS framework simply by considering mapped subdomains and (mapped) NURBS basis functions instead of B-spline basis functions.

Given a subdivision into subspaces, the overlapping additive Schwarz method can be easily built in an algebraic way. We consider the two-level case here, thus including the introduction of a coarse space $S_{\text{coarse}} \subset S_p(\Xi)$. Let A represent the stiffness matrix of the original system. The preconditioner matrix is built as

$$\mathbf{B}_{\text{OAS}} = R_{\text{coarse}}^T A_{\text{coarse}}^{-1} R_{\text{coarse}} + \sum_{\theta} R_\theta^T\, A_\theta^{-1}\, R_\theta. \tag{8.7}$$

Here, θ represents a generic multi-index counting on all the subdomains. The R_θ are restriction matrices with $0, 1$ entries returning the coefficients of the basis functions belonging to the local spaces S_θ, while $A_\theta = R_\theta\, A\, R_\theta^T$ are the local stiffness matrices restricted to the subspace S_θ. Moreover, R_{coarse} is

the fine-to-coarse restriction matrix and A_{coarse} is the coarse stiffness matrix associated with the coarse space S_{coarse}. Each column of R_{coarse} contains the coefficients of a coarse space basis function expressed as linear combination of the fine space basis functions. Note that more general multiplicative and hybrid versions, as well as projection-like operators associated with inexact local solvers, could also be used.

Beirão da Veiga *et al.* (2012*d*) prove the following bound, showing that the resulting solvers are scalable (independent of the number of subdomains) and have an optimal convergence rate depending linearly on the ratio H/h between the subdomain and mesh sizes.

Theorem 8.3. The condition number of the two-level additive Schwarz preconditioned isogeometric operator defined in (8.7) is bounded by

$$\kappa_2(\mathbf{B}_{\text{OAS}}A) \leq C\left(1 + \frac{H}{h\beta}\right),$$

where β is an overlap parameter growing linearly with the overlap and C is a constant independent of h, H (but not of p, k).

The results of extensive two- and three-dimensional numerical tests in Beirão da Veiga *et al.* (2012*d*) confirm the bound above and additionally explore the condition number dependence on p and k, showing that, as for standard spectral element Schwarz preconditioners, there is optimality in p for generous overlap (for both minimal and maximal regularity k) while the growth in p becomes stronger for minimal overlap and in particular for maximal regularity $k = p - 1$. A sample experiment, taken from Beirão da Veiga *et al.* (2012*d*), is shown in Table 8.3. The numerical tests, moreover, show that the above good convergence properties also hold for heterogeneous problems with discontinuous coefficients across subdomain boundaries.

In the more engineering-oriented contribution of Beirão da Veiga *et al.* (2013*c*), the above results are extended to the case of linear elasticity. In the case of compressible elasticity, which has the same elliptic nature as the Laplace problem, the authors easily extend the theorem above into an equivalent one. Moreover, extensive numerical tests are developed for the almost incompressible case, treated with the mixed displacement-pressure formulation of Bressan and Sangalli (2013). Interesting new aspects need to be considered, such as that of the minimal displacement space overlap (with respect to the pressure space) in order to guarantee the inf-sup condition for the local problems too. The results show that similar good behaviour is also obtained for the almost incompressible case; we refer the interested reader to Beirão da Veiga *et al.* (2013*c*).

Table 8.3. Two-level OAS preconditioner in the parametric domain: condition number $\kappa_2(\mathbf{B}_{\mathrm{OAS}}A)$ as a function of the spline polynomial degree p for maximal regularity $k = p-1$ (left) and minimal regularity $k = 0$ (right), with different levels of overlap from symmetric minimal ($r = 0$) to symmetric generous ($r = p$). Fixed $1/h = 32$, 2×2 subdomains, $H/h = 16$.

	$k = p-1$					$k = 0$		
	No prec.	Two-level OAS				No prec.	Two-level OAS	
p		$r = 0$	$r = 2$	$r = 4$	$r = p$		$r = 0$	$r = p$
2	78.12	7.08	4.63	4.11	4.63	554.89	8.98	4.87
3	82.10	6.71	4.24	4.32	4.18	1.07×10^3	8.46	4.88
4	206.71	6.02	4.10	4.29	4.29	1.76×10^3	8.47	4.92
5	1.57×10^3	15.52	4.67	4.61	4.76	1.26×10^4	8.65	4.97
6	1.29×10^4	12.64	4.88	4.66	4.79	1.53×10^5	8.80	4.98
7	1.02×10^5	55.09	6.84	5.21	4.99	1.98×10^6	9.13	4.99
8	2.99×10^5	37.43	7.61	5.35	4.98	1.86×10^6	10.55	4.98
9	1.07×10^6	289.61	13.12	6.62	4.99	2.96×10^6	12.23	4.99
10	1.24×10^6	156.85	13.44	6.20	4.99	6.34×10^6	13.48	4.99

8.3.2. BPX

The Bramble–Pasciak–Xu (BPX) preconditioner, first proposed in Bramble, Pasciak and Xu (1990), can be seen as an abstract additive Schwarz preconditioner where the spaces are obtained by a multilevel decomposition of the discrete space. References to BPX for B-splines are Maes, Kunoth and Bultheel (2007), for triangular splines, and Buffa *et al.* (2013), in the framework of isogeometric methods. Here we briefly summarize the results of Buffa *et al.* (2013) and, as in the previous section, we focus on the Laplace problem.

Assume that we are given a sequence of dyadically refined knot vectors $\Xi_1, \dots, \Xi_J = \Xi$ such that each Ξ_j is the p-open knot vector

$$\Xi_j = \left\{ \underbrace{0, \dots, 0}_{p+1 \text{ times}}, \frac{1}{2^j}, \frac{2}{2^j}, \dots, \frac{2^j-1}{2^j}, \underbrace{1, \dots, 1}_{p+1 \text{ times}} \right\}, \quad \text{for all } j = 1, \dots, J, \tag{8.8}$$

which are taken to be uniform for simplicity. A multilevel decomposition of the spline space is $S_1 \subset S_2 \subset \cdots \subset S_J = S_p(\Xi)$, where

$$S_j = S_p(\Xi_j), \quad \text{for all } j = 1, \dots, J. \tag{8.9}$$

More generally, Ξ_1 can be selected as any coarse knot vector, with possible repeated knots in the interior, and $\Xi_2, \dots, \Xi_J$ can be defined as dyadic refinements. This framework easily extends to higher dimensions by tensor

products and, following the isogeometric paradigm (3.2), is mapped onto the physical space Ω, which inherits a multilevel decomposition $V_1 \subset \cdots \subset V_j = V_h$. Then, the BPX preconditioner proposed in Buffa *et al.* (2013) is given by

$$\mathbf{B}_{\mathrm{BPX}} = I_1^J A_1^{-1} I_J^1 + \sum_{j=2}^{J} I_j^J (\mathrm{diag} A_j)^{-1} I_J^j, \tag{8.10}$$

where I_j^J is the matrix representing the inclusion from the coarser space V_j into the space V_h and is obtained by knot insertion (2.14)–(2.15), $I_J^j = (I_i^J)^T$ is the matrix representing a restriction from the space V_h to the space V_j, and A_j is the stiffness matrix on V_j. Note that (8.10) has a similar structure to (8.7), where an inexact solver (Jacobi iteration) is used on V_j (or equivalently we separate V_j into the one-dimensional spaces formed by each of its basis functions). Indeed, BPX can be seen as an abstract additive Schwarz preconditioner, and this makes possible its mathematical understanding via Bramble *et al.* (1990) and Dahmen and Kunoth (1992), for example. Then, from Buffa *et al.* (2013) and Dahmen and Kunoth (1992) we have the following result.

Theorem 8.4. The condition number of the BPX preconditioned isogeometric operator defined from (8.10) is uniformly bounded, that is,

$$\kappa_2(\mathbf{B}_{\mathrm{BPX}} A) \leq C,$$

where A is the stiffness matrix and C is a constant depending only on the degree p and the regularity k.

Table 8.4 reports the condition number for quadratic/cubic splines on the parametric square, up to a mesh of $10^3 \times 10^3$ elements. It is seen that the preconditioner is robust with respect to the number of levels but suffers from dependence on the degree. This is confirmed for higher p, three-dimensional problems and non-trivial geometries. Buffa *et al.* (2013) show that if the Jacobi solver on the levels is replaced by a more expensive and accurate symmetric successive overrelaxation (SSOR), then robustness with respect to p improves significantly. We refer to Buffa *et al.* (2013) for a more complete numerical testing and discussion.

8.3.3. BDDC

Beirão da Veiga, Cho, Pavarino and Scacchi (2013*b*) consider the same scalar elliptic model problem in order to construct and study BDDC (balancing domain decomposition by constraints) preconditioners for NURBS-based isogeometric methods.

The basic construction starts from a tensor product subdivision of the parameter domain $\widehat{\Omega} = [0,1]^d$ into disjoint rectangular subdomains $\widehat{\Omega}_i$,

Table 8.4. BPX preconditioner in the two-dimensional parametric domain: condition number $\kappa_2(\mathbf{B}_{\mathrm{BPX}}A)$ as a function of the spline polynomial degree p (maximal regularity $k = p - 1$) and the number of levels.

p	$J = 3$	$J = 4$	$J = 5$	$J = 6$	$J = 7$	$J = 8$	$J = 9$	$J = 10$
2	7.31	9.03	9.72	10.1	10.4	10.5	10.6	10.6
3	22.8	40.2	51.8	58.8	63.1	66.0	68.0	69.3

$i = 1, 2, \ldots, N_{\mathrm{sub}}$. We let Γ denote the skeleton of this partition, that is, the union of the boundaries of all the subdomains excluding $\partial\widehat{\Omega}$.

The BDDC is a non-overlapping method that preconditions the Schur complement system associated to the skeleton of the subdomains. In order to keep a general approach, let the integer N_{dof} denote the number of basis functions in $S_{\mathbf{p}}(\boldsymbol{\Xi})$ and let $\Theta := \{1, 2, \ldots, N_{\mathrm{dof}}\}$ represent the index set of all the basis functions. The first step is to divide Θ into two subsets Θ_Γ and its complement Θ_I. We define

$$\Theta_\Gamma = \{j \in \Theta : \mathrm{supp}(\widehat{B}_j) \cap \Gamma \neq \emptyset\},$$

where $\widehat{B}_j$ denotes the jth B-spline basis function. The set Θ_I is, by definition, associated to all the basis functions that have support fully contained in a single subdomain $\widehat{\Omega}_i$. Therefore such degrees of freedom can be eliminated by static condensation solving (possibly in parallel) problems that are local to subdomains. We denote by V_Γ the resulting discrete space after condensation, its dimension being equal to the cardinality of Θ_Γ. The ensuing linear system is the so-called Schur complement system

$$\mathsf{S}_\Gamma \mathbf{u} = \mathbf{b}, \quad \mathbf{u} \in V_\Gamma.$$

Note that in classical C^0 Lagrangian finite elements the space V_Γ is associated to degrees of freedom that 'lie' on the skeleton Γ (typically such degrees of freedom are evaluations at points on Γ) while all the remaining ones, being associated to basis functions that are internal to subdomains, can be statically condensated. This is not true in general for isogeometric methods, since the basis functions may have a larger support due to the higher continuity. This introduces the concept of a 'fat' boundary.

We then subdivide the set Θ_Γ into the set of primal (or coarse) degrees of freedom (Θ_C) and dual (or local) degrees of freedom (Θ_Δ). This choice is fundamental to the good behaviour of the BDDC method. A possible choice associated to the primal Poisson problem in two dimensions is to include in the set Θ_C all (and only) the indices associated to basis functions with support that intersects a *corner* of Γ. Different choices may be needed for different problems or different dimensions. We then introduce a partially

Table 8.5. Full system, Schur complement and BDDC dependence on p in the two-dimensional parametric domain: condition number $\kappa_2(\mathbf{B}_{\mathrm{BDDC}}\mathsf{S}_\Gamma)$ and iteration counts versus p. Fixed mesh size $1/h = 64$, 4×4 subdomains, regularity at the subdomain interface $k_\Gamma = 1$.

$k = p-1,\ k_\Gamma = 1,\ 1/h = 64,\ 1/H = 4$ B-splines, square domain								
p	Full		Schur		BDDC (ρ-scal.)		BDDC (stiff. scal.)	
	κ_2	iter.	κ_2	iter.	κ_2	iter.	κ_2	iter.
2	311.46	72	72.57	37	3.40	12	7.61	16
3	366.81	77	75.99	41	3.82	12	6.12	14
4	477.38	114	90.27	51	4.25	12	5.68	13
5	1.78×10^3	275	114.56	73	4.61	12	5.79	13
6	1.49×10^4	774	338.43	122	4.92	12	6.05	13
7	1.27×10^5	2151	1.00×10^3	202	5.24	12	6.34	12
8	1.11×10^6	5907	2.98×10^3	337	5.50	12	6.64	12
9	1.01×10^7	16541	8.77×10^3	545	5.73	12	6.96	13
10	9.42×10^7	47050	2.56×10^4	868	5.95	12	7.24	13

assembled (larger) discrete space $\widetilde{V}_\Gamma$, in which the values associated to the dual degrees of freedom Θ_Δ are assumed to be multi-valued, being different for different subdomains sharing the same associated basis function.

As the final step we introduce a 'partially broken' elliptic problem that consists in minimizing the same energy expression (for instance the H^1 square seminorm if a pure Laplace problem is considered) on the new discrete space $\widetilde{V}_\Gamma$. We let $\widetilde{\mathsf{S}}_\Gamma$ denote the stiffness matrix associated to this problem. For instance, following the choice above for Θ_C, this problem would represent a new Poisson problem where the domain is assumed to be cut along the edges (but not the corners) of Γ. Note that, thanks to this partial assembly, the new problem is much cheaper to solve, as the interaction between the different subdomains is now reduced to the coarse degrees of freedom in Θ_C.

By introducing weighted restriction and extension operators

$$R : \widetilde{V}_\Gamma \longrightarrow V_\Gamma, \quad R^T : V_\Gamma \longrightarrow \widetilde{V}_\Gamma,$$

the BDDC preconditioner is simply given by

$$\mathbf{B}_{\mathrm{BDDC}} := R\, \widetilde{\mathsf{S}}_\Gamma^{-1} R^T.$$

The (positive) weights in the R, R^T operators must sum to unity, that is, $R\, R^T = I$, with I representing the identity matrix. The choice of such weights also turns out to be fundamental for the good behaviour of the

method. An explicit expression of $\mathbf{B}_{\mathrm{BDDC}}$, in terms of the original stiffness matrix, can be found in Beirão da Veiga *et al.* (2013*b*).

As already mentioned, in the isogeometric case the construction of non-overlapping preconditioners is more challenging because B-spline basis functions are not nodal and have non-local support spanning several elements, depending on their polynomial degree and regularity. Beirão da Veiga *et al.* (2013*b*) construct BDDC preconditioners by defining primal continuity constraints across the generalized 'fat' subdomain interface. As for finite elements, these primal constraints are associated to subdomain vertices and/or averages or moments over edges or faces of the subdomains, but have a higher multiplicity in proportion to the spline regularity. Two different choices for the weights appearing in the restriction/extension operators R, R^T are proposed, the ρ-scaling and the stiffness scaling. By constructing appropriate discrete norms, it is proved that the isogeometric BDDC preconditioner is scalable in the number of subdomains and (for the ρ-scaling) also quasi-optimal in the ratio of subdomain and element sizes. We refer to the above paper for the proof and more details.

Theorem 8.5. The condition number of the BDDC preconditioned isogeometric operator is bounded by

$$\begin{aligned} &\kappa_2(\mathbf{B}_{\mathrm{BDDC}}\mathsf{S}_\Gamma) \le C\big(1+\log^2(H/h)\big) && \rho \text{ scaling},\\ &\kappa_2(\mathbf{B}_{\mathrm{BDDC}}\mathsf{S}_\Gamma) \le C\left(1+\log\left(\frac{H}{h}\right)\right)\frac{H}{h} && \text{stiffness scaling}, \end{aligned}$$

where the constant C is independent of H, h.

We note that the above theoretical results are not uniform in the polynomial degree p, and focus on the two-dimensional case. Although deriving p-estimates would be a very challenging task, extending such results to the three-dimensional case would be straightforward.

Beirão da Veiga *et al.* (2013*b*) present an extensive set of numerical experiments in two and three dimensions that confirm the theoretical estimates and also illustrate the preconditioner performance with respect to the polynomial degree p and the regularity index k, as well as its robustness with respect to discontinuities of the coefficient of the elliptic problem across subdomain boundaries. In particular, it is interesting to note that the ρ-scaling choice for the weights, which is quasi-optimal in the mesh parameters, leads to far worse subdivision of energy for high values of k. As a consequence, a much better condition number is obtained in practice with the stiffness scaling for high values of the regularity index k across the interface. A sample test (for fixed C^1-regularity across the interfaces and variable polynomial degree) taken from Beirão da Veiga *et al.* (2013*b*) is shown in Table 8.5.

8.3.4. Other preconditioners

Here we briefly describe other interesting preconditioning techniques that can be found in the isogeometric literature.

Gahalaut, Tomar and Kraus (2013) introduce (geometric) multigrid methods for isogeometric discretization of the Laplace model problem. The method inherits the theoretical analysis of finite element methods, based on the smoothing property of the relaxation method, and the approximation property of the intergrid transfer operators. Multigrid schemes based on V-, W- and F-cycles are tested numerically and shown to give satisfactory results with respect to the mesh size, and in the presence of variable coefficients. The robustness of the proposed preconditioner for high values of the degree p is not tested.

Finally, Kleiss *et al.* (2012) introduce a FETI (finite element tearing and interconnecting) method for isogeometric analysis, referred as IETI. The paper deals only with the case of a C^0 interface, but also covers non-trivial multi-patch geometries (such as in the presence of T-junctions and triple points), and introduce a preconditioner for the iterative linear solver used for the interface problem in such situations. Numerical tests for $p = 3$ show good performance of the method for complicated multi-patch domains in two dimensions.

Acknowledgements

The authors were partially supported by the European Research Council via the FP7 Ideas Starting Grant *GeoPDEs*, and by the Italian MIUR via the FIRB 'Futuro in Ricerca' Grant RBFR08CZ0S. This support is gratefully acknowledged. Moreover, we are indebted to P. Antolín, A. Bressan, C. Lovadina, M. Martinelli and L. Pavarino for their valuable advice and help.

REFERENCES[3]

R. A. Adams (1975), *Sobolev Spaces*, Vol. 65 of *Pure and Applied Mathematics*, Academic Press.

M. Aigner, C. Heinrich, B. Jüttler, E. Pilgerstorfer, B. Simeon and A.-V. Vuong (2009), 'Swept volume parameterization for isogeometric analysis', Vol. 5654 of *Lecture Notes in Computer Science*, Springer, pp. 19–44.

A. Apostolatos, R. Schmidt, R. Wüchner and K.-U. Bletzinger (2014), 'A Nitsche-type formulation and comparison of the most common domain decomposition methods in isogeometric analysis', *Internat. J. Numer. Methods Engrg* **97**, 473–504.

[3] The URLs cited in this work were correct at the time of going to press, but the publisher and the authors make no undertaking that the citations remain live or are accurate or appropriate.

D. N. Arnold, R. S. Falk and R. Winther (2006), Finite element exterior calculus, homological techniques, and applications. In *Acta Numerica*, Vol. 15, Cambridge University Press, pp. 1–155.

D. N. Arnold, R. S. Falk and R. Winther (2010), 'Finite element exterior calculus: From Hodge theory to numerical stability', *Bull. Amer. Math. Soc.* (NS) **47**, 281–354.

F. Auricchio, L. Beirão da Veiga, C. Lovadina and A. Reali (2010*a*), 'The importance of the exact satisfaction of the incompressibility constraint in nonlinear elasticity: Mixed FEMs versus NURBS-based approximations', *Comput. Methods Appl. Mech. Engrg* **199**, 314–323.

F. Auricchio, L. Beirão da Veiga, A. Buffa, C. Lovadina, A. Reali and G. Sangalli (2007), 'A fully "locking-free" isogeometric approach for plane linear elasticity problems: A stream function formulation', *Comput. Methods Appl. Mech. Engrg* **197**, 160–172.

F. Auricchio, L. Beirão da Veiga, T. J. R. Hughes, A. Reali and G. Sangalli (2010*b*), 'Isogeometric collocation methods', *Math. Models Methods Appl. Sci.* **20**, 2075–2107.

F. Auricchio, F. Calabrò, T. Hughes, A. Reali and G. Sangalli (2012), 'A simple algorithm for obtaining nearly optimal quadrature rules for NURBS-based isogeometric analysis', *Comput. Methods Appl. Mech. Engrg* **249–252**, 15–27.

I. Babuška and T. Strouboulis (2001), *The Finite Element Method and its Reliability*, Numerical Mathematics and Scientific Computation, Oxford Science Publications.

Y. Bazilevs and T. J. R. Hughes (2008), 'NURBS-based isogeometric analysis for the computation of flows about rotating components', *Comput. Mech.* **43**, 143–150.

Y. Bazilevs, L. Beirão da Veiga, J. A. Cottrell, T. J. R. Hughes and G. Sangalli (2006), 'Isogeometric analysis: Approximation, stability and error estimates for h-refined meshes', *Math. Models Methods Appl. Sci.* **16**, 1031–1090.

Y. Bazilevs, V. Calo, J. A. Cottrell, J. A. Evans, T. J. R. Hughes, S. Lipton, M. Scott and T. Sederberg (2010*a*), 'Isogeometric analysis using T-splines', *Comput. Methods Appl. Mech. Engrg* **199**, 229–263.

Y. Bazilevs, V. M. Calo, J. A. Cottrell, T. J. R. Hughes, A. Reali and G. Scovazzi (2007), 'Variational multiscale residual-based turbulence modeling for large eddy simulation of incompressible flows', *Comput. Methods Appl. Mech. Engrg* **197**, 173–201.

Y. Bazilevs, V. M. Calo, T. J. R. Hughes and Y. Zhang (2008), 'Isogeometric fluid–structure interaction: Theory, algorithms, and computations', *Comput. Mech.* **43**, 3–37.

Y. Bazilevs, M.-C. Hsu and M. Scott (2012), 'Isogeometric fluid–structure interaction analysis with emphasis on non-matching discretizations, and with application to wind turbines', *Comput. Methods Appl. Mech. Engrg* **249**, 28–41.

Y. Bazilevs, M.-C. Hsu, J. Kiendl, R. Wüchner and K.-U. Blezinger (2011), '3D simulation of wind turbine rotors at full scale II: Fluid–structure interaction modeling with composite blades', *Internat. J. Numer. Meth. Fluids* **65**, 236–253.

Y. Bazilevs, C. Michler, V. Calo and T. Hughes (2010*b*), 'Isogeometric variational multiscale modeling of wall-bounded turbulent flows with weakly enforced boundary conditions on unstretched meshes', *Comput. Methods Appl. Mech. Engrg* **199**, 780–790.

L. Beirão da Veiga, A. Buffa, D. Cho and G. Sangalli (2012*a*), 'Analysis-suitable T-splines are dual-compatible', *Comput. Methods Appl. Mech. Engrg* **249–252**, 42–51.

L. Beirão da Veiga, A. Buffa, C. Lovadina, M. Martinelli and G. Sangalli (2012*b*), 'An isogeometric method for the Reissner–Mindlin plate bending problem', *Comput. Methods Appl. Mech. Engrg* **209–212**, 45–53.

L. Beirão da Veiga, A. Buffa, J. Rivas and G. Sangalli (2011), 'Some estimates for *h*-*p*-*k*-refinement in isogeometric analysis', *Numer. Math.* **118**, 271–305.

L. Beirão da Veiga, A. Buffa, G. Sangalli and R. Vázquez (2013*a*), 'Analysis-suitable T-splines of arbitrary degree: Definition, linear independence and approximation properties', *Math. Models Methods Appl. Sci.* **23**, 1979–2003.

L. Beirão da Veiga, D. Cho and G. Sangalli (2012*c*), 'Anisotropic NURBS approximation in isogeometric analysis', *Comput. Methods Appl. Mech. Engrg* **209–212**, 1–11.

L. Beirão da Veiga, D. Cho, L. Pavarino and S. Scacchi (2012*d*), 'Overlapping Schwarz methods for isogeometric analysis', *SIAM J. Numer. Anal.* **50**, 1394–1416.

L. Beirão da Veiga, D. Cho, L. F. Pavarino and S. Scacchi (2013*b*), 'BDDC preconditioners for isogeometric analysis', *Math. Models Methods Appl. Sci.* **23**, 1099–1142.

L. Beirão da Veiga, D. Cho, L. F. Pavarino and S. Scacchi (2013*c*), 'Isogeometric Schwarz preconditioners for linear elasticity systems', *Comput. Methods Appl. Mech. Engrg* **253**, 439–454.

D. Benson, Y. Bazilevs, M.-C. Hsu and T. Hughes (2011), 'A large deformation, rotation-free, isogeometric shell', *Comput. Methods Appl. Mech. Engrg* **200**, 1367–1378.

D. Boffi (2007), 'Approximation of eigenvalues in mixed form, discrete compactness property, and application to *hp* mixed finite elements', *Comput. Methods Appl. Mech. Engrg* **196**, 3672–3681.

D. Boffi (2010), Finite element approximation of eigenvalue problems. In *Acta Numerica*, Vol. 19, Cambridge University Press, pp. 1–120.

D. Boffi, F. Brezzi and M. Fortin (2013), *Mixed Finite Element Methods and Applications*, Vol. 44 of *Springer Series in Computational Mathematics*, Springer.

D. Boffi, F. Brezzi and L. Gastaldi (1997), 'On the convergence of eigenvalues for mixed formulations', *Ann. Scuola Norm. Sup. Pisa Cl. Sci.* (4) **25**, 131–154.

D. Boffi, P. Fernandes, L. Gastaldi and I. Perugia (1999), 'Computational models of electromagnetic resonators: Analysis of edge element approximation', *SIAM J. Numer. Anal.* **36**, 1264–1290.

C. de Boor (2001), *A Practical Guide to Splines*, Vol. 27 of *Applied Mathematical Sciences*, revised edition, Springer.

M. J. Borden, M. A. Scott, J. A. Evans and T. J. R. Hughes (2011), 'Isogeometric finite element data structures based on Bézier extraction of NURBS', *Internat. J. Numer. Methods Engrg* **87**, 15–47.

J. H. Bramble, J. E. Pasciak and J. Xu (1990), 'Parallel multilevel preconditioners', *Math. Comp.* **55**, 1–22.

A. Bressan (2011), 'Isogeometric regular discretization for the Stokes problem', *IMA J. Numer. Anal.* **31**, 1334–1356.

A. Bressan (2013), 'Some properties of LR-splines', *Comput. Aided Geom. Design.* **30**, 778–794.

A. Bressan and G. Sangalli (2013), 'Isogeometric discretizations of the Stokes problem: Stability analysis by the macroelement technique', *IMA J. Numer. Anal.* **33**, 629–651.

A. Bressan, A. Buffa and G. Sangalli (2013), Characterization of analysis suitable T-splines. Technical report, IMATI-CNR.

A. Buffa, D. Cho and M. Kumar (2012), 'Characterization of T-splines with reduced continuity order on T-meshes', *Comput. Methods Appl. Mech. Engrg* **201–204**, 112–126.

A. Buffa, D. Cho and G. Sangalli (2010*a*), 'Linear independence of the T-spline blending functions associated with some particular T-meshes', *Comput. Methods Appl. Mech. Engrg* **199**, 1437–1445.

A. Buffa, M. Costabel and M. Dauge (2005), 'Algebraic convergence for anisotropic edge elements in polyhedral domains', *Numer. Math.* **101**, 29–65.

A. Buffa, C. de Falco and G. Sangalli (2011*a*), 'Isogeometric analysis: Stable elements for the 2D Stokes equation', *Internat. J. Numer. Methods Fluids* **65**, 1407–1422.

A. Buffa, H. Harbrecht, A. Kunoth and G. Sangalli (2013), 'BPX-preconditioning for isogeometric analysis', *Comput. Methods Appl. Mech. Engrg* **265**, 63–70.

A. Buffa, J. Rivas, G. Sangalli and R. Vázquez (2011*b*), 'Isogeometric discrete differential forms in three dimensions', *SIAM J. Numer. Anal.* **49**, 818–844.

A. Buffa, G. Sangalli and C. Schwab (2014*a*), Exponential convergence of the *hp* version of isogeometric analysis in 1D. In *Spectral and High Order Methods for Partial Differential Equations: ICOSAHOM 2012* (M. Azaez, H. El Fekih and J. S. Hesthaven, eds), Vol. 95 of *Lecture Notes in Computational Science and Engineering*, Springer, pp. 191–203.

A. Buffa, G. Sangalli and R. Vázquez (2010*b*), 'Isogeometric analysis in electromagnetics: B-splines approximation', *Comput. Methods Appl. Mech. Engrg* **199**, 1143–1152.

A. Buffa, G. Sangalli and R. Vázquez (2014*b*), 'Isogeometric methods for computational electromagnetics: B-spline and T-spline discretizations', *J. Comput. Phys.* B **257**, 1291–1320.

P. G. Ciarlet (2002), *The Finite Element Method for Elliptic Problems*, Vol. 40 of *Classics in Applied Mathematics*, SIAM. Reprint of the 1978 original (North-Holland).

E. Cohen and L. L. Schumaker (1985), 'Rates of convergence of control polygons', *Comput. Aided Geom. Design.* **2**, 229–235.

E. Cohen, T. Lyche and R. Riesenfeld (2013), 'A B-spline-like basis for the Powell–Sabin 12-split based on simplex splines', *Math. Comp.* **82**, 1667–1707.

E. Cohen, T. Martin, R. M. Kirby, T. Lyche and R. F. Riesenfeld (2010), 'Analysis-aware modeling: Understanding quality considerations in modeling for isogeometric analysis', *Comput. Methods Appl. Mech. Engrg* **199**, 334–356.

E. Cohen, R. Riesenfeld and G. Elber (2001), *Geometric Modeling with Splines: An Introduction*, Vol. 1, A. K. Peters.

N. Collier, L. Dalcin, D. Pardo and V. M. Calo (2013*a*), 'The cost of continuity: Performance of iterative solvers on isogeometric finite elements', *SIAM J. Sci. Comput.* **35**, A767–A784.

N. O. Collier, L. Dalcin and V. M. Calo (2013*b*), PetIGA: High-performance isogeometric analysis. arXiv:1305.4452

N. O. Collier, D. Pardo, M. Paszynski and V. M. Calo (2012*a*), Computational complexity and memory usage for multi-frontal direct solvers in structured mesh finite elements. arXiv:1204.1718

N. Collier, D. Pardo, L. Dalcin, M. Paszynski and V. M. Calo (2012*b*), 'The cost of continuity: A study of the performance of isogeometric finite elements using direct solvers', *Comput. Methods Appl. Mech. Engrg* **213–216**, 353–361.

M. Costabel and M. Dauge (2006), Maxwell eigenmodes in tensor product domains. Technical report, University of Rennes.

J. A. Cottrell, T. Hughes and A. Reali (2007), 'Studies of refinement and continuity in isogeometric structural analysis', *Comput. Methods Appl. Mech. Engrg* **196**, 4160–4183.

J. A. Cottrell, T. J. R. Hughes and Y. Bazilevs (2009), *Isogeometric Analysis: Toward Integration of CAD and FEA*, Wiley.

J. A. Cottrell, A. Reali, Y. Bazilevs and T. J. R. Hughes (2006), 'Isogeometric analysis of structural vibrations', *Comput. Methods Appl. Mech. Engrg* **195**, 5257–5296.

N. Crouseilles, A. Ratnani and E. Sonnendrücker (2012), 'An isogeometric analysis approach for the study of the gyrokinetic quasi-neutrality equation', *J. Comput. Phys.* **231**, 373–393.

W. Dahmen and A. Kunoth (1992), 'Multilevel preconditioning', *Numer. Math.* **63**, 315–344.

M. Dauge (2014), Benchmark computations for Maxwell equations for the approximation of highly singular solutions. http://perso.univ-rennes1.fr/monique.dauge/benchmax.html

L. De Lorenzis, İ. Temizer, P. Wriggers and G. Zavarise (2011), 'A large deformation frictional contact formulation using NURBS-based isogeometric analysis', *Internat. J. Numer. Methods Engrg* **87**, 1278–1300.

R. Dimitri, L. De Lorenzis, M. Scott, P. Wriggers, R. Taylor and G. Zavarise (2014), 'Isogeometric large deformation frictionless contact using T-splines', *Comput. Methods Appl. Mech. Engrg* **269**, 394–414.

T. Dokken, T. Lyche and K. F. Pettersen (2013), 'Polynomial splines over locally refined box-partitions', *Comput. Aided Geom. Design* **30**, 331–356.

M. Dörfel, B. Jüttler and B. Simeon (2010), 'Adaptive isogeometric analysis by local h-refinement with T-splines', *Comput. Methods Appl. Mech. Engrg* **199**, 264–275.

R. Echter and M. Bischoff (2010), 'Numerical efficiency, locking and unlocking of NURBS finite elements', *Comput. Methods Appl. Mech. Engrg* **199**, 374–382.

T. Elguedj, Y. Bazilevs, V. Calo and T. J. R. Hughes (2008), '$\bar{B}$ and $\bar{F}$ projection methods for nearly incompressible linear and non-linear elasticity and plasticity using higher-order NURBS elements', *Comput. Methods Appl. Mech. Engrg* **197**, 2732–2762.

J. A. Evans and T. J. R. Hughes (2013*a*), 'Isogeometric divergence-conforming B-splines for the Darcy–Stokes–Brinkman equations', *Math. Models Methods Appl. Sci.* **23**, 671–741.

J. A. Evans and T. J. R. Hughes (2013*b*), 'Isogeometric divergence-conforming B-splines for the steady Navier–Stokes equations', *Math. Models Methods Appl. Sci.* **23**, 1421–1478.

J. A. Evans and T. J. R. Hughes (2013*c*), 'Isogeometric divergence-conforming B-splines for the unsteady Navier–Stokes equations', *J. Comput. Phys.* **241**, 141–167.

J. A. Evans, Y. Bazilevs, I. Babuška and T. J. R. Hughes (2009), 'n-widths, sup-infs, and optimality ratios for the k-version of the isogeometric finite element method', *Comput. Methods Appl. Mech. Engrg* **198**, 1726–1741.

C. de Falco, A. Reali and R. Vázquez (2011), 'GeoPDEs: A research tool for isogeometric analysis of PDEs', *Adv. Engrg Softw.* **42**, 1020–1034.

K. Gahalaut, S. Tomar and J. Kraus (2013), 'Algebraic multilevel preconditioning in isogeometric analysis: Construction and numerical studies', *Comput. Methods Appl. Mech. Engrg* **266**, 40–56.

C. Garoni, C. Manni, F. Pelosi, S. Serra-Capizzano and H. Speleers (2014), 'On the spectrum of stiffness matrices arising from isogeometric analysis', *Numer. Math*, to appear.

C. Giannelli and B. Jüttler (2013), 'Bases and dimensions of bivariate hierarchical tensor-product splines', *J. Comput. Appl. Math.* **239**, 162–178.

C. Giannelli, B. Jüttler and H. Speleers (2012), 'THB-splines: The truncated basis for hierarchical splines', *Comput. Aided Geom. Design.* **29**, 485–498.

H. Gómez, V. Calo, Y. Bazilevs and T. J. R. Hughes (2008), 'Isogeometric analysis of the Cahn–Hilliard phase-field model', *Comput. Methods Appl. Mech. Engrg* **197**, 4333–4352.

H. Gómez, T. J. R. Hughes, X. Nogueira and V. M. Calo (2010), 'Isogeometric analysis of the isothermal Navier–Stokes–Korteweg equations', *Comput. Methods Appl. Mech. Engrg* **199**, 1828–1840.

S. Govindjee, J. Strain, T. J. Mitchell and R. L. Taylor (2012), 'Convergence of an efficient local least-squares fitting method for bases with compact support', *Comput. Methods Appl. Mech. Engrg* **213–216**, 84–92.

R. Hiptmair (2002), Finite elements in computational electromagnetism. In *Acta Numerica*, Vol. 11, Cambridge University Press, pp. 237–339.

S. Hosseini, J. J. Remmers, C. V. Verhoosel and R. Borst (2013), 'An isogeometric solid-like shell element for nonlinear analysis', *Internat. J. Numer. Methods Engrg* **95**, 238–256.

T. J. R. Hughes, J. A. Cottrell and Y. Bazilevs (2005), 'Isogeometric analysis: CAD, finite elements, NURBS, exact geometry and mesh refinement', *Comput. Methods Appl. Mech. Engrg* **194**, 4135–4195.

T. J. R. Hughes, J. A. Evans and A. Reali (2014), 'Finite element and NURBS approximations of eigenvalue, boundary-value, and initial-value problems', *Comput. Methods Appl. Mech. Engrg* **272**, 290–320.

T. J. R. Hughes, A. Reali and G. Sangalli (2008), 'Duality and unified analysis of discrete approximations in structural dynamics and wave propagation:

Comparison of p-method finite elements with k-method NURBS', *Comput. Methods Appl. Mech. Engrg* **197**, 4104–4124.

T. J. R. Hughes, A. Reali and G. Sangalli (2010), 'Efficient quadrature for NURBS-based isogeometric analysis', *Comput. Methods Appl. Mech. Engrg* **199**, 301–313.

K. A. Johannessen, T. Kvamsdal and T. Dokken (2014), 'Isogeometric analysis using LR B-splines', *Comput. Methods Appl. Mech. Engrg* **269**, 471–514.

A. Karatarakis, P. Karakitsios and M. Papadrakakis (2014), 'GPU accelerated computation of the isogeometric analysis stiffness matrix', *Comput. Methods Appl. Mech. Engrg* **269**, 334–355.

R. B. Kellogg (1974/75), 'On the Poisson equation with intersecting interfaces', *Applicable Anal.* **4**, 101–129.

J. Kiendl, Y. Bazilevs, M.-C. Hsu, R. Wüchner and K.-U. Bletzinger (2010), 'The bending strip method for isogeometric analysis of Kirchhoff–Love shell structures comprised of multiple patches', *Comput. Methods Appl. Mech. Engrg* **199**, 2403–2416.

J. Kiendl, K.-U. Bletzinger, J. Linhard and R. Wuchner (2009), 'Isogeometric shell analysis with Kirchhoff–Love elements', *Comput. Methods Appl. Mech. Engrg* **198**, 3902–3914.

S. K. Kleiss, C. Pechstein, B. Jüttler and S. Tomar (2012), 'IETI: Isogeometric tearing and interconnecting', *Comput. Methods Appl. Mech. Engrg* **247/248**, 201–215.

R. Kraft (1997), Adaptive and linearly independent multilevel B-splines. In *Surface Fitting and Multiresolution Methods: Chamonix–Mont-Blanc, 1996*, Vanderbilt University Press, pp. 209–218.

M.-J. Lai and L. L. Schumaker (2007), *Spline Functions on Triangulations*, Vol. 110 of *Encyclopedia of Mathematics and its Applications*, Cambridge University Press.

B.-G. Lee, T. Lyche and K. Mørken (2001), Some examples of quasi-interpolants constructed from local spline projectors. In *Mathematical Methods for Curves and Surfaces: Oslo, 2000*, Vanderbilt University Press, pp. 243–252.

X. Li and M. A. Scott (2014), 'Analysis-suitable T-splines: Characterization, refineability, and approximation', *Math. Models Methods Appl. Sci.* **24**, 1141.

X. Li, J. Zheng, T. Sederberg, T. Hughes and M. Scott (2012), 'On linear independence of T-spline blending functions', *Comput. Aided Geom. Design* **29**, 63–76.

S. Lipton, J. A. Evans, Y. Bazilevs, T. Elguedj and T. J. R. Hughes (2010), 'Robustness of isogeometric structural discretizations under severe mesh distortion', *Comput. Methods Appl. Mech. Engrg* **199**, 357–373.

J. Maes, A. Kunoth and A. Bultheel (2007), 'BPX-type preconditioners for second and fourth order elliptic problems on the sphere', *SIAM J. Numer. Anal.* **45**, 206–222.

A. Mantzaflaris and B. Jüttler (2014), Exploring matrix generation strategies in isogeometric analysis. In *Mathematical Methods for Curves and Surfaces* (M.-L. Mazure *et al.*, eds), Vol. 8177 of *Lecture Notes in Computer Science*, Springer, pp. 364–382.

T. Martin, E. Cohen and R. Kirby (2009), 'Volumetric parameterization and trivariate B-spline fitting using harmonic functions', *Comput. Aided Geom. Design* **26**, 648–664.

J. Melenk, K. Gerdes and C. Schwab (2001), 'Fully discrete *hp*-finite elements: Fast quadrature', *Comput. Methods Appl. Mech. Engrg* **190**, 4339–4364.

P. Monk (2003), *Finite Element Methods for Maxwell's Equations*, Oxford University Press.

P. Morin, R. H. Nochetto and K. G. Siebert (2002), 'Convergence of adaptive finite element methods', *SIAM Rev.* **44**, 631–658.

J.-C. Nédélec (1980), 'Mixed finite elements in $\mathbb{R}^3$', *Numer. Math.* **35**, 315–341.

V. Nguyen, P. Kerfriden, M. Brino, S. Bordas and E. Bonisoli (2014), 'Nitsche's method for two and three dimensional NURBS patch coupling', *Comput. Mech.*, to appear.

V. P. Nguyen, S. P. A. Bordas and T. Rabczuk (2012), Isogeometric analysis: An overview and computer implementation aspects. arXiv:1205.2129

S. Pauletti, M. Martinelli, N. Cavallini and P. Antolín (2013), Igatools: An isogeometric analysis library. Technical report, IMATI-CNR.

M. Petzoldt (2001), Regularity and error estimators for elliptic problems with discontinuous coefficients. PhD thesis, Freie Universität, Berlin.

R. Picard (1984), 'An elementary proof for a compact imbedding result in generalized electromagnetic theory', *Math. Z.* **187**, 151–164.

L. Piegl and W. Tiller (1997), *The NURBS Book*, Springer.

A. Ratnani and E. Sonnendrücker (2012), 'An arbitrary high-order spline finite element solver for the time domain Maxwell equations', *J. Sci. Comput.* **51**, 87–106.

D. F. Rogers (2001), *An Introduction to NURBS: With Historical Perspective*, Morgan Kaufmann.

T. Rüberg and F. Cirak (2012), 'Subdivision-stabilised immersed B-spline finite elements for moving boundary flows', *Comput. Methods Appl. Mech. Engrg* **209–212**, 266–283.

M. Ruess, D. Schillinger, A. I. Özcan and E. Rank (2014), 'Weak coupling for isogeometric analysis of non-matching and trimmed multi-patch geometries', *Comput. Methods Appl. Mech. Engrg* **269**, 46–71.

D. Schillinger, L. Dedè, M. A. Scott, J. A. Evans, M. J. Borden, E. Rank and T. J. Hughes (2012), 'An isogeometric design-through-analysis methodology based on adaptive hierarchical refinement of NURBS, immersed boundary methods, and T-spline CAD surfaces', *Comput. Methods Appl. Mech. Engrg* **249–252**, 116–150.

D. Schillinger, J. Evans, A. Reali, M. Scott and T. Hughes (2013), 'Isogeometric collocation: Cost comparison with Galerkin methods and extension to adaptive hierarchical NURBS discretizations', *Comput. Methods Appl. Mech. Engrg* **267**, 170–232.

L. L. Schumaker (2007), *Spline Functions: Basic Theory*, third edition, Cambridge University Press

M. Scott (2011), T-splines as a design-through-analysis technology. PhD thesis, The University of Texas at Austin.

M. Scott, M. Borden, C. Verhoosel, T. Sederberg and T. J. R. Hughes (2011), 'Isogeometric finite element data structures based on Bézier extraction of T-splines', *Internat. J. Numer. Methods Engrg* **88**, 126–156.

M. Scott, X. Li, T. Sederberg and T. J. R. Hughes (2012), 'Local refinement of analysis-suitable T-splines', *Comput. Methods Appl. Mech. Engrg* **213–216**, 206–222.

T. Sederberg, D. Cardon, G. Finnigan, N. North, J. Zheng and T. Lyche (2004), 'T-spline simplification and local refinement', *ACM Trans. Graph.* **23**, 276–283.

T. Sederberg, J. Zheng, A. Bakenov and A. Nasri (2003), 'T-splines and T-NURCCSs', *ACM Trans. Graph.* **22**, 477–484.

H. Speleers (2013), 'Multivariate normalized Powell–Sabin B-splines and quasi-interpolants', *Comput. Aided Geom. Design* **30**, 2–19.

H. Speleers, C. Manni, F. Pelosi and M. L. Sampoli (2012), 'Isogeometric analysis with Powell–Sabin splines for advection–diffusion–reaction problems', *Comput. Methods Appl. Mech. Engrg* **221/222**, 132–148.

T. Takacs and B. Jüttler (2011), 'Existence of stiffness matrix integrals for singularly parameterized domains in isogeometric analysis', *Comput. Methods Appl. Mech. Engrg* **200**, 3568–3582.

T. Takacs and B. Jüttler (2012), 'Regularity properties of singular parameterizations in isogeometric analysis', *Graph. Models* **74**, 361–372.

İ. Temizer, P. Wriggers and T. Hughes (2012), 'Three-dimensional mortar-based frictional contact treatment in isogeometric analysis with NURBS', *Comput. Methods Appl. Mech. Engrg* **209–212**, 115–128.

R. Vázquez, A. Buffa and L. Di Rienzo (2012), 'NURBS-based BEM implementation of high-order surface impedance boundary conditions', *IEEE Trans. Magn.* **48**, 4757–4766.

R. Vázquez, A. Buffa and L. Di Rienzo (2014), 'Isogeometric FEM implementation of high order surface impedance boundary conditions', *IEEE Trans. Magn.*, to appear.

A.-V. Vuong, C. Giannelli, B. Jüttler and B. Simeon (2011), 'A hierarchical approach to adaptive local refinement in isogeometric analysis', *Comput. Methods Appl. Mech. Engrg* **200**, 3554–3567.

W. A. Wall, M. A. Frenzel and C. Cyron (2008), 'Isogeometric structural shape optimization', *Comput. Methods Appl. Mech. Engrg* **197**, 2976–2988.

W. Wang, Y. Zhang, L. Liu and T. J. Hughes (2013), 'Trivariate solid T-spline construction from boundary triangulations with arbitrary genus topology', *Comput. Aided Design* **45**, 351–360.

W. Wang, Y. Zhang, M. Scott and T. J. R. Hughes (2011), 'Converting an unstructured quadrilateral mesh to a standard T-spline surface', *Comput. Mech.* **48**, 477–498.

E. L. Wilson (1974), 'The static condensation algorithm', *Internat. J. Numer. Methods Engrg* **8**, 198–203.

G. Xu, B. Mourrain, R. Duvigneau and A. Galligo (2011), 'Parameterization of computational domain in isogeometric analysis: Methods and comparison', *Comput. Methods Appl. Mech. Engrg* **200**, 2021–2031.

G. Xu, B. Mourrain, R. Duvigneau and A. Galligo (2013), 'Optimal analysis-aware parameterization of computational domain in 3D isogeometric analysis', *Comput. Aided Design* **45**, 812–821.

Y. Zhang, W. Wang and T. J. R. Hughes (2012), 'Solid T-spline construction from boundary representations for genus-zero geometry', *Comput. Methods Appl. Mech. Engrg* **249–252**, 185–197.